Application of Data Mining for Assessment of Material Properties: Creep Behavior of High-Temperature Steels

Anwendung von Neuronalen Netzen zur Beurteilung des Langzeitstandbruch-Verhaltens von warmfesten Stählen

Dissertation

zur Erlangung des akademischen Grades

Doktoringenieurin / Doktoringenieur
(Dr.-Ing.)

von Dipl.-Ing. (Universität Neusatz) Daniel Balos

geb. am 29. Oktober 1971 in Belgrad, Serbien

genehmigt durch die Fakultät für Maschinenbau
der Otto-von-Guericke-Universität Magdeburg

Gutachter:

Prof. Dr.-Ing. habil. Jens Strackeljan

Prof. Dr.-Ing. Martin Heilmaier

Prof. Dr.-Ing. habil. Karl Maile

Promotionskolloquium am 20.05.2009

Ehrenerklärung

Ich versichere hiermit, dass ich die vorliegende Arbeit ohne unzulässige Hilfe Dritter und ohne Benutzung anderer als der angegebenen Hilfsmittel angefertigt habe. Die Hilfe eines kommerziellen Promotionsberaters habe ich nicht in Anspruch genommen. Dritte haben von mir weder unmittelbar noch mittelbar geldwerte Leistungen für Arbeiten erhalten, die im Zusammenhang mit dem Inhalt der vorgelegten Dissertation stehen. Verwendete fremde und eigene Quellen sind als solche kenntlich gemacht

Ich habe insbesondere nicht wissentlich:

- Ergebnisse erfunden oder widersprüchliche Ergebnisse verschwiegen,
- statistische Verfahren absichtlich missbraucht, um Daten in ungerechtfertigter Weise zu interpretieren,
- fremde Ergebnisse oder Veröffentlichungen plagiiert,
- fremde Forschungsergebnisse verzerrt wiedergegeben

Mir ist bekannt, dass Verstöße gegen das Urheberrecht Unterlassungs- und Schadensersatzansprüche des Urhebers sowie eine strafrechtliche Ahndung durch die Strafverfolgungsbehörden begründen kann.

Ich erkläre mich damit einverstanden, dass die Dissertation ggf. mit Mitteln der elektronischen Datenverarbeitung auf Plagiate überprüft werden kann.

Die Arbeit wurde bisher weder im Inland noch im Ausland in gleicher oder ähnlicher Form als Dissertation eingereicht und ist als Ganzes auch noch nicht veröffentlicht.

Stuttgart, 21.05.2009

Declaration of Honor

I hereby declare that I produced this thesis without prohibited external assistance and that none other than the listed references and tools have been used. I did not make use of any commercial consultant concerning graduation. A third party did not receive any nonmonetary perquisites neither directly nor indirectly for activities which are connected with the contents of the presented thesis.

All sources of information are clearly marked, including my own publications.

In particular I have not consciously:

- Fabricated data or rejected undesired results
- Misused statistical methods with the aim of drawing other conclusions than those warranted by the available data
- Plagiarized data or publications
- Presented the results of other researchers in a distorted way

I do know that violations of copyright may lead to injunction and damage claims of the author and also to prosecution by the law enforcement authorities. I hereby agree that the thesis may need to be reviewed with an electronic data processing for plagiarism.

This work has not yet been submitted as a doctoral thesis in the same or a similar form in Germany or in any other country. It has not yet been published as a whole.

Stuttgart, 21.05.2009

Acknowledgements

Special thanks goes to Prof. Dr. Jens Strackeljan for support in the area of data mining and neural network training with his experience and to Dr. Jovanovic, for support and advice on critical steps during the whole course of the work presented here.

I am grateful to my colleague and longtime advisor Prof. Dr.-Ing. Karl Maile for the unconditional support, enthusiasm, knowledge and trust along this long research path we have behind us.

Dr. Wolfgang Müller also deserves my deep gratitude for all the support and collaboration in the project from which this work has resulted.

I am indebted to Stiftung Stahlanwendungsforschung im Stifterverband für die Deutsche Wissenschaft e.V , and in particular to members of the FDBR and the Working Group W12 - Restlebensdauer for their expertise, support and data.

Also, a special help goes to all the colleagues participating in the UNCERT and UNCERT-AM projects, which resulted in standardization efforts and CEN WA 11 “Measurement uncertainties in mechanical tests on metallic materials”, where initial data analysis using clustering and neural networks did take place.

I am looking forward to further continuation of the work and collaboration with all the mentioned colleagues in the same field in the future.

Finally, I would like to thank to my family for their love, unfailing support and help.

Daniel Balos, November 2008

Table of Content

List of Figures

List of Tables

1 Introduction

Part of this work has been presented in the following publications and events:

1. D. Balos, K. Maile und W. Müller: Abschlussbericht des Forschungsprojekts Bewertung der Streubänder im Langzeitverhalten von warmfesten Stählen mit Hilfe der Anwendung von Data Mining-Methoden (AVIF 198), 2007
2. Presentation at 29. Vortragsveranstaltung 2006 "Langzeitverhalten warmfester Stähle und Hochtemperaturwerkstoffe", November 2006, under title „Anwendung von neuronalen Netzen zur Ermittlung des schmelzenabhängigen Zeitstandverhaltens“ by D. Balos, A. Klenk und K. Maile, Materialprüfungsanstalt Univ. Stuttgart (MPA), W. Müller, Institut für Metallformung, TU Freiberg

Equipment and components for high-temperature purpose can be designed and used either in high-temperature tensile range or in the creep range. The point where the design curve of yield strength cuts the corresponding creep curve (for component design lifetime) represents the point after which design for creep has to be considered. This approach is generally accepted in both German / European norms (TRD 301:1979, EN 12952-3:2001), where the designer is explicitly required to determine the maximum allowable stresses ([EN 12952-3:2001], Table 6.3.1 and [TRD 301:1979], Table 5) Figure 1, as well as in the ASME code ([ASME BPVC: 2004], Section II – Materials, Part D), where this point is not defined, but can be identified in the maximum allowable stress diagrams – see Figure 2. Furthermore, in ASME BPVC: 2004, Section II, Part D, Appendix 1, the principles of determination of the curves are given, based on 100.000 hours values and multiplier F_{av} of recommended value of 0.67 for temperatures up to 815°C (1500 F). In more details, ASME BPVC: 2004 Section VIII, Division 1 defines the allowable stress as minimum values obtained by:

- 67% of the average value of 100,000-hour creep rupture strength
- 80% of the minimum value of 100,000-hour creep rupture strength
- 100% of the average value of stress that produces a creep rate of 0.01% per 1,000 hours

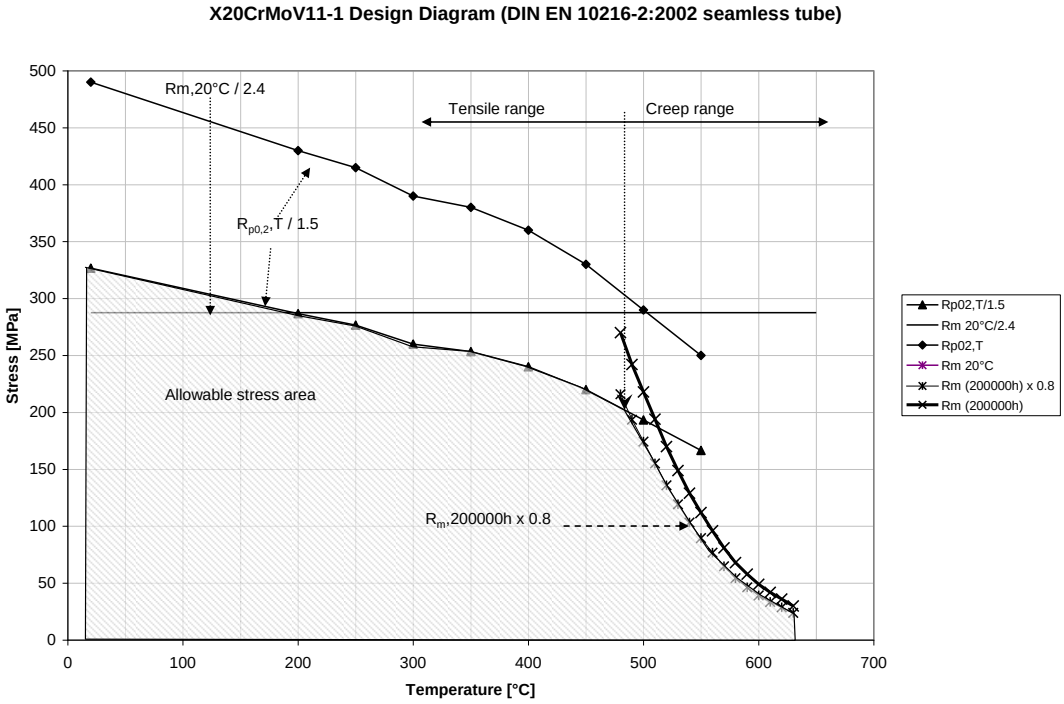

Figure 1: Maximum allowable stress determination for X20CroMoV11-1, according to EN 12952-3:2001, Table 6.3-1, material properties according to EN 10216-2:2002

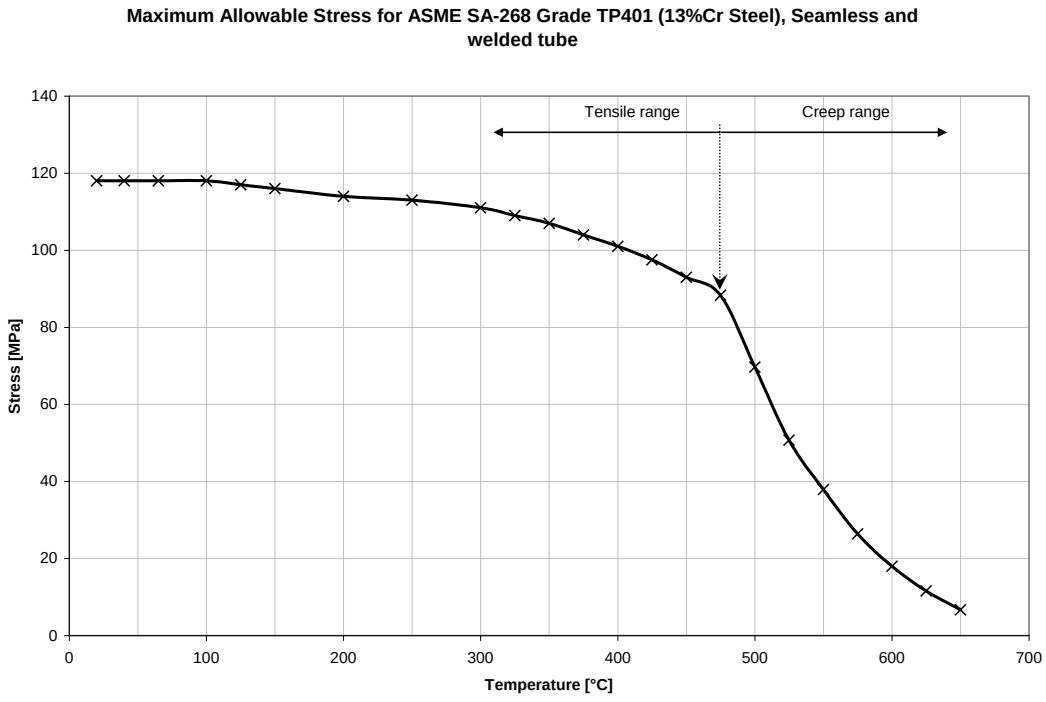

Figure 2: Maximum allowable stresses for SA-268 TP401, according to ASME BPVC: 2004 Section II, Part D (Metric)

For the determination of the minimal wall thickness of components in the creep range, the maximum allowable stress depends on two parameters, namely on de-

sign (operating) temperature and component design lifetime. In the example shown on Figure 1, 200.000 operating hours has been assumed for the component design lifetime; however, for the components that are expected to operate in the creep range for short duration (i.e. less than 10.000 hours), the corresponding $R_{m/t}$, where t=10.000 hours can be used. If the value of temperature and design operating hours lies between two given values in the standard (i.e. in EN 10216-2:2002), linear extrapolation in double logarithmic scale is to be used.

The values for $R_{m/t}$ are obtained by performing creep tests. In those tests, a specimen of the given material is put under constant load, and is kept under constant temperature. During the test, the elongation of the specimen can be measured. Using those values, after subtracting the elastic deformation elongation, the values for creep strain are obtained. Standard methods for creep testing are defined in corresponding standards, i.e. [EN 10291: 2000].

Obtaining the time to rupture is the main purpose of creep tests. Applied temperature, stress in the component as well as the time to rupture are the main parameters used in analysis of creep results for the given material. As with all mechanical tests, the results (in this case time to rupture vs. applied stress) form a scatter of the points that are further analyzed with different numerical methods. All available methods aim to determine the average, middle value for the creep rupture strength – see Figure 3. However, since the scatter band is wide, for the design purposes the 20% lower boundary is used. This is necessary in order to assure that, if the specific heat is used for component construction that corresponds to the minimal requirements for the given materials, the component will not fail.

Technically it is commonly accepted that the scatter band lies in the range of ± 20% around the average rupture strength curve. However, for some materials (as for the X20CrMoV11-1), creep tests are available that show even larger scatter, mainly due to the fact that lot of data comes from the samples and heats that were used for the purpose of the determination of the minimal and maximal chemical composition requirements; thus this data would not qualify under this specification presently (see chapter 1).

As a consequence of the use of 20% lower scatter bound values for the design and remaining life estimation of components, and since the position of the specific heat out of which the component was constructed is not known, the resulting values of the calculations (i.e. for remaining life assessment) could be as much as

300% lower than if it would be known that the components heat lies in the upper part of the scatter band.

There are two possibilities to obtain more precise component life time exhaustion, and those are:

- Construction of heat-specific average creep rupture strength curves
- Determination of the position of the heat-specific curve inside the scatter band using a kind of correlation based on available data for the heat.

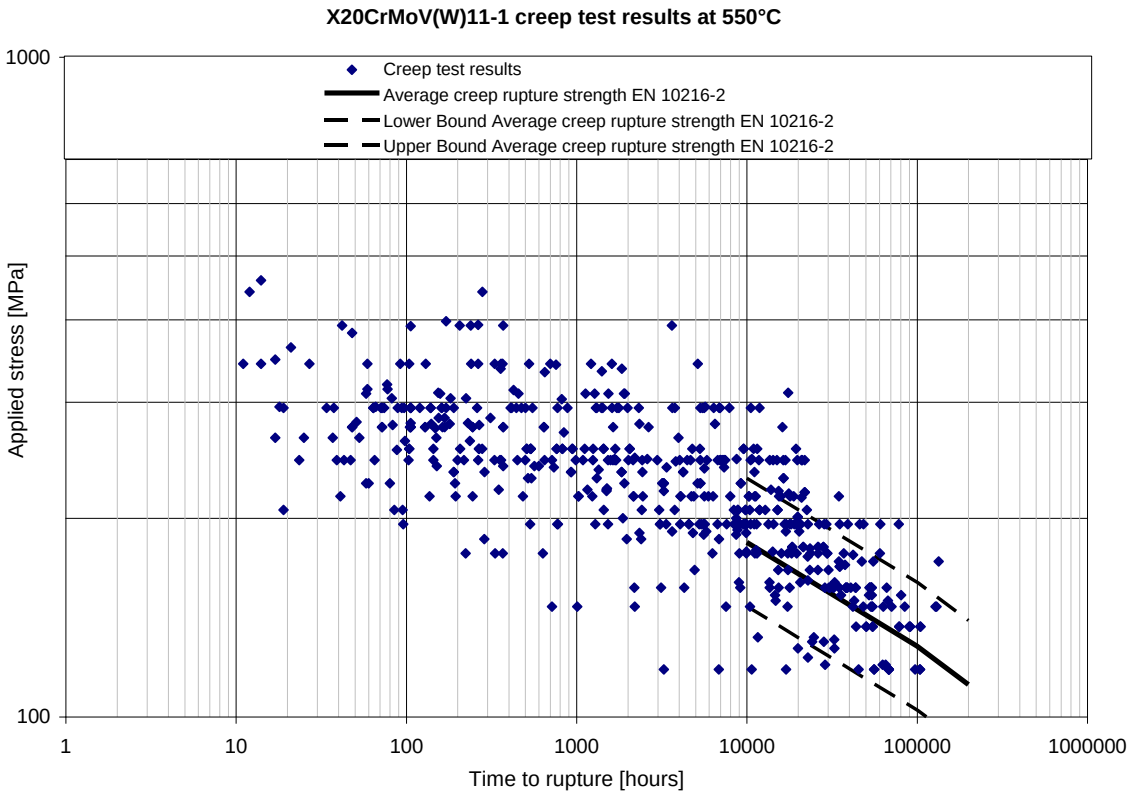

Figure 3: Creep rupture strength at 550°C – results for the material X20CrMoV11-1, (German “Arbeitsgemeinschaft warmfester Stähle“) and average creep rupture strength line according to EN 10216-2:2002

2 Goal of the research

The main cause of the scatter in the creep test results is the micro structural behavior of the material. This includes the influence of the chemical composition, heat treatment, product form and geometry of the components.

The following factors have to be considered for the design of creep experiments to this goal:

- at least 5 tests are needed to be performed for each of the possible combination of parameters, possibly more, possibly performed by more than one testing organization; in order to achieve statistically unbiased results
- the duration of the tests should be representative for the envisaged design life time of the components (typically 100.000 or 200.000 hours); even if the recommendations of the ECCC for the extrapolation are applied (i.e. 3x the real duration of the tests); this means having tests of duration between 1000 and 70.000 hours; this is a lengthy process, as the longest test would take more than 8 years.

If we assume that for the given material (i.e. X20CrMoV11-1) one can vary each of the basic elements in the chemical composition only 10 times (C, Cr, Mo, Ni, V), and only 5 different types of heat treatment and quenching are to be considered, at 3 different temperatures (500, 550 and 600°C), and with 5 different load levels (in order to obtain different time to rupture estimates),further taking into account that each of those has to be repeated at least 5 times, one can come to a number of tests: 10x10x10x10x10x5x5x3x5 = 37.500.000 tests. Even if the requirement to have 5 experiments for each possible case to be tested is abandoned, there are still a staggering number of 7.500.000 tests to be performed.

These numbers of tests are not realistic and never realized; even if the whole capacity of creep testing in the world would have been engaged (estimated at several couple of tens of thousands of testing units), it would take almost a century to fully perform the experiment.

In the practice, the tests are performed on given, existing samples, for the given conditions, and existence of couple of hundreds or even thousands of experi-

mental results are used for qualification of a material for the use in the creep range. Time to market and necessary qualification of the material tends to increase the pressure towards even quicker results, in shorter time.

On the other hand, designers and users of high-temperature components know that the calculated component life-time exhaustion in reality gives only a very rough statement about the component's real damage – i.e. a component that has reached 75% of its life exhaustion (according to the average rupture strength curve x 0.8) at 150.000 hours, can in reality be further exploited from any time between 50.000 and 250.000 (5 to 28 years) further operating hours until it fails due to creep damage.

A more precise prediction of failure due to creep based on component's material properties – i.e. by positioning the heat more precisely in the scatter band would enable users and designers to utilize the resources available, and bring along very tangible economic benefits.

To this goal, the work presented here aims to demonstrate innovative ways of utilization of modern data analysis tools for the purpose of better prediction of time to rupture and position of the specific heat in the scatter band for the given steel. Further on, the influences of different parameters that are known from the material fabrication and utilization experience are once more critically evaluated.

For the demonstration of the modeling using neural networks (NN), material grade X20CrMoV11-1 and its modifications X20 (1.4922), X22 (1.4923) and X21 (1.4926) have been chosen. The modeling has been done using the chemical composition, heat treatment, and annealing, tensile properties at room temperature – in other words, the data required with the new component delivery according to the applicable standards (i.e. EN 10216-2:2002, mandatory and optional tests – Table 13).

3 State of the Art and Alternative Methods

3.1 Deformation and failure in the creep range

If the components are operated in the creep range, the behavior as shown on Figure 4, showing the dependency between plastic creep deformation and damage can be observed [Maile 99].

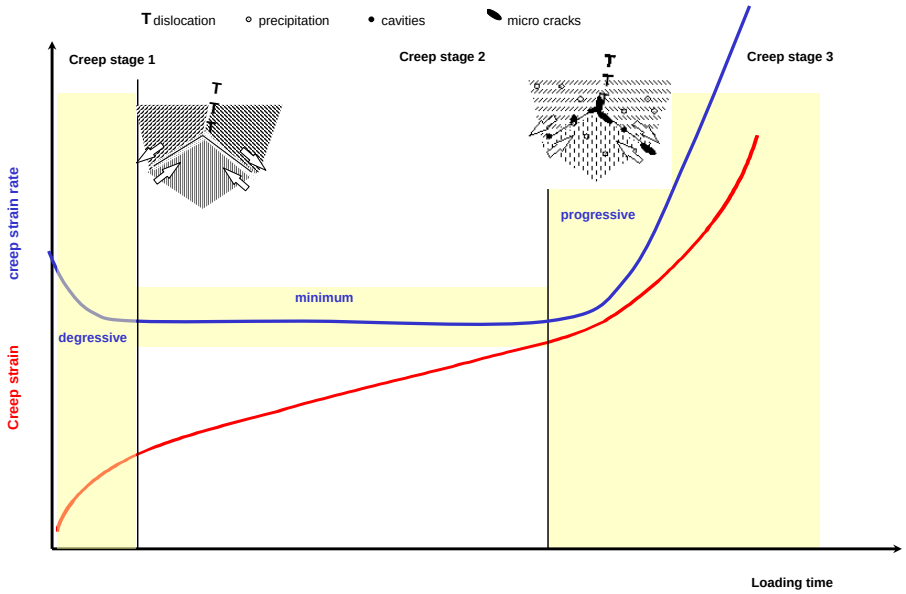

Figure 4: Development of creep strain and creep strain rate over time and schematic illustration of micro structural changes in material

During the phase of primary creep, the creep strain rate decreases, and the main cause of this phenomenon is seen in the increase of density of dislocations in the material. In the phase of secondary creep, a balance of hardening and softening mechanisms is present; therefore the creep strain rate is almost constant. Aside from changes in the micro structure like formation of precipitates, other thermally activated processes in the microstructure can take place like: Pearlite decomposition, coagulation and precipitation of carbides etc. These processes are independent from material, time and temperature. All the changes in the microstructure up to this point are reversible, and their effects can be mitigated trough i.e. heat treatment.

Irreversible creep damage appears in the form of cavities, dependent on material and load (stress, temperature and time). In connection with the metallurgical changes (sub-grain growth, particle coarsening and increase of particle distances),

the creep strain rate increases significantly. As the damage progresses, chains of cavities appear mostly on the grain boundaries, as well as micro cracks. They tend to grow in the direction of load. This phase is known as tertiary creep phase.

The optical-microscope visible damage in the form of creep cavities is dependent on type of material and its microstructure, temperature and load (stress and multi-axiality) [Maile 04]. Multiaxiality of the load reduces the deformability of the material, therefore promoting the cavitations processes.

In the area of high operating hours (> 10^5 h), important for design and use consideration, the creep strength is mostly influenced by thermo dynamical stability of the microstructure and dislocations in the microstructure. This is illustrated on the example of the 12% Cr steels. According to [Schnabel 87], a drop in the creep strength can be seen for the material X19CrMoVNbN11-1 (Cr content 10-11.5%) at 600°C - Figure 5. After having much higher creep rupture property at lower operating hours, after about 10.000 hours it shows a sharp drop towards the values of X20CrMoV11-1. This drop is also visible for 550°C, but at much higher operating hours - Figure 6. The recovery effects, i.e. recrystallization of martensitic laths are considered as primary cause of this drop.

The creep rupture strength of stainless steels depends on precipitates in the matrix. It is well known that creep rupture strength increases with the increase in the amount of precipitated carbides and the precipitation of carbides is promoted by solution treatment at a high temperature, to bring an increasing amount of dissolved carbon. Therefore, solution treatment is generally conducted at temperatures high enough to dissolve carbides in the matrix [MINAMI 87].

The stability of $M_{23}C_6$ particles in relation to the particle size and density creates the conditions for delay in the recrystallization. The hardening of particles composed from $M_{23}C_6$ carbides (Cr), MN nitrides (V, Nb) and Laves Phase (Fe_2(Mo, W)) can be seen as critical for the long-term conservation of creep strength. Further role have the stable nitrides; in the cases when they are dissolved, a drop in creep strength is registered.

Also, Z-Phase, appearing at temperatures ≥600°C can be connected to the decrease of creep strength. Z-Phase, according to [Danielsen 06], has been found in X20-materials after 150.000 hours at 600°C.

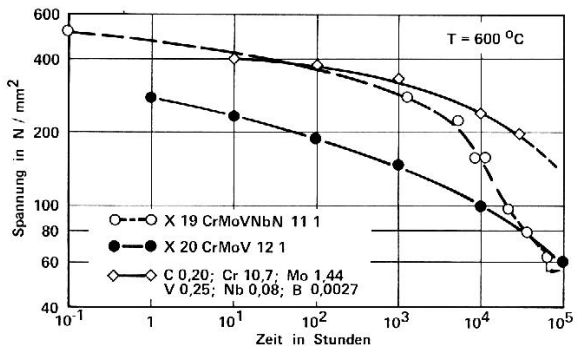

Figure 5: Creep rupture isothermal curves for 12% Cr steels at 600°C [Schnabel 87]

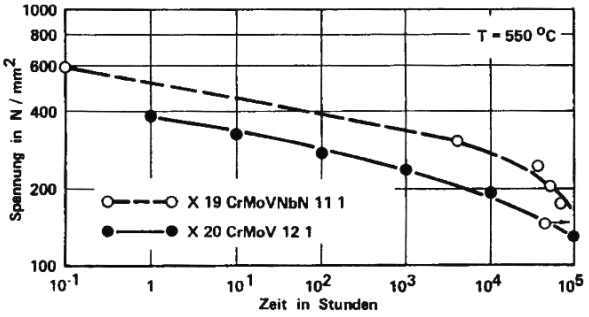

Figure 6: Creep rupture isothermal curves for 12% Cr steels at 550°C [Schnabel 87]

3.2 Evaluation of creep test results – average values, extrapolation

During the creep tests specimens are subjected to static load at constant temperature, with the main goal being to determine the creep strain development in time and time to rupture for the given stress. Smooth surface probes are normally used; notched probes are used to determine the susceptibility of the material to creep notch embrittlement. This susceptibility is present when the time to rupture of a notched specimen is shorter than one of the smooth surface specimen subjected to the same stress. It is to be noted that the nominal stress considered represents the stress determined by the ratio of load and starting cross sectional area of the specimen. The actual stress in the specimen will change/increase during the time as a consequence of specimen elongation, contraction of cross-section, oxidation and internal damage caused by creep cavities.

Creep tests can be performed as uninterrupted and interrupted tests. Uninterrupted tests are performed with measurement of specimen elongation against measurement rod, in other words, the strain is determined during the test out of elastic and plastic deformation of the specimen. Interrupted tests are performed in such a manner that the test is being interrupted in regular intervals and specimen elongation (without load) measured at room temperature. After this, the specimen is again subjected to the same load and kept for further time interval at the (same) test temperature; this is repeated until the break occurs.

Time-rupture curve gives the dependency of creep rupture strength over the time. Creep rupture strength is in the case of creep testing equal to the test stress (as described above), and the time is the time the specimen needed until rupture.

If the plastic creep strain ε_f is plotted against the time until rupture, then the creep-strain curve is obtained. This curve is temperature and material dependent. These curves can be used for determination of stresses needed to achieve, for the given time, the given strain limit (i.e. 1%), in i.e. real component in a power plant. This is shown as an example on Figure 7, for 1%-strain at 100.000 hours.

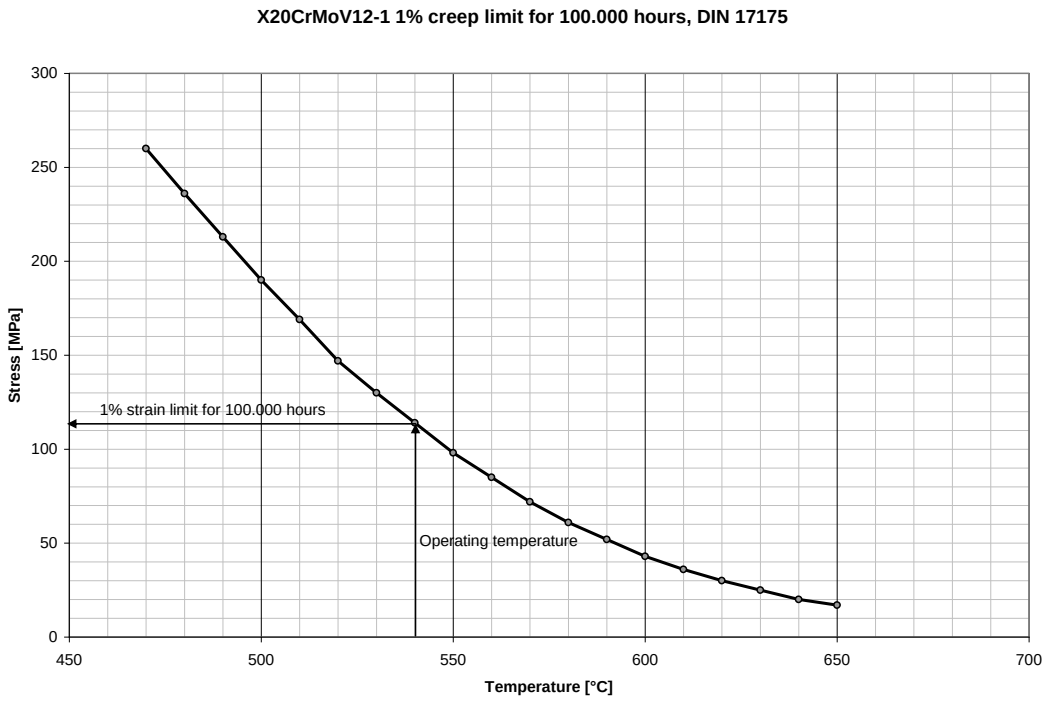

Figure 7: 1% strain creep limit for 100.000 hours, X20CrMoV12-1, DIN 17175

Creep tests are normally performed according to the standard testing procedures, defined in corresponding standards, i.e. EN 10291-2000: Metallic Materials - Uniaxial Creep Testing In Tension - Method of Test, or ASTM E 139 - Standard Test Methods for Conducting Creep, Creep-Rupture, and Stress-Rupture Tests of Metallic Materials, or ISO 204:1997 – Metallic Materials – Uninterrupted uniaxial creep testing in tension – method of test.

Creep tests are characterized by relatively broad scatter, influenced by two main groups of factors:

- Material scatter
- Uncertainties in the test procedure

Uncertainties in the test procedure are the consequence of the uncertainties in the measuring the initial, intermediate and final results of the tests, due to the limitations of the measurement equipment [CEN CWA 15261-3:2005]. These include:

- measurement of initial and subsequent dimensions of the specimen (i.e. tolerance on the measurement of the diameter and length of the specimen),
- load control,
- time to rupture, and
- temperature control.

Material scatter inside one of the steel specification is primarily a consequence of the variations in the properties of the heat (i.e. chemical composition, heat treatment), as well as inhomogeneity of the heat itself. This inhomogeneity is the consequence again of the light differences in the chemical composition and heat treatment. Inside one semi-finished product (i.e. tube), the properties can vary, as effect of the fabrication process, for example, segregation, micro structural changes, temperature variation along the product during the heat-treatment, etc.

According to the standards (i.e. ISO 6303:1981, EN 12952-2:2001, Annex B), a scatter of rupture stress strength of around ±20 % is allowed, see Figure 8. This scatter includes both experimental and material properties scatter.

Figure 8 shows clearly that the nominal scatter of ±20 % has significant influence on the remaining life assessment of the components. For the given stress of 111 MPa, lower-bound curve gives about 80.000 operating hours, the average creep strength curve gives about 200.000 hours, and the upper bound curve yields 400.000 operating hours. Due to the fact that the curve has logarithmic nature and has a slope less than -45°, the smallest change in the stress level yields significant changes in the time to rupture values.

ECCC [ECCC 05] (European Collaborative Creep Committee) has issued, based on the existing national and international standards, recommendations for conducting the creep tests; these recommendations define the basic requirements for conducting the creep tests, all with the goal, among others, to minimize the influence test-related scatter on the results of testing.

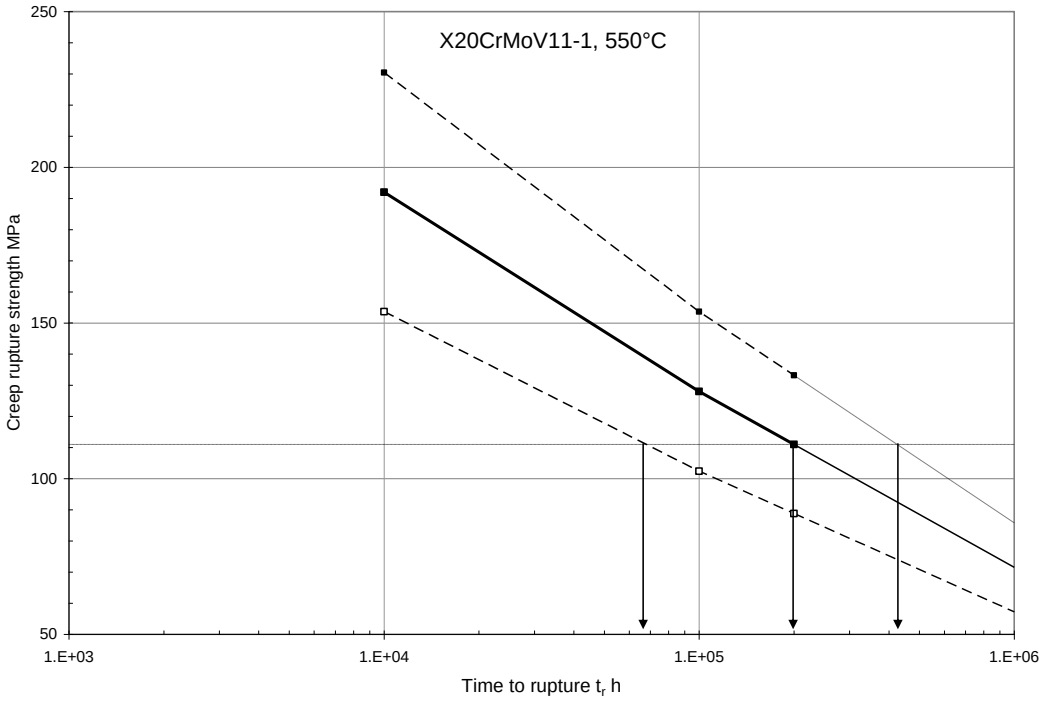

Figure 8: Influence of the scatter band on the remaining life assessment, example X20CrMoV11-1, 550°C, stress level 111 MPa

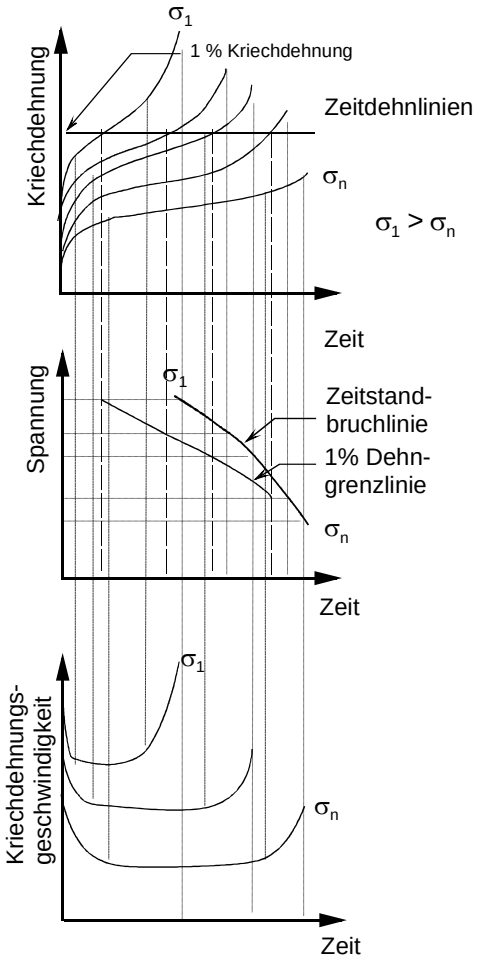

Figure 9: Graphical presentation and evaluation of creep test results

In the process of determination of average creep rupture curves, a combination of mathematical/analytical methods supported by computers and expert/manual opinion has been broadly accepted and proven in Germany. This combination of mathematical/statistical methods and expert advice gives as a rule more reliable long-time creep values as application of pure analytical methods. Analytical methods for determination of the average rupture curves are quite sensitive to the quality and quantity of the results available, whereas the expert opinion can give necessary corrections and advice.

Furthermore, the analytical description of the dependency between temperature, time to rupture and stress requires a commonly accepted, physically and metallurgical based model that does not exist as such, at least not in the commonly accepted form. This is particularly visible in the Figure 10 and Figure 11, where the evaluation of two commonly used steels X10CrMoVNb9-1 and X6CrNi18-11 have been evaluated, using various recommended methods, according to ECCC.

Out of these examples it is visible that, especially in the area of 100.000 hours and more, the models diverge, i.e. scatter in their prediction of the creep behavior. Furthermore, it is clear that some of the curves, in cases of extrapolations outside the area covered by the data points, might result in the unrealistic or physically impossible values.

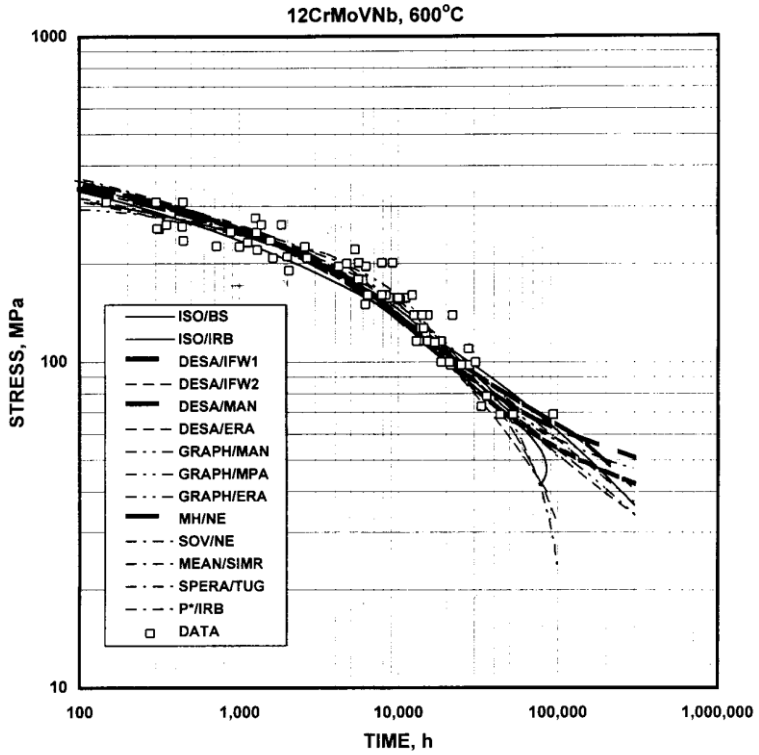

Figure 10: Example of determination of average creep rupture curve based on different analytical methods, material X10CrMoVNb9-1, 600°C, ECCC

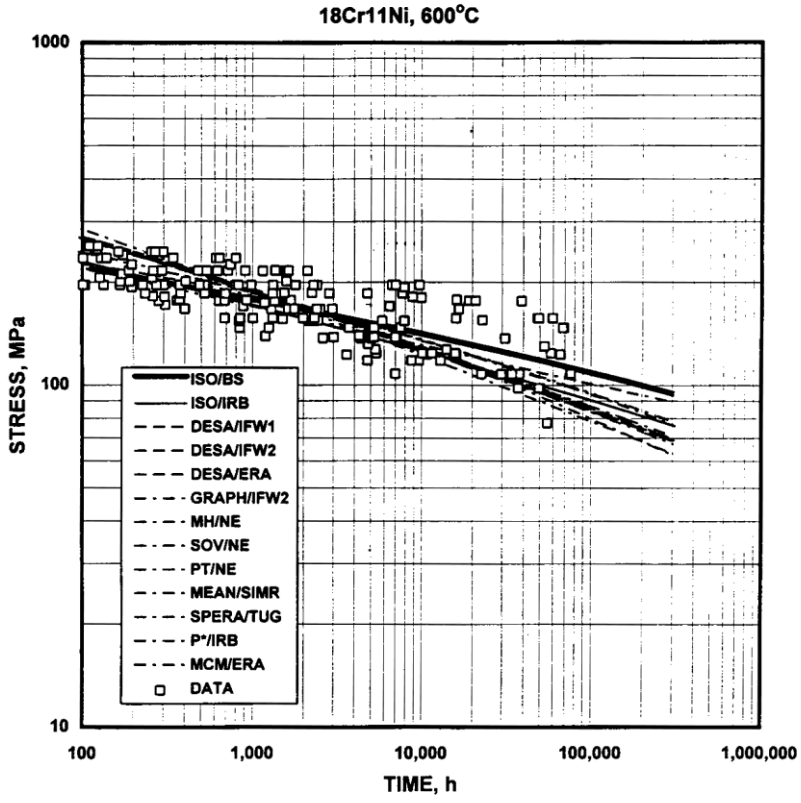

Figure 11: Example of determination of average creep rupture curve based on different analytical methods, material X6CrNi18-11, 600°C, ECCC

3.2.1 Time-Temperature Parameters

One of the common ways to interpret the results of the creep testing for the given material is application of time-temperature parametric equations. The purpose of the time-temperature parameters is to interpret the results of the creep tests with an analytical form in a compact form, allowing interpolation and extrapolation and to provide a simple means of comparing of the behavior of the materials and of rating them in a relative matter [Howard 88]. Time-temperature parameters have physical basis in chemical rate theory based on Arrhenius equation. There are more than 30 existing, proposed equations, and most of them are based on the generalized Mendelson-Roberts-Manson generalized equation [ECCC 05]:

$$P(\sigma) = \frac{\sigma^q (\log t_r - \log t_a)}{(T - T_a)^R},$$

where σ is applied stress [MPa], t_r is time to rupture [hours], T absolute temperature [K] and t_a [hours], T_a [K] are reference time and temperature respectively.

Table 1 gives an overview of some of the time-temperature parametric equations, as well as the parameters to be determined and suggested methods for the determination of them.

Table 1 Overview of the selected time-temperature parameters

Parameter name	Equation(s)	Remarks
Garofalo rupture (modified)	$\log t_r = a_0 + a_1 \log\sigma + a_2\sigma$ $\log t_r = c_0 + c_1 T \log\sigma + c_2 T\sigma + c_3 T\sigma + c_4 T$ where : T - Temperature [K] t_r - time to rupture [hours] σ - stress [MPa]	Parameters to be determined: a_0, a_1, a_2, c_0, c_1, c_2, c_3, c_4 Method: linear regression

Parameter name	Equation(s)	Remarks
Goldhoff-Sherby	$P_{GS} = \frac{\log t_r - \log t_a}{\frac{1}{T} - \frac{1}{T_a}} = f(\sigma)$ $f(\sigma) = \sum_{i=0}^{n} b_i X^i$ where : X - σ or $\log\sigma$ n - polynomial order (3 or 4) T - Temperature [K] t_r - time to rupture[hours] σ - stress [MPa]	Parameters to be determined: t_a, T_a, b_i (i=0-n) Method: linear regression for t_a, T_a by stepwise variation
Larson-Miller	$f(\sigma) = T(C + \log t_r)$ $f(\sigma) = \sum_{i=0}^{n} b_i (\log\sigma)^i$ where : n - polynomial order T - Temperature [K] t_r - time to rupture[hours] σ - stress [MPa]	Parameters to be determined: C, b_i, n Method: linear regression, C optimized for smallest residual sum of squares over time to rupture
Mendelson-Roberts-Manson	$f(\sigma) = \frac{\sigma^q (\log t_r - \log t_a)}{(T - T_a)^R}$ $f(\sigma) = \sum_{i=0}^{n} b_i (\log\sigma)^i$ where : n - polynomial order (usually 5) T - Temperature [K] t_r - time to rupture[hours] σ - stress [MPa]	Parameters to be determined: q, R, T_a, t_a, n, b_i Method: maximum likelihood method with stepwise variation

Parameter name	Equation(s)	Remarks
Manson-Brown	$f(\sigma) = \frac{\log t_r - \log t_a}{(T - T_a)^k}$ $f(\sigma) = \sum_{i=0}^{n} b_i (\log \sigma)^i$ where : n - polynomial order (usually 5) T - Temperature [K] t_r - time to rupture [hours] σ - stress [MPa]	Parameters to be determined: T_a, t_a, k, b_i Method: maximum likelihood method with stepwise variation Special case of Manson equation, where q=0
Manson-Haferd / ISO 6303	$f(\sigma) = \frac{\log t_r - \log t_a}{(T - T_a)}$ $f(\sigma) = \sum_{i=0}^{n} b_i (\log \sigma)^i$ where : n - polynomial order (usually 5) T - Temperature [K] t_r - time to rupture [hours] σ - stress [MPa]	Parameters to be determined: T_a, t_a, b_i Method: linear regression, stepwise variation Special case of Manson-Brown with k=1 Flexible for most engineering alloys, good extrapolation for good source data
Manson-Succop	$f(\sigma) = \log t_r + CT$ $f(\sigma) = \sum_{i=0}^{n} b_i (\log \sigma)^i$ where : n - polynomial order T - Temperature [K] t_r - time to rupture [hours] σ - stress [MPa]	Parameters to be determined: C, b_i, n Method: linear regression, C optimized for smallest residual sum of squares over time to rupture

Parameter name	Equation(s)	Remarks
Monkman-Grant	$\log t_r + m \log \frac{d\varepsilon_m}{dt} = C$ where : t_r - time to rupture[hours] $\frac{d\varepsilon_m}{dt}$ - minimum creep rate [%/h]	Parameters to be determined: m, C Method: linear regression
Norton	$\frac{d\varepsilon_m}{dt} = a\sigma^n$ where : $\frac{d\varepsilon_m}{dt}$ - minimum creep rate [%/h] σ - stress [MPa]	Parameters to be determined: a, n Method: linear regression
Orr-Sherby-Dorn	$f(\sigma) = \log t_r - \frac{Q}{2.303RT}$ $f(\sigma) = \sum_{i=0}^{n} b_i (\log \sigma)^i$ where : n - polynomial order T - Temperature [K] t_r - time to rupture[hours] σ - stress [MPa] $R = 8.317$ [J/mol/K]	Parameters to be determined: Q, b_i, n Method: linear regression, Q optimized for smallest residual sum of squares over time to rupture More conservative than the Larson-Miller model

Parameter name	Equation(s)	Remarks
Soviet algebraic standard method	$\log t_r = a + \sum_{i=1}^{n} b_i (\log T)^i + \sum_{i=1}^{m} c_i (\log \sigma)^i + d\frac{1}{T} + f\frac{\sigma}{T}$ where: n, m - polynomial order T - Temperature [K] t_r - time to rupture [hours] σ - stress [MPa] There are six variations: 1. $n = 1, m = 1,\ b_1 = 2, c_1 = -3$ 2. $n = 1, m = 1,\ b_1 = 2, c_1 = -\frac{2400}{T}$ 3. $n = 1, m = 3, b_1 = 2$ 4. $n = 1, m = 4,\ c_i = \frac{c_i'}{T}$ 5. $n = 5, m = 5$ 6. $n = 6, m = 6, c_i = \frac{c_i'}{T}$	Parameters to be determined: a, b_i, c_i,, d, f Method: linear regression, least squares method
MAN Creep equation	$\log t_r = \frac{\frac{k_2}{\log\left(\frac{\sigma}{k_1}\right)} + k_3}{T} + k_4$ T - Temperature [K] t_r - time to rupture [hours] σ - stress [MPa]	Parameters to be determined: k_1, k_2, k_3, k_4 Method: linear regression
Minimum Commitment Method (MCM)	$\log t_r + A \cdot P(T) \log t_r + P(T) = G(\sigma)$ $P(T) = \frac{R_1}{(T - T_a)} - R_2\left(\frac{1}{T} - \frac{1}{T_a}\right)$ $G(\sigma) = B + C\log\sigma + D\sigma + E\sigma^2$ T - Temperature [K] t_r - time to rupture [hours] σ - stress [MPa]	Parameters to be determined: T_a, A, B, C, D, E, R_1, R_2 Method: linear regression two stages Common form has A=0

Parameter name	Equation(s)	Remarks
SPERA	$t_r = t_0 \cdot F_1(T) \cdot F_2(\sigma)$ $F_1(T) = e^{\frac{Q}{RT}}$ $F_2(\sigma) = \sigma^{B_0} \cdot 10^{(B_1\sigma + B_2\sigma^2)}$ where: T - Temperature [K] t_r - time to rupture [hours] σ - stress [MPa] R = 8.317 [J/mol/K]	Parameters to be determined: t_0, Q, B_0, B_1, B_2 Method: linear regression, optimization over Q
TGL-Time	$\log t_r = T(h \cdot \mathrm{sgn}(k_1)) \cdot \sqrt{h^2 + \frac{(\log\sigma - k_2)}{k_1}}$ $h = \frac{-k_3}{2k_1}$ where: T - Temperature [K] t_r - time to rupture [hours] σ - stress [MPa]	Parameters to be determined: k_1, k_2, k_3, k_4 Method: linear regression, variation over k_4
TGL-Stress	$\log\sigma = b_0 + b_1 P + b_2 P^2$ $P = \frac{T(C_k + \log t_r)}{10000}$ where: T - Temperature [K] t_r - time to rupture [hours] σ - stress [MPa]	Parameters to be determined: b_0, b_1, b_2, C_k Method: linear regression, variation over b

3.3 Methods of assessment of a heat inside the scatter band

3.3.1 Iso-Stress test

Iso-stress test represents a series of creep tests at the same level of stress, but at the much higher temperature points over the design/operating temperature. The goal is the assessment of time to rupture at the levels of stress that are similar to the design/operating stress levels, and then extrapolate them on the temperature axis.

The specimens for iso-stress test are usually made out of the same heat as the real-life component, and are subjected to the same level of stress as the component. Usually, this is done in order to assess the state of the already existing com-

ponent, exposed to service conditions. As the testing on the same operating temperature would lead to the very long test duration (equal or close to the expected life of the component), the temperature is increased, while the stress level is kept constant. As shown on the Figure 12, the values are then extrapolated to the operating temperature. This in turn represents the basis for the assessment of the component condition.

There are few problems that are coupled with the application of this method:

- since the tests are usually of short duration (< 10^4 h), and in cases when material tested was not exposed to service conditions, or very short, the changes in the microstructures that normally do occur in the material in service are not going to develop, and in addition the creep mechanisms will be influenced by the relatively high load; as a consequence, the behavior of the real component will be different than obtained from the test results
- If the test temperatures are too high, being too close to the annealing or phase-change temperature, the material will thermally age or microstructure phase will change. As a result, the usability of the results obtained on the real component will be limited. This is the case when the points do not lie on a straight line in high-temperature region.

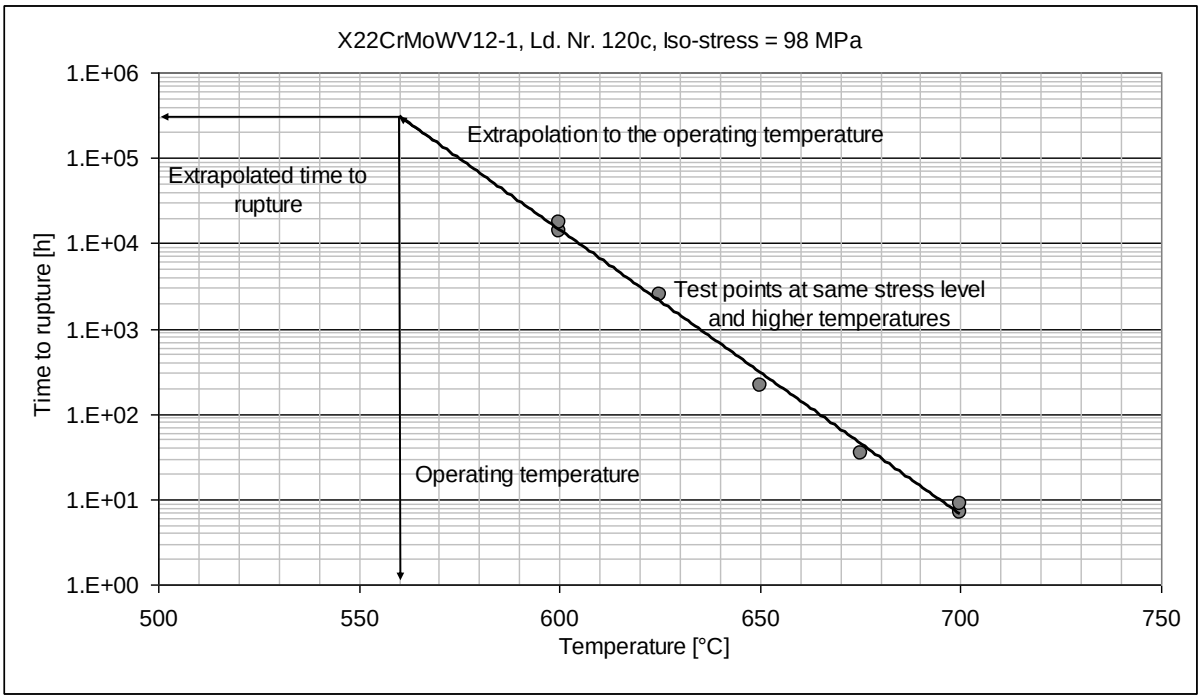

Figure 12: Iso-stress test (example)

3.3.2 Isothermal test

In contrast to the Iso-stress test, isothermal testing is performed at constant temperature. When applying the isothermal method the load is varied, usually being the same as the component that has to be tested - Figure 13. Isothermal test results can be used to reduce uncertainties associated with Iso-stress method. However, the stress levels should be selected in such a way that the test duration expected is representative to the component predicted life duration. If the test duration is too short, the same remark (1) as for the Iso-stress method applies.

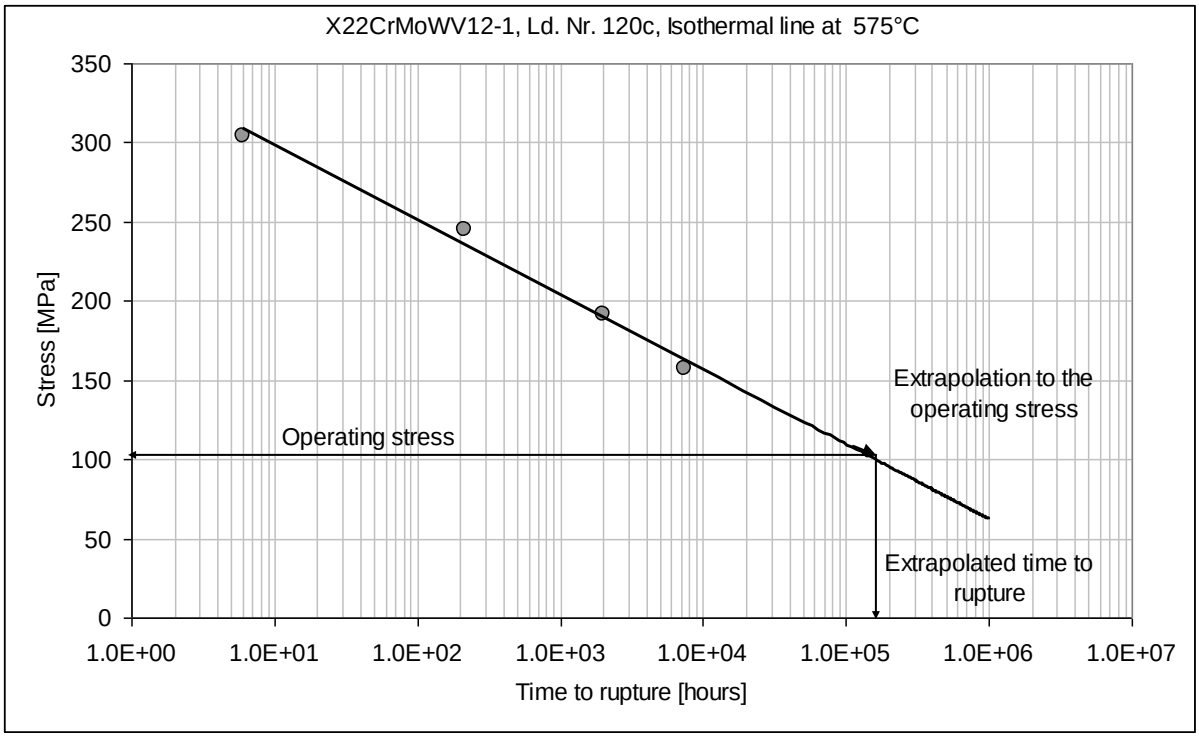

Figure 13: Isothermal method (example)

3.3.3 Z-Factor

The assessment of the dependencies between creep strength and the corresponding parameters can be achieved using the so called Z-Factor ("Z" stands for "Zeitstand" or creep), according to the [Melzer 91, Melzer 92]:

Z = real creep strength / material creep strength (Average standard value – i.e. EN 10216-2:2002)

In the recent research performed in AIF project [AiF 92], for the steel 15CrMoV5-10, the following dependencies between creep strength and parameters have been examined (based on 22 heats, 150 specimens and at 5 test temperatures):

- Destructively measurable: 0,2-%-proof strength at room temperature, tensile strength at room temperature
- Non-destructively measurable: hardness, Microstructure (microstructure classification according to [Schenk 85]), coercitive field strength, remaining magnetic field strength, chemical composition

The corresponding curves showing the dependencies are schematically shown on Figure 14.

It has been shown that if considering each of the elements separately, scatter bands tend to be very wide. Therefore, an average value that connects multiple properties / information about the material or component can be used:

$$Z = \frac{1}{n}\sum_{i=1}^{n} Z_i$$

Z_i –Single dependency factor (i.e. creep strength/hardness)

This simplified approach can be seen as a simple, yet powerful tool for engineers to quantify the state of the components in a power plant; the engineer is in this way in a position to have better overview of the state of the component, and to better plan the inspection intervals, minimizing the effort needed for preparation (i.e. removal of the insulation) and inspection time, and at the same time minimizing the outage time. However, there is still need for work in this area to establish and test Z-Factor curves for each of the material of interest and its parameters.

The main problem of the Z-Factor implementation is that the ratio measured/expected for the creep values is not constant over time and temperature, as discussed in 5.3.

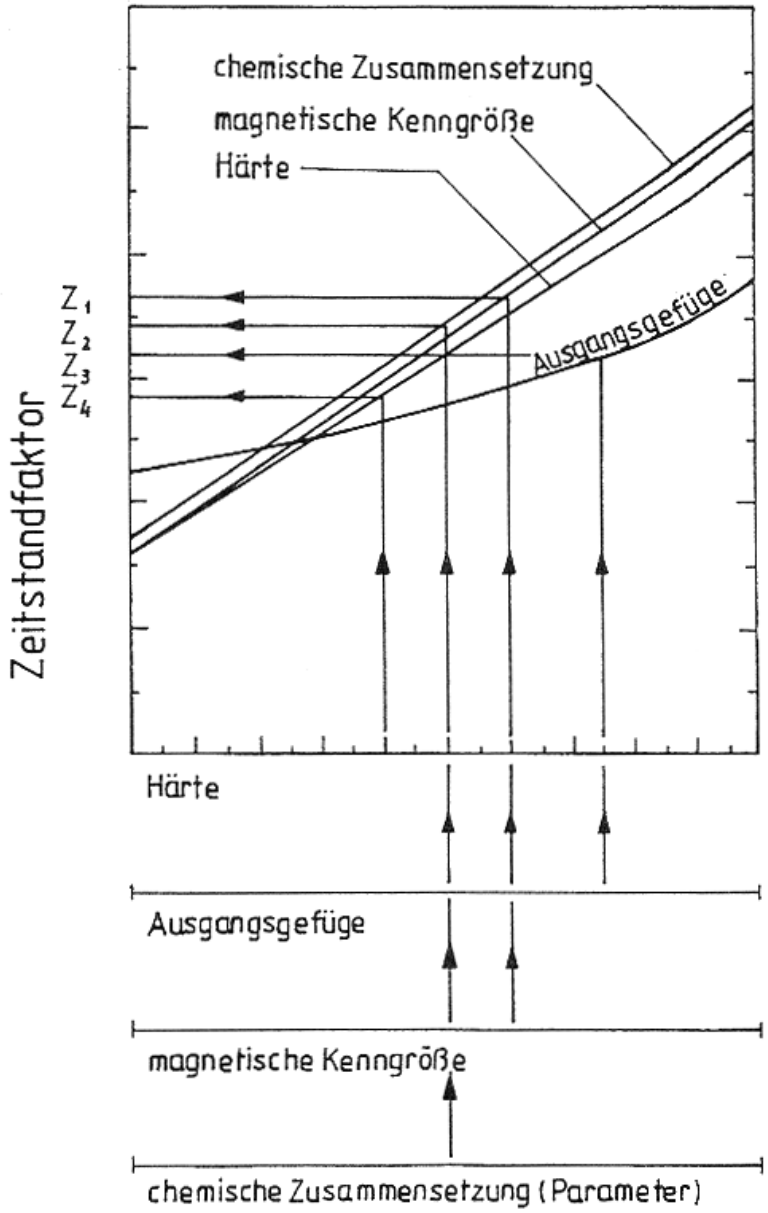

Figure 14: Schematic dependencies of Z-Factor and nondestructively measurable parameters

3.4 Neural Networks[1]

Neural networks are biologically inspired mathematical models. For example, animals are able to react adaptively to changes in their external and internal environment, and they use their nervous system to this goal. Model simulating by its structure the nervous system can be used to mimic this behavior.

[1] This chapter corresponds to the theoretical introduction of the software package DataEngine, MIT GmbH, Aachen, used for practical application in this work.

Nervous system is consisting from neurons and their links (synapses). Therefore, similar structure, consisting of neurons and links between them, as a copy of the nervous system model represents the mathematical copy of the biological nervous system.

The foundation of most of the neural network models are three basic characteristics that lead to three basic concepts of the artificial neural networks [DataEngine 02]:

- Knowledge is distributed over many neurons within the nervous system; this represents the structure of the neuron
- Neurons can communicate with one another using their synapses; this represents the network topology
- Nervous system is adaptable; this represents the adaptation or the learning rule.

3.4.1 Neuron structure

Neurons form the processing units of the neural networks. They consist of four components:

1. a connection function
2. an input function
3. an activation or transfer function, that can have multiple forms:
    - i.e. McCullogh-Pitts model (spike rate model) or linear function represented by the formula f(z) = z
    - sigmoidal function, that has the form $f(z) = \frac{1}{1+e^{=z}}$
    - Gaussian function, in the form $f(z) = e^{-\frac{\|z-w\|}{2a^2}}$,
    - Tanh function, in the form $f(z) = \frac{e^{z} - e^{-z}}{e^{z} + e^{-z}}$
    - Other functions are possible, the only requirement is that a derivative of the function exists; this is important for the backpropagation or any similar learning algorithm.

4. an output function

A typical neuron is schematically presented in Figure 15.

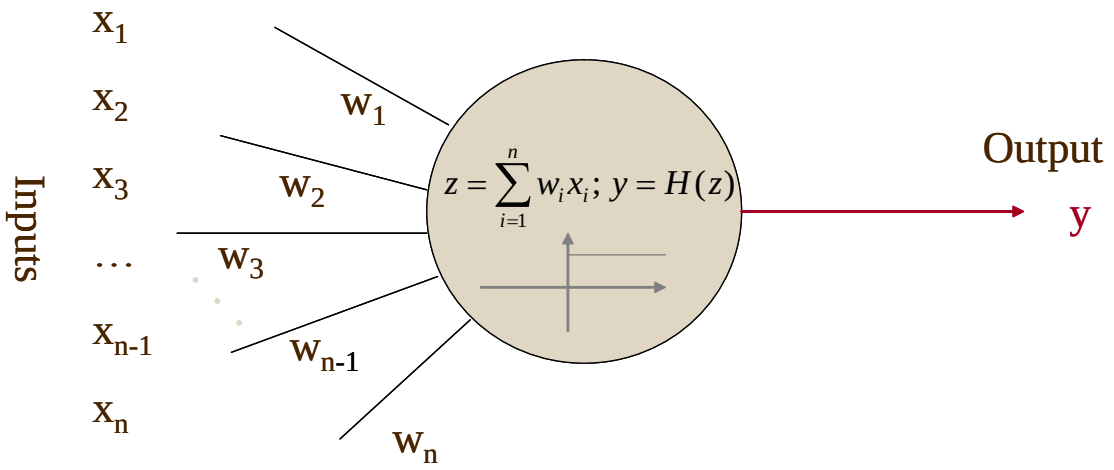

Figure 15: Basic schematic structure of a neuron

A neuron receives signals via several input connections [DataEngine 02]. These are weighted at the input to a neuron by the connection function, and the weights employed define the coupling strength (synapses) of the connections and are established during the learning process, in the course of which they are modified according to given patterns and a learning rule. The input function compresses these weighted inputs into a scalar value, the so-called network activity at this neuron, using usually simple summation. In such cases, the network activity, which results from the connection function and the input function, is the weighted sum of the input values. The transfer function determines a new activation status on the basis of the current network activity, if appropriate taking the previous status of the neuron into account. This new activation status is transmitted to the connecting structure of the network via the output function of the neuron, which is generally a linear function, which is also known as the excitation of the neuron.

3.4.2 Neuronal Network Topology

An artificial neural network is composed of many artificial neurons that are linked together according to specific network architecture. The objective of the neural network is to transform the inputs into meaningful outputs. A layered connecting structure is generally employed, whereby the layer containing input signals is referred to as the input layer; the layer containing outputs is known as the output layer; and the layers located between these are known as hidden layers. The neu-

rons are generally fully connected on a layer-by-layer basis. The number of layers often determines the performance of a network. A distinction can be made between feed-forward, lateral and feedback connections for the method of linking the different layers. Typical schematic representation of the feed-forward topology is shown on Figure 16.

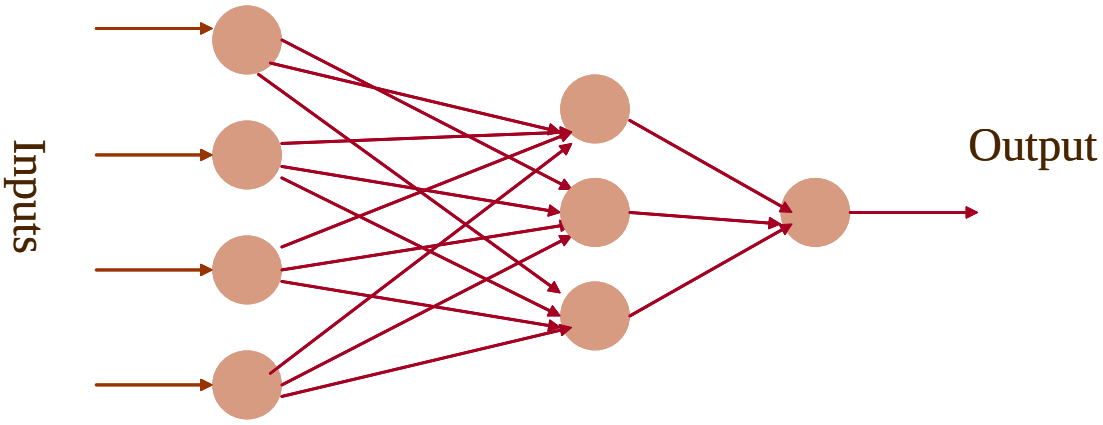

Figure 16: Typical feed-forward neural network topology

3.4.3 Learning or adaptation rules

The connecting structure and the choice of processing units determine the structure of a network. In order to carry out classification, the network must be taught a task by presenting it with examples in a training phase; the knowledge gathered is distributed throughout the network in the connection weights. The weights are adjusted in this phase to fit the problem, using learning rules.

The training phase normally proceeds as follows: random values are initially assigned for the weights of the neurons. Patterns from a training data record are then presented to the network and the weightings are adapted on the basis of the learning rule and training pattern until a convergence criterion, e.g. a defined error threshold, is attained. A test phase is then carried out, in which unknown test patterns are presented to the network to establish the extent to which the network has been trained.

Selection of the patterns for the training phase is a particularly important aspect. These patterns must describe the task as completely as possible, as in later use the network will only be able to provide good results for problems which it has learnt. This means that patterns must be selected which cover all classes and, where possible, describe the boundary ranges between the classes.

The learning processes can be divided into:

- supervised - in addition to the input patterns, the desired corresponding output patterns are also presented to the network in the training phase. The network calculates a current output from the input pattern, and this current output is compared with the desired output. An error signal is obtained from the difference between the generated and the required output. This signal is then employed to modify the weights in accordance with the current learning rule, as a result of which the error signal is reduced. The best-known and most commonly employed network model here is the multilayer perception with back-propagation learning rule
- unsupervised (self-organizing) - the network is required to find classification criteria for the input patterns independently. The network attempts to discover common features among the presented input patterns via a "similarity comparison", and to adapt its weight structure accordingly. The neurons thus form independent pattern classes and become pattern detectors. This method is similar in effect to clustering algorithms or vector quantification methods. An example of this process is provided by Kohonen's self-organizing feature maps, which organize themselves with the aim of converting signal similarity into proximity between excited neurons.
- stochastic strategies - employ random processes and probability distributions to minimize a suitably defined energy function of the network. This process corresponds to that of crystal growth: in order to obtain a crystal with the minimum errors in its lattice structure, it must be cooled very slowly, to ensure that the atoms/molecules have sufficient time to find those positions at which the total energy of the structure becomes minimal. As long as the temperature remains sufficiently high, individual molecules and atoms can change positions, resulting in an increase in the total energy. This may result in departures from local minima. As the temperature falls, the probability of this occurring diminishes. Examples of this process, which by analogy with thermodynamics is also referred to as simulated annealing, are Boltzmann machines.

3.4.4 Network Model

A large number of neural models exist, and each of these models is available in various forms. The network types which are most commonly employed in practice

are multilayer perception with backpropagation learning – for the supervised learning, and Kohonen's self-organizing feature maps - for unsupervised learning. These both models have a long history of successful application for various data behavior modeling, starting from financial, medical sectors towards traffic control and modeling of physical phenomena.

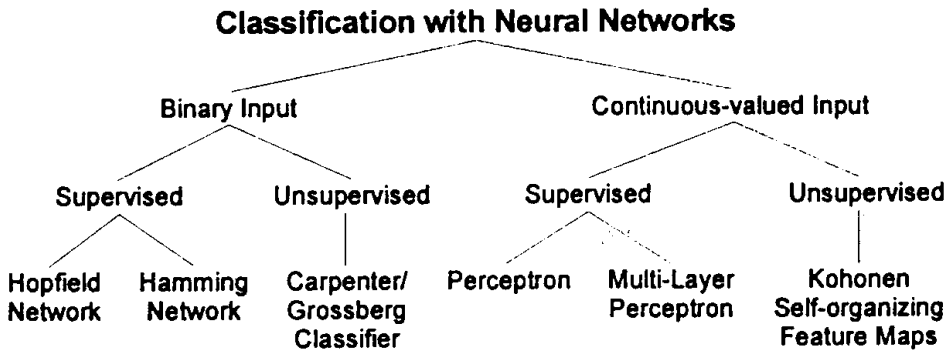

Figure 17: Types of different neural networks [DataEngine 02]

3.4.5 Multilayer Perception (MLP) Network

Multilayer perception is a network model in which the neurons are configured in layers, whereby the neurons of a layer are generally all connected with the neurons of the following layer. As connections exist only from the input layer in the direction of the output layer, this is a feed-forward network. This network is able to process analogue input patterns and learns in supervised mode, employing the back-propagation algorithm (alternatively also quick propagation learning rule), that represents an adaptation rule which is able to generate an error signal for the hidden layers from the error signal at the output layer. The error of the network is defined as the square distance between the required status (stipulated output pattern) and the actual status of the output pattern generated on the basis of current network weights upon definition of an input pattern. This results in an error function which is dependent on the weighting factors via the activation function. Back-propagation can employ different methods, apart from the basic algorithm, such as:

- momentum learning method (taking into account the change of the weight from the previous step and thus strengthening the longer-term trend of the weight-changing process),
- weight-decay (by modifying the cost function of back-propagation, and taking into account change of weights in each of the steps; this prevents crea-

tion of large weights in the network and allows pruning – removal of irrelevant neural connections).

- SuperSAB (using individual learning rates for each of the weights)
- Resilient propagation (operates with an individual weight delta per connection in place of a learning rate).

The performance capability of the MLP network is strongly dependent on the number of hidden layers, as these are responsible for the network's representation capabilities. For modeling complex problems with high need of partitioning of the possible outcome space, at least 1 or 2 hidden layers have to be defined.

3.4.6 Learning Rate

A problem during the training of a MLP is the choice of a suitable learning rate. It is dependent both on the nature of the problem to be examined and on the network's architecture (or design). Two different factors play a determining role in the choice of learning rate. A high learning rate can be chosen so that the neural network learns fast; greater adjustments of the weights leading to a faster convergence. This effect is in general desired, in that the learning process takes place faster. However, when approaching the sought after minimum, large adjustments of the weights are no longer advantageous, the actual minimum only being approached approximately. The optimal values for the weights in this case not being achieved but rather being passed over as a result of too large an adjustment of the weights. A small learning rate is therefore desirable so that the achieved result is as precise as possible.

When using MLP for the approximation of functions it can often be observed that the error, even after a long period of learning, rarely falls below the order of magnitude of the learning rate used. The final result remaining inaccurate, meaning that the neural network has learnt poorly. A method for solving this problem, on many occasions, is by not using a constant learning rate, i.e. high learning rate is chosen at the beginning of the training, and then gradually decreased. There is no universal rule in which way the learning rate should be reduced in order to achieve this desired effect. Another variant for changing the learning rate is the use of a continuously decreasing learning rate. At each step the learning rate is multiplied by a value in the near to, but less than 1.0 (learning decay rate). Repeated multiplica-

tion by decay constant continuously transforms the initial learning rate to an eventual value of 0.0. For values in the near to 1.0, the process corresponds to the learning rate decaying exponentially. A reasonable decay constant for the learning rate has proved to be in the range of 1.0 - 10E-6 = 0.999999 and 1.0 - 10E-9 = 0.999999999. In cases of doubt a decay constant close to one should be chosen.

3.4.7 Setup of MLP

In the case of multilayer perception network, the question of how many neurons should be employed in the hidden layers poses itself. Choosing too few neurons results in the problem not being solved accurately enough. Too many neurons however, have the disadvantage that the desired generalization of the neural network is lost, the networks tending to learn the training examples by heart ("over fitting"). Taken to the extreme, so many weights may be available in the network that every training pattern is represented separately by a weight from the neural network. Indeed the network is able to reproduce the training models exactly, but will produce a considerable error when presented with other data even if only slightly different to the original training data. Too many weights reduce the general applicability of a network.

As a guideline when choosing the network size, one can say that a too big network learns by heart, while smaller networks produce better generalizations.

The network size is in general chosen heuristically, whereby the number of neurons available, or its degree of freedom, is identified with the number of synaptic weights and then set in relation to the number of the training examples. As a rule-of-thumb, the number of examples should be between about two and four times as many as the number of weights in the neural network. Such an approximation can be regarded as being suitable for a number of problems, it cannot though be thought of as universal rule.

3.4.8 Training Procedure

Successful training of a neural network is revealed by the fact that the network is able both to reproduce known data with a minimal error and to classify unknown data (i.e. data not employed in the training phase) correctly. It is thus necessary to interrupt training of the network repeatedly in order to carry out test phases aimed at establishing whether the required accuracy of approximation has been attained.

3.4.9 Data Pre-processing

Neural networks have already been deployed with great success in a diverse range of applications. In some instances, the results obtained have been of surprisingly good quality. Due to the fact that only relatively little preliminary knowledge is required to train a neural network and on account of the black box character, data is often presented to the network without any further processing steps. However, the degree of care which is invested in preparing the data is of decisive importance to the network's learning speed and the quality of approximation attained by the network. Every hour which is invested in preparing the data may save days in training the network.

The first questions to be considered here are of a very general nature:

- Is sufficient data available and does this data contain the correct information?
- Does the available data cover the range of the variables concerned as completely as possible?
- Are there borderline cases which are not covered by the data?
- Does the data contain irrelevant information?
- Are there transformations or combinations of variables (e,g. ratios) which describe the problem more effectively than the individual variables themselves?

3.4.10 Application of neural networks on creep properties of materials

As pointed out by [Badeshia 01], neural networks are seen as feasible tools for modeling of mechanical properties of materials, and, even more, for development and prediction of properties of new alloys. 2 ¼ Cr1Mo steel was investigated, based on chemical composition and heat treatment, as those two groups of elements have greatest influence of the microstructure, and thus on creep properties of a material. The results were presented in [Badeshia 01], Figure 18, where the error bars outside the specified area of 0.1-0.2% C indicate the lack of data.

According to [Badeshia 01], a neural network can be used for modeling of creep behavior of weld metal based on knowledge of creep strength of wrought plates. Figure 19 shows the comparison between modeled and measured creep rupture

strength for welds of NF616 steel [Cole 00] and [Badeshia 01]. The neural network can capture interactions between the inputs because it is nonlinear. It can be interrogated to make predictions and to see how these depend on various combinations of inputs. There is strong fundamental evidence that a well-designed neural network is the best way of extrapolating empirical data. The method should now be more widely exploited in the assessment of creep data [Badeshia 05].

This application has been published and is available mostly for austenitic steels and alloys in the project “Materials Algorithms Project” of Cambridge University (http://www.msm.cam.ac.uk/map/).

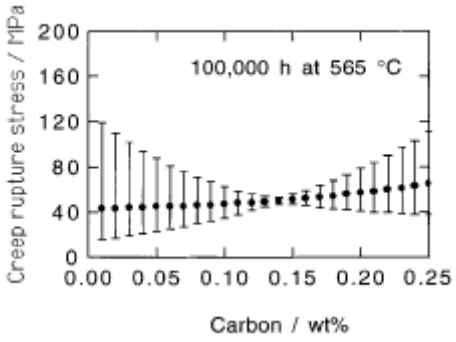

Figure 18: 2¼Cr1Mo steel calculated creep rupture strength at 565 °C, 100 000 h as a function of the carbon concentration [Badeshia 01]

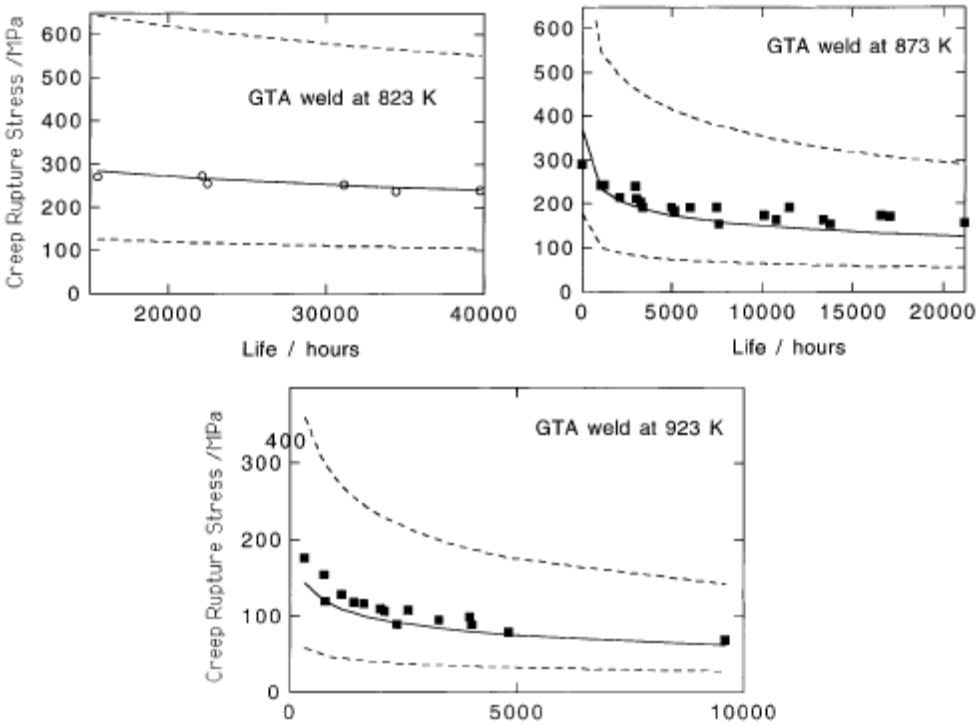

Figure 19: Comparison of calculated and measured creep rupture strength for NF616 type welding alloys [Badeshia 01]

In regards of application of data mining techniques and use of fuzzy clustering method of creep test data, the work was performed by [Jovanovic 99] and shown in the final report of the UNCERT project (Project reference SMT4-CT97-2165). Further, in the same work, the path has been identified for prediction of missing data in creep test data processing using neural networks.

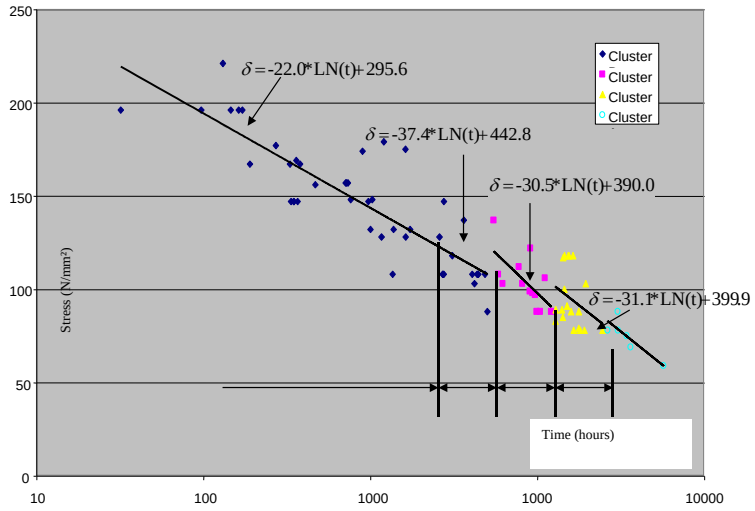

Figure 20 Statistical analysis on clusters identified by DataEngine for 2.25 CrMo1Mo specimens [Jovanovic 99]

Work from [Stackeljan 96] gives a procedure for selection of minimum of features required for the network prediction of the experiment outcome. The described method identifies the procedure for the selection of the optimal minimum of the features for the neural network training and implementation. In the same work the both classical and evolutionary methods for feature selection are described.

4 Modeling of Creep Strength Behavior of 9-12% Cr Steels and Model Material X20CrMoV11-1 Using Neural Networks

4.1 Introduction

The main goal of this work is to demonstrate the feasibility of the application of the modern data mining and neural network methods on the 9-12% Cr steels to the prediction of long-term creep behavior of steels. To this purpose, the model steel X20 CrMoV 11-1 has been selected, due to the fact that broad database of test results has been available; furthermore, due to the long history of application of the material, the variation of the chemical composition and heat treatment is much greater than for other materials in the class, like P91, P92, E911 and others. This represents a good input for a neural network, since it can obtain more information about particular parameter influence coming outside of the current specification. On the other hand, this specification does not contain the microelements like Nb, B, Co that are crucial for the development of new materials. Therefore, further work in this area focusing on the influence of the new parameters is recommended.

The adopted specification of the X20CrMoV 11-1are defined [EN 10216-2:2002] as:

- Cast analysis – chemical composition (C, Si, Mn, P, S, Cr, Mo, Ni, (Al), Cu, Nb, V, W) – Table 2 of EN 10216-2:2002
- Heat-treatment specification (requirement 7.3.3 of EN 10216-2:2002) – austenizing temperature, austenizing cooling medium, tempering temperature, tempering cooling medium
- Tensile test at room temperature – proof stress $R_{p0,2}$, tensile strength R_m, rupture elongation A_{min} longitudinal and transversal - according to Table 4: Mechanical properties of EN 10216-2:2002

The use of each of the inputs as listed above has been separately investigated in the literature, but a strong correlation between each of the inputs and resulting creep strength has not been found. Yet, combination of all those influence factors does correlate to the creep strength, as it is known from the production and service experience. Therefore, models using neural networks had to be investigated and the results of this work are presented here.

4.2 9-12%Cr Steels

In the 80s and 90s of the previous century, a new generation of ferritic-martensitic steels with 9-12% Cr have been developed. They represent an alternative to the use of austenitic materials for high temperature, high pressure boilers and boiler component parts. The addition of the microelements (N, Nb, B) as well as addition of the W has resulted in the significant increase in the creep resistant properties of the new materials, and significant reduction of required wall thickness of the components (Figure 21) [Melzer 03]. Further work is still in the progress, and it is to be expected that the new steels of this specification will be developed that have up to 180 MPa creep strength values for 600°C and 100.000 hours of operation.

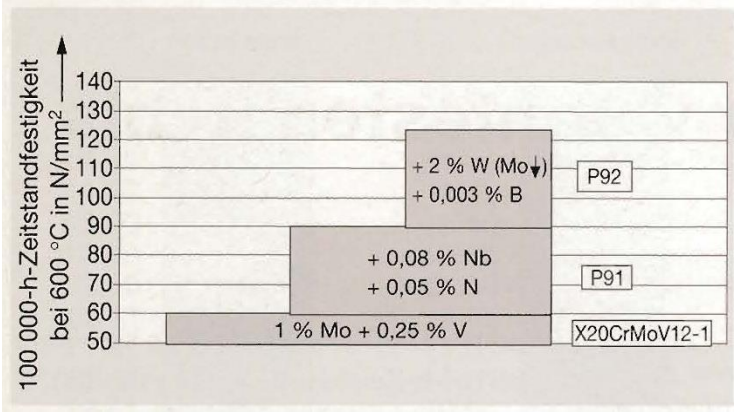

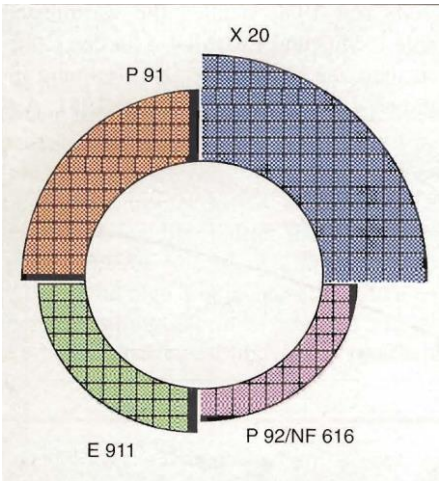

Figure 21: Creep strength and wall thickness change for different 9-12%Cr steels [Melzer 03]

4.3 Model material X20CrMoV11-1

X20CrMoV11-1 has been widely used for tubing, headers and piping in Europe. The steel was developed in 1960s together with a modification for bars and forgings with an increased C-content (0.20 – 0.26 %) - X22CrMoV12-1 as well as a modification with an additive of W - X22CrMoWV12-1, X20CrMoWV12-1. It has been developed out of stainless martensitic steel with 13% Chromium content [Jesper 85].

During the 50s, the 13% Chromium steels were used primarily for turbine parts, mostly due to the poor weld ability of these steels. As, in mid 50s, the welding problems have been solved, these steels became more used in the power plant boiler and piping area, mostly due to stable long-term creep properties. After the mid-90s, this steel is being replaced with 9-12% Cr steels, as the operating temperature of the new power plants increased. The maximum long term service temperature for tubes and pipes of X20CrMoV11-1 is generally limited to 565 °C.

X20CrMoV11-1 steel was specified under designation X20CrMoV12-1 in DIN 17175, as well as in the ISO 9329-2 under designation X20CrMoNiV11-1-1 whereas in the British standard it is known as ST762. ISO designation for forging specification was F40, and for cast specifications C40H (ISO 4991 - Steel Castings for Pressure Purposes).

In the new, harmonized EU standardization it became the current designation X20CrMoV11-1, and it is also identified by the Material number 1.4922. ASME and ASTM never adopted this steel in their specification. Therefore, it is primarily used in European power plants, but has been in put in exploitation on all continents [Kalwa 85]. Even more, some national regulations also adopted this material – for example, Indian Boiler Regulation endorses this material (Regulation 48, 53b, etc.).

Until 1984, more than 100,000 metric tons of X20 tube and pipe had been supplied by Mannesmann alone [Kalwa 85]. The cumulative operating time with the material steel had been more than 4 million hours up to this year [Kalwa 85]. It might be considered that this number of operating hours has more than doubled in the last 25 years.

4.3.1 Classification

X20CrMoV11-1 is a stainless tempering steel. It has three distinct specifications – i.e. one specification for seamless steel tubes, steel forgings and rolled or forged bars and steel castings [EN 10213-2:1995]. The latest one is not considered in this work.

X20CrMoV11-1 belongs to, according to [IS0 15608: 2000], group 6 – high vanadium alloyed Cr-Mo-(Ni) steels, and it is classified under subgroup 6.4 – Steels with 7.0%<Cr≤12,5%, 0,7% < Mo ≤ 1,2% and V ≤ 0,35%

4.3.2 Chemical composition

X20CrMoV11-1 and its modifications have the chemical composition according to different standards as given in the Table 2. Due to the high Cr- and Mo-content X20CrMoV11-1 steel shows a distinctive martensitic microstructure, which permits its use as thick pipe material.

Table 2: Chemical requirements for X20CrMoV11-1 and its modifications according to different standard specifications

Standard	Designation / steel number	Chemical composition , %											
		C	Si	Mn	P	S	Cr	Mo	Ni	V	Al	Cu	W
EN 10216-2:2002	X20CrMoV11-1 (1.4922)	0.17 0.23	0.15 0.50	≤1.00	≤0.025	≤0.020	10 12.50	0.8 1.20	0.30 0.80	0.25 0.35	≤0.40	≤0.30	
ISO 9329-2: 1997	X20CrMoNiV11-1-1	0.17 0.23	0.15 0.50	≤1.00	≤0.030	≤ 0.030	10.00 12.50	0.80 1.20	0.30 0.80	0.25 0.35	≤0.02	≤0.25	
DIN 17175	X20CrMoV12-1 (1.4922)	0.17 0.23	≤0.50	≤1.00	≤0.030	≤0.030	10.00 12.50	0.80 1.20	0.30 0.80	0.25 0.35			
IISO 9327-2: 1999	X20CrMoV12-1	0.17 0.23	≤0.40	0.30 1.00	≤ 0.035	≤0.030	10.00 12.50	0.80 1.20	0.30 0.80	0.25 0.35	≤0.025		
EN 10222-2: 2000	X20CrMoV11-1 (1.4922)	0.17 0.23	≤0.40	0.30 1.00	≤0.025	≤0.015	10 12.50	0.8 1.20	0.30 0.80	0.25 0.35			
EN 10302: 2002	X20CrMoV11-1 (1.4922)	0.17 0.23	≤0.50	≤1.00	≤0.030	≤0.030	10 12.50	0.8 1.20	0.30 0.80	0.25 0.35			
EN 10302: 2002	X22CrMoV12-1 (1.4923)	0.18 0.24	≤0.50	0.40 0.90	≤0.025	≤0.015	11 12.50	0.8 1.20	0.30 0.80	0.25 0.35			
EN 10302: 2002	X20CrMoWV12-1 (1.4935)	0.17 0.24	0.10 0.50	0.30 0.80	≤0.025	≤0.015	11 12.50	0.8 1.20	0.30 0.80	0.20 0.35			0.4 0.6
EN 10088: 2005	X20CrMoV11-1 (1.4922)	0.17 0.23	≤0.40	0.30 1.00	≤0.025	≤0.015	10 12.50	0.8 1.20	0.30 0.80	0.25 0.35			

Standard	Designation / steel number	Chemical composition , %											
		C	Si	Mn	P	S	Cr	Mo	Ni	V	Al	Cu	W
EN 10088: 2005	X22CrMoV12-1 (1.4923)	0.18 0.24	≤0.50	0.40 0.90	≤0.025	≤0.015	11 12.50	0.8 1.20	0.30 0.80	0.25 0.35			
EN 10088: 2005	X20CrMoWV12-1 (1.4935)	0.17 0.24	0.10 0.50	0.30 0.80	≤0.025	≤0.015	11 12.50	0.8 1.20	0.30 0.80	0.20 0.35			0.4 0.6
EN 10269: 1999	X22CrMoV12-1 (1.4923)	0.18 0.24	≤0.50	0.40 0.90	≤0.025	≤0.015	11 12.50	0.8 1.20	0.30 0.80	0.25 0.35			

4.3.3 Heat treatment

Heat treatment is very important for X20CrMoV11-1, and the influence of the heat-treatment on the mechanical properties of the steel is discussed later in 4.4.1.

The purpose of the heat-treatment is to achieve the austenitization of the metallographic structure of the material, and if the standard cooling down in air up to room temperature is applied a residual austenite content of approximately 2 – 5 % could be stated, influenced by the specific chemical composition of the heat. A change in the standardized heat treatment conditions leads to modifications in the microstructure and thus to a decrease of the long term creep strength.

The steel may be welded if the relevant measures required for the material are fulfilled. Specific care is required in welding: correct pre and post weld heat treatment should be done in order to avoid cracking. Pre heating up to 450°C is necessary in dependence of thickness. After welding an intermediate cooling down below 130°C should be performed in order to optimize the martensite formation in the deposit material (if similar to X20CrMoV12-1) and heat affected zone. Post heat treatment should be done at a temperature ranging from 750°C and 770°C.

The different heat-treatment requirements are shown in the Table 3.

Table 3: Heat treatment of X20CrMoV12-1 according to different standards

Standard	Designation/ steel number	Austenizing temperature / cooling medium, °C	Tempering temperature / cooling medium, °C	Additional remarks
EN 10216-2:2002	X20CrMoV11-1 (1.4922)	1020-1080/air	730-780/air	For cases when wall thickness above 25 mm or T/D > 0.15 it might be necessary to apply quenching and tempering; steel tubes treated in such a way shall be designated by the steel name supplemented by the symbol “+QT”

Standard	Designation/ steel number	Austenizing temperature / cooling medium, °C	Tempering temperature / cooling medium, °C	Additional remarks
ISO 9329-2: 1997	X20 CrMoNiV 11-1-1	1020-1080/air	730-780/air	
DIN 17175	X20CrMoV12-1 (1.4922)	1020-1070/air	730-780/air	
ISO 9327-2: 1999	X20CrMoV12-1	1020-1070/air, oil, water	730-780	
EN 10222-2: 2000	X20CrMoV11-1 (1.4922)	1020-1070/air, oil	730-780/air, furnace	
EN 10302: 2002	X20CrMoV11-1 (1.4922)	1020-1070/air, oil	720-780/min. 2h	+QT
EN 10302: 2002	X22CrMoV12-1 (1.4923)	1020-1070/air, oil		+QT (d ≤ 250)
EN 10302: 2002	X20CrMoWV12-1 (1.4935)	1020-1070/air, oil 1020-1070/air, oil	720-780/min. 2h 680-740/min. 2h	+QT 700 +QT 800
EN 10269: 1999	X22CrMoV12-1 (1.4923)	1020-1070/air, oil, water 1020-1070/air, oil, water	680-740/min 2h 660-720/min 2h	+QT1 +QT2

4.3.4 Mechanical properties (requirements) at room temperature

Table 4 gives the overview of different mechanical properties requirements at room (ambient) temperature. This particular steel has more heat treatment requirements and product forms, and mechanical properties vary with those requirements.

Table 4: Mechanical properties requirements according to different standards and specifications at room (ambient) temperature

Standard	Designation / steel number	Wall thickness T_{min} / Other condition	R_{p02}/R_{eH}, MPa	Tensile Strength R_m, MPa	Rupture elongation A_{min} %	
					Longitudinal	Transversal
EN 10216-2:2002	X20CrMoV11-1 (1.4922)	For all specified 0-100	490	690-840	17	14
ISO 9329-2: 1997	X20 CrMoNiV 11-1-1	For all specified 0-60	490	690-840	17	14
DIN 17175	X20CrMoV12-1 (1.4922)	For all specified 0-60	490	690-840	17	14
IISO 9327-2: 1999	X20CrMoV12-1	≤ 200 200 < T_{min} ≤ 300	500 (R_{eH}) 500 (R_{eH})	700-850 700-850	16 14	14 14
EN 10222-2: 2000	X20CrMoV11-1 (1.4922)	For all specified 0-330	500	700-850	16	14
EN 10302: 2002	X20CrMoV11-1 (1.4922)		500	700-850	16	
EN 10302: 2002	X22CrMoV12-1 (1.4923)	≤ 160	600	700-850	14	
EN 10302: 2002	X20CrMoWV12-1 (1.4935)	+ QT 700 +QT800	500 600	700-850 800-950	16 16	

Standard	Designation / steel number	Wall thickness T_{min} / Other condition	R_{p02}/R_{eH}, MPa	Tensile Strength R_m, MPa	Rupture elongation A_{min} %	
					Longi-tudinal	Trans-versal
EN 10269: 1999	X22CrMoV12-1 (1.4923)	+QT1 ≤ 160 mm +QT2 ≤ 160 mm	600 700	800-950 900-1050	14 11	

4.3.5 Minimum 0,2%-proof strength values at elevated temperatures

The overview of minimum 0,2%-proof strength values requirements according to different standards and specifications is given in the Table 5. From the table it is obvious that values according to EN 10216-2:2002, DIN 17175, EN 10222-2: 2000 and EN 10302: 2002 (X20+QT700) are essentially the same. Also, values given for EN 10302: 2002 (X22) EN 10302: 2002 (X20+QT800) and EN 10269: 1999 (X22+QT1) are also identical. Hence, on the Figure 5 only 5 distinct lines are visible.

It is to note that different heating treatments give (i.e. additional quenching and tempering for X20 and X22 specifications) much higher mechanical properties as for the basic specification (i.e. X20 according to EN 10216-2:2002). This is even more visible on the Figure 22, where it is obvious that most of the standard specifications are positioned at the middle thick line. The relatively visible difference between ISO and EN curves can be explained by use of ISO2605-1: 1976 or ISO2605-2: 1976 (both now withdrawn) standard for estimation of tensile properties at elevated temperatures, whereas the EN curves indicate application of ISO2605-3: 1985 (since 2003 in modified form as EN 10314: 2002) standard that yields less conservative values of $R_{p0,2}$ at elevated temperatures [RDC].

Table 5: Minimum 0,2%-proof strength values at elevated temperatures

Temp. [°C]	X20CrMoV11-1 (EN 10216-2:2002)	X20 CrMoNiV11-1-1 (ISO 9329-2)	X20CrMoV12-1 (DIN 17175)	X20CrMoV12-1 (ISO 9327-2)	X20CrMoV11-1 (EN 10222-2)	X20CrMoV11-1 (EN 10302)	X22CrMoV12-1 (EN 10302)	X20CrMoWV12-1 +QT700 (EN 10302)	X20CrMoWV12-1 +QT800 (EN 10302)	X22CrMoV12-1 +QT1 (EN 10269)	X22CrMoV12-1 +QT2 (EN 10269)
	R_{p02} [MPa]										
50						465	585	465	585	585	681
100					460	460	560	460	560	560	650
150				390	445	445	545	445	545	545	625
200	430	349	430	362	430	430	530	430	530	530	600
250	415	328	415	340	415	415	505	415	505	505	575

Temp. [°C]	X20CrMoV11-1 (EN 10216-2:2002)	X20 CrMoNiV11-1-1 (ISO 9329-2)	X20CrMoV12-1 (DIN 17175)	X20CrMoV12-1 (ISO 9327-2)	X20CrMoV11-1 (EN 10222-2)	X20CrMoV11-1 (EN 10302)	X22CrMoV12-1 (EN 10302)	X20CrMoWV12-1 +QT700 (EN 10302)	X20CrMoWV12-1 +QT800 (EN 10302)	X22CrMoV12-1 +QT1 (EN 10269)	X22CrMoV12-1 +QT2 (EN 10269)
	R_{p02} [MPa]										
300	390	317	390	328	390	390	480	390	480	480	550
350	380	310	380	322	380	380	450	380	450	450	518
400	360	305	360	316	360	360	420	360	420	420	485
450	330	292	330	302	330	330	380	330	380	380	440
500	290	272	290	280	290	290	335	290	335	335	390
550	250		250		250	250	280	250	280	280	330

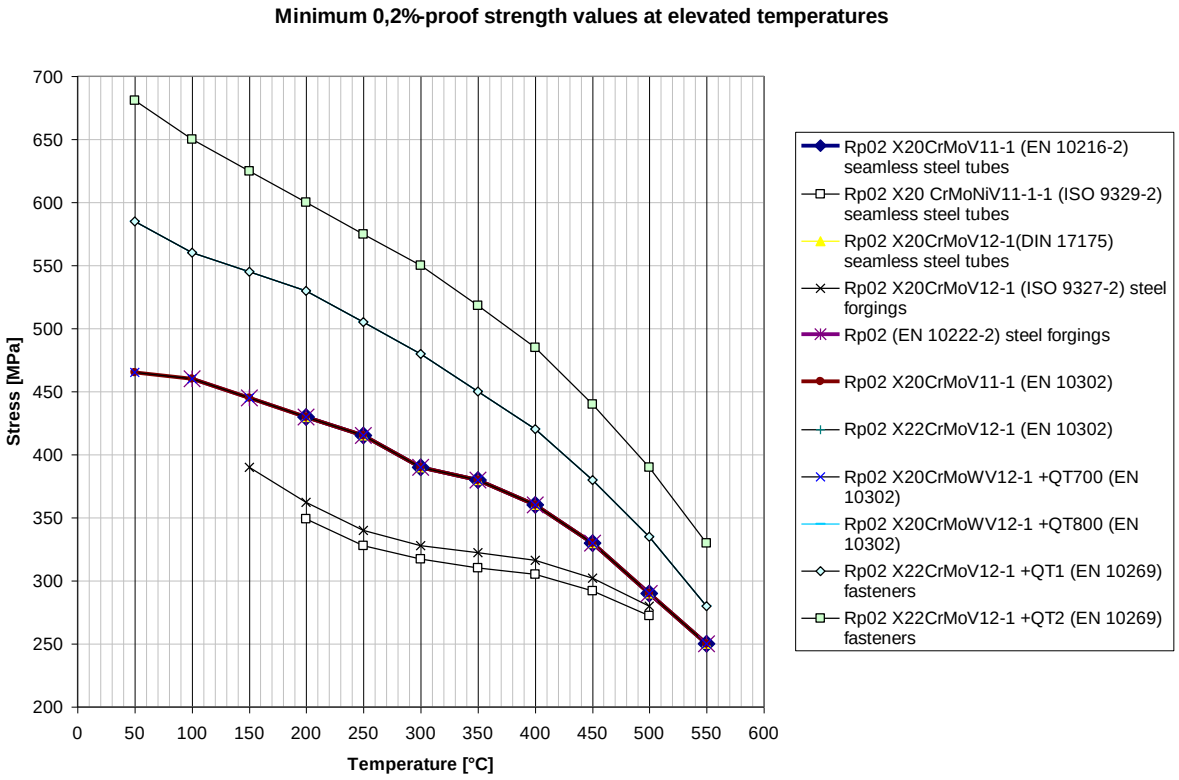

Figure 22: Minimum 0,2%-proof strength values at elevated temperatures, different standards and specifications[2]

[2] Please note: values between some specifications differ in few points, hence the lines on the graph do overlap

4.3.6 Creep rupture strength values

An overview of creep rupture strength values is given in

Table 7. A graphical comparison of values is shown on Figure 23, where it is clearly visible that the grade X20CrMoWV12-1 has better creep properties as the basic X20 specification at lower temperatures, whereas this difference disappears at temperatures higher than 550°C. Also, comparing the tables of data for similar specification, it can be noted that in the later specifications (i.e. EN 10216-2:2002), the values for lowest temperature are starting from 480°C, whereas in the older specifications (i.e. DIN 17175), the lowest temperature given is at 470°C. As when comparing with the diagram of maximum allowable stresses (Figure 1), the temperature of 470°C falls into the area that is dominated by the time independent tensile strength. Further, the values between two main specifications (EN 10216-2:2002 and DIN 17175) differ at most at most about 8-10 MPa (in the low-temperature area, i.e. about 480-500°C), and for 200.000 hours EN 10216-2:2002 gives slightly better values for the temperatures above 580°C. Since these values are outside normal operating conditions for this material (about max. 550°C), these differences have very little practical impact. For the purpose of the further work, the values given in EN 10216-2:2002 are used, since they are also referenced in the EN 12952-2:2001 as required values.

The values in

Table 7 show that for forging EN standards generally supply only the values up to 100.000 hours, whereas ISO specification goes up to 250.000 hours. The values for all EN specifications are identical, i.e. there was no correction in this area as it is the case with seamless pipe specification. Also to be noted is that EN-values are, especially in lower temperature, much higher than ISO-values (difference of about 30-40 MPa), whereas around 550°C (temperature of normal operation of this material) the difference is minimal, and EN values are slightly lower than ISO values.

Important to note is also that generally the curve for forgings has different slope than the curve for seamless pipes (Figure 23).

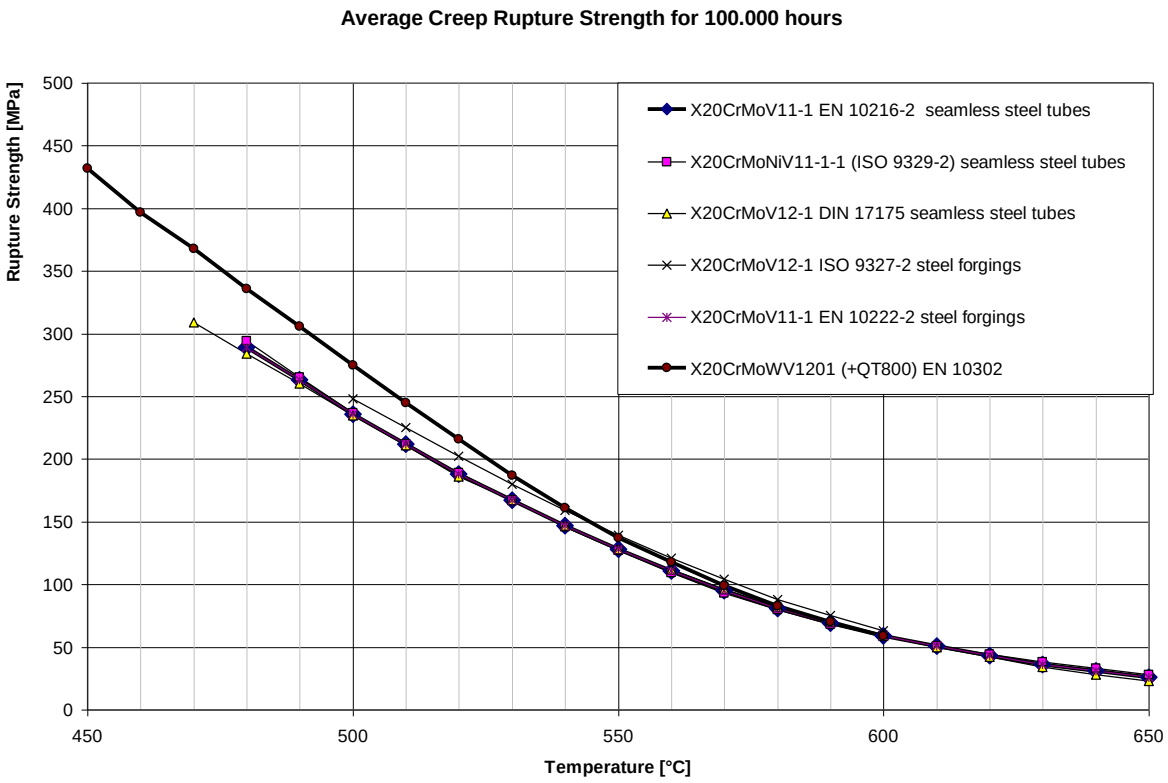

Figure 23: Comparison of selected average creep rupture strength values for 100.000 hours

Table 6: Average creep rupture strength values for seamless pipes and X20CrMoWV12-1, quenched and tempered at 700°C.

Temp. [°C]	X20CrMoV11-1 EN 10216-2:2002 X20CrMoV11-1 EN 10222-2: 2000			X20CrMoNiV11-1-1 (ISO 9329-2: 1997)							X20CrMoV12-1 DIN 17175 X20CrMoV11-1 X20CrMoV11-1 X20CrMoWV12-1 (+QT700) EN 10302: 2002		
	Time to rupture [hours]												
	10^4	10^5	$2x10^5$	10^4	$3x10^4$	$5x10^4$	10^5	$1.5x10^5$	$2x10^5$	$2.5x10^5$	10^4	10^5	$2x10^5$
	Average creep rupture strength [MPa]												
470											368	309	285
480	348	289	270	350	324	311	294	284	277	371	345	284	262
490	319	263	242	319	293	281	265	255	247	242	319	260	237
500	292	236	218	290	265	254	237	228	221	215	294	235	215
510	269	212	194	264	240	228	212	203	196	190	274	211	191
520	247	188	170	240	216	205	189	179	172	167	253	186	167
530	225	167	149	216	194	183	167	157	151	145	232	167	147
540	205	147	129	196	173	162	146	137	130	125	213	147	128
550	184	128	112	176	153	142	127	118	112	107	192	128	111
560	165	111	96	157	135	124	109	101	95	90	173	112	96

Temp. [°C]	X20CrMoV11-1 EN 10216-2:2002 X20CrMoV11-1 EN 10222-2: 2000			X20CrMoNiV11-1-1 (ISO 9329-2: 1997)							X20CrMoV12-1 DIN 17175 X20CrMoV11-1 X20CrMoV11-1 X20CrMoWV12-1 (+QT700) EN 10302: 2002		
	Time to rupture [hours]												
	10^4	10^5	$2x10^5$	10^4	$3x10^4$	$5x10^4$	10^5	$1.5x10^5$	$2x10^5$	$2.5x10^5$	10^4	10^5	$2x10^5$
	Average creep rupture strength [MPa]												
570	147	95	81	139	117	107	93	86	80	76	154	96	81
580	130	81	68	123	102	92	80	73	68	65	136	82	68
590	113	69	58	107	88	79	68	62	58	56	119	70	58
600	97	59	49	93	75	68	59	54	50	48	101	59	48
610	84	51	42	81	65	59	51	46	44	41	87	50	40
620	72	43	36	71	57	51	44	40	38	36	73	42	33
630	61	36	30	62	50	45	38	35	32	30	60	34	27
640	52	31		54	44	39	33	30			49	28	22
650	44	26		48	38	34	28				40	23	18
660				42	33	29							
670				37	29								

Table 7: Average creep rupture strength values for forgings and X20CrMoWV12-1, quenched and tempered at 800°C

Temperature [°C]	X22CrMoV12-1 EN 10302 X20CrMoWV1201 (+QT800) EN 10302 X22CrMoV12-1 EN 10269			X20CrMoV12-1 ISO 9327-2						
	Time to rupture [hours]									
	10^4	10^5	$2x10^5$	10^4	$3x10^4$	$5x10^4$	10^5	$1.5x10^5$	$2x10^5$	$2.5x10^5$
	Average creep rupture strength [MPa]									
450	480	432								
460	451	397								
470	422	368								
480	394	336								
490	366	306								
500	338	275		294	271	261	248	239	234	229
510	312	245		274	250	238	225	219	213	208
520	286	216		253	228	217	202	197	190	185
530	261	187		232	208	195	180	175	167	161

Temperature [°C]	X22CrMoV12-1 EN 10302 X20CrMoWV1201 (+QT800) EN 10302 X22CrMoV12-1 EN 10269			X20CrMoV12-1 ISO 9327-2						
	Time to rupture [hours]									
	10^4	10^5	$2x10^5$	10^4	$3x10^4$	$5x10^4$	10^5	$1.5x10^5$	$2x10^5$	$2.5x10^5$
	Average creep rupture strength [MPa]									
540	235	161		213	187	175	159	150	143	137
550	211	137		192	167	155	139	128	122	117
560	187	118		173	148	136	121	110	104	100
570	165	99		154	130	119	104	94	89	84
580	143	83		136	113	102	88	80	76	72
590	122	70		119	97	87	75	68	64	60
600	103	59		101	81	74	63	57	53	50

4.3.7 Metallurgy

The high-temperature strength of this material is achieved by the addition of the carbide-forming elements molybdenum and vanadium, which also determine the precipitation sequence. The materials with 12 % Cr and additions of molybdenum, vanadium and nickel fill the gap between the low-alloy ferritic steels and the high-temperature austenitic steels. As in the case of all high-chromium steels, there is no bainite transformation, and $M_{23}C_6$ is precipitated already, often in dendritic form, on the austenite grain boundaries before the start of the transformation. In the vanadium-alloyed steels, traces of MX may also form in the austenite. Pre-eutectoid ferrite does not occur, since the steel is hyper-eutectoid on account of the high chromium content ([Petri 83] Page 330, Steel X 20 CrMoV 12 1 (Material No. 1.4922)).

Some of the investigations for X20CrMoV12.1 steam pipes indicated that severe softening did not occur after long-term service exposure at elevated temperature. A particularly important aspect of the microstructure is the distribution of carbide particles. Some work on 12CrMoV pipe steels indicated that the carbides of $M_{23}C_6$, M_7C_3, M_2X, and MX (M denotes the metal elements, and X denotes non-metallic elements of C and N) were found in their as-received heat treatment or after creep exposure test conditions, which were believed to be decisive factors for precipitation hardening, as well as high creep strength [Zheng-Fei].

4.4 Physical and metallurgical characterization of the data

Before the data can be evaluated, the known influences have to be discussed. In this chapter, an overview of the state-of-the art for the material X20CrMoV11-1 is given.

4.4.1 Influence of heat treatment on creep strength

The least expensive way to obtain high creep-rupture strength is by giving the alloy a high temperature solution anneal. Austenitic grain size of 63.5μm (ASTM E112: 1996 grain size 5) or coarser gives much better creep and rupture strength than does a finer grain size. However, coarse grained materials lose thermal fatigue resistance as they gain creep strength. Material with grain size coarser than 89.8μm (ASTM E112 grain size 4) will be unsatisfactory in liquid quench applications. X20CrMoV11-1 usually is characterized with the primary austenite grains of size of 35-89.8 μm (ASTM E112 grain size 4-6) – see Figure 24.

Creep damage (prematurely) found on the power plant components fabricated out of X20CrMoV11-1 material is usually resulting of improper heat treatment [Bendick 92]. According to the research done by [Bendick 92], the following conditions have negative influence on creep strength:

1. the speed of cooling after the austenitization was too low
2. cooling between solution annealing and tempering was not low enough
3. temperature of austenitization was too low [Jesper 85, Fabritius 85]

If the tempering temperature is higher than 780°C, in cases of product types seamless pipe and plate, and at higher Ni-content, it can result in partial austenitization during the tempering, and, as a result, with the material that contains higher content of non stress-relieved martensitic structures [Kalwa 91], which can, in turn, lead to lower creep strengths at temperatures above 530°C [Bendick 93].

The dependency between critical duration of cooling and chemical composition of the material is show on Figure 24. The dependency between austenitization temperature and creep strength is shown on Figure 25.

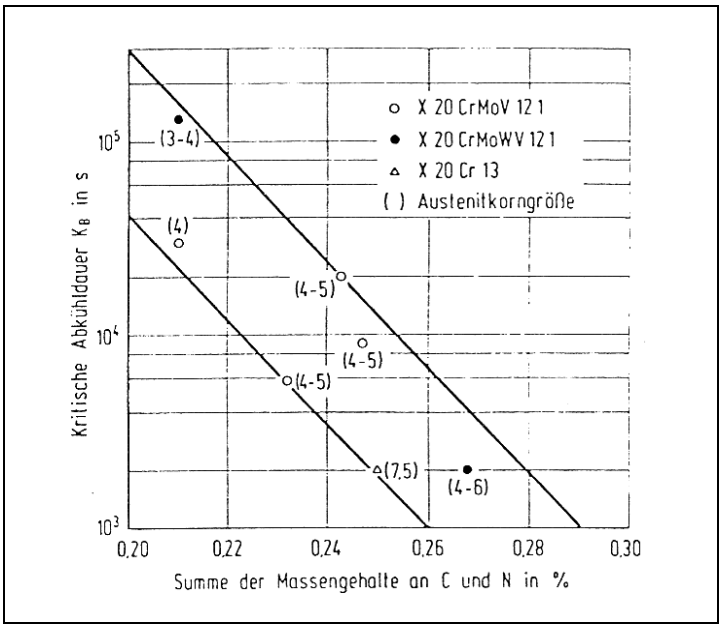

Figure 24: Critical cooling duration K_B needed for the start of transformation towards the ferrite-carbide-phase in dependency of sum of C and N [Jesper 85]

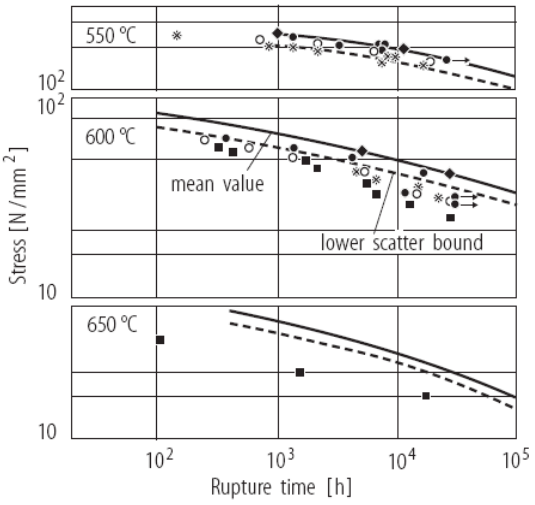

L = air	$R_p/R_{p0.2}$ [N/mm²]	R_m [N/mm²]
■ 1/2 h, 920 °C/L; 2 h, 780 °C/L	459	724
* 1/2 h, 925 °C/L; 2 h, 780 °C/L	558	755
○ 1/2 h, 975 °C/L; 2 h, 750 °C/L	605	805
● 1/2 h, 1000 °C/L; 2 h, 750 °C/L	603	810
◆ 1/2 h, 1050 °C/L; 2 h, 750 °C/L	606	814

Figure 25: Influence of temperature of heat treatment on creep strength [Maile 04a]

4.4.2 Effects of chemical composition

According to some literature sources [Jesper 85, Schinn 60], influence of **Tungsten** (W) is not identifiable, see Figure 26. Tungsten is a large, heavy atom used as a strengthening addition. It is a carbide forming element, that is, it reacts with the carbon in the alloy to form a hard particle, which may incorporate other carbide forming elements such as chromium. Tungsten also promotes formation of sigma phase, and of delta ferrite [Kelly 07]. The carbide forming properties are main reason this element is added to modifications of X20.

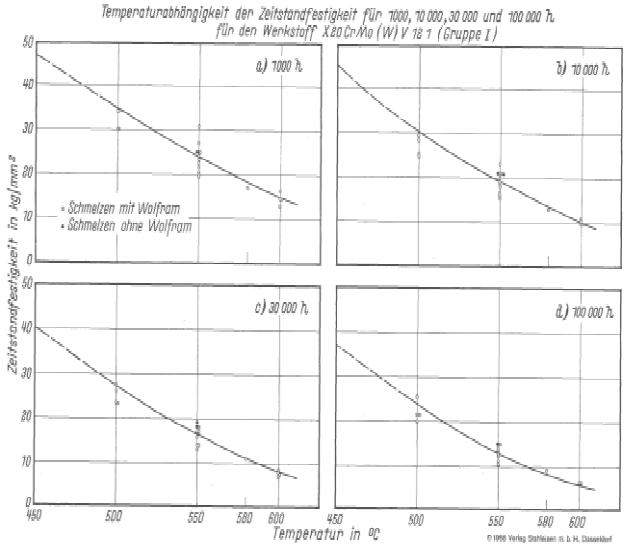

Figure 26: Effect of W on creep strength

The **carbon** content has, according to the Figure 27, important influence on the creep strength [Schieferstein 60], therefore the carbon content should be kept lower. Carbon is an “austenitizing element”, and tends to retard or prevent formation of delta ferrite and sigma phase. Carbon may actually be dissolved in the alloy, or, more commonly, it is present as small, hard particles called carbides. These are chemical compounds of carbon with chromium, molybdenum, tungsten, titanium, ziconium or columbium (niobium) [Kelly 07].

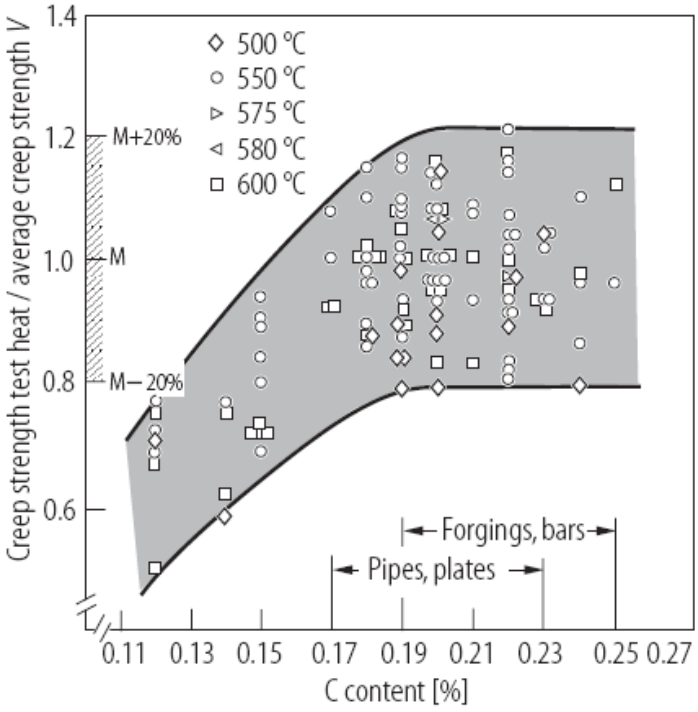

Figure 27: 12%Cr-Steels – C-content and 10^5 h creep strength [Schieferstein 60]

Chromium is the one element present in all heat resisting alloys. Oxidation resistance comes mostly from the chromium content (the same is true of aqueous corrosion resistance). Chromium adds to high temperature strength, and to carburization resistance. Metallurgically speaking, chromium tends to make the atomic structure “ferritic”, that is, with a body centered cubic (BCC) crystal structure. High chromium content contributes to sigma phase formation too. Both the tendency to form ferrite, and to form sigma phase are counteracted by nickel [Kelly 07]. According to [Schinn 60], too low or too high content of Cr in 12% Cr-steels does not influence the creep strength.

Molybdenum is another large, heavy atom used to increase high temperature creep-rupture strength. About 3% is the maximum that can be tolerated in a heat resistant alloy without serious oxidation problems in the high temperature range. Molybdenum promotes sigma phase formation, unless counterbalanced by austenitizing elements such as nickel, cobalt, etc., and is a ferritizer. Molybdenum is also a carbide forming element. Molybdenum helps weldability in austenitic alloys, both stainless and nickel base. In 12% Cr-Steels, according to [Jesper 85], Molybdenum content of about 1% with at the same time **Vanadium-content** of 0.15-0.35% has positive effect on creep strength. Mo and V additions are, as carbide-forming elements, most important factors in chemical composition for the creep strength of X20CrMoV11-1 [Petri 83]. According to [Melzer 03], molybdenum is the most important element that contributes to the creep strength of the steel, with a maximum of about 1.2% concentration, whereas the V content of more than 0.35% influence negatively the weldability and ductility.

Phosphorus is harmful to weldability. Phosphorus cannot be removed during the refining process. To produce alloys with low phosphorus, one must start with low phosphorus raw materials.

Sulfur is normally regarded as an impurity. It has the benefit of improving machinability [Kelly 07]. To improve hot workability, the steel mill normally refines the metal to very low sulfur content. This is fairly easy to do with current melting processes, such as the AOD (argon-oxygen decarburization) or ESR (electro-slag remelt) furnaces. Sulfur is also detrimental to weldability. Along with simply removing the sulfur in the refining process, the harmful effects of S on hot working and welding may be reduced to a degree by the addition of some manganese.

For X20CrMoV11-1 steels, the content of sulfur and phosphorus was continuously sunken. In this way, the impact toughness of the steel could be improved, as well as the weldability. The influence of S and P content on creep strength is not known. However, with the sulfide content reduction, the number of cavities can be reduced, but this cannot be brought in the connection with creep strength, according to [VGB 05], as the appearance of the “cavities” linked with the sulfide particles, it can be considered as deformation induced gap between the hard particle and the ductile grain matrix.

A small amount of **nitrogen** serves to strengthen austenitic heat resisting alloys. Too much nitrogen can embrittle them. Nitrogen is also an “austenitizing” element. It tends to retard or prevent delta ferrite and sigma phase formation. Together with Nb and V it forms MX particles, which are important for the optimization of creep strength especially in 9-11% Cr steels. A balanced B/N content is assumed to prevent the dissolution of MX particles at high temperatures in service.

Silicon improves carburization and oxidation resistance, as well as resistance to absorbing nitrogen at high temperature [Kelly 07]. At high enough levels, silicon improves resistance to alkali metal hot corrosion. Silicon can decrease weldability in some, not all, alloys. The metallurgical effects of silicon are that it tends to make the alloy ferritic, or to form sigma phase. Silicon decreases the solubility of carbon in the metal (technically it increases the chemical “activity” of carbon in the alloy). A silica (silicon oxide) layer, just under the chromium oxide scale on the alloy, is what helps the alloy resist carburization.

Aluminum is added in austenitic, heat-resistant steels at the 1 to 5% level for oxidation resistance. Aluminum is a ferritizing element, and promotes sigma phase formation. It is used in the age hardening (precipitation hardening) alloys. For X20CrMoV11-1, the limit is set to 0.4% according to the latest specification, other specification do not specify or put the values to much lower (i.e. 0.02% limits).

Nickel is present, anywhere from 8% up to 80%, in all of the “austenitic” heat resistant alloys [Kelly 07]. When added to a mix of iron and chromium, nickel increases ductility, high temperature strength, and resistance to both carburization and nitriding. Nickel decreases the solubility of both carbon and nitrogen in austenite. High nickel is bad for sulphidation resistance. Nickel tends to make the atomic structure “austenitic”, that is, with a face centered cubic (FCC) crystal structure.

Nickel counteracts, but doesn't necessarily stop, the tendency for an alloy to form sigma phase.

Manganese is used in steelmaking to improve hot workability. It is mildly detrimental to oxidation resistance, so is limited to 2% maximum in most heat resistant alloys. Manganese improves weldability, and is added to many austenitic weld fillers. Manganese is usually considered an austenitizing element. It increases solubility for nitrogen, and has for decades been used, both as a partial substitute for nickel and to permit a substantial nitrogen addition [Kelly 07].

Copper—molten copper and copper base alloys penetrate the grain boundaries of any austenitic iron, nickel-chromium-iron or nickel-chromium alloy. Even carbon steel, austenitized by immersion in molten copper, can have the austenite grain boundaries outlined by copper metal. It is known from literature [Kelly 07] that stainless steel welds generally do not crack unless contaminated, possibly by zinc or copper, more rarely by aluminum. Copper tends to embrittle the alloys; therefore its content should be kept at minimum for all high temperature applications. Also, it has strengthening effect; therefore it is used for improving the creep strength in various alloys, such as 23Cr-18Ni-3Cu-1.5W-Nb-N steel, for applications up to 750°C [Masuyama 04].

4.4.2.1 Other elements, present in new 9-12% Cr steel specifications

Cobalt is an austenitizing element, like nickel [Kelly 07]. High cost and variations in availability tend to limit the use of cobalt alloys to gas turbine engine applications. In higher concentration it tends to increase strength and enhance oxidation resistance at high temperatures.

Titanium is added in small amounts, about 0.3-0.7%, for strength in austenitic alloys [Kelly 07]. Around 0.1—0.2%Ti is used, as part of steel mill melting practice, in deoxidation of nickel alloys. Ti is strong carbide former. Titanium also promotes sigma phase and delta ferrite, but it is normally used in such small amounts as to be inconsequential in this respect. In aqueous corrosion alloys titanium is referred to as a "stabilizing" element, in some cases for austenitic steels. Titanium metal itself, although it has a very high melting point (3040°F/1671°C), is not really a heat resistant metal. Titanium alloys are used up to about 600°F (316°C) in aerospace applications.

Columbium (Cb) also called **niobium** (Nb) is added at the 0.4 to 0.8% level for strength in several heat resisting alloys [Kelly 07]. The low amount of Cb is harmful to weldability, while higher amounts are beneficial. Columbium is very harmful to oxidation resistance, practically speaking around 980°C and higher. Columbium is a strong carbide former, a ferritizing element and promotes sigma phase formation.

Addition of 0.08% of the Nb in P91 and addition of 0.003% of B in P92 have resulted in the significant increase of creep strength of the new generation of steels [Melzer 03].

Zirconium is strong carbide former.

The **rare earth elements cerium**, **lanthanum** and **yttrium** are used singly or in combination to increase oxidation resistance in austenitic alloys both wrought and cast, and in the newer ferritic heat resistant alloys. The technology has been known, but little used, since about 1940 in Germany.

Cerium is added as an alloy of several rare earths, called mischmetal [Kelly 07]. For chemistry control purposes, steel mills analyze only for Ce. Residual cerium oxides in the metal may contribute to creep-rupture strength.

Boron increases creep-rupture strength, and is used at rather low concentrations, 0.002% is typical [Kelly 07]. Boron is somewhat harmful to weldability of nickel alloys, so nickel alloy weld filler is often made without boron, even though the matching base metal alloy has a boron addition. Boron is an interstitial element and tends to concentrate at the grain boundaries. It is used in high temperature braze alloys.
Borides have stabilizing effects on MX, M23 and C6 phases.

According to [Morinaga 94], it is possible to quantify the influence of chemical composition on creep strength with two parameters – Md and Bo. Both parameters are based on atomistic analysis of valence of bonding forces in the atomic grid. Bo represents the main source of strength of binding of dissolved elements and Iron atom in the flat-centered atomic grid. Md correlates with the electron-charge and atomic diameter of the element considered. According to [Morinaga 94], these two parameters can be used for optimization of steels, in the way that Bo is maximized and Md minimized. However, the metallurgical basis, or the relation with the creep strength is challenged by [Badeshia 01]. An empirical relation between creep

strength and valence forces has been given by [Morinaga 94] for δ-Ferrite-free steels.

Furthermore, [Badeshia 05] gives table of elements that strongly influence formation of carbides, see Figure 28. Another source [Marx 86], gives an overview of the chemical elements on different properties of steel (Figure 29).

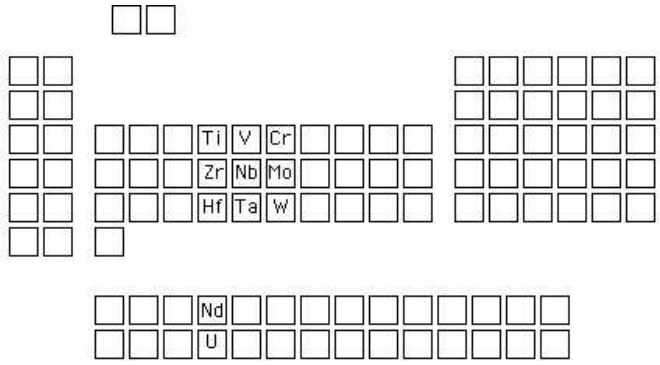

Figure 28: Periodic table of elements showing the positions of strong carbide forming elements [Badeshia 05]

	Strength	Creep Strength	Thermal resistence	Scaling resistance	Elongation	Hardness	Through-hardening	Impact strength	malleability	machinability	Corrosion Resistance
C	++		+		--	++	++	--	-	-	
Mn	++				-	+	++	+	+		+
Si	++			++	-	+	++		-		+
Al				++				-			
Ni	+				-			+	++		+
Cr	++	++	++	++	-	+	++				+
Mo	+	++	++		-	+	+		-		+
V	+	++	+			+	+				+
W	+		+		-	+	+	-			
Cu	+				--	+		--			++
S									+	++	
P	+		+		-	+		-			+
Ti	+					+		+			
Ta	++	++			+			+			
Nb	++	++			+			+			

+ - increasing influence

++ - strong increasing influence

- - decreasing influence

-- - strongly decreasing influence

Figure 29: Influence of different chemical elements on the properties of the steel [Marx 86]

4.4.3 Relation between creep and tensile strength

The increase in tensile strength through cold working of about 17% results in the short-time range of up to 15.000 h with better creep strength properties. However, due to thermally-induced relaxation of the material, in the range above 10^5h, this effect largely disappears [Dobers 73]. This is also true for the drop of creep strength due to higher level of deformation in the range of 20-40% [Wilhelmsson 80].

Historical, but even today used classification in strength classes (see Table 8) is a result of different heat treatment.

Table 8: Strength classes for X20CrMoV11-1

Class	R_{p02} (MPa)	Tensile strength R_m (MPa)	Austenitization	Tempering
1	≥ 490	638 – 883	1030-1050°C	720-780°C (mostly above 750°C)
2	≥ 589	785 – 932	980-1100°C	670-780°C (mostly under 750°C)
3	≥ 785	≥ 932	980-1150°C	620-680°C (mostly under 660°C)

The resulting different creep strength values are shown on Figure 30, Figure 31, and Figure 32. [AGW 69]. These diagrams show the dependency of 105 values from the initial strength of the material, and this dependency is presented on Figure 33, for 550°C, where the linear regression formula with coefficients of 1/15 and 8.167, based on linear regression of data, is employed. This is also visible in the comparison of standard data – see Figure 23.

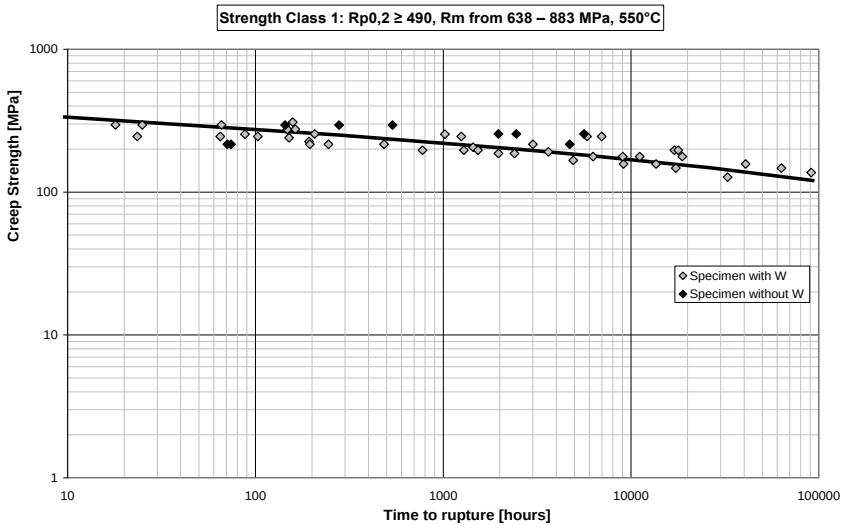

Figure 30: Creep strength for strength class 1

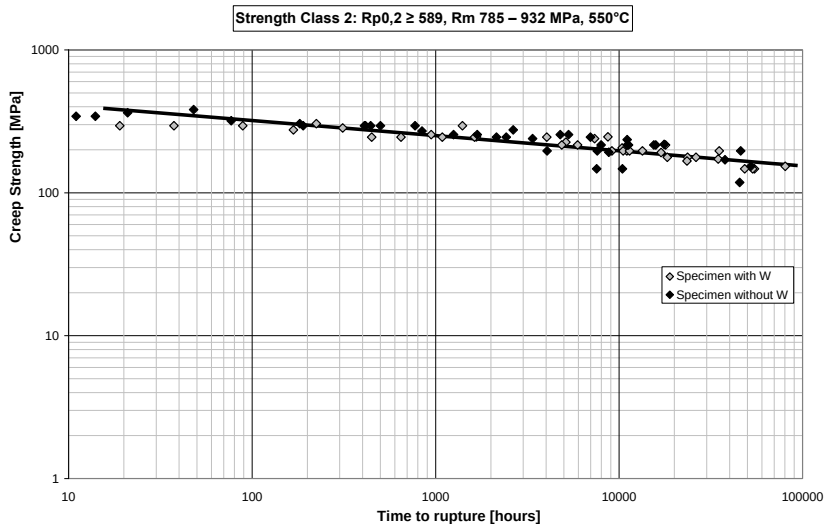

Figure 31: Creep strength for strength class 2

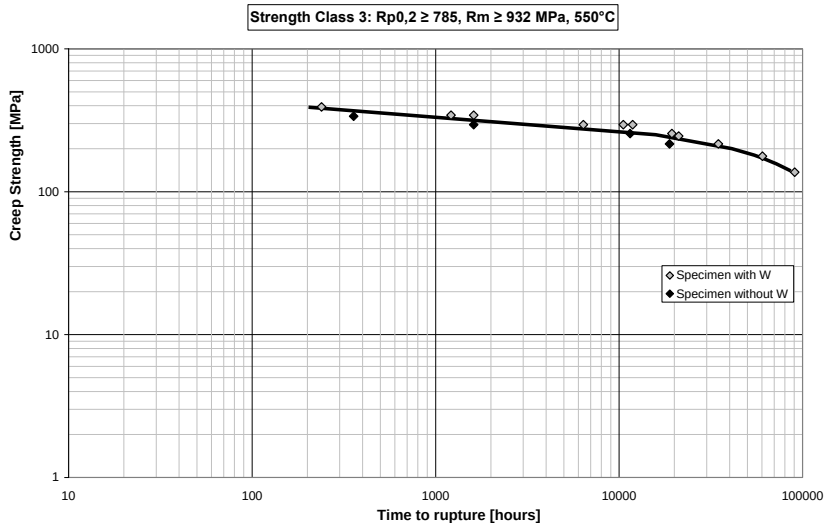

Figure 32: Creep strength for strength group 3

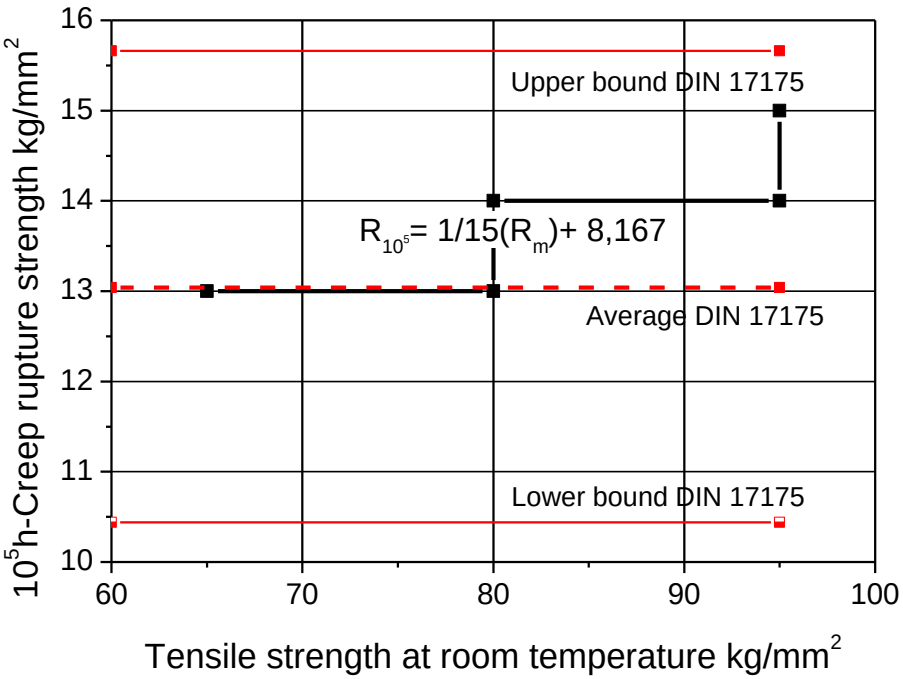

Figure 33: Relation between 10^5h-creep strength and tensile strength at room temperature; scatter band according to DIN 17175.

4.4.4 Influence of microstructure

The presence of δ-Ferrite does not influence the creep strength of X20CrMoV11-1, according to [Schieferstein 60]. [Morinaga 94] reports, on the contrary, that δ-Ferrite has, in general, a negative influence on creep strength. Elements such as Ni, Co and Cu are suppressing the formation of δ-ferrite.

When normal heat-treated, the microstructure of X20CrMoV11-1 can contain, apart from tempered martensite, also non-tempered martensite and deltaferrite up to 5% [Petri 82], however, in this amount it does not have negative impact on creep strength.

4.5 Dataset

For the purpose of the work presented here, X20CrMoV11-1 data has been selected. Initial dataset contained the following material sub-specifications:

- X20CrMoV12-1 with 847 individual creep tests
- X22CrMoV12-1 with 505 individual creep tests
- X20CrMoWV12-1 with 269 individual creep tests

- G-X22CrMoV12-1 with 266 individual creep tests
- G-X22CrMoWV12-1 with 228 individual creep tests
- X22CrMoWV12-1 with136 individual creep tests

with total of 2251 data points (individual creep tests). Graphically, the distribution of the data is shown on Figure 34. The actual number of total available points was slightly higher (2829), but only creep tests ending with rupture were considered (2251). The bulk of the data points not considered were creep tests ended before specimen break, but there were also 16 unspecified, and a small number of tests that failed for different reasons, but were reported.

The data is covering 178 distinct casts and 236 different chemical analyses.

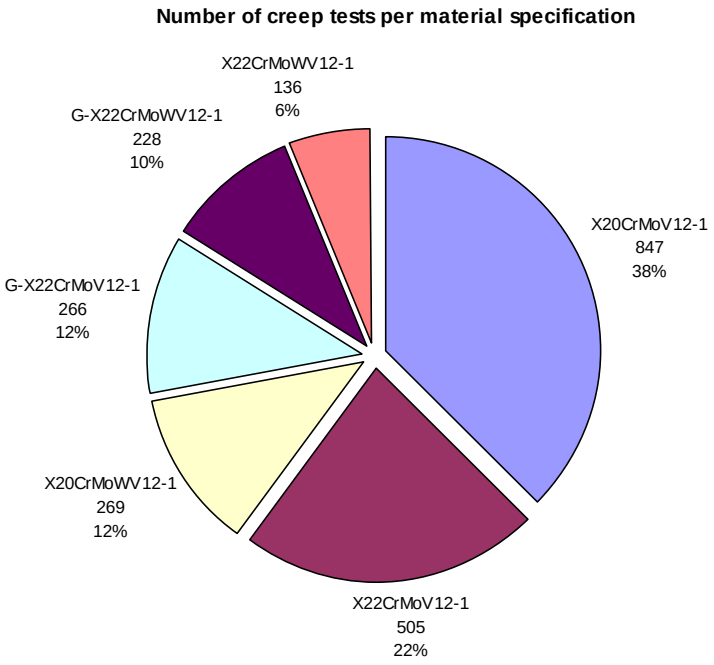

Figure 34: Distribution of number of individual creep test results

As already stated, the cast iron specification of X20CrMoV11-1 has different properties, slightly different chemical composition (i.e. higher carbon content), and different purpose. Therefore, the G-X22 and G-X20 specifications were not considered.

Furthermore, the welded components tests were also not considered, as the data sets did not contain information regarding chemical composition (inhomogeneous specimens).

After this reduction, the data is covering 129 distinct casts and 177 different chemical analyses – see Table 9.

Table 9: Initial data set without cast iron specification and welded components

Material	Number of chemical analyses	Number of creep tests
X20CrMoV12-1	78	798
X20CrMoWV12-1	26	269
X22CrMoV12-1	62	489
X22CrMoWV12-1	11	136
Total	**177**	**1692**

As the data used for this analysis has been produced during the very long period of time (987 points, i.e. more than a half was already published in 1969 [AGW 69]), and since the purpose of some of the experiment was to investigate the single effects of i.e. chemical composition variation, different heat treatment, etc., the data is characterized by the following:

1. Data sets are not always compliant with current specification for the material; if only compliant data sets were used, then only 37 different cast analyses and 314 distinct data points / creep tests available for analysis
2. Data provided in one data set is not necessarily complete, i.e. not giving all the information as desired for the purpose
3. For some datasets it can be deduced that they have been used for special purposes (i.e. unusual heat treatment, variable chemical composition, etc.), but explicit verification of these facts could not be found in the data available for the analysis. This is in contrary with the 987 data points published in 1969 [AGW 69], where 3 basic strength borders were given – see Table 8, and then special variations identified by class 1S, 2S, 4S (not individually identified in the tables).

Selected features to be considered were, grouped by level of appearance:

- Level of heat/cast:
  - Cast analysis – chemical composition (in % by mass)
    - C
    - Si
    - Mn
    - P
    - S
    - Cr
    - Mo
    - Ni

        - (Al)
        - Cu
        - V
        - W
        - N
        - Co
    - Heat-treatment specification:
        - austenizing temperature (°C)
        - austenizing cooling medium (-)
        - austenizing duration (minutes)
        - tempering temperature (°C)
        - tempering cooling medium (-)
        - tempering duration (minutes)
    - Tensile properties at room temperature
        - $R_{p0,2}$ - 0,2% proof strength or R_{eh} (MPa)
        - tensile strength R_m, (MPa)
        - Elongation A_{min} (%)
        - Reduction of area Z (%)
- Level of testing temperature
    - Tensile properties at the test temperature:
        - $R_{p0,2}$ - 0,2% proof strength or R_{eh} (MPa)
        - tensile strength R_m, (MPa)
        - Elongation A_{min} (%)
        - Reduction of area Z (%)
- Level of single specimen:
    - Specimen characteristics
        - Type of specimen (notched, smooth) (k/z)
        - Type of product (-)
        - Production Process (-)
- Level of creep test
    - Creep test parameters:
        - Temperature (°C)
        - Applied stress (MPa)
    - Creep test results:
        - Time to rupture (h)
        - Hardness before the test

- Hardness after the test
- Elongation A (%)
- Reduction of area Z (%)
- Time to 0,2% strain (hours)
- Time to 0,5% strain (hours)
- Time to 1% strain (hours)

Further, other fields containing additional information, like comments, type of test, testing institution, type of rupture have been evaluated and considered as input for the features mentioned above.

Graphically, this is represented in Figure 35.

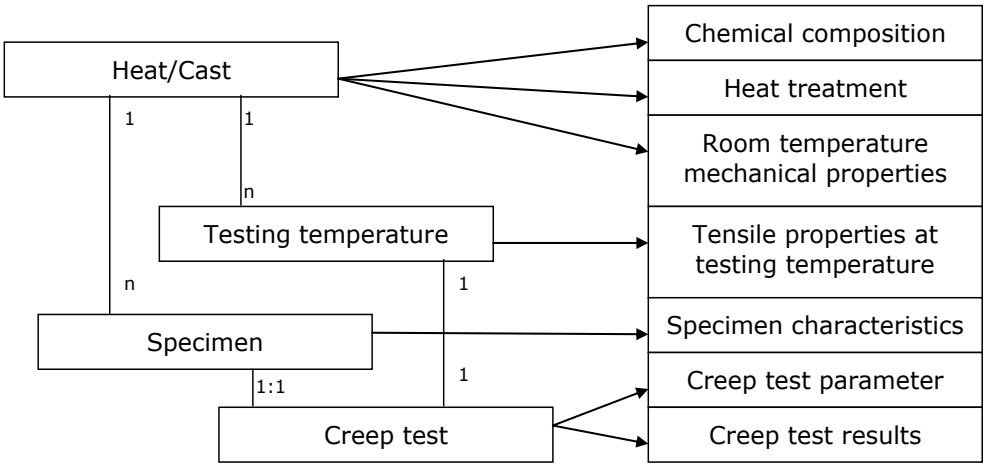

Figure 35: Data structure by the source of data

The following table shows the overview of data availability, minimal and maximal values, as well as mean values and standard deviations for each single feature.

Table 10: Overview of features, availability, and basic statistics in the dataset

Feature	No of points	% Availability	Min. value	Max. value	Mean value	Std. deviation
Material Specification	1692	100%	-	-	-	-
Cast No	1692	100%	-	-	-	-
Type of Test	1692	100%	-	-	-	-
Cast Analysis	1692	100%	-	-	-	-
Product Form	1692	100%	-	-	-	-
Type of Specimen	1692	100%	-	-	-	-
Production Process	533	31.5%	-	-	-	-
Comment	20	1.2%	-	-	-	-
Testing institution	753	44.5%	-	-	-	-
P	1153	68.1%	0.008	0.031	0.014	0.004
S	1160	68.6%	0.002	0.017	0.01	0.003

Feature	No of points	% Availability	Min. value	Max. value	Mean value	Std. deviation
C	1692	100%	0.1	0.26	0.205	0.031
Si	1639	96.9%	0.14	0.72	0.338	0.075
Mn	1615	95.4%	0.24	1.39	0.503	0.158
Al	526	31.1%	0.002	0.05	0.015	0.015
Cr	1692	100%	10.2	13.7	11.949	0.599
Co	421	24.9%	0.02	0.18	0.075	0.048
Cu	762	45%	0.007	0.18	0.096	0.047
Mo	1692	100%	0.58	1.39	1.077	0.15
Ni	1561	92.3%	0.07	1.52	0.43	0.256
V	1692	100%	0.15	0.82	0.341	0.098
W	773	45.7%	0.01	0.82	0.356	0.239
N	759	44.9%	0.009	0.056	0.024	0.011
R_{p02} (RT)	620	36.6%	428	853	667.09	99.037
R_m (RT)	1684	99.5%	629.5	1334	843.675	104.909
A (RT)	1618	95.6%	7	27	18.892	3.282
Z (RT)	1618	95.6%	14	67	54.929	6.5
R_{eH} (RT)	1038	61.3%	394	1216	663.43	144.761
Test Temperature	1692	100%	450	800	567.586	40.918
Tensile Test Temperature	866	51.2%	450	800	567.471	42.735
R_{p02} (Test Temperature)	508	30%	59	534	343.33	90.41
R_m (Test Temperature)	866	51.2%	119.5	777	467.589	109.202
A (Temperature)	858	50.7%	12	81.7	27.874	9.485
Z (Temperature)	858	50.7%	48.6	96.3	75.545	9.8
R_{eH} (Temperature)	311	18.4%	212	626	377.22	103.441
Duration Until 0,1% Strain	278	16.4%	0.15	10000	571.212	1262.291
Duration Until 0,5% Strain	550	32.5%	0.3	48000	2000.313	4532.563
Duration Until1% Strain	748	44.2%	0.5	72000	4568.105	8816.743
Stress	1692	100%	16	686	210.829	96.215
Time to Rupture	1692	100%	0.05	225008	11719.985	22038.224
Hardness Before	532	31.4%	148	344	267.974	39.165
Hardness After	350	20.7%	187	349	256.763	34.108
A Creep	1419	83.9%	2.8	93.5	30.687	14.781
Z Creep	1375	81.3%	1.6	96	62.979	22.338
Heat Treatment	1692	100%	-	-	-	-
Austenitization Temperature	1687	99.7%	950	1150	1045.347	32.472
Austenitization Medium	1614	95.4%	-	-	-	-
Austenitization Duration	1207	71.3%	10	300	57.756	55.894
Tempering Temperature	1687	99.7%	570	850	717.807	48.268
Tempering Duration	1600	94.6%	60	900	166.156	136.27
Tempering Medium	1547	91.4%	-	-	-	-
Strength Class	987	58.3%	-	-	-	-
Type of Rupture	304	18%	-	-	-	-

4.5.1 Data visualization and data selection application

For the purpose of the easier data analysis, where only aggregated and visualized data might help the work of data selection and results interpretation, data selection and data visualization, a small dedicated application has been created. This application has two parts: a) database and b) visual, web-based interface towards the database.

For the purpose of the data selection, a dedicated database was created, based on the structure corresponding to the ECCC recommendations for the creep test data collation and storage [ECCC 05]. The relations and tables are shown on the Figure 36.

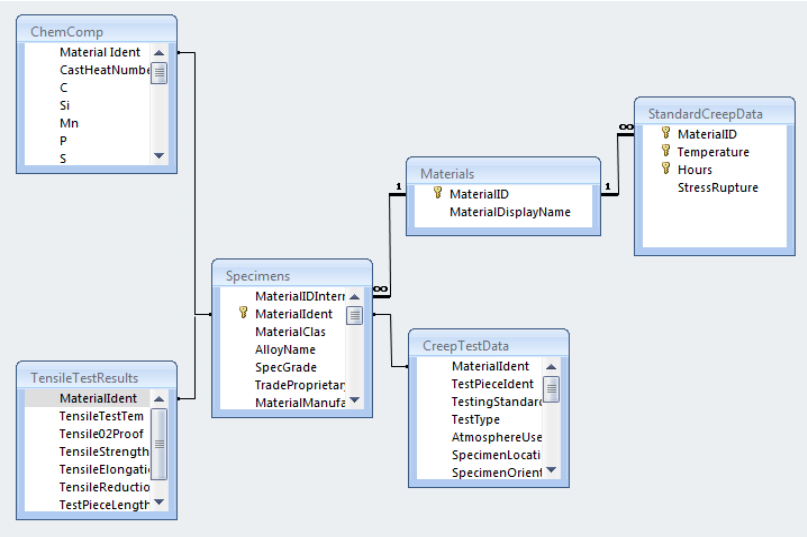

Figure 36 Database structure

As input for the web application (interface towards data), a set of queries based on various criteria have been created in order to aggregate the data in the form suitable for the analysis. The queries are fairly complex, since results and data from material specification, specimen data, tensile testing at both room and high temperature are needed to be joined in a suitable way. The sample query is shown on Figure 37, and the results on Figure 38.

```
SELECT FullSetCreepData.MaterialIDInternal, FullSetCreepData.MaterialsChemCompTensileRT.MaterialIdent,
FullSetCreepData.MaterialClas, FullSetCreepData.AlloyName, FullSetCreepData.SpecGrade,
FullSetCreepData.TradeProprietary, FullSetCreepData.MaterialManufacturer,
FullSetCreepData.MaterialsImported.CastHeatNumber AS Expr1, FullSetCreepData.PrimaryMeltprocess,
FullSetCreepData.DeoxidationProcess, FullSetCreepData.SecondaryMeltProcess, FullSetCreepData.CastingProcess,
FullSetCreepData.CastOrHeatWeightPrimary, FullSetCreepData.CastOrHeatWeightSecondary,
FullSetCreepData.ProductForm, FullSetCreepData.ProductDimensions, FullSetCreepData.ProcessingRoute,
FullSetCreepData.ProductFabricator, FullSetCreepData.LocationOf, FullSetCreepData.SizeHeatTreated,
FullSetCreepData.Operation, FullSetCreepData.NormalizationTemperature,
FullSetCreepData.NormalizationDuration, FullSetCreepData.NormalizationQuenchMedium,
FullSetCreepData.TemperingTemperature, FullSetCreepData.TemperingDuration,
FullSetCreepData.TemperingQuenchMedium, FullSetCreepData.Tempering2Temperature,
FullSetCreepData.Tempering2Duration, FullSetCreepData.Tempering2QuenchMedium,
FullSetCreepData.ChemComp.CastHeatNumber, FullSetCreepData.C, FullSetCreepData.Si, FullSetCreepData.Mn,
FullSetCreepData.P, FullSetCreepData.S, FullSetCreepData.Cr, FullSetCreepData.Mo, FullSetCreepData.Ni,
FullSetCreepData.V, FullSetCreepData.[Al sol], FullSetCreepData.[Al tot], FullSetCreepData.B,
FullSetCreepData.Nb, FullSetCreepData.[N sol], FullSetCreepData.[N tot], FullSetCreepData.As,
FullSetCreepData.Co, FullSetCreepData.Cu, FullSetCreepData.Pb, FullSetCreepData.Sn, FullSetCreepData.Ti,
FullSetCreepData.W, FullSetCreepData.Zr, FullSetCreepData.RTMaterialIdent, FullSetCreepData.TensileTestRT,
FullSetCreepData.TensileO2ProofRT, FullSetCreepData.TensileStrengthRT, FullSetCreepData.TensileElongationRT,
FullSetCreepData.TensileReductionAreaRT, FullSetCreepData.TestPieceLengthRT,
FullSetCreepData.TestPieceCrossSectionRT, FullSetCreepData.CreepTestData.MaterialIdent,
FullSetCreepData.TestPieceIdent, FullSetCreepData.TestingStandard, FullSetCreepData.TestType,
FullSetCreepData.AtmosphereUsed, FullSetCreepData.SpecimenLocation, FullSetCreepData.SpecimenOrientation,
FullSetCreepData.TestPieceLength, FullSetCreepData.TestPieceDiameter, FullSetCreepData.SpecimenHeat,
FullSetCreepData.CreepTestTemperature, FullSetCreepData.AppliedInitialStress, FullSetCreepData.TestStatus,
FullSetCreepData.CurrentTestDuration, FullSetCreepData.TimeToRupture,
FullSetCreepData.CreepTestElongationAtRupture, FullSetCreepData.CreepTestReductionAreaRupture,
FullSetCreepData.CreepTestrTimeTo1PercentPlasticStrain, FullSetCreepData.MinimumCreepRate,
FullSetCreepData.Comments, FullSetCreepData.TESTER, TensileHT.HTMaterialIdent, TensileHT.TensileTestHT,
TensileHT.TensileO2ProofHT, TensileHT.TensileStrengthHT, TensileHT.TensileElongationHT,
TensileHT.TensileReductionAreaHT, TensileHT.TestPieceLengthHT, TensileHT.TestPieceCrossSectionHT
FROM FullSetCreepData LEFT JOIN TensileHT ON (FullSetCreepData.MaterialsChemCompTensileRT.MaterialIdent =
TensileHT.HTMaterialIdent) AND (FullSetCreepData.CreepTestTemperature = TensileHT.TensileTestHT);
```

Figure 37 Sample query for joining the data

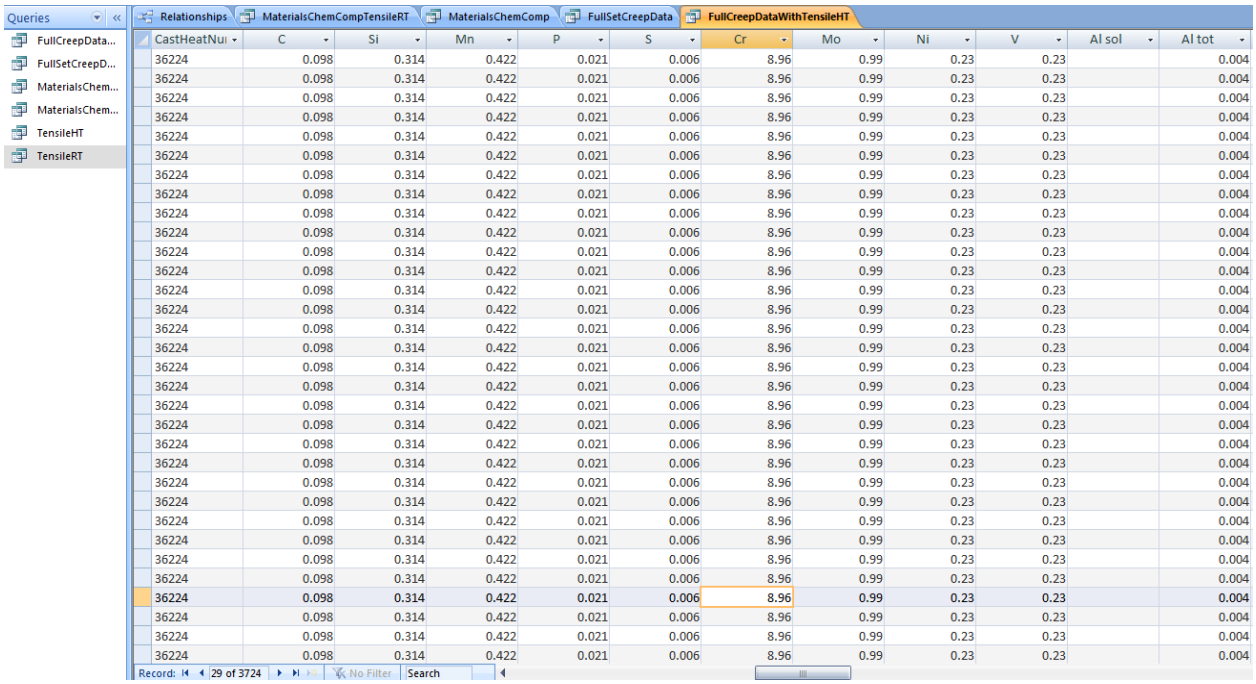

Figure 38 Sample query output based on data join

The main purpose of the visualization part of the application was to allow easy data selection and visualization of the results of the data selection through the queries. A sample data selection and visualization screen is shown on Figure 39. The main features are the existence of predefined filters (levels), as well as filters over test duration (short and long). Further, data selection can be on-line done, by applying filters over any of the existing columns in the data table (or combination of them).

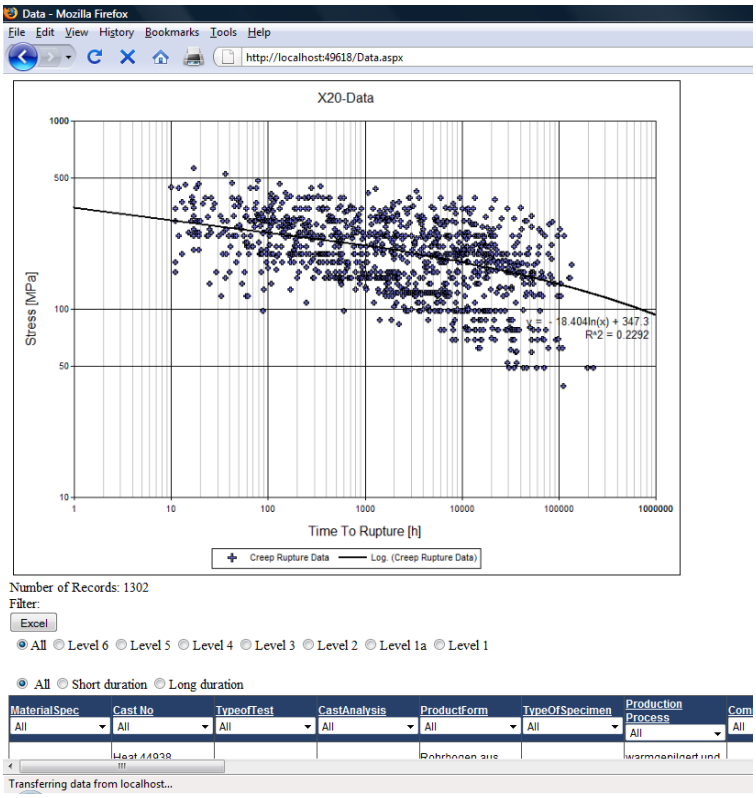

Figure 39 Sample data selection screen

A full data statistics about the columns is automatically created – see Figure 40. This feature does allow the selection of features for different data groupings, and the outputs are shown in i.e. Table 10.

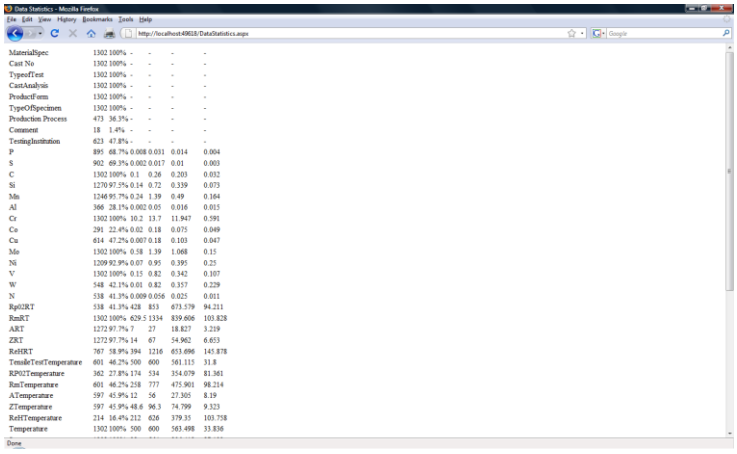

Figure 40 Data statistics screen.

Further, a series of visualization helping tools have been created – i.e. tools for visualization of pairs of features with the corresponding regressions and trend lines, allowing one-click creation of couple of hundreds of graphs - Figure 41. The results of selected graphs are given in i.e. Figure 48 and Figure 49.

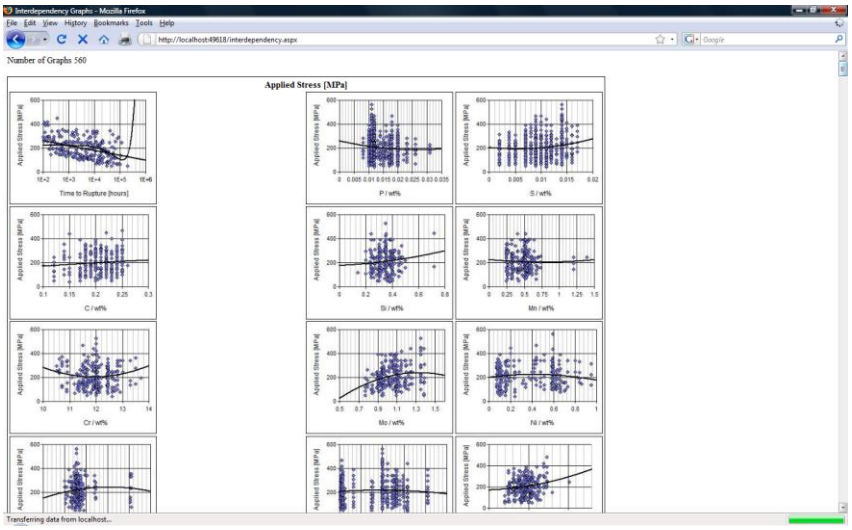

Figure 41 Interdependency graphs examples

Further, for the purpose of analysis of single casts behavior over given temperature, dedicated tools have been created, as shown on Figure 42. This feature allows i.e. creation of about 40 individual graphs by one-click. Also, trend lines for single casts and temperatures are also automatically created – more than 200 for the given model material X20, as shown on Figure 43.

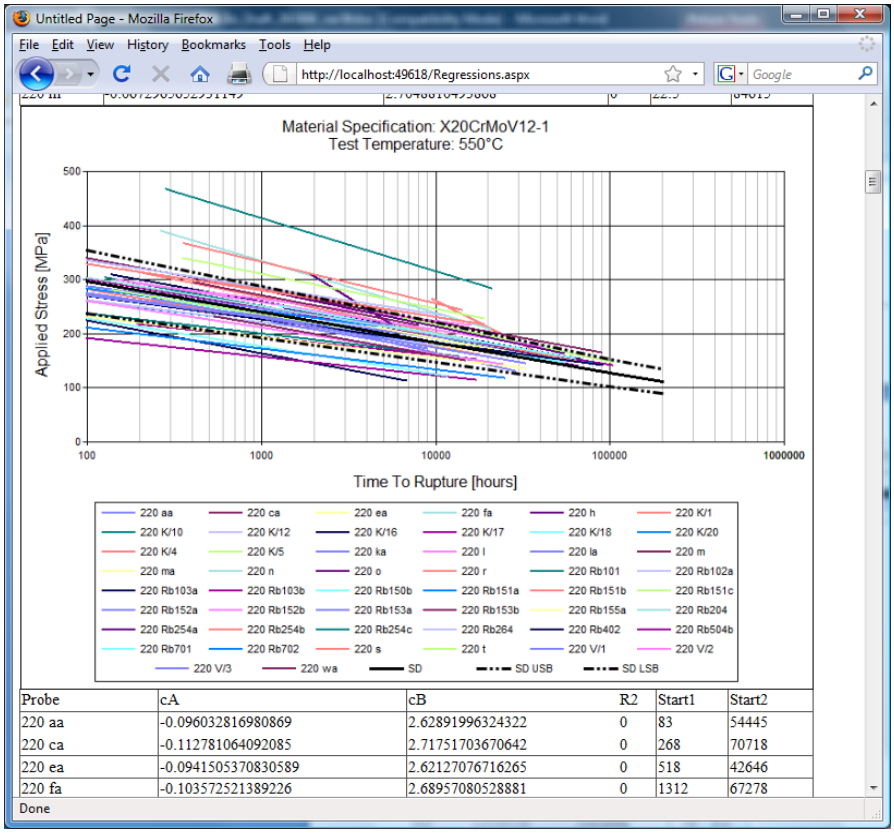

Probe	cA	cB	R2	Start1	Start2
220 aa	-0.096032816980869	2.62891996324322	0	83	54445
220 ca	-0.112781064092085	2.71751703670642	0	268	70718
220 ea	-0.0941505370830589	2.62127076716265	0	518	42646
220 fa	-0.103572521389226	2.68957080528881	0	1312	67278

Figure 42 Cast and temperature data analysis

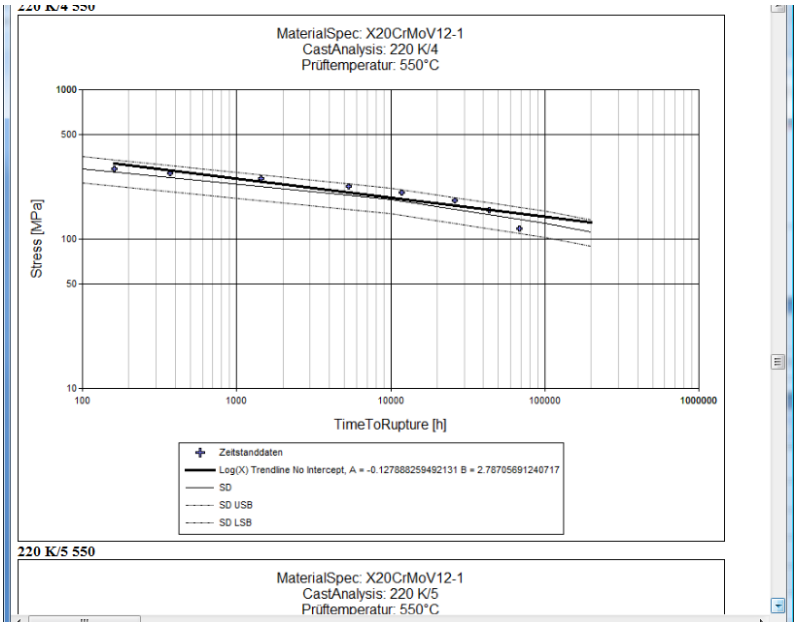

Figure 43 Single cast/temperature analysis

Finally, a series of small utilities have been created for the calculation of single time-temperature parameters as given in the Table 1, for the purpose of the comparison of the results achieved by application of neural networks over the data and of the conventional time-temperature parameters. An example of such an analysis is given in Figure 140.

This application can be applied to further data sets and can be used as starting point for analysis of data sets other than the selected one for this work. One example of the application to the P91 data set is given on Figure 44.

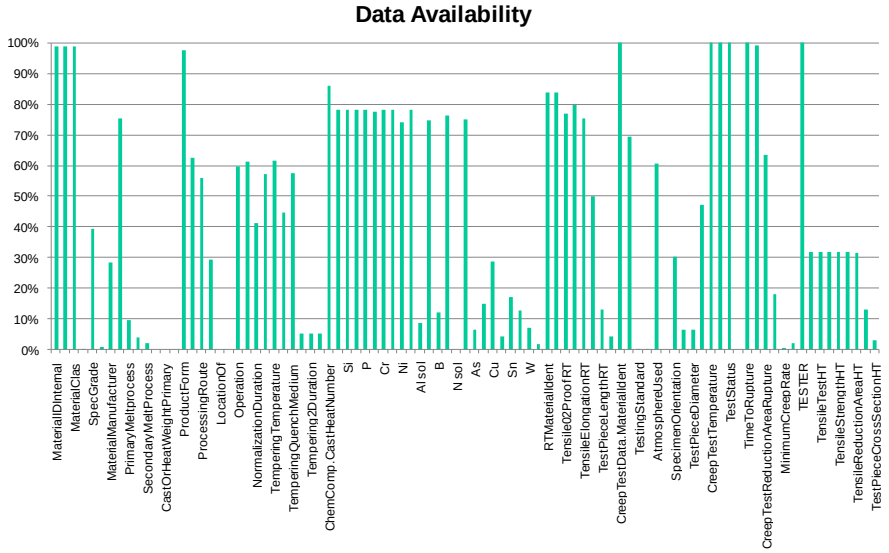

Figure 44 Example of application of the data analysis tool on the P91 data set (ca. 3720 data points)

4.5.2 Selection of features for the data analysis

Based on standard requirements and on data availability (Table 10), the basic set of parameters has been selected, and data grouped in levels; furthermore, the data test points below 450°C (5 data points) and above 650°C (71 data points) were not considered; also, all data tests close to tensile test behavior (duration shorter than 10 hours) have been eliminated (42 points). Further, one specimen with no heat-treatment specification has been removed (5 data points). Specimens where no tensile test data was available for room temperature were also removed (40 records)

Further, due to the fact that not all features are available in the same amount, grouping according to availability of features has been performed, and 6 subgroups of data have been identified.

The availability of data, selection and grouping of feature after further data reduction is shown in Table 11. Out of this table it is clear that data coverage in the data matrix 1535 creep tests x 37 features is in the range of 75%. Therefore, the grouping of data has been performed in data levels, starting with minimum number of features, and most data points, then introducing more features and thus reducing the number of data points, as the points without full data cannot be used for training of the network.

The treatment of missing values in the manner that the data points are removed rather than replacing missing values with defaults – be it minimal, average or maximal value has been selected due to the fact that the correlations between output(s) expected – i.e. carbon content and time to rupture is not strong (Figure 48), thus, introducing other values will rather confuse the network than bring any new information.

As the number of points decrease and number of features (inputs) increase, the capability of the neural network to model the dependency gets limited.

Table 11: Overview of data availability, selection of features and aggregation

Feature	No of points	% Availability	Min. value	Max. value	Mean value	Std. deviation	Data aggregation level / use
Material Specification	1535	100%	-	-	-	-	Grouping
Cast No	1535	100%	-	-	-	-	Grouping
Cast Analysis	1535	100%	-	-	-	-	Grouping
Product Form	1535	100%	-	-	-	-	Grouping
Type Of Specimen	1535	100%	-	-	-	-	Grouping

Feature	No of points	% Availability	Min. value	Max. value	Mean value	Std. deviation	Data aggregation level / use
Production Process	503	32.8%	-	-	-	-	Information
Comment	20	1.3%	-	-	-	-	Information
Testing Institution	710	46.3%	-	-	-	-	Information
P	1046	68.1%	0.008	0.031	0.014	0.004	1-4
S	1053	68.6%	0.002	0.017	0.01	0.003	1-4
C	1535	100%	0.1	0.26	0.204	0.031	1-6
Si	1482	96.5%	0.14	0.72	0.339	0.074	1-5
Mn	1458	95%	0.24	1.39	0.5	0.165	1-5
Al	462	30.1%	0.002	0.05	0.016	0.016	1
Cr	1535	100%	10.2	13.7	11.958	0.598	1-6
Co	370	24.1%	0.02	0.18	0.074	0.049	1
Cu	711	46.3%	0.007	0.18	0.099	0.047	1-3
Mo	1535	100%	0.58	1.39	1.074	0.149	1-6
Ni	1422	92.6%	0.07	0.95	0.411	0.246	1-5
V	1535	100%	0.15	0.82	0.342	0.102	1-6
W	686	44.7%	0.01	0.82	0.346	0.24	1-2
N	678	44.2%	0.009	0.056	0.024	0.011	1-2
$R_{p0,2}$ (RT)	1535	100%	394	1216	668	131.832	1-6
R_m (RT)	1535	100%	629.5	1334	845	107.942	1-6
A (RT)	1501	97.8%	7	27	18.85	3.353	-
Z (RT)	1501	97.8%	14	67	54.97	6.592	-
Tensile Test Temperature	779	50.7%	500	600	562	30.815	-
$R_{P0,2}$ (Temperature)	457	29.8%	174	534	356	81.431	-
R_m (Temperature)	779	50.7%	258	777	479	99.157	-
A (Temperature)	773	50.4%	12	56	27.073	7.948	-
Z (Temperature)	773	50.4%	48.6	96.3	74.702	9.007	-
R_{eH} (Temperature)	287	18.7%	212	626	379	104.433	-
Temperature	1535	100%	500	600	564	32.776	1-6
Stress	1535	100%	39	686	211	88.732	1-6
Duration Until 0,1% Strain	260	16.9%	0.15	10000	590	1301.42	-
Duration Until 0,5% Strain	528	34.4%	0.3	48000	2050	4609.363	-
Duration Until 1% Strain	709	46.2%	1	72000	4674	8981	-
Time to Rupture	1535	100%	10	225008	12336	22752	1-6
Hardness Before	471	30.7%	148	344	267	39.8	-
Hardness After	309	20.1%	187	348	257	33.1	-
A Creep	1291	84.1%	2.8	93.5	30.342	14.468	-
Z Creep	1249	81.4%	1.6	93.9	62.231	22.106	-
Heat Treatment	1535	100%	-	-	-	-	Information
Austenitization Temperature	1535	100%	950	1150	1045	33.655	1-6
Austenitization Medium	1487	96.9%	-	-	-	-	Grouping
Austenitization Duration	1098	71.5%	10	300	58	55.679	-
Tempering Temperature	1535	100%	570	850	717	49.255	1-6
Tempering Duration	1451	94.5%	60	900	170	139.898	-
Tempering Medium	1396	90.9%	-	-	-	-	Grouping
Strength Class	872	56.8%	-	-	-	-	Grouping

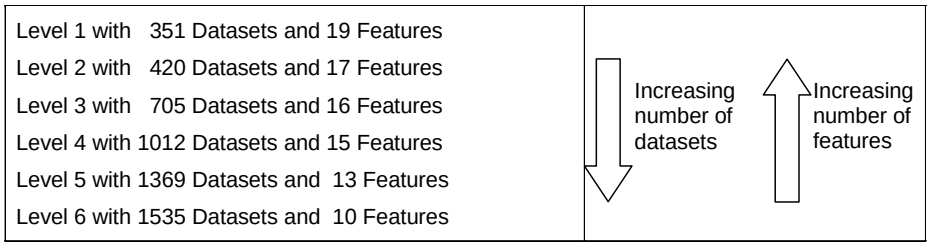

Table 12: Graphical representation of data grouping

Statistical analysis of the data frequency has been performed, against the main features (stress, testing temperature, time to rupture) and the results are shown on Figure 45, Figure 46 and Figure 47. From Figure 45, it is obvious that the most of

the tests performed are in the short-time area, with the highest frequency in the region up to 2000 hours. Only few points are present in the normal creep design area of component life-time of 100.000-200.000 hours. Figure 46 shows the applied stress frequency, where it is obvious that the normal creep limits of 100-130 MPa at 540°C, are in the lower left part of the applied stress frequency diagram, which is in line with the Figure 45 – i.e. higher levels of stresses are leading to the shorter times to rupture. Finally, Figure 47 shows temperature distribution, where it is obvious that 3 main target temperatures of 500, 550 and 600°C take up most of the test numbers. These three diagrams clearly demonstrate the gap between creep testing and design in creep region – i.e. the long-time properties are usually derived from short-term creep tests on much higher stress levels. Temperature coverage is, in contrast, equivalent to the design application of the material, suggesting the isothermal nature of testing approach applied for the testing.

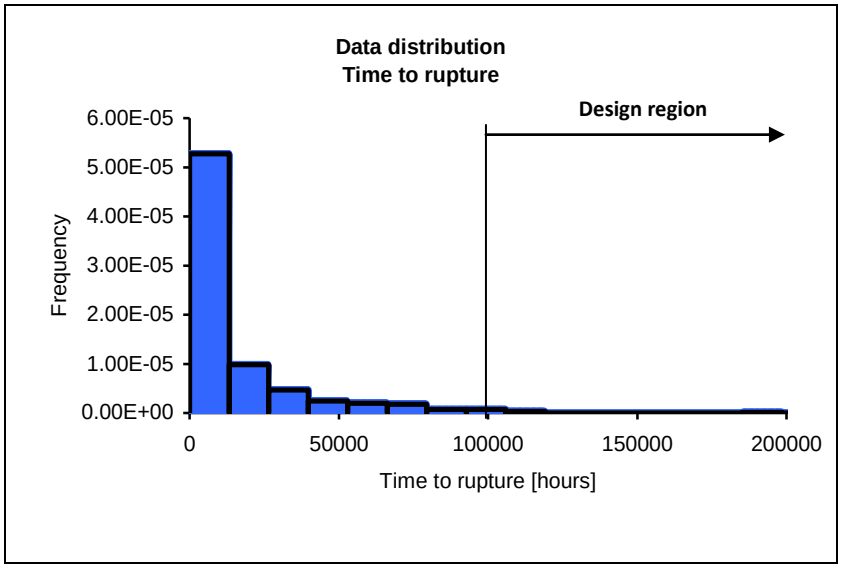

Figure 45: Distribution of time to rupture data points vs. design region

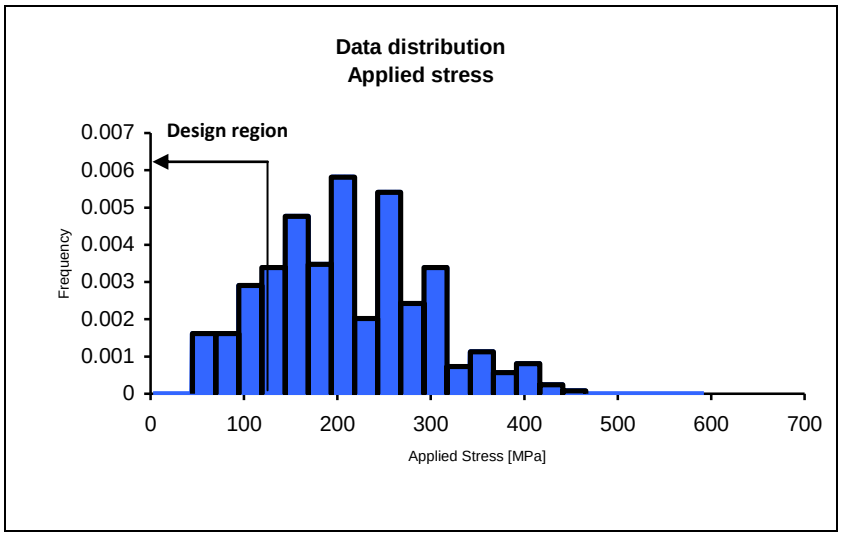

Figure 46: Distribution of applied stress vs. design region

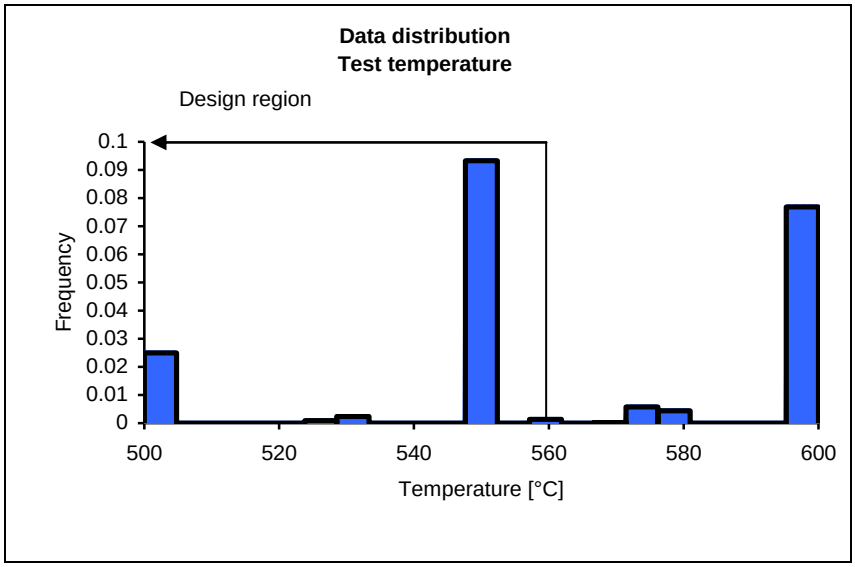

Figure 47: Distribution of temperature of test vs. design region

Figure 48 shows the plots of individual features presented against logarithm of time to rupture. As expected, the graphs show no easily identifiable correlations, with the only exception being the quite start dependency between time to rupture and time to strain of levels 0.1, 0.5 and 1%, where the dependency gets stronger with the strain level increase, i.e. 1% strain vs time to rupture.

Rupture time has better correlation than 0.1% strain. Furthermore, the dependency between applied stress and time to rupture is relatively strong, although not so strong as if only one temperature level would be selected.

The main reason for this analysis was to visualize the inputs that neural network faces as input distribution. Full visualization (all features against other features) has been performed and total of 1260 graphs have been analyzed.

The most interesting correlations are shown on Figure 49. It is interesting to note the very strong dependence of the tensile properties at room temperature from tempering temperature, as well as strong dependence between R_m and $R_{p0,2}$ at

room and elevated temperatures. Also, dependency between different strain levels is strong, as shown on the example of 0.1 vs. 0.5 % strain dependency.

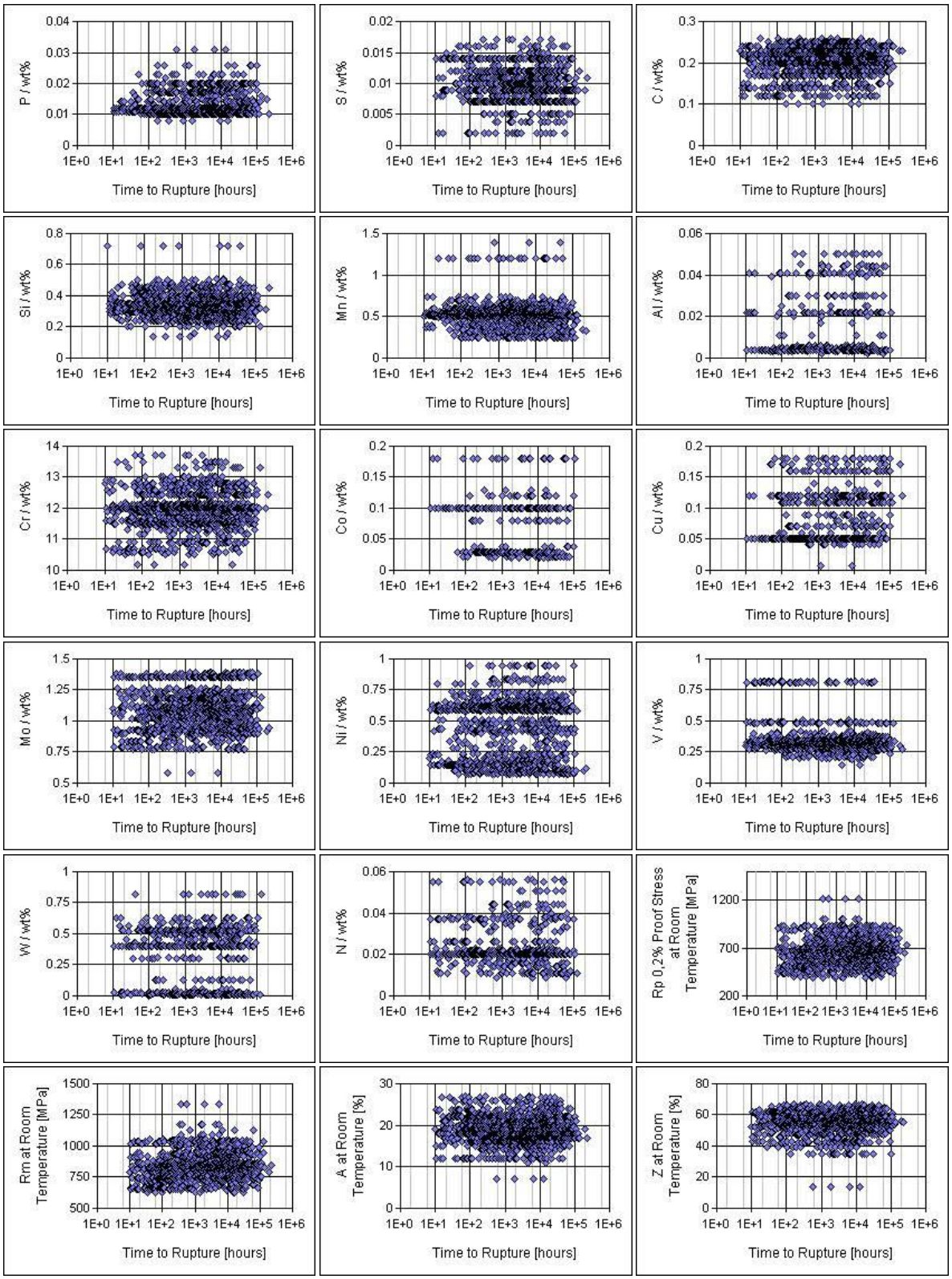

Figure 48: Distribution of different features against the time to rupture

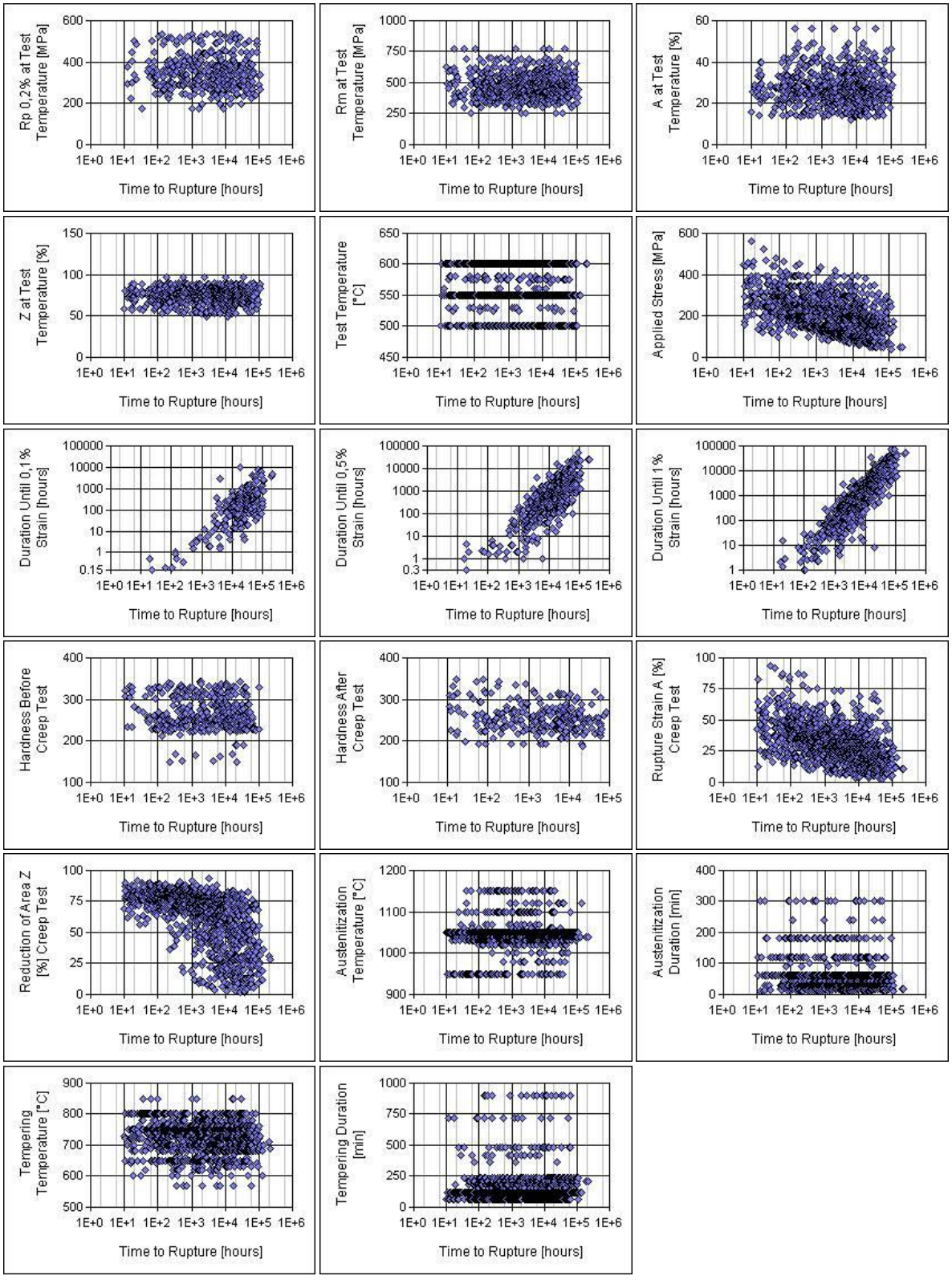

Figure 48: Continued

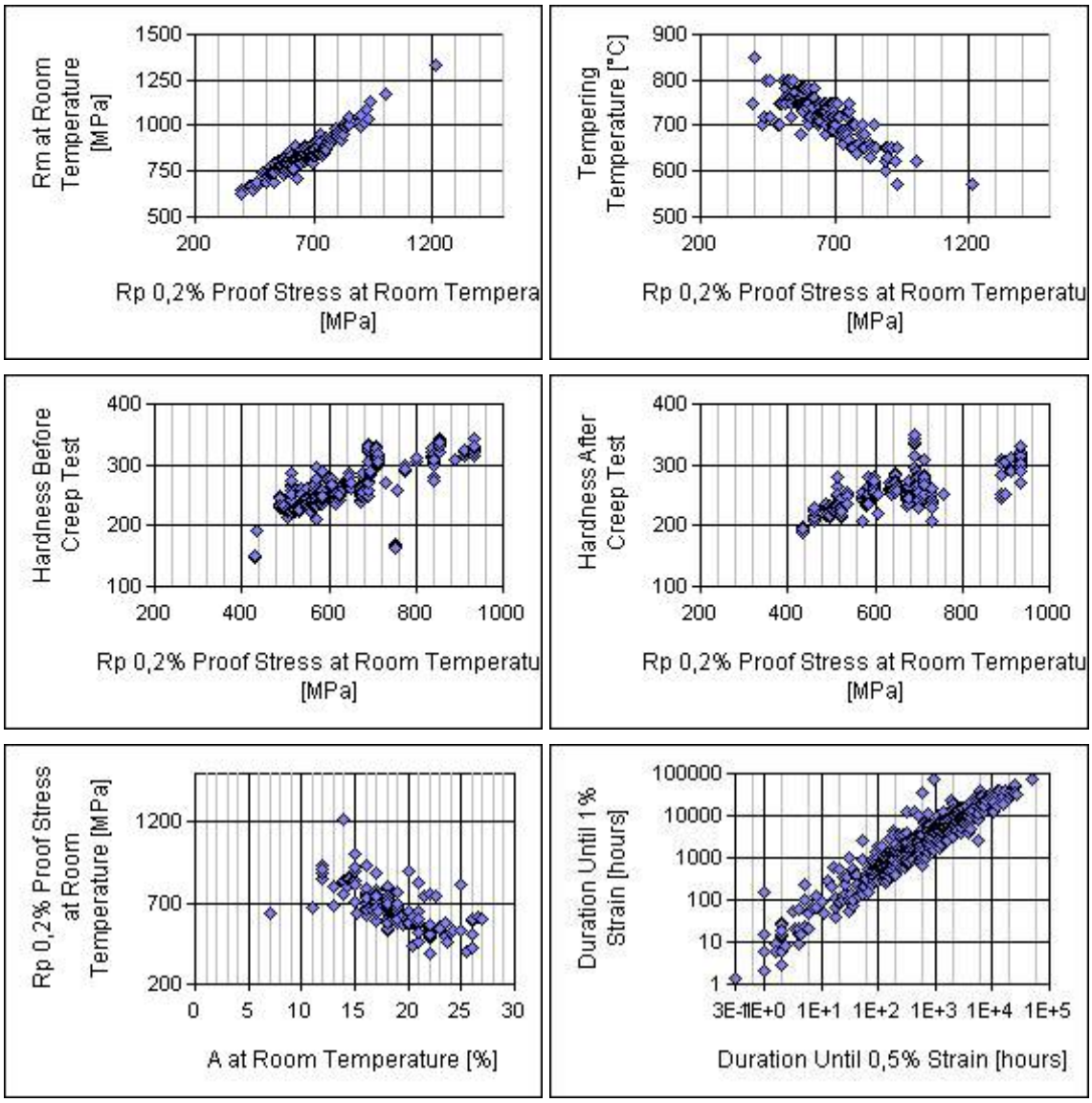

Figure 49: Other selected interdependencies from dataset

4.6 Modeling

For the modeling of the dependency of creep strength and/or time to rupture, multilayer perception (MLP) neural networks were used. These networks are build on layers and are having concise structure, therefore being easily adjustable to the complexity of the application – i.e. number of neurons, layers can be easily adjusted. MLP can be considered as a “black box” for the user, able to, trough training, find as good as possible dependency between input and output values, that are, at the same time, representing respectively input and output layers.

For the construction of neural networks the software program “DataEngine”, MIT GmbH Germany [DataEngine 02] was used. The process of building the network was performed trough following steps:

1. definition of inputs and outputs and their normalization, if needed
2. definition of training, test and recall data subsets
3. definition of network structure – number of hidden layers and neurons, transfer functions
4. adjustment of learning parameters – learning rate, moments, stop conditions
5. training of the network – training procedure, stop conditions
6. validation of the network – using the data that is not included in the training set, in case of unsatisfactory results new start of training with modified parameters
7. Implementation / use of MLP, once that learning process results are acceptable.

Since both time to rupture for the given stress as well creep strength for the given time to rupture can be considered as output values, for all defined data levels both models were trained. As a result, **12 data models have been constructed**, six for each of data levels, with 2 alternative outputs (either time to rupture or creep rupture strength).

Once the MLP have been constructed, it can be used for calculations – determination of outputs based on inputs; variation of input parameters is usually in the same borders as they were defined in the input dataset.

The results can be graphically represented and analyzed. To this purpose, the software provides tools that can be used for calculation, variation and sensitivity analysis of the model. With those tools one can analyze how much the variation in the input parameters changes the values of output parameters (i.e. time to rupture, rupture stress). For visualization of those influences, following graphical options are available:

- Minimum / Maximum Graph

  This graphical representation shows the rate of change of the outputs (time to rupture, rupture stress), in dependence of input variables - Figure 50. This variation is performed around the selected working point (i.e. one of the datasets), or around new, user-defined data point (by inputting the individual data in the interface). It shows the effect of variation of each of the inputs in its predefined range on the output (in the case on Figure 50, it is rupture strength). It is a horizontal, non-ordered tornado diagram used normally for assessment of sensitivity of outputs on inputs change. It is to be noted that the resulting variations are point-specific, i.e. for other data points it changes slightly, as it is 2D representation of n-dimensional space.

- Curve-plot

  This graphical representation, Figure 51, shows the change of the output variable over the percent change/variation of individual inputs. Percent change represents the change inside the validity borders of the input variables, defined at the setup level of the neural network. Again, this is done around the current data point, and the 0% value represents the current value for the given data point; and the appearance of this diagram changes slightly with the data point, as, again, it represents a variation of variables in n-dimension space in two dimensions. The percent variation is, as already mentioned, related to the range of validity of the input variable – for example, if the C content is being varied between 0.11 and 0.29%, and the current value is 0.20, then the variation for C content is possible in the both directions of 50% (0.09 down and 0.09 up in percentage weight content).

- Sum of differentials graph

  In this type of chart, for each input the derivations occurring when the input is changed are added up. The resulting totals are displayed in a bar chart - Figure 52.

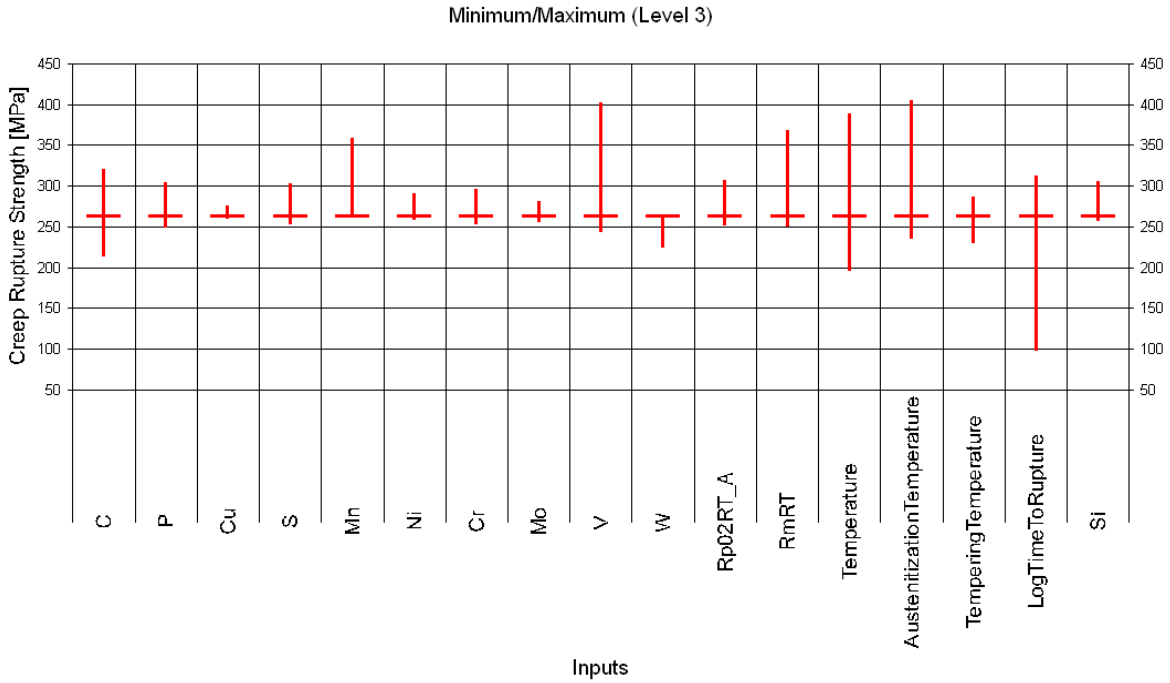

Figure 50: Graphical representation of minimum and maximum of the output variable, based on changes/variation of individual inputs

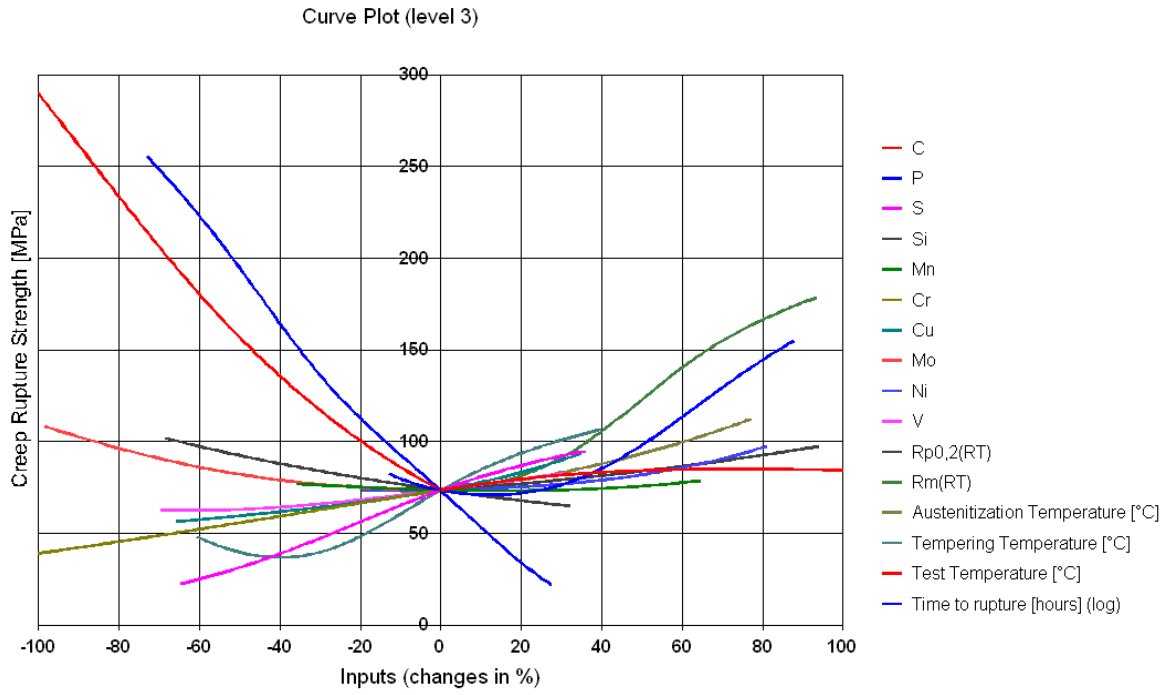

Figure 51: Change of output parameters in dependence of input variable variation in percentage (relative to the minimum and maximum of the input variable)

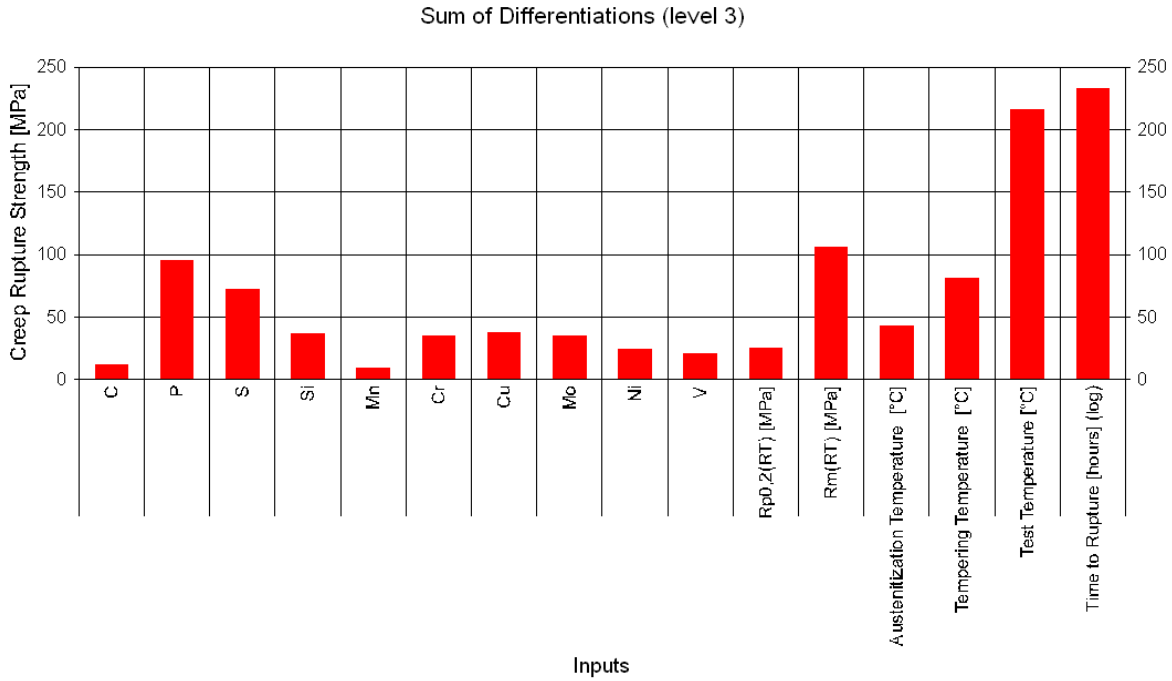

Figure 52: Sum of differentials graph

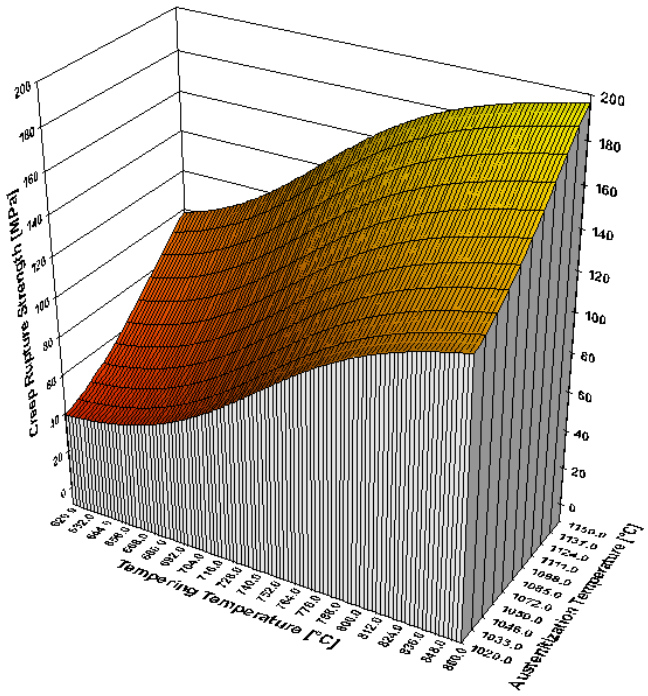

Figure 53: Creep Rupture strength in dependency of tempering and austenitization temperature

While using sensitivity analysis to determine how much single input variation influences the change of outputs (either time to rupture or creep strength), the analysis of the exact influence of each of the inputs on the outputs is only to be determined

using examples / concrete input of data. The visualization of the process is again linked to only one or two dimensions (Figure 53, showing the dependency between creep strength, austenitization and tempering temperature), while the exact change is again dependent on the influence of all the factors, and varies from one point to another. It is to be noted that the variations between the influence graphs for different data points usually keep the same tendency. Therefore it is useful to check the dependencies for each of the data points analyzed. This can be done quite conveniently with the DataEngine program.

4.7 Influence of the data structure on the model

One of the basic prerequisite for the modeling using neural networks is existence of enough representative data. Furthermore, the data reliability and accuracy influences the quality of the results. One of the best measures of the quality of the neural network model is the correlation coefficient as well as the graphical representation of modeled and measured values. To this goal, the Figure 54 to Figure 65 show the values of time to rupture vs. predicted time to rupture and creep rupture strength vs. predicted creep rupture strength. Correlation coefficient is a measure of the dependency between model and experimental values. As higher, or closer to, values of 1 or -1 it comes, the dependency is higher. If the values is 0, then it means that virtually no correlation between x and y values exists.

It is generally to note that the correlation coefficient for creep rupture strength higher lies higher as for the time to rupture, Figure 66.

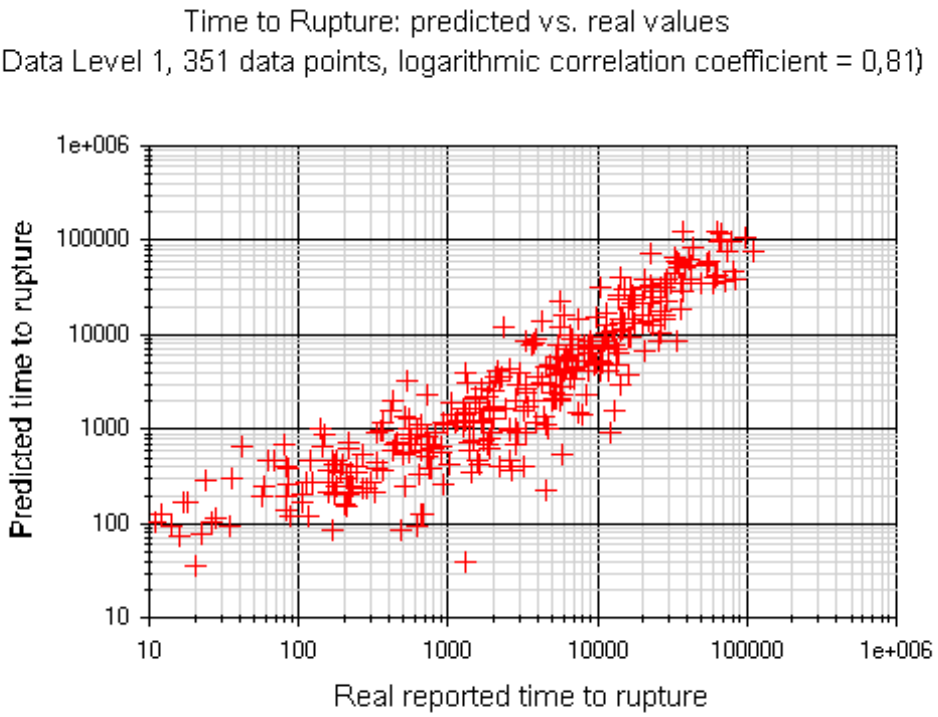

Figure 54: Comparison of model and experimental values, data level 1, output variable time to rupture

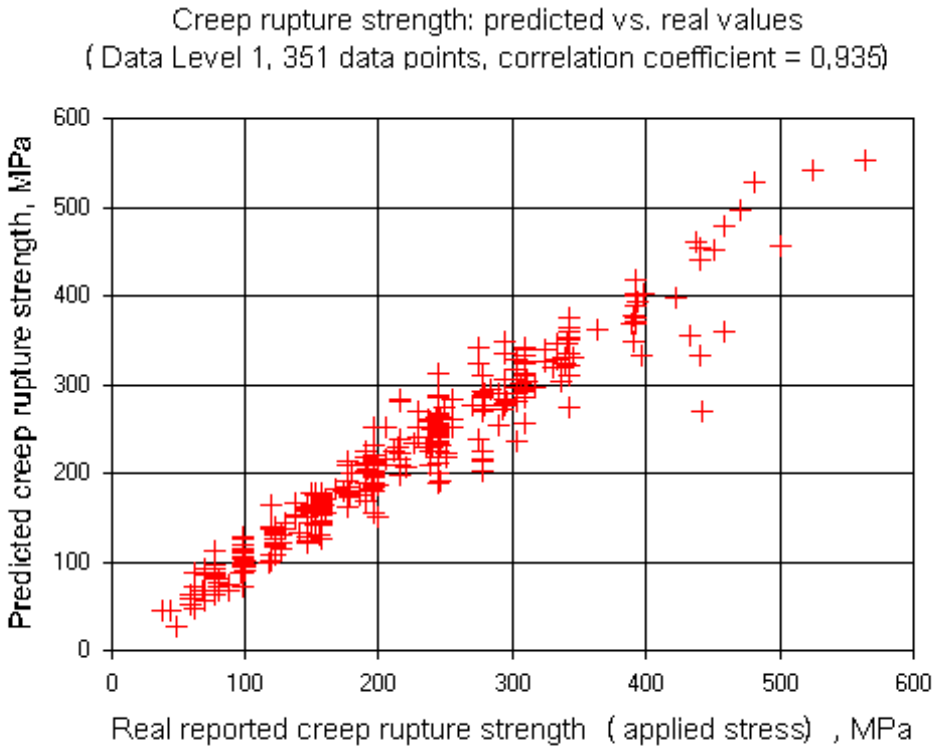

Figure 55: Comparison of model and experimental values, data level 1, output variable creep rupture strength

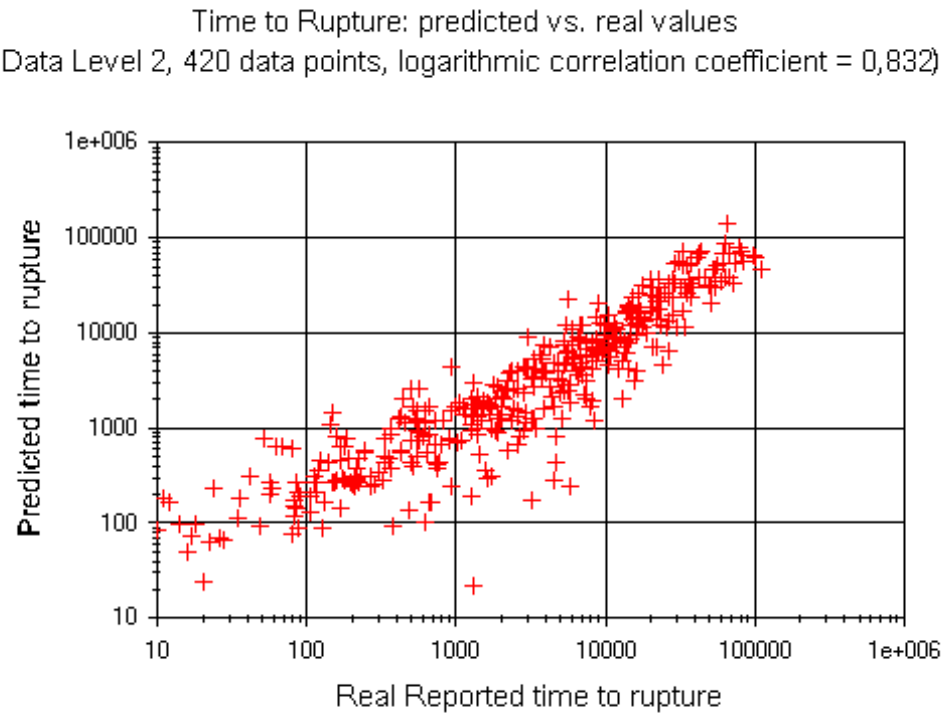

Figure 56: Comparison of model and experimental values, data level 2, output variable time to rupture

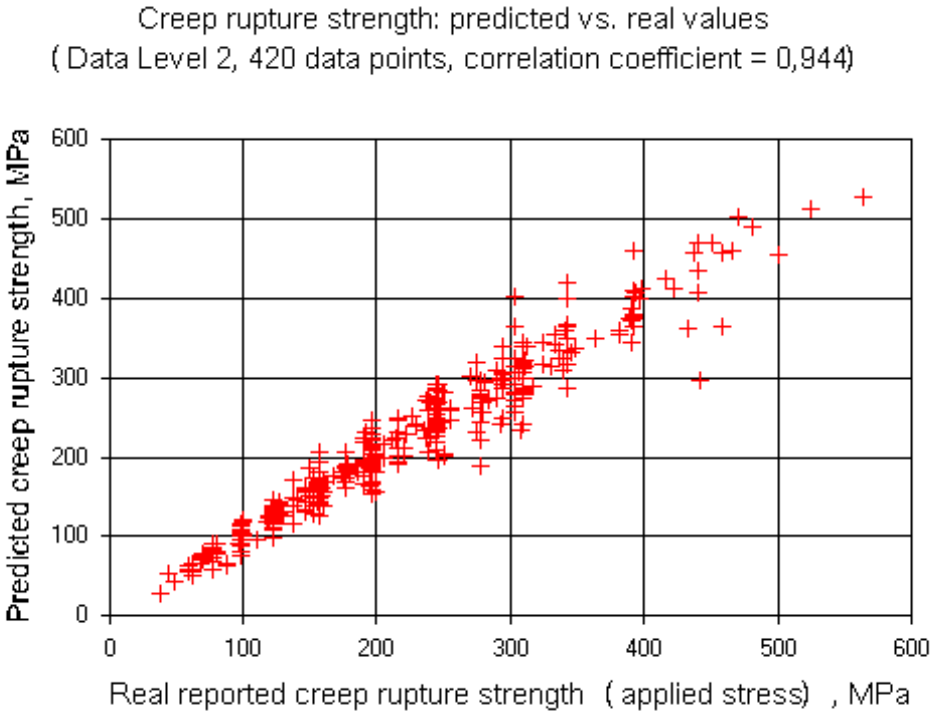

Figure 57: Comparison of model and experimental values, data level 2, output variable creep rupture strength

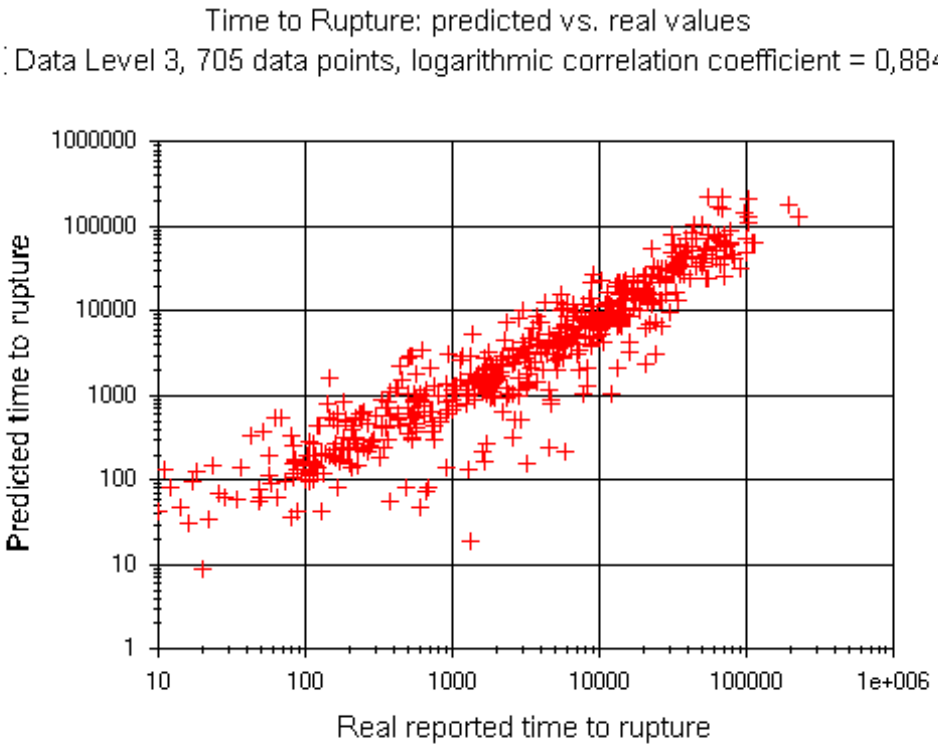

Figure 58: Comparison of model and experimental values, data level 3, output variable time to rupture

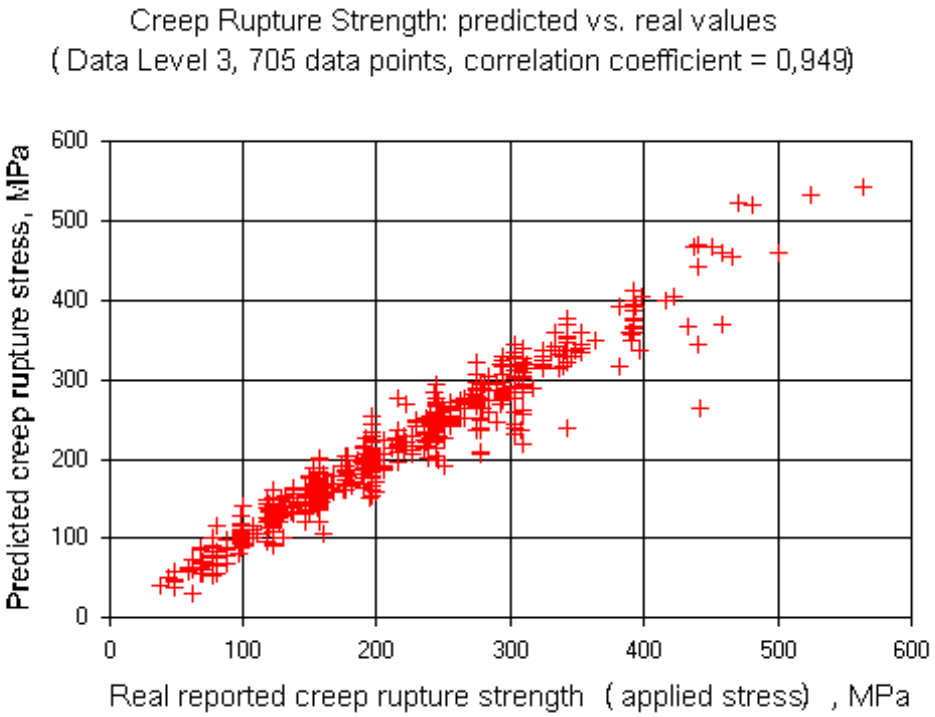

Figure 59: Comparison of model and experimental values, data level 3, output variable creep rupture strength

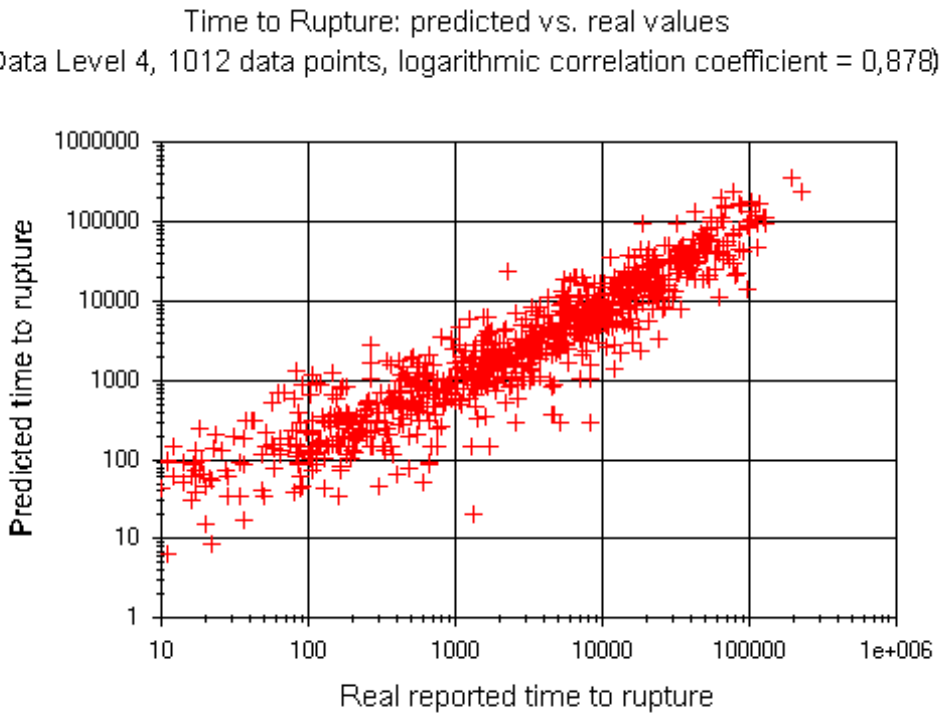

Figure 60: Comparison of model and experimental values, data level 4, output variable time to rupture

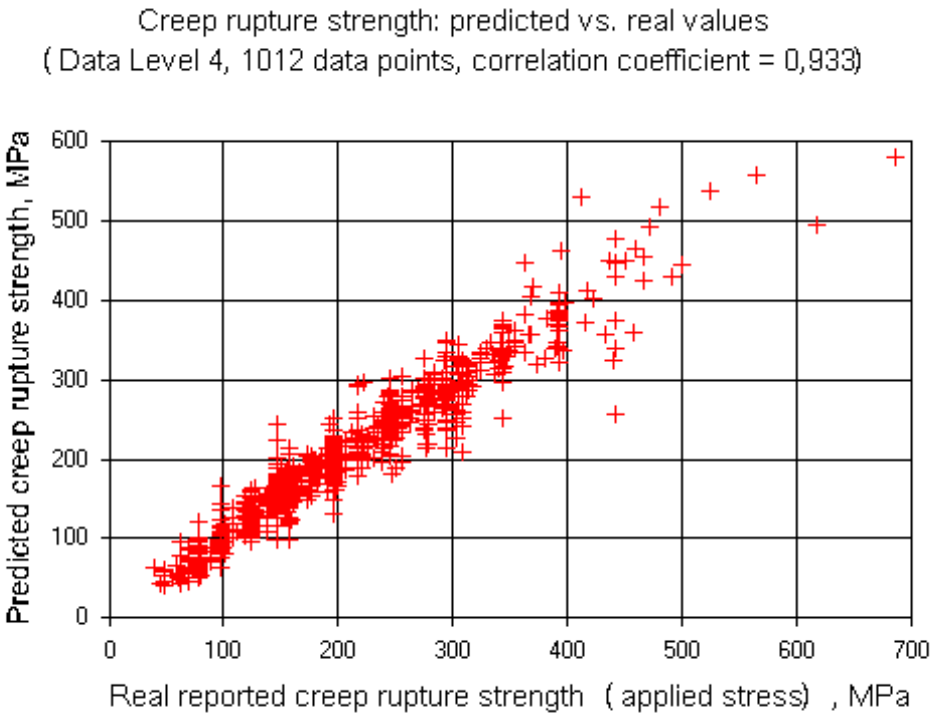

Figure 61: Comparison of model and experimental values, data level 4, output variable creep rupture strength

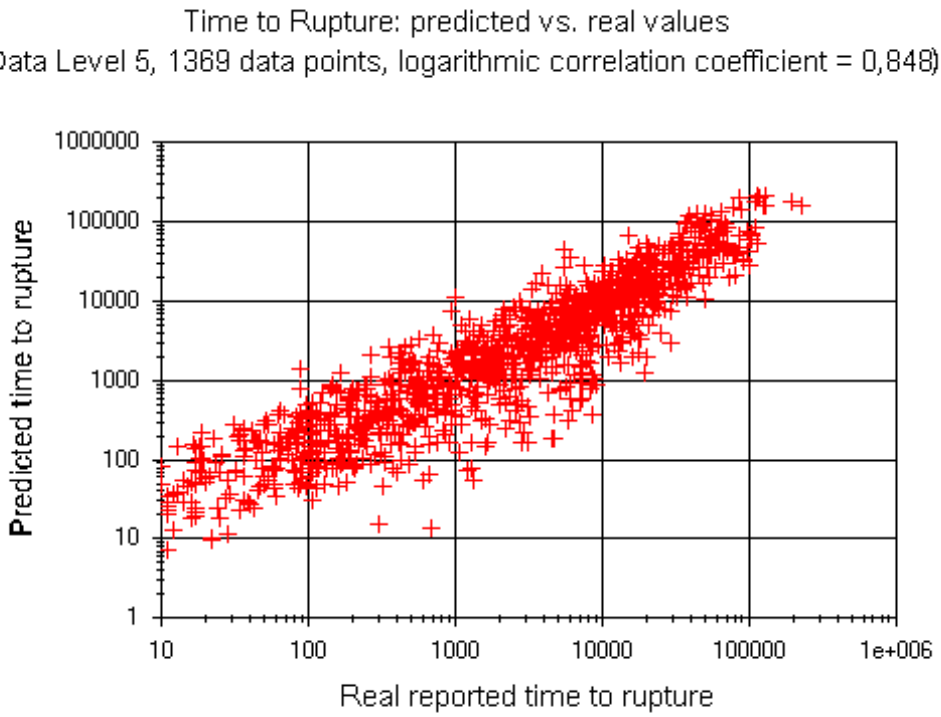

Figure 62: Comparison of model and experimental values, data level 5, output variable time to rupture

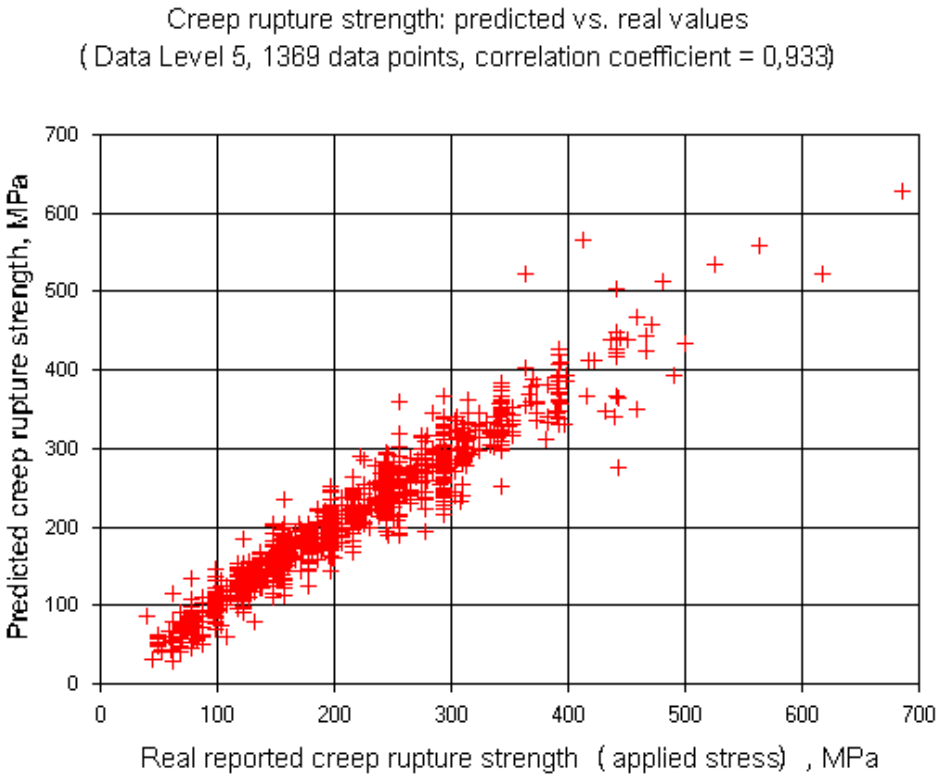

Figure 63: Comparison of model and experimental values, data level 5, output variable creep rupture strength

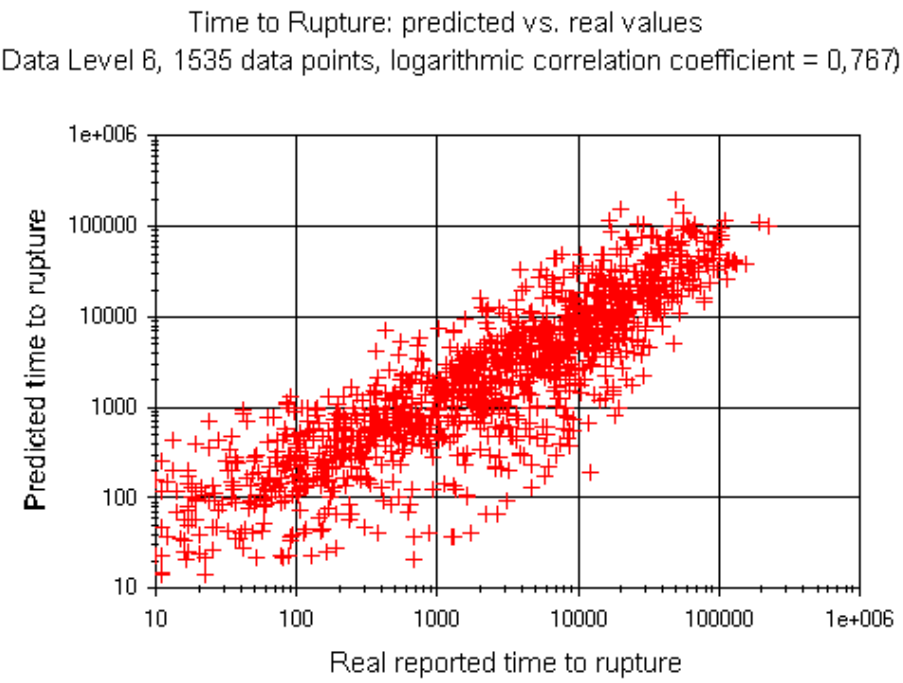

Figure 64: Comparison of model and experimental values, data level 6, output variable time to rupture

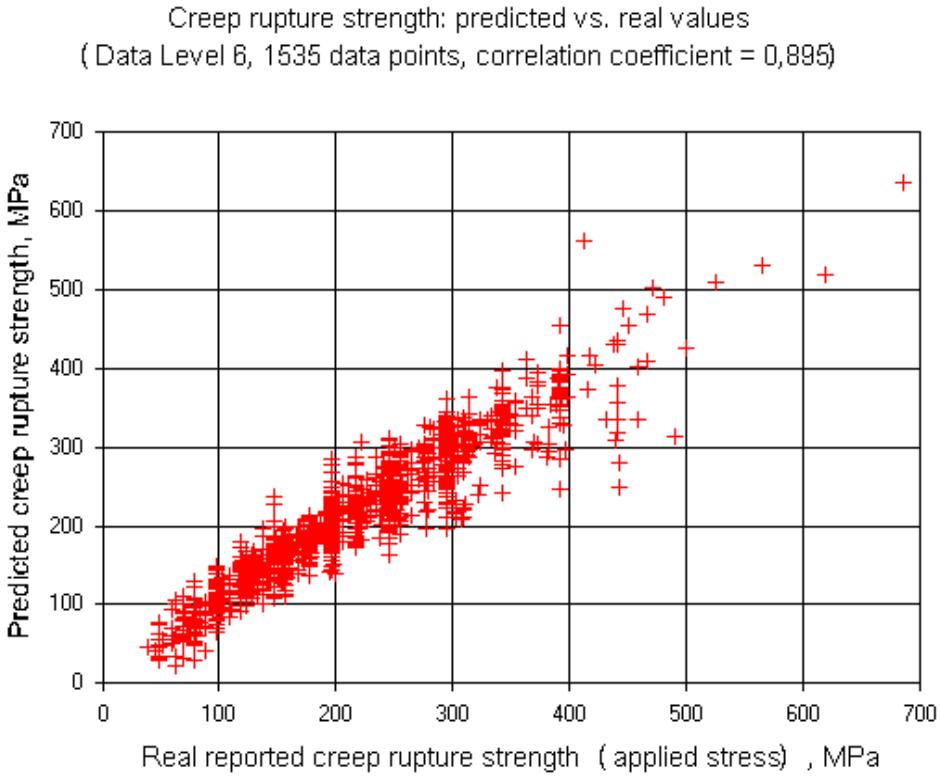

Figure 65: Comparison of model and experimental values, data level 6, output variable creep rupture strength

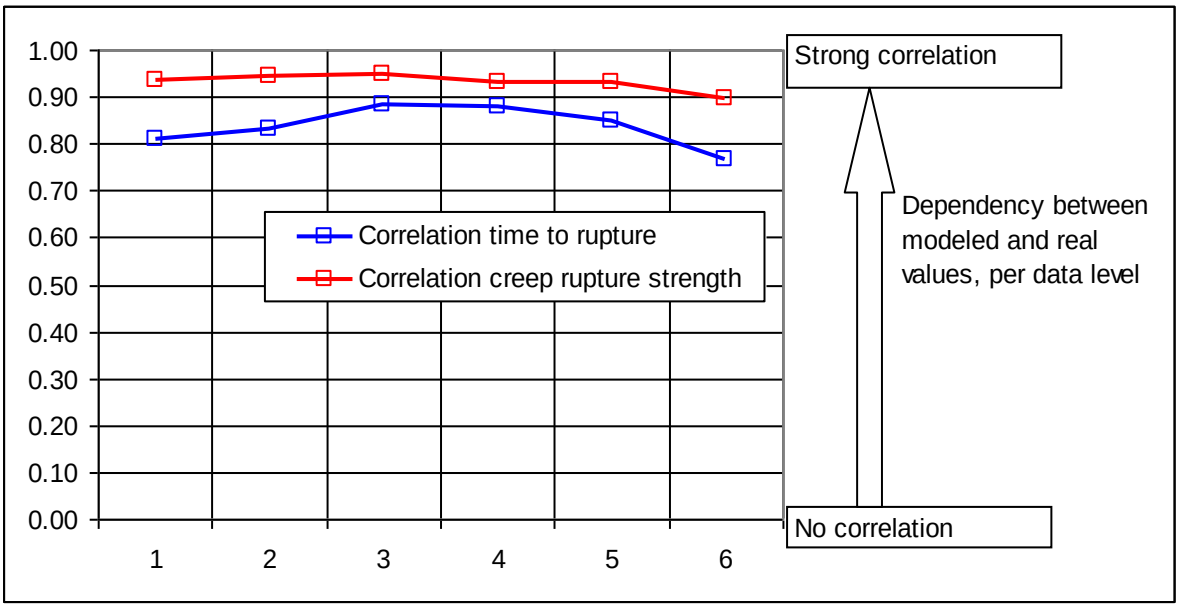

Figure 66: Correlation between model and real outputs

As a consequence of the analysis, it is obvious that the best results have been achieved for the data level 3-4, i.e. this data level represents the optimum of available data points and features considered. Data level 6 has smaller number of features, and the networks are not able to predict the variations in behavior based on the available features. On the other hand, data levels 1 and 2 contain too few data points for a reliable modeling of the outcome based on too many features.

4.8 Verification of Neural Network models

From the i.e. Figure 63, - creep rupture strength for the data level 5 temperatures between 500 - 600°C, it is visible that in the technically significant area (creep rupture strength less than 200 MPa), the data scatter is relatively small, which, in consequence, means that the models deliver relatively good prediction in this range.

The functional application of the neural networks is applied on the selected cast analyses. To this goal, the inputs of the individual cast analyses are inputted, and then the corresponding input (stress for output time to rupture or time to rupture for output creep rupture strength) is varied for same values as in the individual tests and for selected standard values (i.e. time to rupture 10.000, 100.000 hours). Then, the predicted values are plotted against measured values, and the corresponding standard values, with the defined standard scatter band of ±20% is also

plotted, in order to visually access the behavior of the individual cast analysis against the trend established for the whole population.

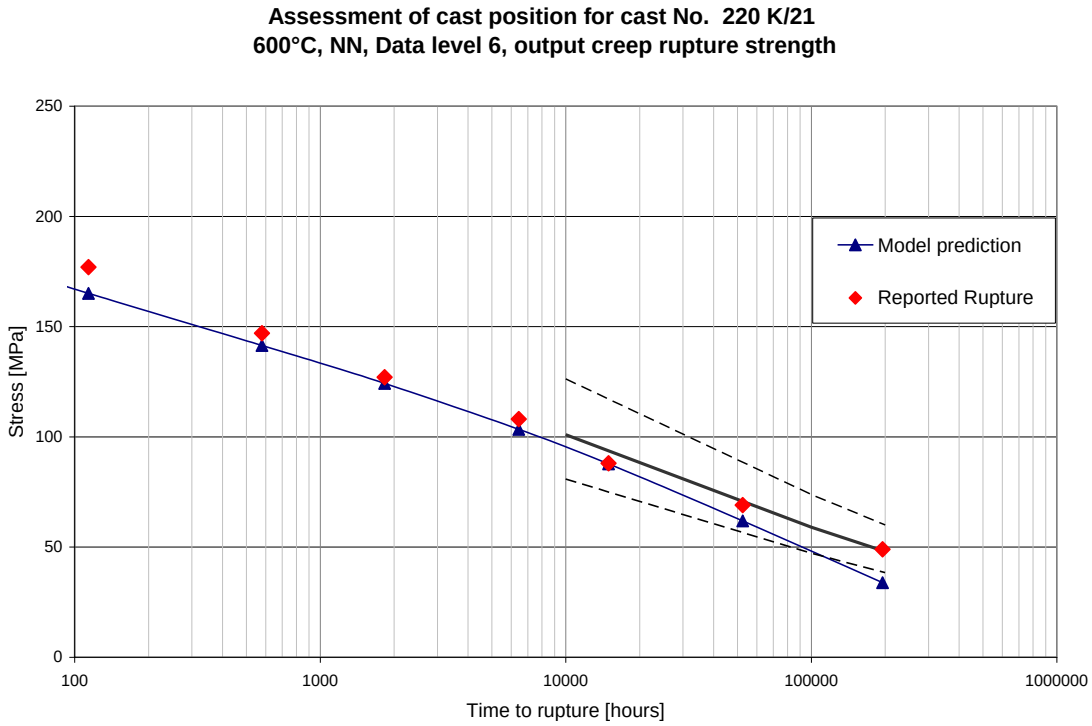

Figure 67: Comparison of model prediction (▲), experimental data (◆) and average creep rupture strength values and corresponding scatter band of the material X20CrMoV11-1 (thick and dashed lines), cast analysis 220K/21 – 600°C, data level 6

Figure 67 shows good prediction of the properties compared with the experimental values, especially in the short-term range. This is also a result of the fact that this data set has small scatter of the points, i.e. homogeneity of the data is quite high. On the other hand, the prediction in the long-time range shows significant discrepancies.

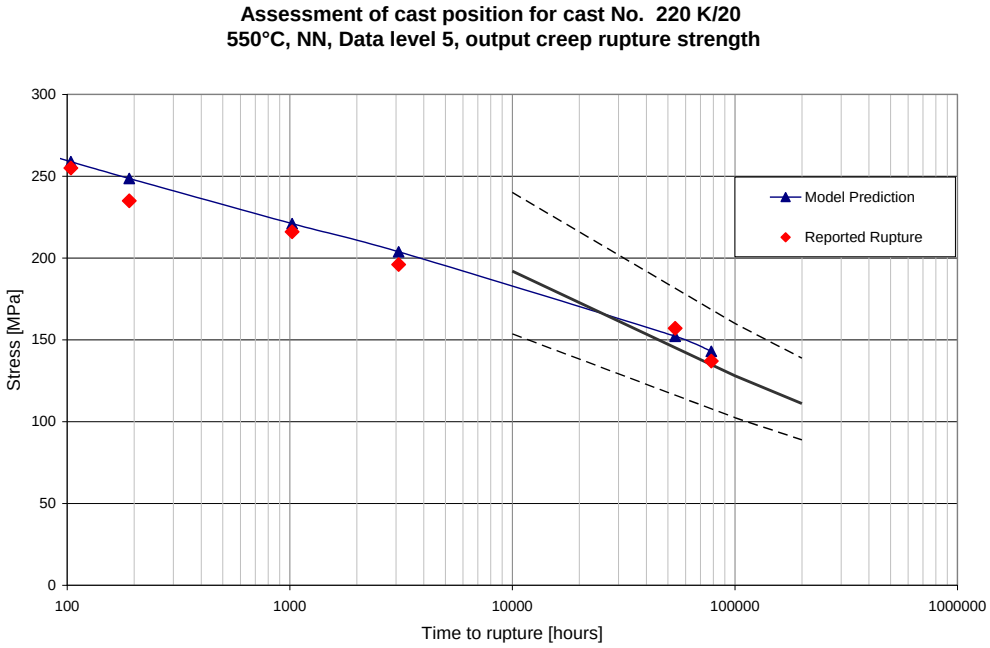

Figure 68: Comparison of model prediction (▲), experimental data (◆) and average creep rupture strength values and corresponding scatter band of the material X20CrMoV11-1 (thick and dashed lines), cast analysis 220K/20 – 550°C, data level 5

Figure 68 also shows very good agreement between model prediction and experimental data. In this case, it is to note that the general direction of the behavior of the cast has different behavior compared with the general population/standard values, resulting with the intersection of the standard line at about 30.000 hours.

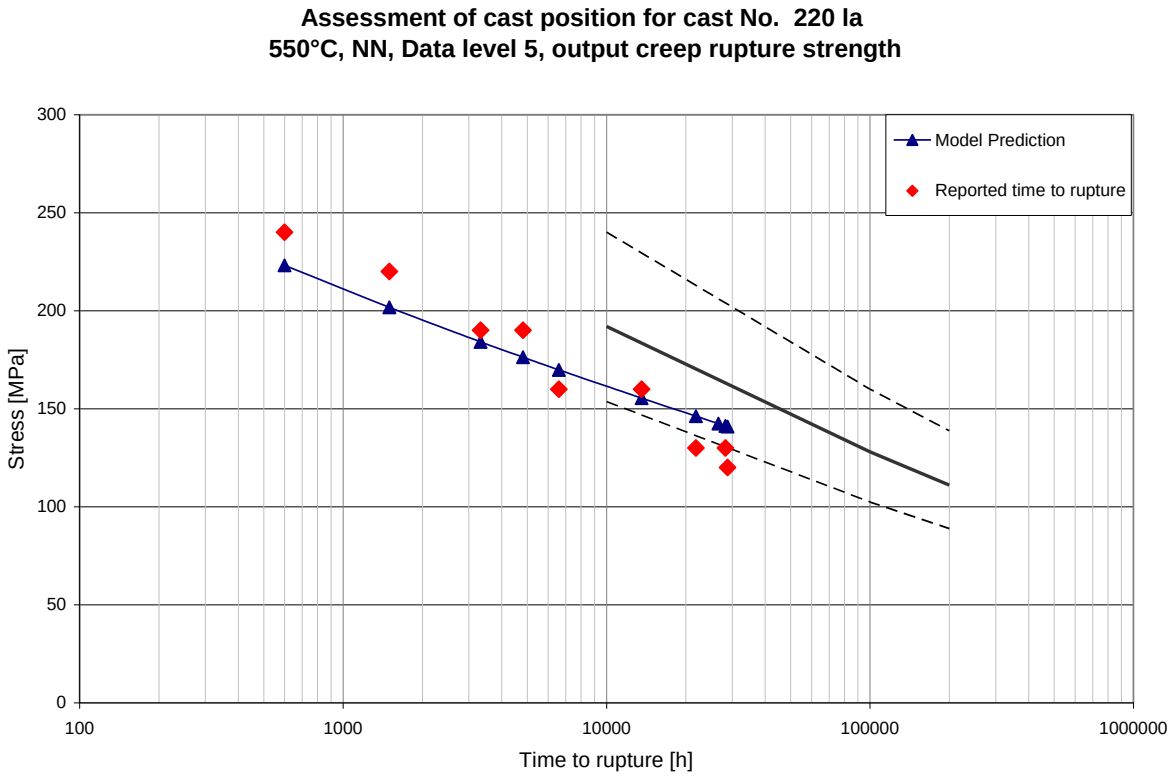

Figure 69: Comparison of model prediction (▲), experimental data (◆) and average creep rupture strength values and corresponding scatter band of the material X20CrMoV11-1 (thick and dashed lines), cast analysis 220 Ia – 550°C, data level 5

Figure 69 shows a cast is inhomogeneous. Although close, two data populations (one above and one below lower scatter band) is visible. The network tries to average the influences, and tends to be more conservative in the short-term, whereas the long-term data prediction is rather too high. This illustrates the effects of the existence of multiple data populations on the overall capability of the network, giving space for further improvement.

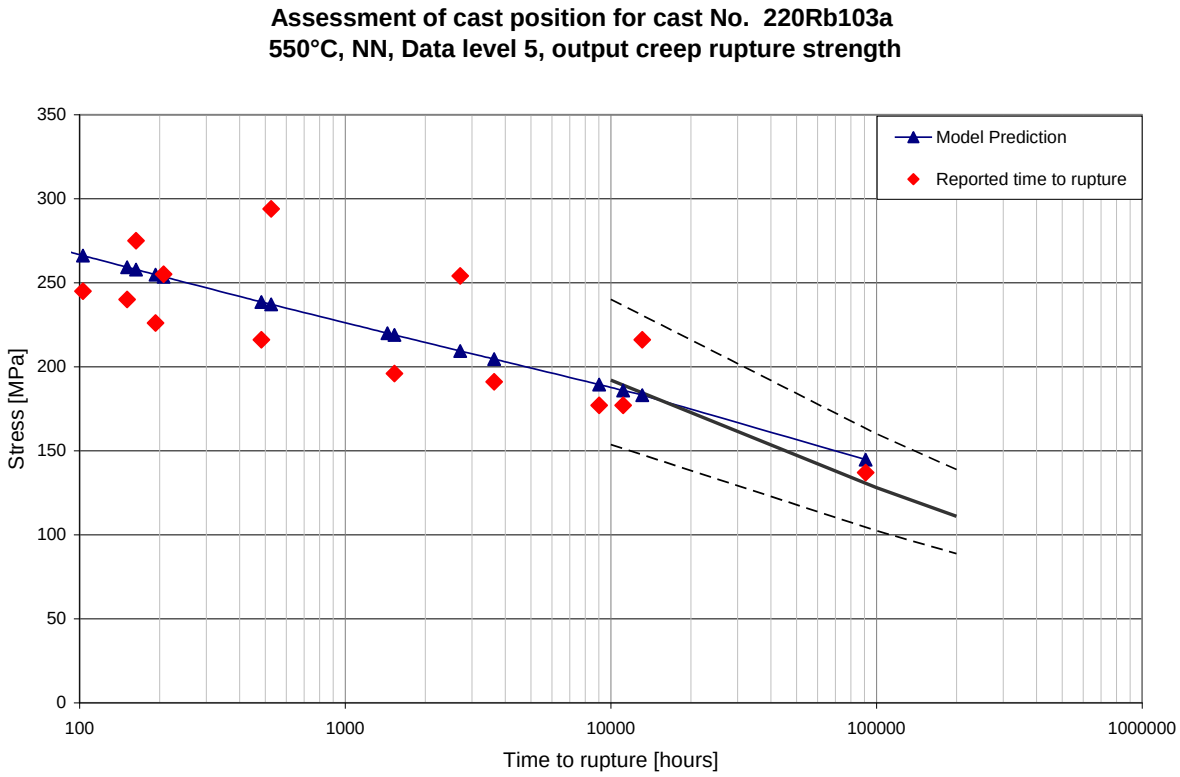

Figure 70: Comparison of model prediction (▲), experimental data (◆) and average creep rupture strength values and corresponding scatter band of the material X20CrMoV11-1 (thick and dashed lines), cast analysis 220 Rb103a – 550°C, data level 5

Data set shown on Figure 70 has rather high scatter in the short-time range. Additionally, it is to be noted that the distinct population of specimens are clearly visible (3 data points in the upper part of the diagram). Neural network tries to average all values, giving rather optimistic results for the overall population, but also conservative for the sub-population. This, again indicates existence of multiple data populations in the data set, stressing even more the need to tackle this issue.

Figure 71 shows a cast analysis that was not used either for training or verification of the neural network. The network clearly fails to predict the behavior of the cast inside the scatter band. It indicates an average cast, whereas the real behavior is clearly on the lower scatter bound, and below. However, assessment of the same cast position using the data level 3 neural network model shows that the network predicts the behavior of the cast, especially in the technically interesting range of long-time creep, quite well, i.e. it indicates that the cast position lies under the lower scatter bound - Figure 72.

These examples clearly demonstrate following:

1. neural network can be used to predict the position of the cast inside the scatter band, i.e. to indicate the trends, especially in the long-time creep area, indicating that it can recognize the trends in the data, and even be used for limited extrapolation
2. simple models with small number of inputs (data level 5 and 6) are able to predict the behavior of the standard casts, they fail to do so for more complicated cases
3. inclusion of additional characteristics of the cast (data level 3) allows the neural network to predict the behavior of the more complicated cases, as demonstrated with the last example.
4. the trend of almost all casts, determined using neural network models shows different trend than given trough standard data; in some cases it comes to intersection with the average creep rupture strength line, leading to the higher values of the predicted creep strength in the long-time range
5. multiple data populations within single casts exist, influencing the ability of the network to accurately predict the behavior; therefore this should be considered in the training; or the existence of multiple populations should be made “known” to the network i.e. by flagging them (0 for base population, 1 for secondary population), or using other techniques such as fuzzy clustering.

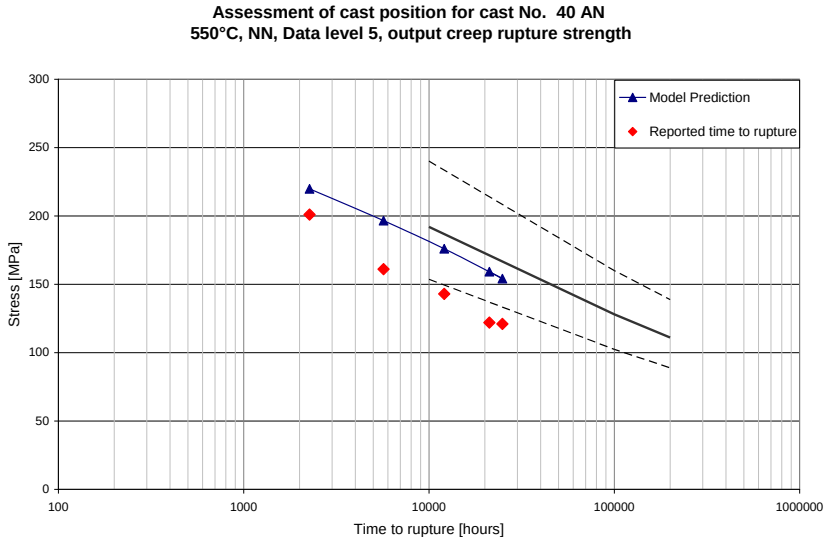

Figure 71: Comparison of model prediction (▲), experimental data (◆) and average creep rupture strength values and corresponding scatter band of the material X20CrMoV11-1 (thick and dashed lines), cast analysis 40 AN – 550°C, data level 5

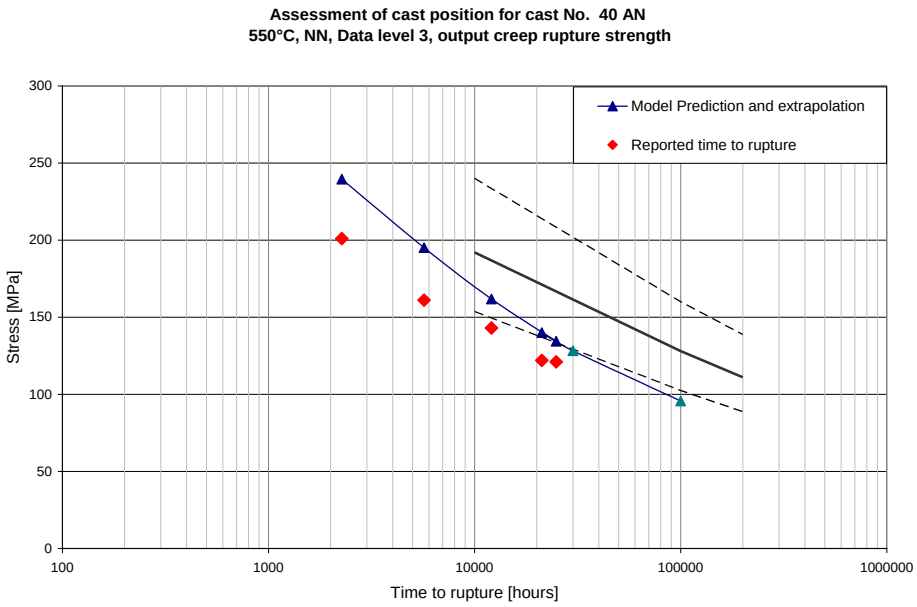

Figure 72: Comparison of model prediction (▲), experimental data (◆) and average creep rupture strength values and corresponding scatter band of the material X20CrMoV11-1 (thick and dashed lines), cast analysis 40 AN – 550°C, data level 3

For the optimization of the neural network models, the following elements deserve more attention:

- check the influence of the subpopulations – i.e. notched/smooth specimens on the results; remove notched specimens from the data pool
- check the general trend of single casts (isothermal method) against the standard data
- influence of single inputs might be better investigated if the analysis would be limited to single stress range(s) and temperature(s) – for example, the influence of each of the chemical composition elements on time to rupture. Also, clustering (i.e. according to the strength class as already discussed in 4.4.3) needs to be investigated.

5 Optimization of the model

The optimization of the model was done in the following steps:

1. Data for notched specimens has been removed (data set is reduced to 1302 data points), largely removing identified subpopulations in the cast data sets.
2. Data for W was set to be 0 for all the casts that do not contain W by specification, in order to include this element as important carbide-forming element into the analysis at all levels; it is safe to assume 0 or close-to-zero values for those specifications.
3. Isothermal curves for each of the cast analysis and temperature has been constructed, using the procedure as described in 3.3.2.
4. Time to rupture has been determined according to the constructed isothermal curves for applicable stress levels and interesting times to rupture. Non-compliant extrapolation (stress level more than 1.5 of the min/max in the data set, as well as more than 3 times maximum measured time to rupture) were not performed.
5. The dependency of creep strength and inputs has been assessed for fixed temperature and time to rupture, extreme influences have been remove and data set reduced to 982 points.
6. Clustering possibilities have been assessed
7. The networks were again trained with the selected data and with the standardized (isothermal data) for data level 6 and data level 3, and results presented and discussed.

5.1 Optimized data set

After the removal of the notched specimens, the number of available data sets for the analysis has been reduced – see Table 13, by percent more in the lower levels than in higher, i.e. data level 5 for the new data set has less (327) data points

then data level 6 of the original data set (351). This could be interpreted that the creep tests performed with notched specimens have been more documented and better prepared than those that did not involve notch effect testing.

Level 1 with 272 Datasets and 19 Features Level 2 with 327 Datasets and 17 Features Level 3 with 611 Datasets and 16 Features Level 4 with 868 Datasets and 15 Features Level 5 with 1177 Datasets and 13 Features Level 6 with 1302 Datasets and 10 Features	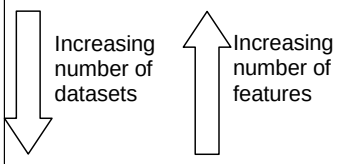

Table 13: Graphical representation of data grouping after removal of notched specimens

5.2 Evaluation of isothermal behavior of single casts

The available data has first been evaluated using isothermal method, and corresponding graphs have been plotted, in order to check if the behavior predicted by the neural network as shown in the Figure 68, can be repeated. Figure 73 shows that at temperature of 500°C, some of the casts, initially above the average line, have slope which is lower than the average line, thus, in cases of extrapolation from short-term creep towards long-term creep, they cut the upper-bound line. This kind of behavior is in conflict with the general notion that usually, in cases when the tests run longer, the cast behavior is such that those points would remain inside the scatter band. Further, the casts in the lower area of scatter band usually have very similar slope to the average (standard) line, showing plausible behavior. Both of the phenomena can be observed at 550°C - Figure 74. On the contrary, Figure 75 shows that the tendency of the single casts to behave differently than the average (standard) line decreases. Also is to note that some of the lines show other tendency than the overall population; this is mainly due to either small number of points available (3-4) and/or the cases when the number of points are concentrated around one stress level (i.e. the test being both iso-stress and isothermal). Those casts were not considered in the further examination with the application of isothermal lines.

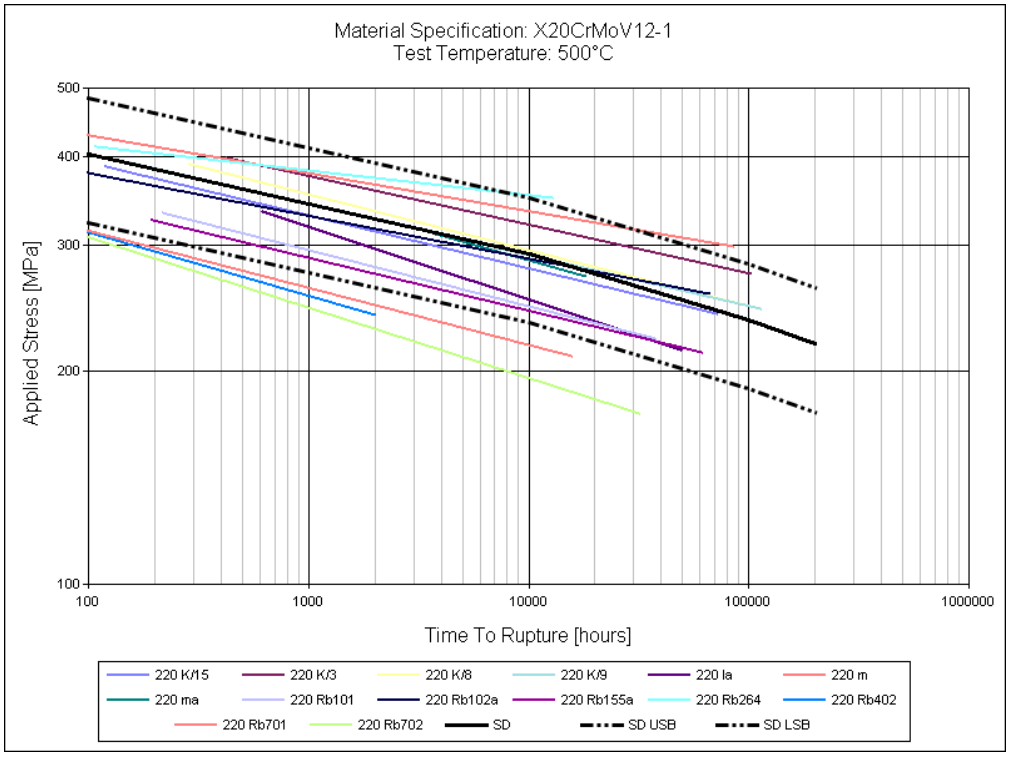

Figure 73: Isothermal lines for different casts compared to standard specification (SD), test temperature 500°C

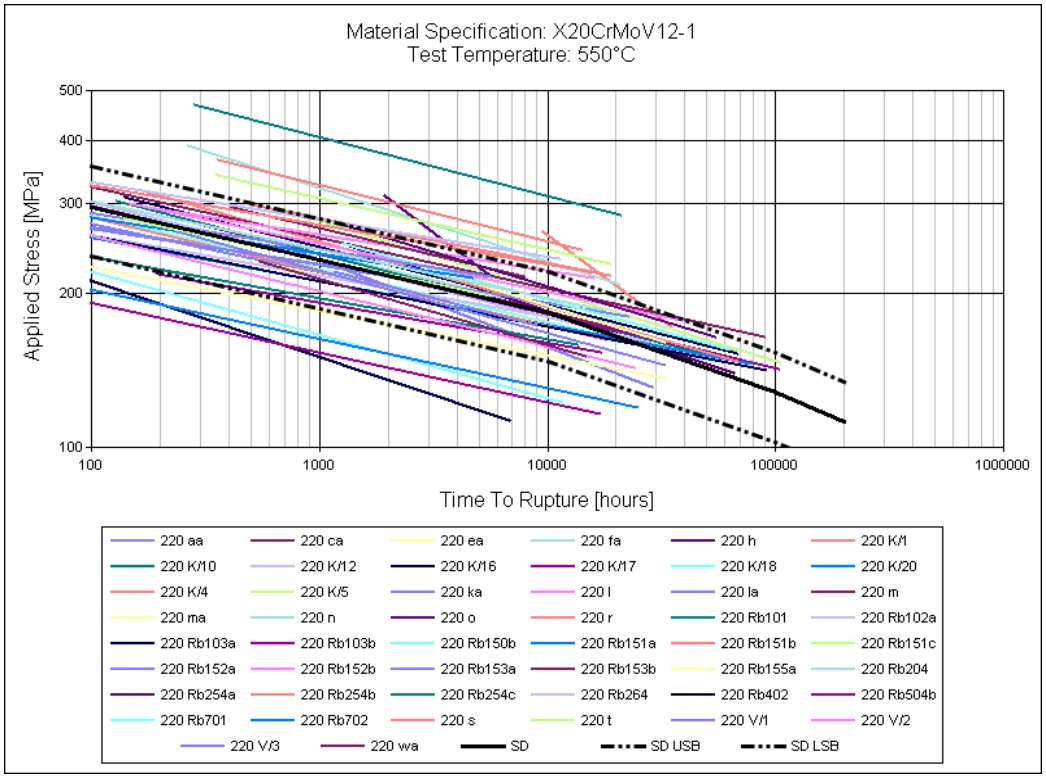

Figure 74: Isothermal lines for different casts compared to standard specification (SD), test temperature 550°C

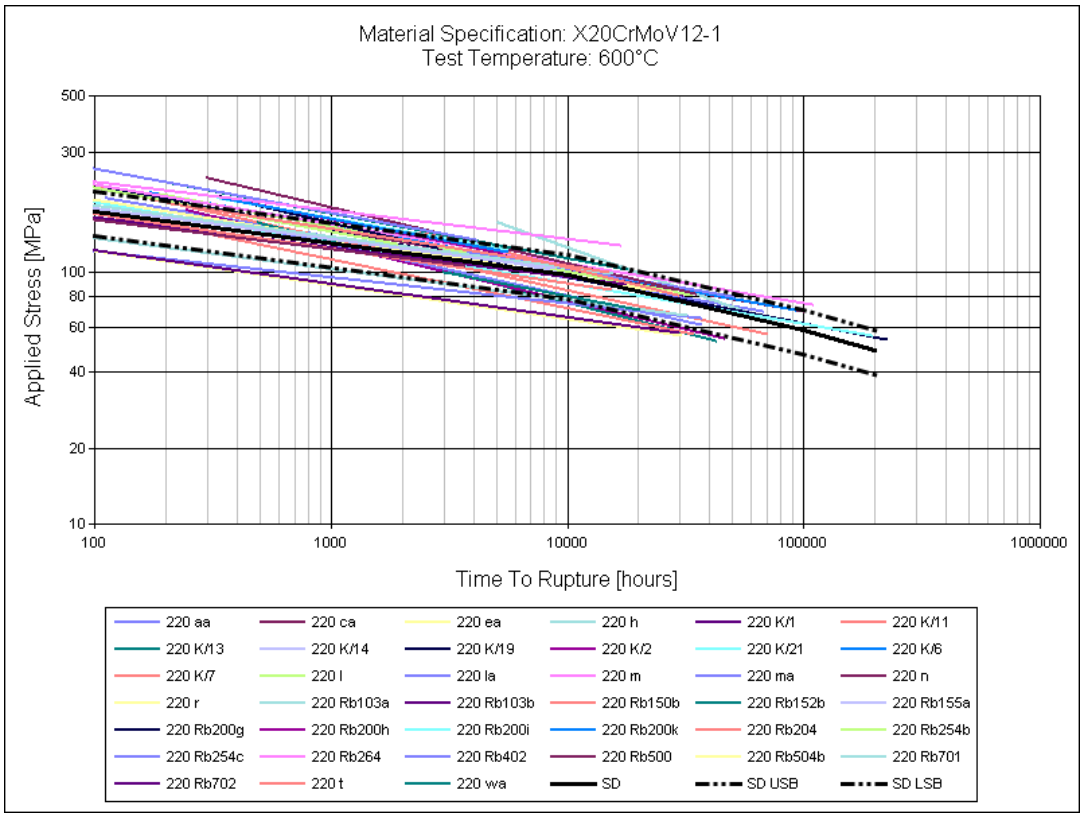

Figure 75: Isothermal lines for different casts compared to standard specification (SD), test temperature 600°C

As already demonstrated on Figure 69, neural networks generally follow the cast trend line, i.e. tend to have the same slope and intercept (simplified in linear form) as the cast itself. In order to obtain better results in the long-time creep area that is, as shown on Figure 45, very poorly covered with tests, two options have been explored:

1. Introduce the correction trough data modification
2. Use clustering of the data.

Both options have been explored and the results are presented here.

5.3 Analysis of Isothermal Coefficients

In order to assess the behavior of the casts in the scatter band, the regression coefficients for simplified isothermal lines were analyzed.

Both forms of possible isothermal regression were analyzed – simple logarithmic one and double-logarithmic:

simple logarithmic : $\sigma = A_1 + B_1 \cdot \log(t)$
double logarithmic : $\log(\sigma) = A_2 + B_2 \cdot \log(t)$
σ – applied stress [MPa]
t – time to rupture [hours]
A_1, A_2 – intercept
B_1, B_2 – slope

The analysis was done using both double-log scale and in normal-log scale (log for time, normal for stress). Casts showing deviant behavior (i.e. being outside the 2 sigma distance from the average value either by the intercept or slope parameter criterion, as well as casts showing poor data fit – i.e. R2 < 0.75 for linear and R2 < 0.975 in log-log scale) were removed. Overall, 12 cast analyses has been removed (220a, 120y, 220 Rb265b, 220 Rb155d, 220 Rb155e, 220 o, 220 K/1, 220/301, 220 Rb601, 220 n, 220 Rb 254c and 220 V/3, 220 s, 220 h), with approx. 130 creep tests. It is to note that from 14 removed cased analyses, 10 were having tempering temperature at or below specification (i.e. in the range of 570-680°C). Furthermore, one cast (220 h) was showing generally much steeper falling tendency while at the same time having the tempering temperature of 800°C – again outside the allowable range. This only stresses the importance of the appropriate heat treatment, as all of the removed casts were showing abnormally falling slopes, i.e. in order magnitude of 2, compared with the standard specifications for heat treatment.

Figure 76 shows the results of the removal of the casts as specified above. It is generally to note that the tendency of the lines remains flatter than the standard data. Furthermore, Figure 77 shows (linear, for sake of easier understanding of phenomena) that the tendency of the casts tends to remain the same compared to 550°C at 600°C, whereas the standard data suggests otherwise. Although the figure suggests otherwise, the comparison of mean values for slope and intercept for 500, 550 and 600°C - Figure 78, shows that there is a tendency in data to have almost linear behavior in the slope and intercept change over the temperature, the standard specification suggests otherwise; this might be seen as a consequence of analytical formula applied for determination of standard values, rather than different data set behavior. The standard specification suggests flatter curve at 600°C than the experimental data, thus making the standard specification too op-

timistic. The interception of the lines between standard and experimental data in both cases lies at about 560°C, which is about the limit of this steel's recommended application. This can be interpreted also in the following way: standard data tends to be more conservative than experimental data in the area of application (below 560°), when using isothermal method.

Figure 79 shows the same analysis as performed in normal-log scale in log-log scale. This figure suggests that the population has on average much milder slope than the standard data would suggests, in almost parallel direction (i.e. as if the standard data would be translated by a factor); on the other hand, the intercepts are decreasing with the temperature according to the averages for the experimental data, whereas the standard data suggests otherwise. This is mainly due to log-log nature of this regression – slope and intercept have power of base 10 nature in this scale. This can be also interpreted in such a way that in log-log space, standard data tends to be more conservative than the whole population, which confirms the recommendations to interpolate those values in double-logarithmic scale as defined in i.e. EN 12952-3:2001.

During this exercise it was found that for isothermal method application for this material, a normal-log scale gives better results that can be better interpreted. Also, with this it has been shown that application of parametric methods (i.e. Z-Factor) can be applied only punctually, i.e. for selected times and temperatures, as both the experimental data and the standard data do not have a constant ratio; this might be only the case as seen in the Figure 79, but that would mean constant ratio in logarithmic terms, not in the terms of absolute ratio as defined in 3.3.3.

Figure 80 shows calculated Z-Factor for a single cast, it is clear that in this case a constant dependency cannot be established, i.e. Z experimental/Z average is not constant, but varies in quite broad range from 0.8 to 1.05. However, application of Z-Factor on single temperature and single target time (i.e. 100.000 or 200.000 hours) has potential for application, i.e. using Z-Factor for target temperature and time for i.e. design or verification purpose is feasible.

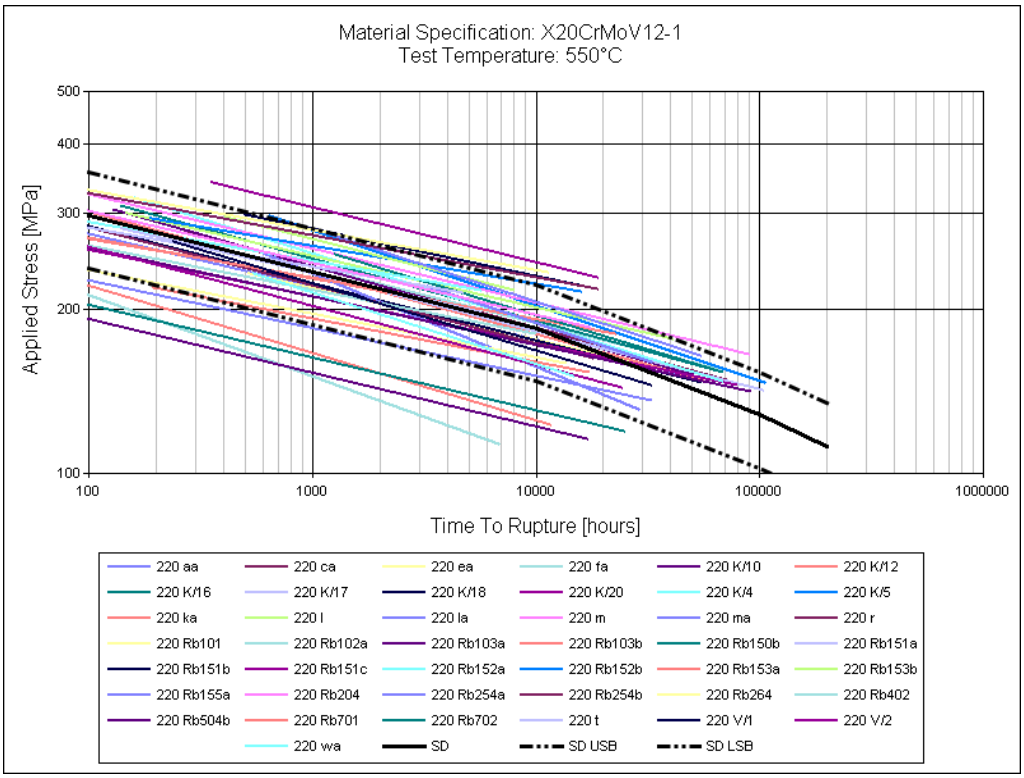

Figure 76: Isothermal lines for different casts compared to standard specification (SD), test temperature 550°C, after removal of extremes in regarding slope and intercept

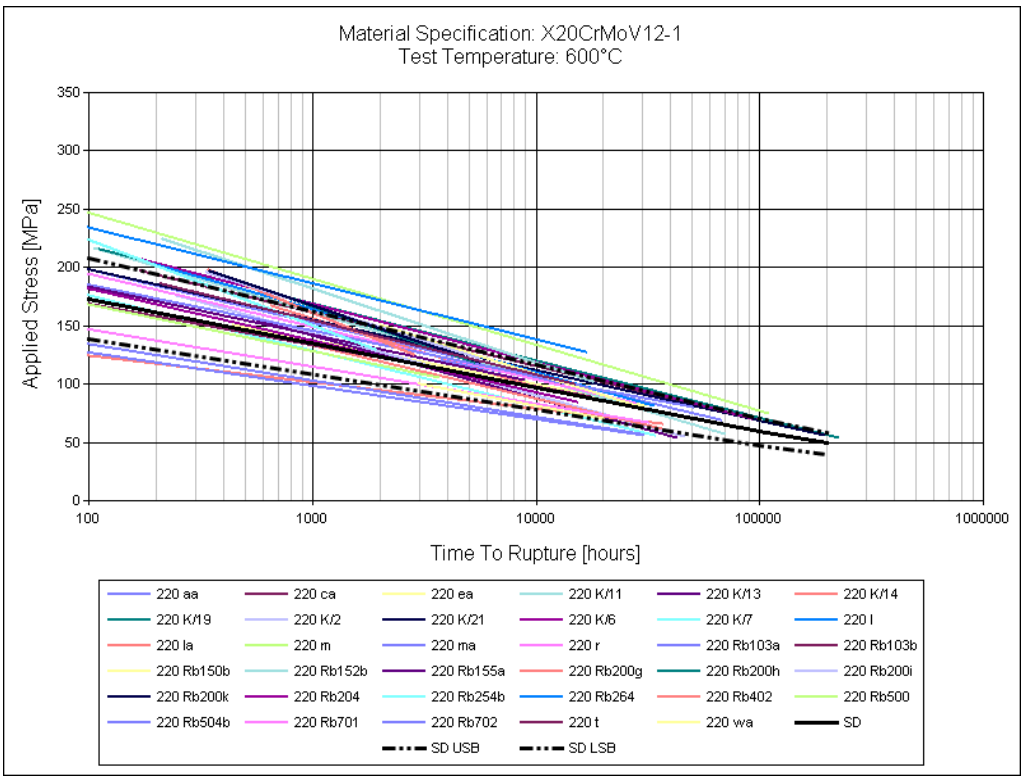

Figure 77: Isothermal lines for different casts compared to standard specification (SD), test temperature 600°C, after removal of extremes in regarding slope and intercept, linear representation

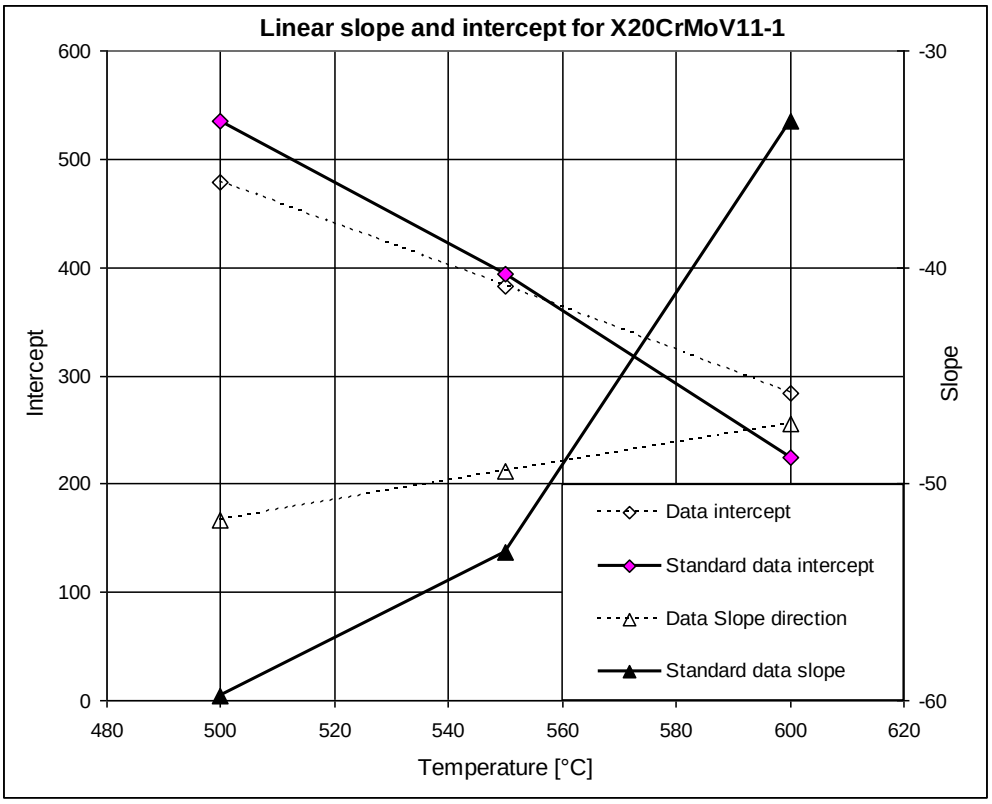

Figure 78: Comparison of standard and data population behavior for X20CrMoV11-1 specification, normal-log scale, formula y = A+B*log(x)

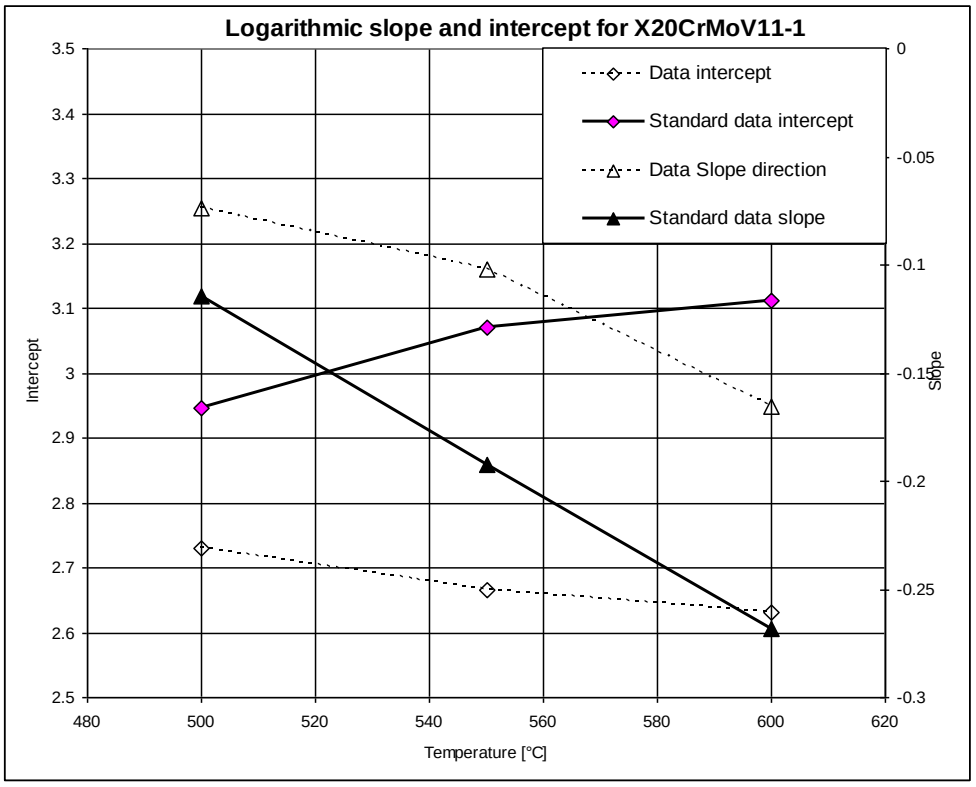

Figure 79: Comparison of standard and data population behavior for X20CrMoV11-1 specification, log-log scale, log(y) = A+B*log(x)

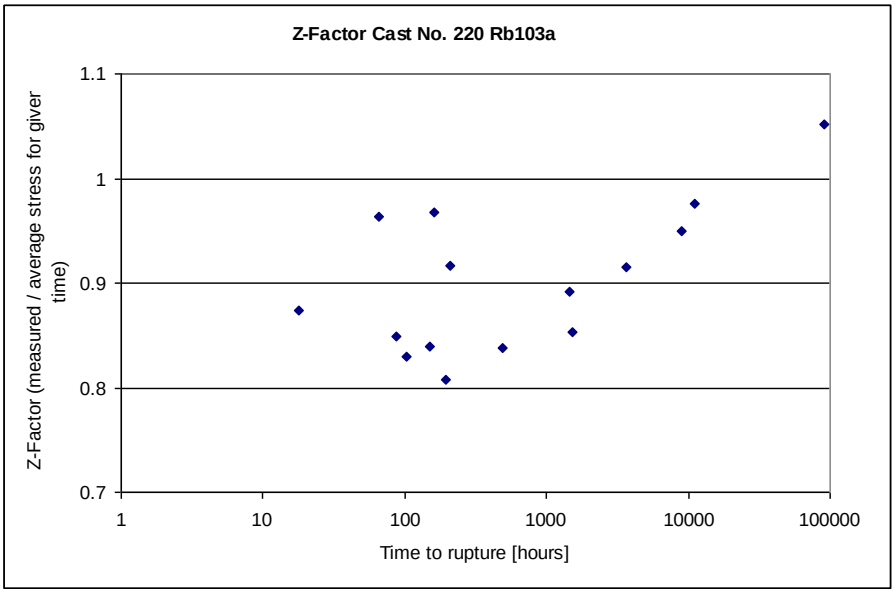

Figure 80: Z-Factor calculated for single cast 220 Rb 103a, temperature 550°C

5.4 Construction of standardized data set

In order to be able to access the effects of single inputs on creep rupture strength and/or time to rupture, using isothermal method, values for standard values were calculated.

The following points were calculated for each of the remaining casts:

- Time to rupture for the following stress levels: 275, 250, 225, 200 at 500°C; 200, 175, 150, 125, 110 at 550°C and
  150, 125, 100, 75, 60, 50 at 600°C
- Creep rupture stress for 5.000, 10.000, 50.000 and 100.000 hours
- No extrapolation was done if it resulted in stress levels 1.5 greater than maximal and 1.5 times smaller than minimal for the given task
- No extrapolation was done if it resulted in times to rupture 3 times greater or 3 times smaller than the respective maximum and minimum for the given cast.

A family of isothermal curves is shown on Figure 81: Family of isothermal lines for X20CrMoV11-1. It is to note that the technically not interesting area for analysis (i.e. time shorter than 5000 hours and stress levels above 200 MPa) are removed from the analysis.

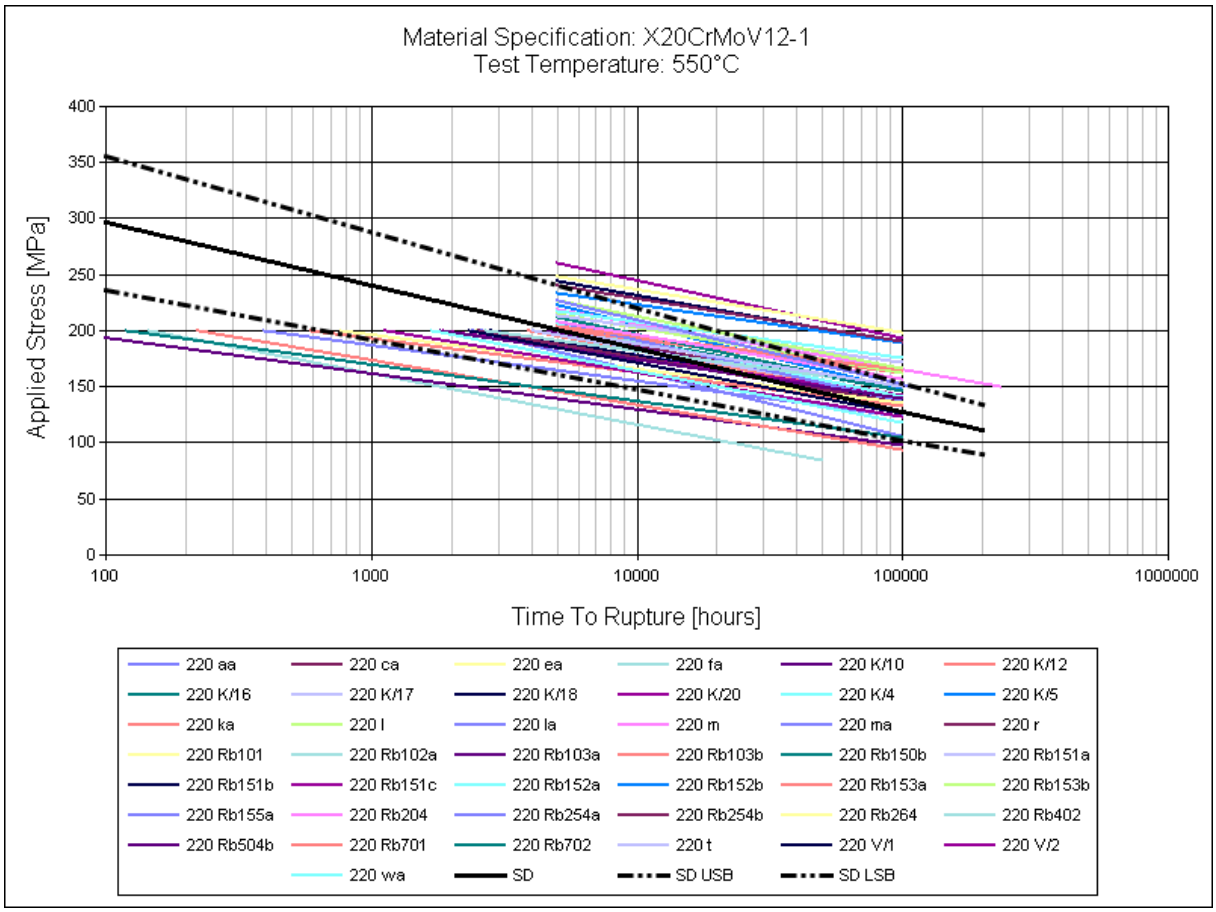

Figure 81: Family of isothermal lines for X20CrMoV11-1, temperature 550°C

The creation of standardized data set allows first of all, with a degree of error, to perform dependency analysis of single inputs on the i.e. rupture stress or time to rupture, at given temperature, while holding the other two most influential variables constant. In other words, it is possible to perform the punctual analysis of i.e. influence of carbon content on creep strength by using standardized values of i.e. 10.000 hours to rupture and fixed temperature level (i.e. 550°C). This also gives the possibility to analyze cast behavior at given temperature, without having to take into account single test results. Some of the examples, together with automatic trend lines, without any assessment of their physical/metallurgical correctness, are shown on Figure 82 up to Figure 90. It is to note the similarity of the results obtained by trending the data in Figure 83 and expert evaluation shown on Figure 27. Further, the dependency between creep strength and R_m at room temperature has been shown to be strong Figure 87, as already shown on Figure 33. Further on, the influence of the tempering and austenitization temperature on creep strength has the same behavior as shown on Figure 53. It is to note that the this behavior

detected by the network is generated by the extreme values, being outside the allowable range for tempering and austenitization temperatures, therefore, those casts have been excluded from further analysis (casts 220 Rb402 with 22 data points, 220 Rb701 with 23 data points, 220 Rb702 with 28 data points, 220 Bt805 with 3 data points, 220 ia with 4 data points, 220 Rb507 with 2 data points, 220 Rb506 with 15 data points, 220 Rb254a with 7 data points, 220 Rb205 with 3 data points, 220 Rb200i with 6 data points, 220 Rb200k with 6 data points, 220 z with 9 records, 220 y with 4 records, 220 Rb300 with 7 records, 220 t with 7 data points, 220 Rb200f with 6 data points, 220 Rb200e with 6 data points, 220 Rb200b with 6 data points, 220 Rb600 with 4 data points, and 220 Rb254b with 8 data points). This still leaves 982 data points for further analysis. Figure 91 shows that austenitization influence as shown on Figure 89 completely disappears.

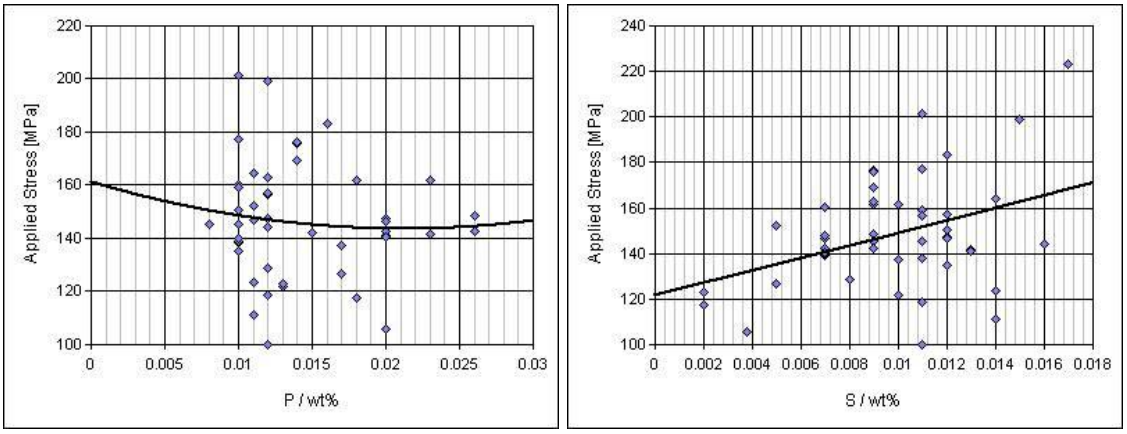

Figure 82: Influence of P and S on creep rupture strength at 100.000 hours and 550°C

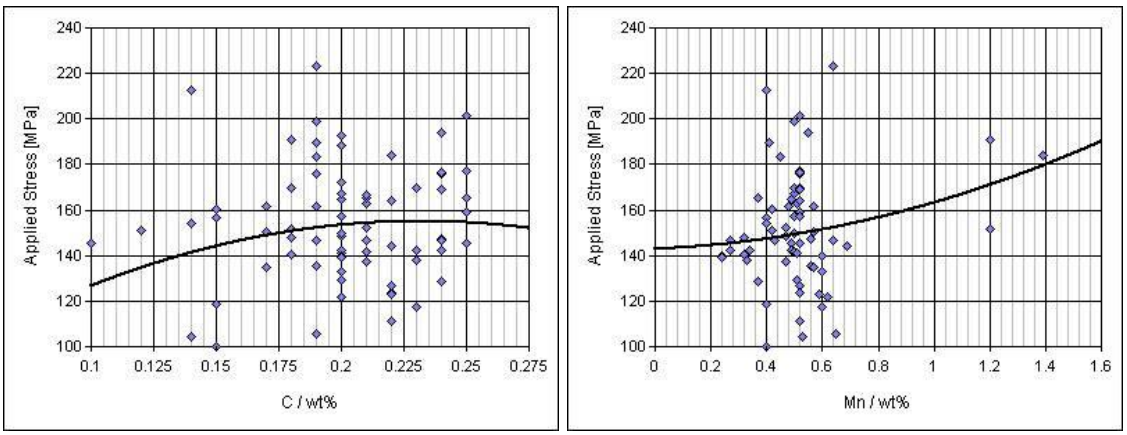

Figure 83: Influence of C and Mn on creep rupture strength at 100.000 hours and 550°C

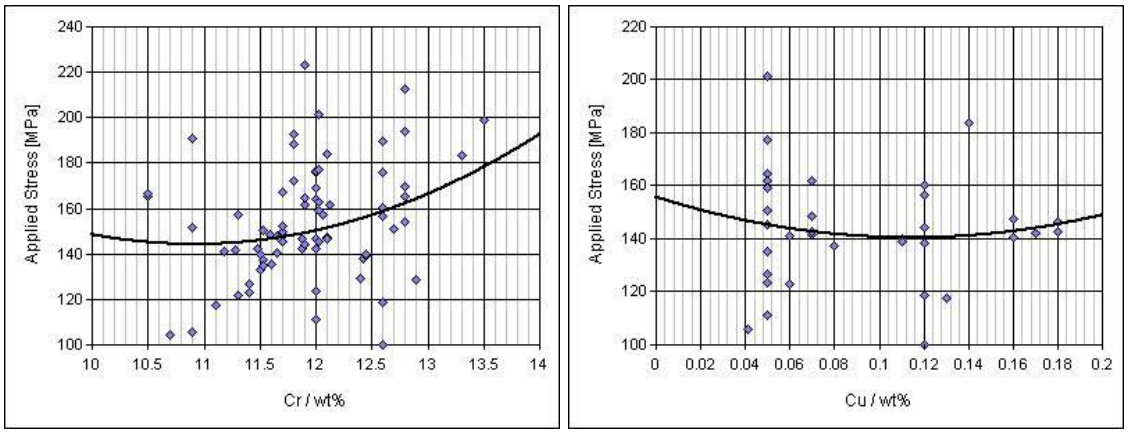

Figure 84: Influence of Cr and Cu on creep rupture strength at 100.000 hours and 550°C

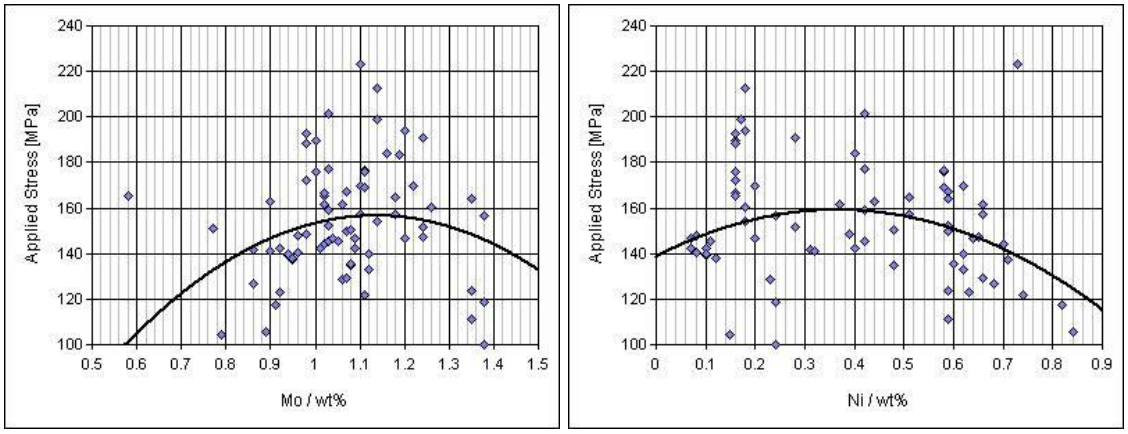

Figure 85: Influence of Mo and Ni on creep rupture strength at 100.000 hours and 550°C

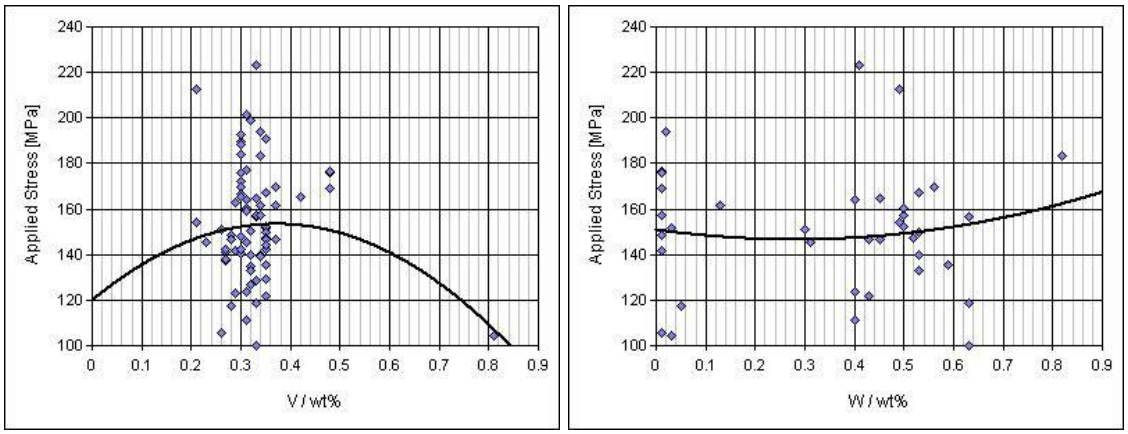

Figure 86: Influence of V and W on creep rupture strength at 100.000 hours and 550°C

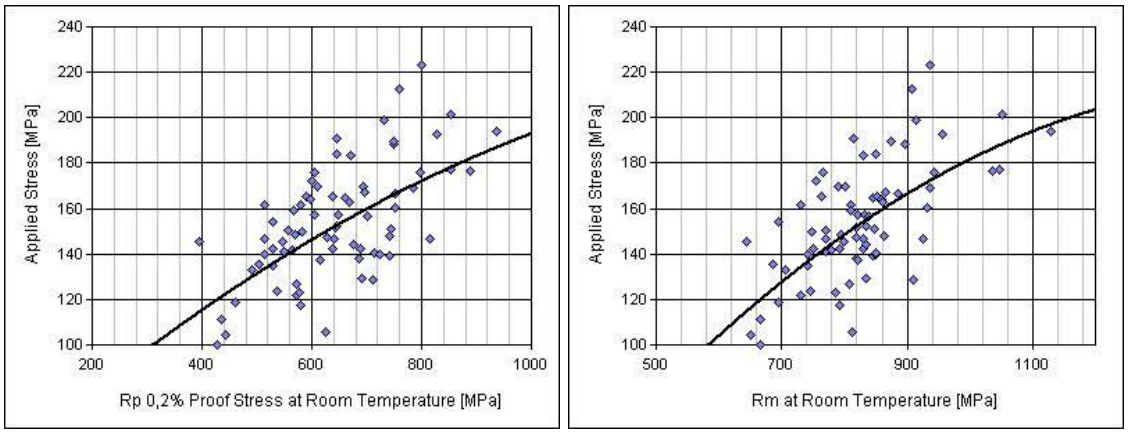

Figure 87: Influence of $R_{p0,2}$ proof stress on room temperature on creep rupture strength at 100.000 hours and 550°C

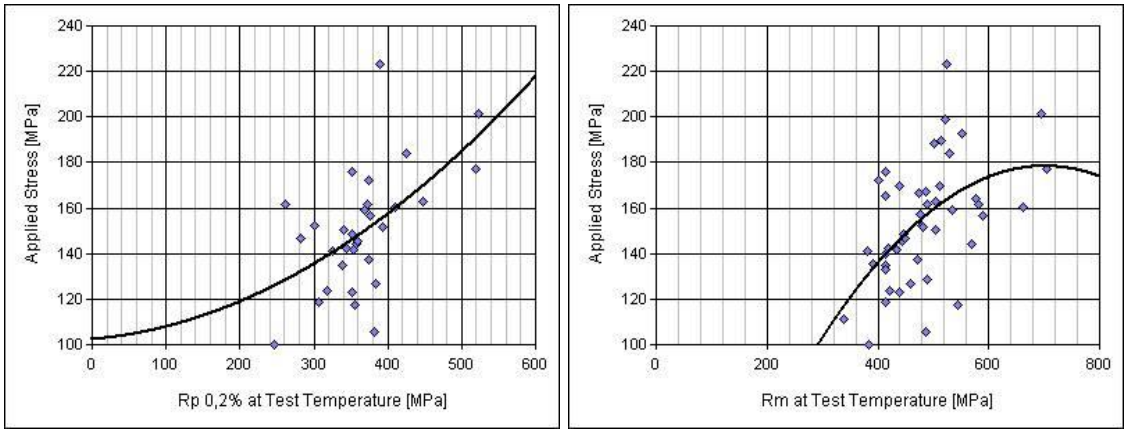

Figure 88: Influence of R_m on test temperature on creep rupture strength at 100.000 hours and 550°C

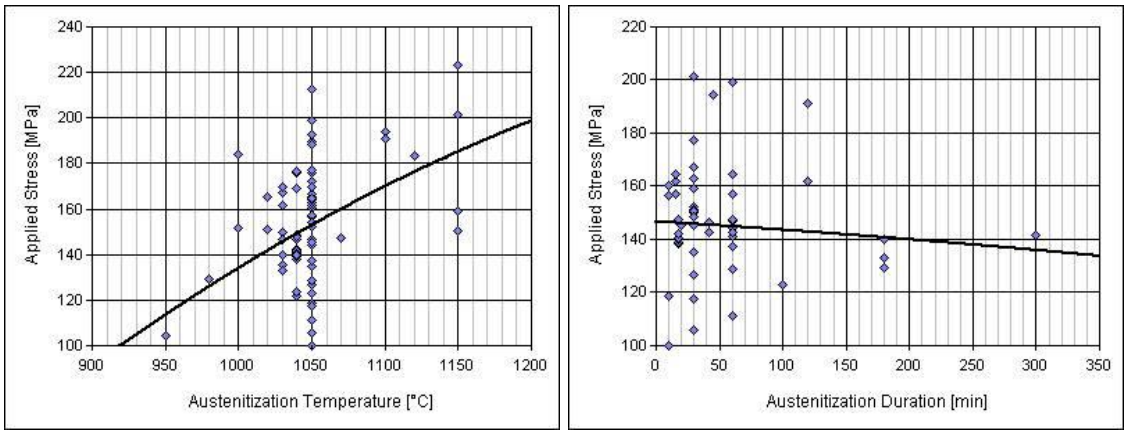

Figure 89: Influence of austenitization temperature and duration on creep rupture strength at 100.000 hours and 550°C

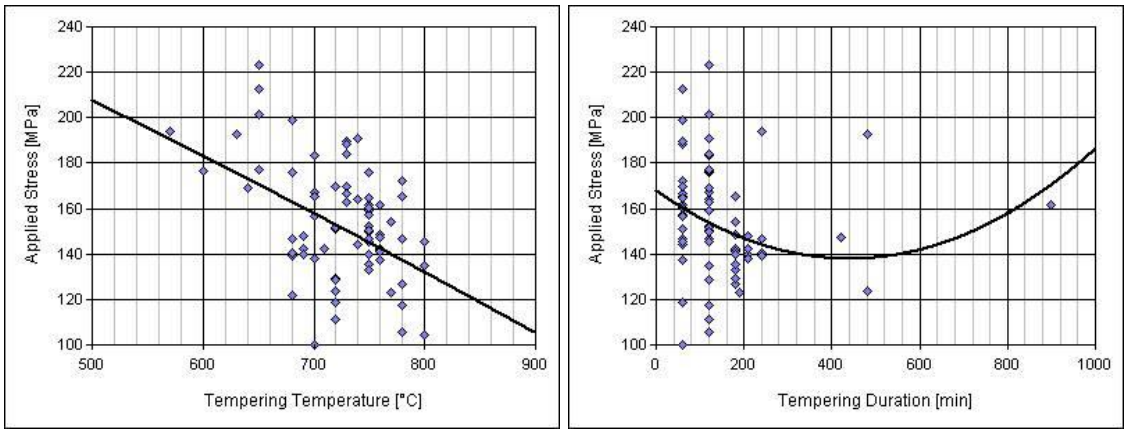

Figure 90: Influence of tempering temperature and duration on creep rupture strength at 100.000 hours and 550°C

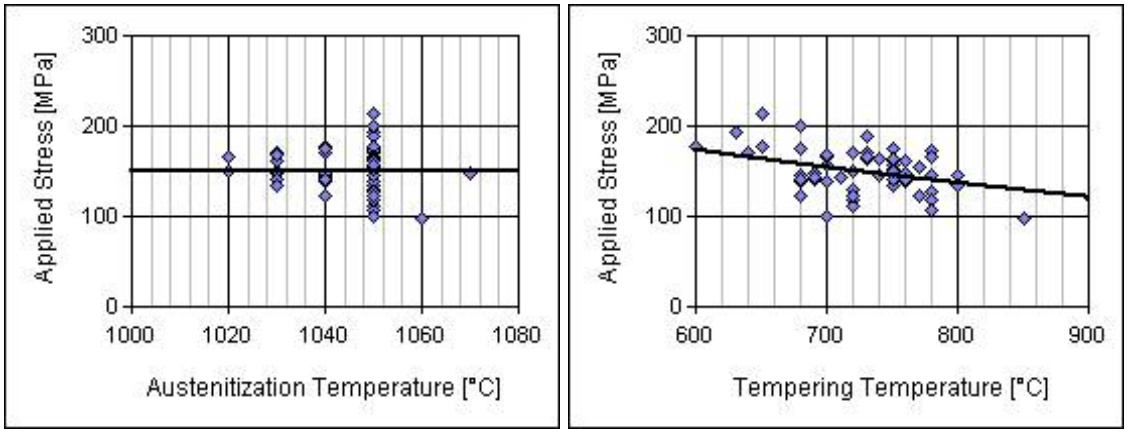

Figure 91: Influence of austenitization and tempering temperature on creep rupture strength at 100.000 hours and 550°C, after the removal of casts with non-compliant austenitization temperatures (1020-1080°C)

5.5 Clustering

Clustering is a partitioning process of the overall data into clusters of similar data, by using either selection of typical cases for each of the cluster and then determining how close according to the selection criteria others are. The other option is to cluster the data by using expert opinion, in this case the metallurgical dependencies and previous knowledge about material behavior. Creep mechanism indeed does not represent one single behavior but rather different behavior of the material in different stages of creep and temperature, as shown on Figure 92 [DIMM]. Here it is demonstrated that an inflexion point exists for transition between diffusive creep (less deformation) by the lower stress levels, and creep due to intergranular dislocations by the higher stress levels.

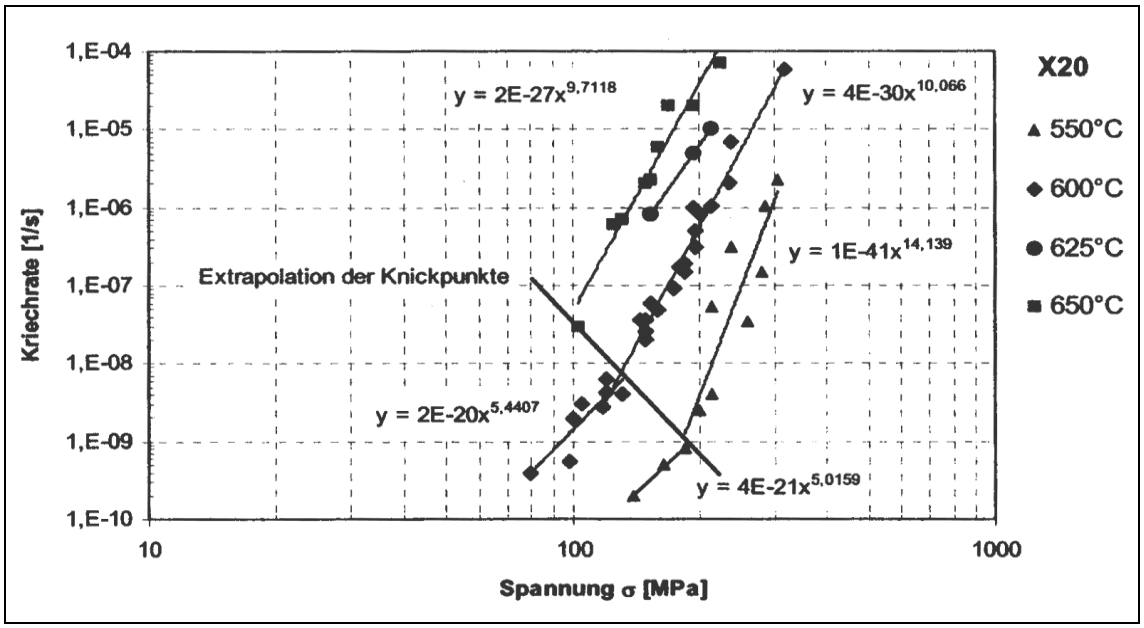

Figure 92: Creep mechanisms for steel X20CrMoV11-1 [Polcik 98]

Therefore, it is meaningful to test the feasibility of training two pools of neuronal networks, defined by the stress and time to rupture, and defined by the inflexion line as shown on Figure 92. The borders for clustering are defined in Table 14. Further, according to the Figure 92, below 550°C, the clustering does not apply.

Table 14: Clustering scheme

Cluster	Temperature	Applied stress (MPa)	Time to rupture (hours)
Short-time	550	> 180	< 10000
Long-time	550	< 180	> 10000
Short-time	600	> 130	< 5000
Long-time	600	< 130	> 5000

Based on the clustering scheme suggested, one network for short-time and long-time creep was trained, taking only X20CrMoV11-1 (X20CrMoV12-1) specification.

The effect of clustering is shown on Figure 93 and Figure 94. Even with small amount of data available for the training – see Figure 45, the long-time cluster has determined correctly that the given cast is located in the lower part of the scatter band, using minimum inputs (data level 6). Much better results, mainly due to more data available in the short-term cluster, is shown on Figure 93, where accurate prediction of the position of the cast is scatter band has been obtained again

using minimum of data. This shows that clustering might be a way of better data assessment, giving good results in both short-time and long-time creep clusters, however, the lack of enough tests of sufficient duration (at least two tests, possibly three in each of the cluster for the correct trend assessment) yields relatively imprecise performance of the network in the long-time cluster and reduces the number of outcomes for network to learn drastically. Improving model with more inputs is also impractical, while it implies training a more complex network with less data points available.

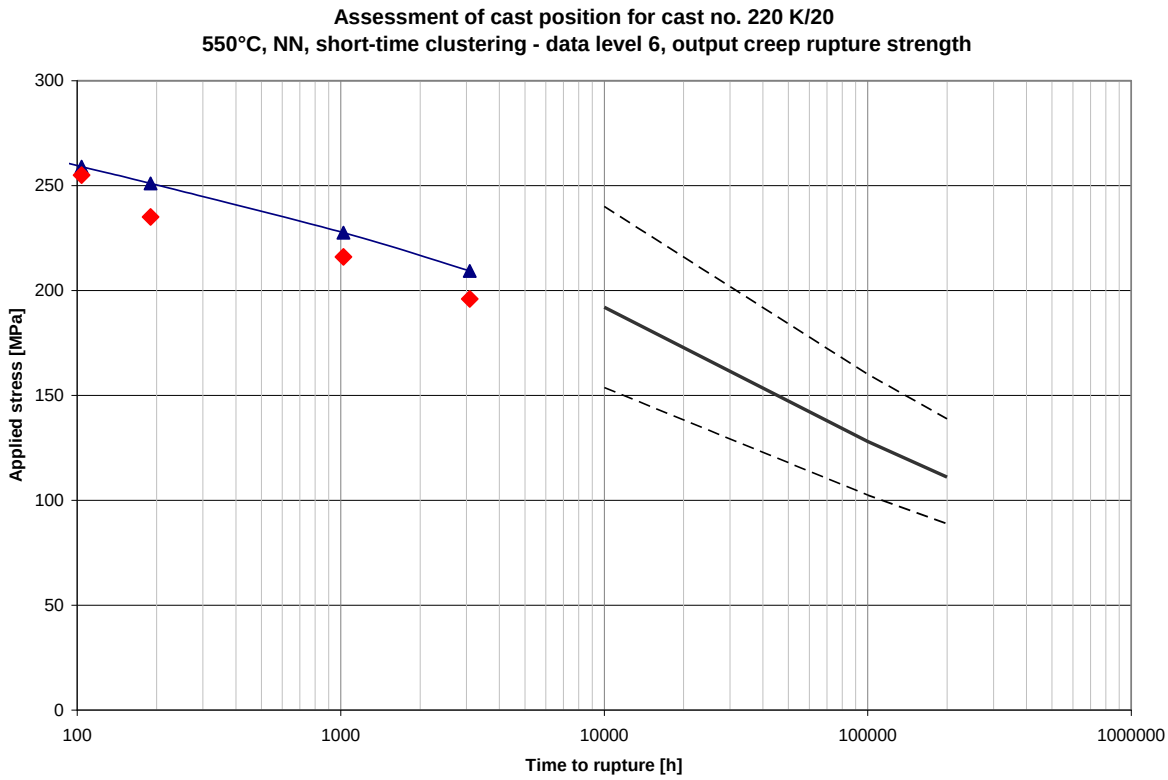

Figure 93: Comparison of model prediction (▲), experimental data (◆) and average creep rupture strength values and corresponding scatter band of the material X20CrMoV11-1 (thick and dashed lines), cast analysis 220 K/20 550°C, data level 6 – 550°C, short-time data

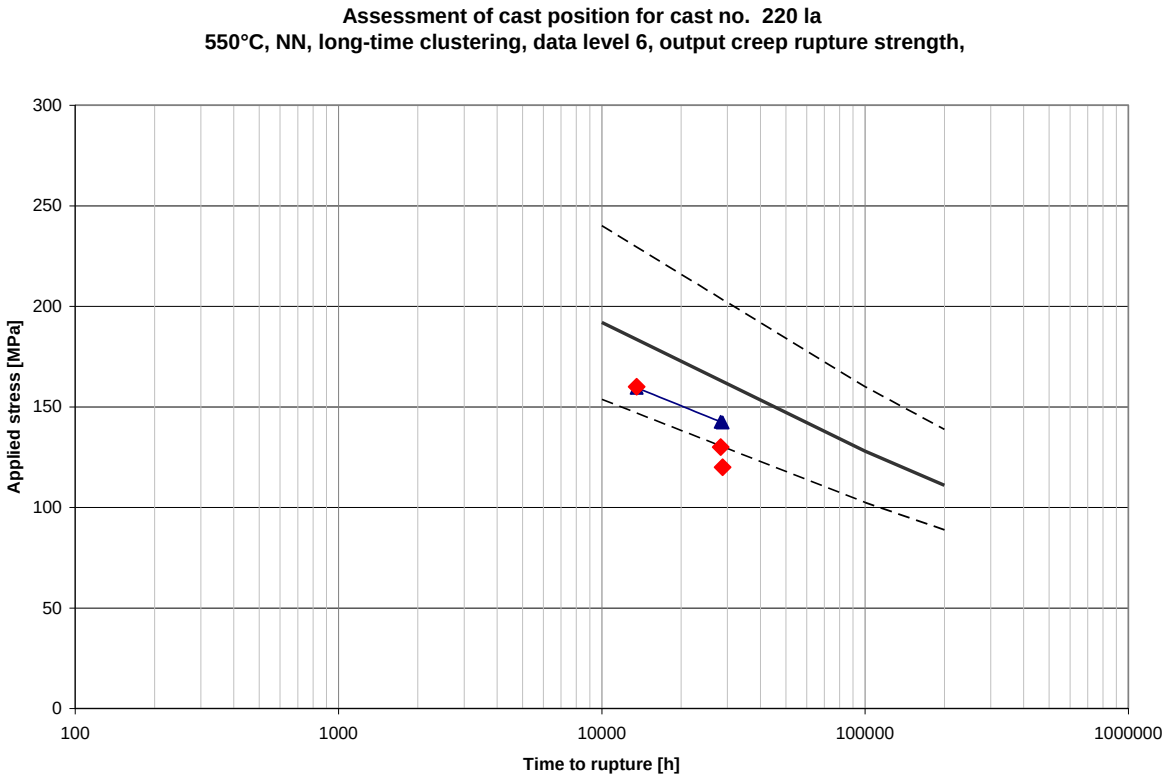

Figure 94: Comparison of model prediction (▲), experimental data (◆) and average creep rupture strength values and corresponding scatter band of the material X20CrMoV11-1 (thick and dashed lines), cast analysis 220 Ia – 550°C, data level 6 – 550°C, long-time data

Further clustering possibilities would be the use of classification according to the strength class, as described in 4.4.3, or by using the different designations available in the dataset (X20, X21 and X22), or by product form; however this kind of classification would yield from the data amount available to a single very populated cluster with most of the data, see i.e. Figure 34, and the rest of the clusters having not enough data points for feasible neural network testing.

5.6 Optimized data set neural network training

After the successive data removal as described in previous chapters, a data set of total 982 data points has been left for analysis. The value of W-content has been set to zero for all casts without W in specification, effectively giving the possibility to use W as input already on the level 6 of data analysis. Furthermore, the training was performed only with output being creep rupture strength, as it has been demonstrated that this gives much better results. Table 15 shows the overall data

availability; level 1 and level 2 of data analysis were not included in the further analysis due to significant decrease of available data points; therefore the training was repeated for levels 6 – 3.

Level 1 with 183 Datasets and 20 Features Level 2 with 219 Datasets and 18 Features Level 3 with 500 Datasets and 17 Features Level 4 with 721 Datasets and 16 Features Level 5 with 919 Datasets and 14 Features Level 6 with 982 Datasets and 11 Features	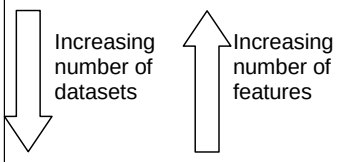

Table 15: Graphical representation of data grouping after successive data elimination

Figure 95 to Figure 98 show the effect of the training on the results. As one can notice, the fitting i.e. the results achieved in prediction of the properties based on data have improved, and the fit remains stable in both low and high stress areas. Also, data reduction vs. achieved results shows that already at data level 5 has already reached the optimum of learning; further reduction in data sets leads to better fit; however this might be attributed to the smaller variability of the data in the dataset due to the number reduction. On the other hand, application of the neural network on “unknown” specimens shows that data level 3 still indeed has better ability to recognize true behavior of the cast.

Figure 99 illustrates the same data set as shown on Figure 98, but with the data points used for training and for validation colored displayed separately. As it is visible from the Figure 99, the deviation of the data is almost the same for validation and for training data, showing properly trained state of the network.

From metallurgical point of view the fact that the predictor on level 5 has better performance compared with data level 6 can be explained by the fact that since the data level 5 includes data for Mn, Si and Ni, and, as discussed in 4.4.2, they do influence the metallographic structure of the material and thus represent relevant information about the property of the cast.

Much better results for data fitting might be attributed to the following actions (in order of influence):

1. Removal of notched specimens from dataset
2. Removal of extreme values, especially for heat treatment

3. Introduction of W as one more input for all levels

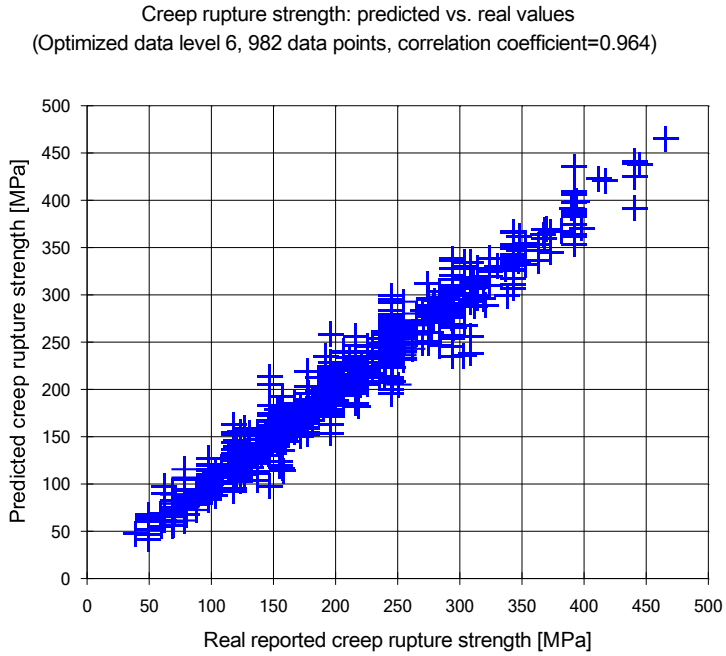

Figure 95: Comparison of model and experimental values, optimized data level 6, output creep strength

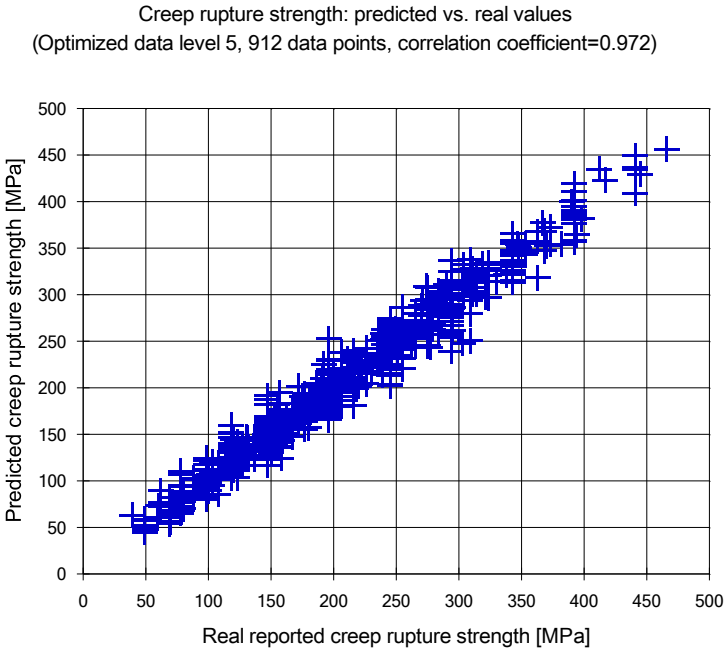

Figure 96: Comparison of model and experimental values, optimized data level 5, output creep strength

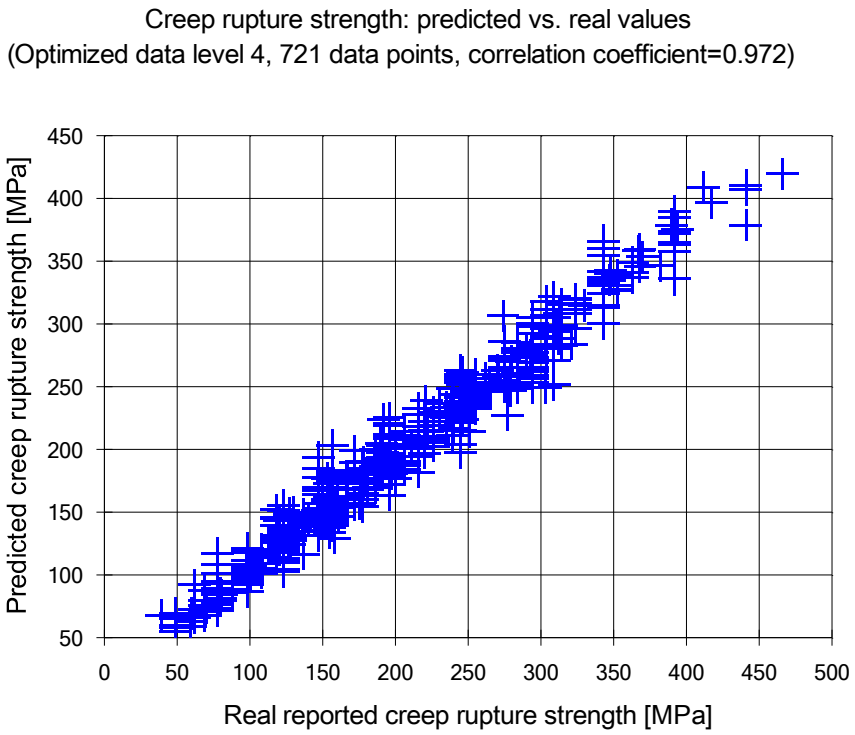

Figure 97: Comparison of model and experimental values, optimized data level 4, output creep strength

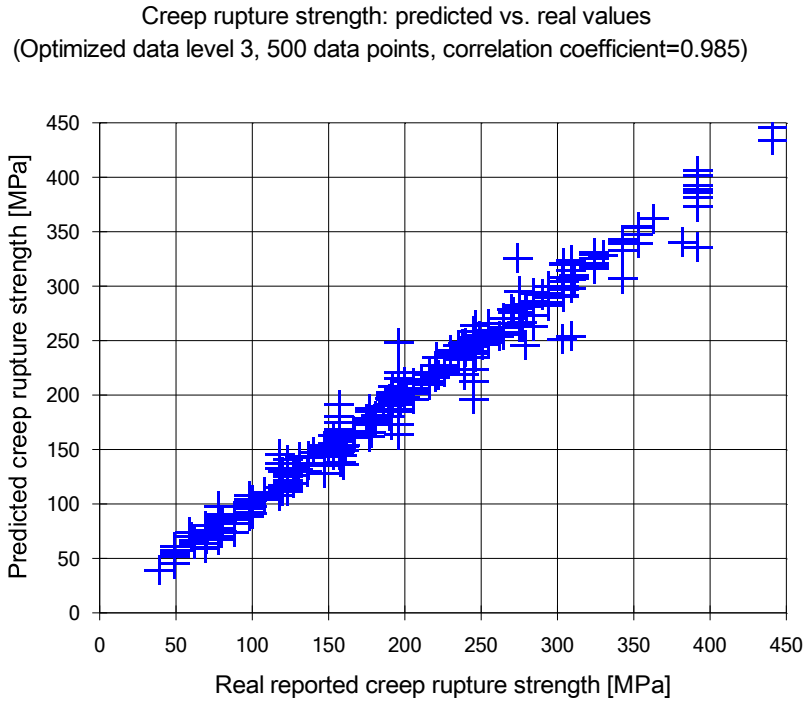

Figure 98: Comparison of model and experimental values, optimized data level 3, output creep strength

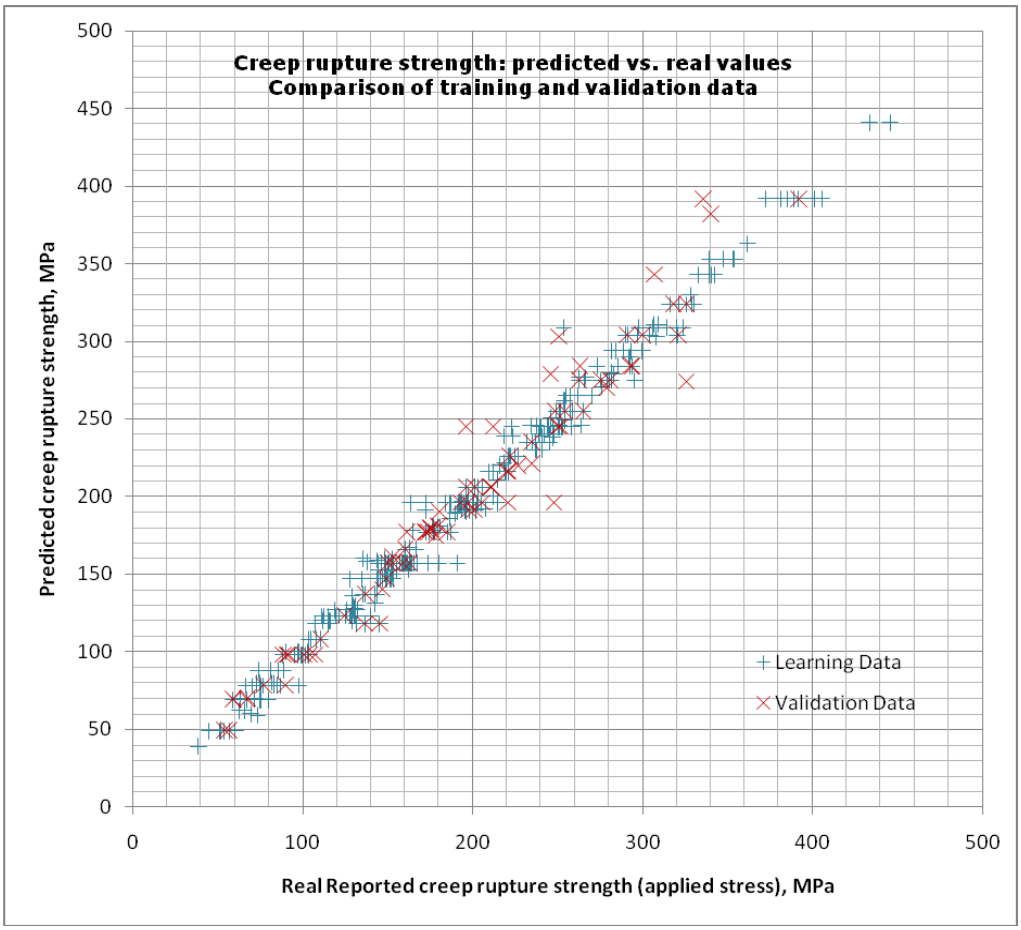

Figure 99: Comparison of model and experimental values, optimized data level 3, output creep strength, training vs. validation data

5.7 Metallurgical interdependencies

The literature citations provided in the 4.4.2 regarding the influence of individual chemical elements from chemical composition are usually based on a limited number of tests, at least regarding the model material X20CrMoV11-1 and its family, and therefore have only limited statistical basis. From the data analyzed so far, these aspects can be checked and/or verified.

It is to note that, due to the n-dimension of the network topology, where n is number of inputs to the network, the analysis of influence of each of the inputs individually on the output is of local character, i.e. it shows the effect of variation of the given input on the output (creep rupture strength) while keeping all other inputs constant. In any other point on the network configuration this influence might be completely of different behavior, i.e. the network might in one particular configuration consider a parameter as “positive” and in other “negative”. A good example is

the assessment of the C content on the creep rupture strength – in some cases, the schematic representation shown on Figure 27 and on Figure 100 gives almost identical behavior; however, in some other cases, i.e. as shown on Figure 101, the network has applied completely different pattern (i.e. showing negative influence). Furthermore, Figure 102 shows the effect of sparse data in some regions – since, as shown on Figure 48, the area below 0.17% C content has only limited number of points, and also since the 0.14% values are characterized by lower values of creep rupture strength, visible on Figure 27, the network “correctly” recognizes this pattern and applies it on the data. It is interesting to note that this effect, at the same working point, completely disappears at already 10.000 hours - Figure 103. Further, Figure 27 is showing creep strength at 10^5 hours; metallurgical influences at i.e. 10^3 or 10^4 hours creep strength might differ from this behavior.

This obviously stresses the need to have data population for the neural network of similar density in all directions, in order to obtain meaningful results. The areas with lower data point density tend to confuse the network and introduce patterns that are not physically explainable.

In order to investigate the influences of each single element, a point was fixed for investigation, represented by the mean values from the overall population, as given in Table 10, adjusted to the average values as in specification – given in Table 2, with the temperature set to 550°C, time to rupture to 100.000 hours, austenitization temperature set to 1050°C and tempering temperature set to 740°C. In each of the cases, both W content of 0 and 0.5 was investigated. The resulting data point is given in the Table 16.

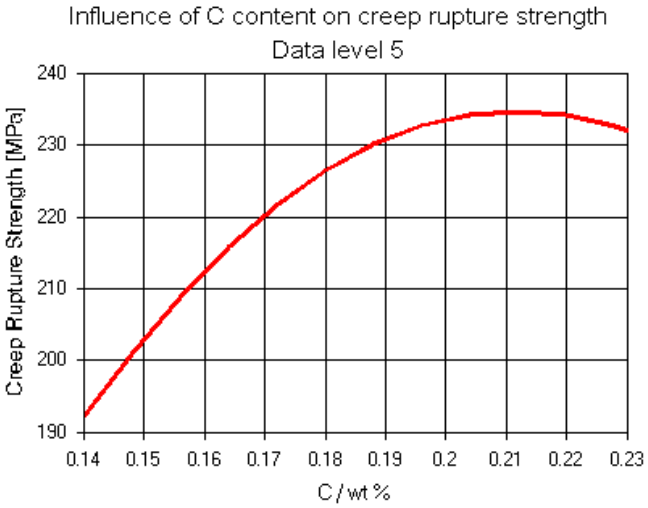

Figure 100: Influence of C content on creep rupture strength, optimized data level 5, working point specimen K/11, time to rupture 100.000 hours, 500°C

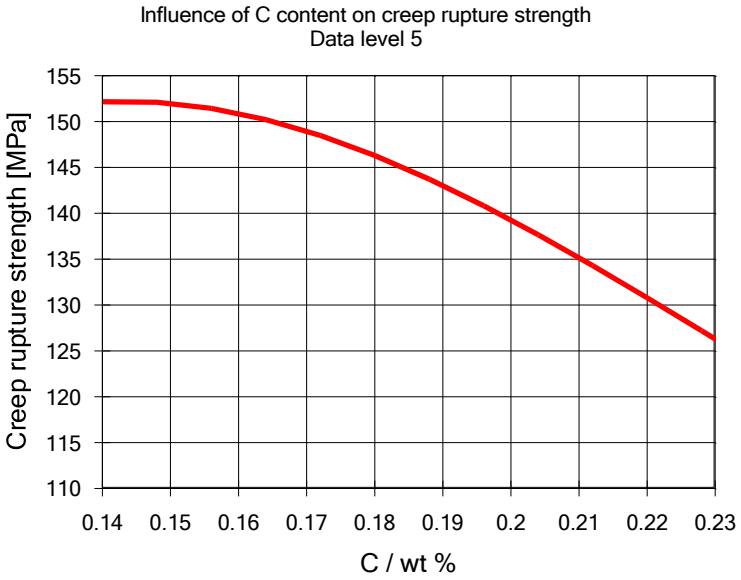

Figure 101: Influence of C content on creep rupture strength, optimized data level 5, working point specimen K/3, time to rupture 100.000 hours, 550°C

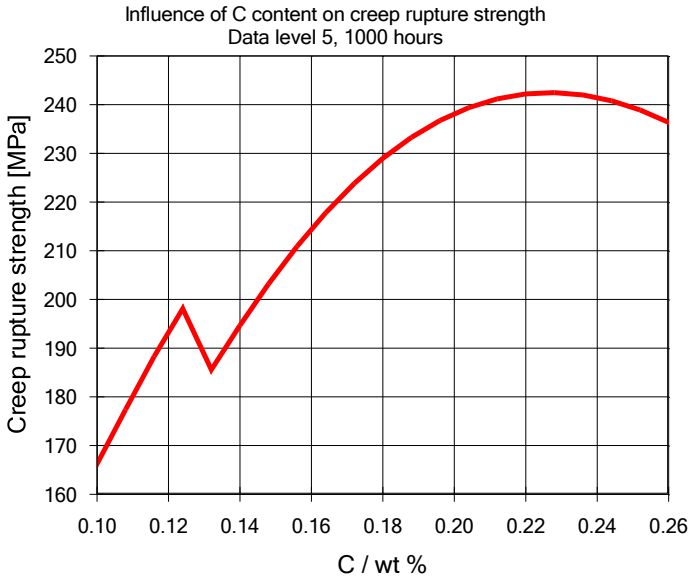

Figure 102: Influence of C content on creep rupture strength, optimized data level 5, working point specimen 220 fa, time to rupture 1.000 hours, 550°C

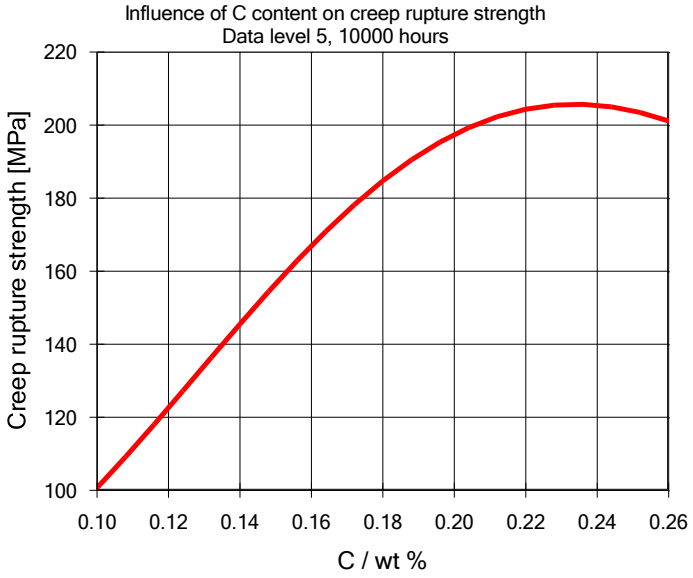

Figure 103: Influence of C content on creep rupture strength, optimized data level 5, working point specimen 220 fa, time to rupture 10.000 hours, 550°C

Table 16: Mean point of the data set used for analysis

Feature	P	S	C	Si	Mn	Cr	Cu	Mo	Ni	V	W
Mean value	0.015	0.015	0.20	0.25	0.5	11.0	0.1	1.00	0.5	0.3	(0) 0.5

Feature	$R_{p0,2}$ (RT)	R_m (RT)	Austenitization Temperature	Tempering Temperature	Temperature	Time to rupture
Mean value	660	840	1050	740	550	100000

5.8 Influence of elements and their interpretation in the neural network

5.8.1 Influence of C content

From point of view of its importance in building the carbides that have positive influence on creep rupture strength, it would be expected that the increase of carbon content would provide a higher creep rupture strength. However, as already visible from the Figure 27, and later on from Figure 83, an increase of C content over 0.19% does not yield a significantly visible increase in the creep strength. On the other hand, the values below 0.17%, as lower limit specified in the Table 2 for X20CrMoV11-1, should be kept, as, based on sparse data available below this concentration, lower carbon content tends to give lower creep rupture strength values. The potential for variation is therefore limited. Figure 106, Figure 105 and Figure 104 show the influence as given by the neural network for the mean data point. All figures show no significant influences, and effects of data scarcity are clearly visible for both optimized data level 5 and 3. As shown already on Figure 100, Figure 101, Figure 102 and Figure 103, network interprets C content differently in different configurations, for different times to rupture. Figure 107 shows evaluation of raw experimental data; Figure 83 shows the evaluation of isothermal data calculated to 100.000 operating hours. Generally, all networks tend to interpret the lower content on C as mild negative influence, whereas the values over about 0.17% are usually giving in essence flat trends, i.e. reproducing the expert evaluation as given on Figure 27.

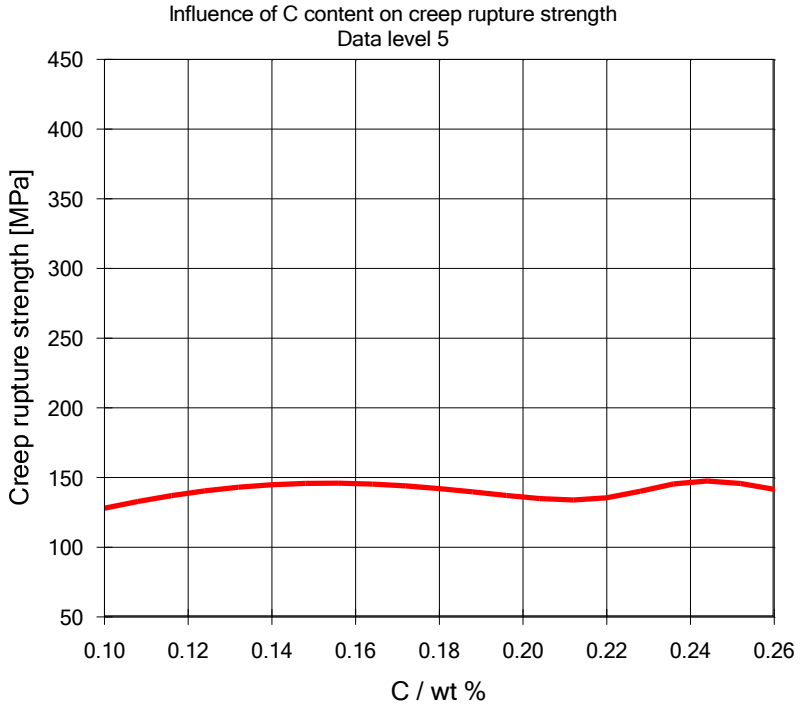

Figure 104: Influence of C content on creep rupture strength, optimized data level 5

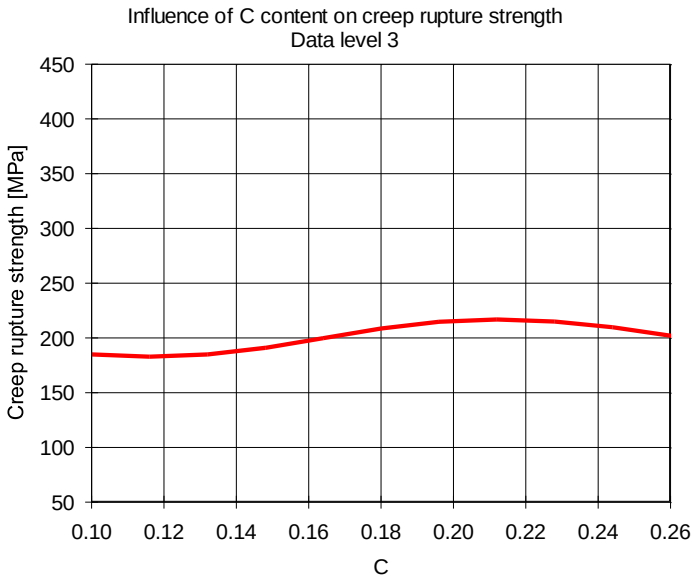

Figure 105: Influence of C content on creep rupture strength, optimized data level 3

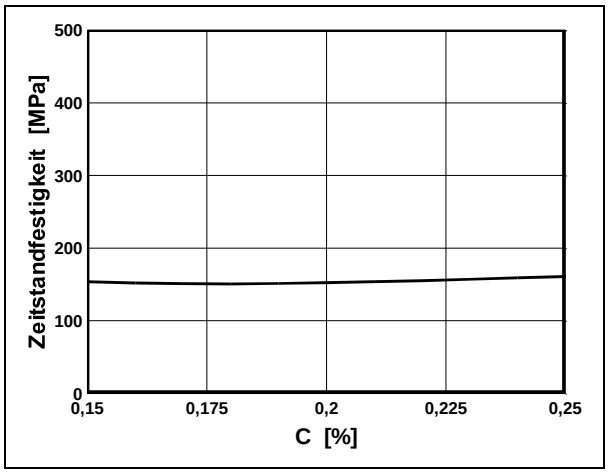

Figure 106: Influence of C content on creep rupture strength, data level 1 (non-optimized) [AVIF 198]

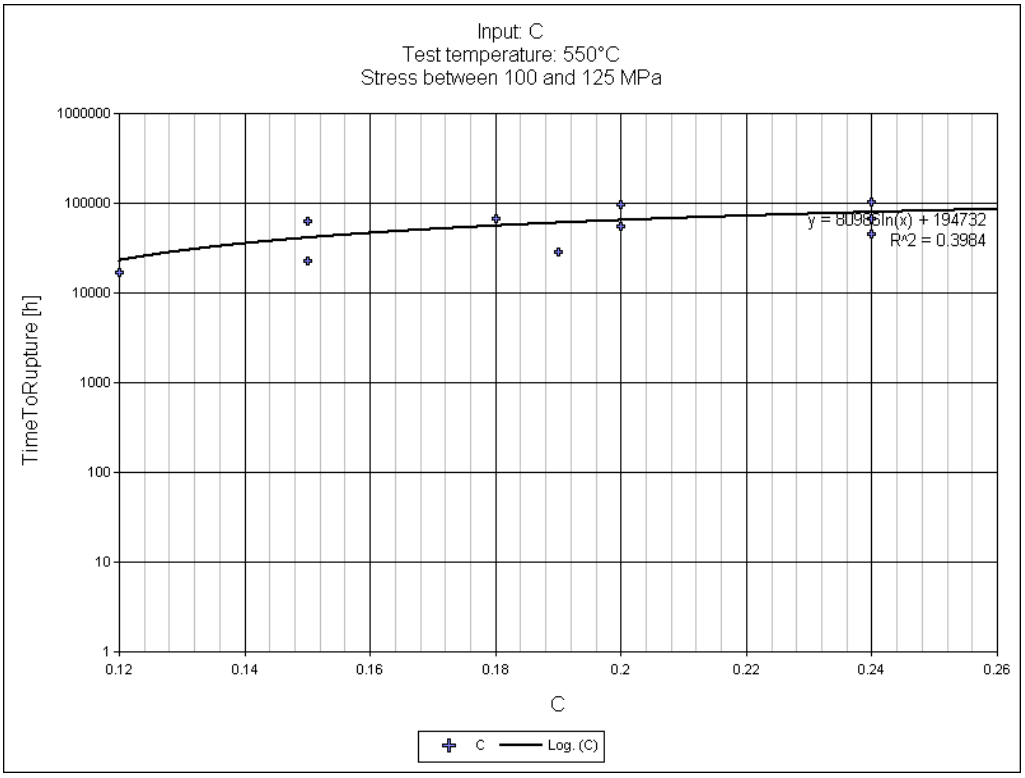

Figure 107: Influence of C content on creep rupture strength, data experimental data, applied stress level of 100-125 MPa

5.8.2 Influence of Mo content

From metallurgical point of view, Mo stabilizes the $M_{23}C_6$ particles in the metallographic structure of the material. On the other hand, the Mo and V content should be considered according to the metallurgical analyses and prescribed values for the material (Mo: 0,8 - 1,2%, V: 0,22 - 0,35%). These concentration boundaries are considered as optimal by [Jesper 85].

Figure 108 shows the different interpretation of the networks at level 5 and level 3, generally a mild increase of creep rupture strength with the increase of Mo content; this is also to be seen from the experimental data evaluation, as on Figure 109. Figure 85 (isothermal evaluation of the data) confirms the optimal region as defined by [Jesper 85].

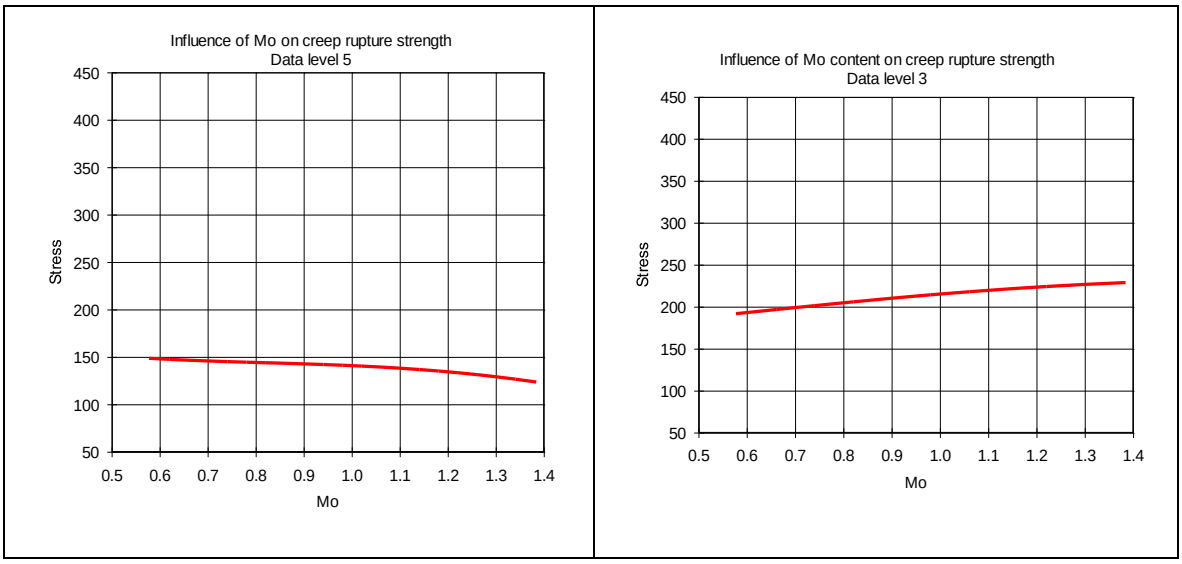

Figure 108: Influence of Mo concentration on the creep rupture strength as interpreted by the neural network – optimized data level 5 (left) and level 3(right)

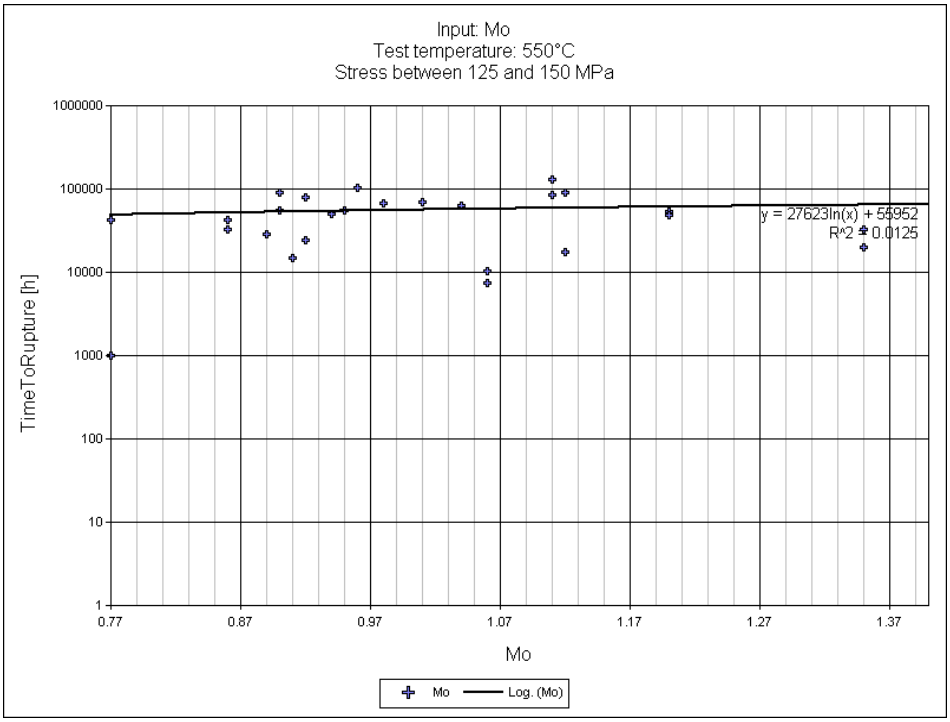

Figure 109: Influence of Mo content on creep rupture strength, data experimental data, applied stress level of 100-125 MPa

5.8.3 Influence of P and S concentration

Negative influence of P and S concentration on creep rupture strength was seen in connection with the formation of oxides and sulfides on the grain boundaries but also in the grains themselves, considered as cavities. However, it is found that they represent hard particles, linked to the deformation mechanisms, and not to the diffusion processes. Further, the concentration of P and S has been drastically reduced with the development of the new methods of material production. Furthermore, the THTR-casts fabricated in the 80s, characterized by very low concentrations of P and S, were all positioned in the lower scatter band. This can be also connected to the relatively high tempering temperatures (760-780°C) [Schubert 92].

Figure 110 shows the evaluation of P and S influence by applying the neural network on the mean data point. In comparison with the direct data evaluation - Figure 111 and Figure 112, as well as with the isothermal evaluation - Figure 82, it is generally to conclude that the small concentrations of P and S tend to increase the creep rupture strength. However, since the concentrations of both elements (in cases when reported) were below the maximal concentrations, the negative influence reported for high concentrations could not be verified.

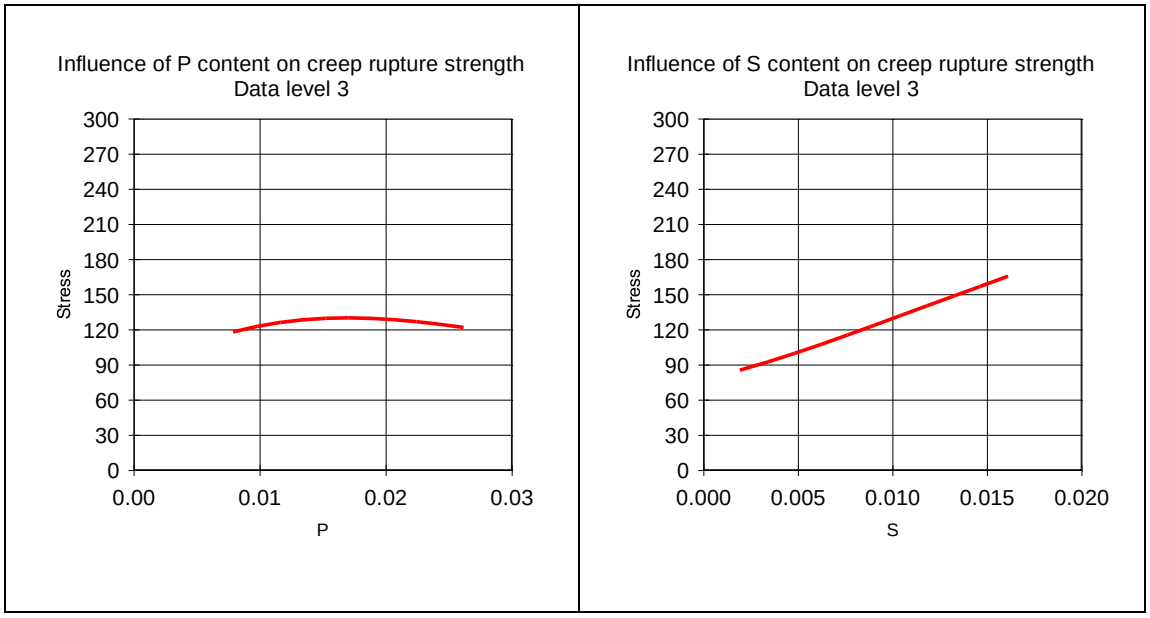

Figure 110: Influence of P and S concentration on the creep rupture strength as interpreted by the neural network – optimized data level 3

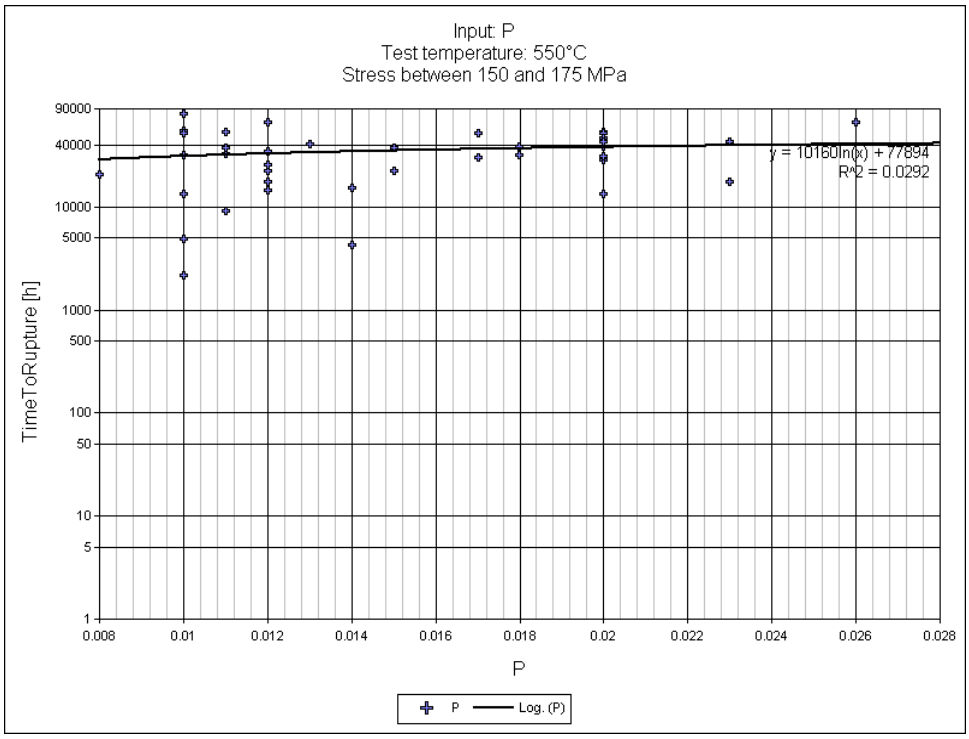

Figure 111: Influence of P content on creep rupture strength, experimental data, applied stress level of 150-175 MPa

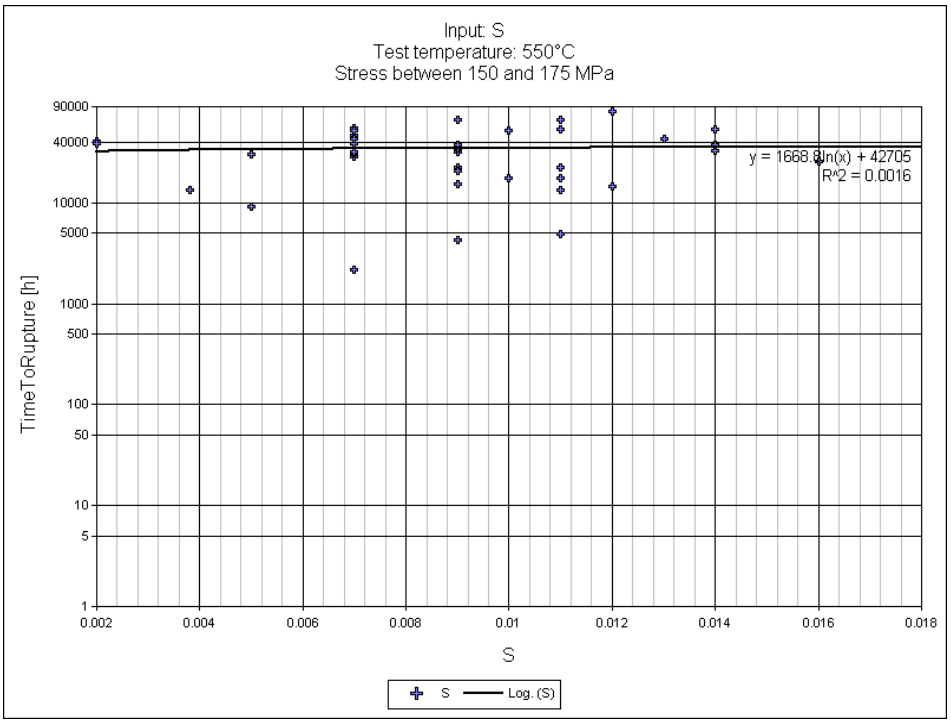

Figure 112: Influence of S content on creep rupture strength, experimental data, applied stress level of 150-175 MPa

5.8.4 Influence of Cr content

The development of modern martensitic steels for higher temperatures than those that are limiting for X20CrMoV11-1 shows that increase in creep rupture strength is achieved by decrease of Cr content below 11% or, whenever possible, below 10%. This is explained by the fact that higher Cr content changes the metallographic structure at temperatures higher than 600°C, in the following ways:

- Laves Phase becomes more coarse
- decreases thermal stability of $M_{23}C_6$ particles
- smaller number or no MX particles in the microstructure in the initial microstructure
- Unstable M_2X in the initial microstructure.

This all leads to the appearance of the Z-phase during the application of the material at temperatures higher than 600°C [Mayer 06], consuming the MX particles.

Figure 113 shows the effect as interpreted by the network that demonstrates that Cr content, due to temperatures lower than 600°C, does not have great influence on the creep rupture strength. Level 5 data shows a small variation, whereas clearly level 3 give very flat dependency, with an optimum (very weak one) at the content of 11.5-12.5%.

Figure 114, similar to Figure 84 shows a small increase in the data for some stress levels and temperatures; however, this effect is mostly due to statistically insignificant presence of couple of casts in the area outside the specification (at about 13-13.5% Cr content).

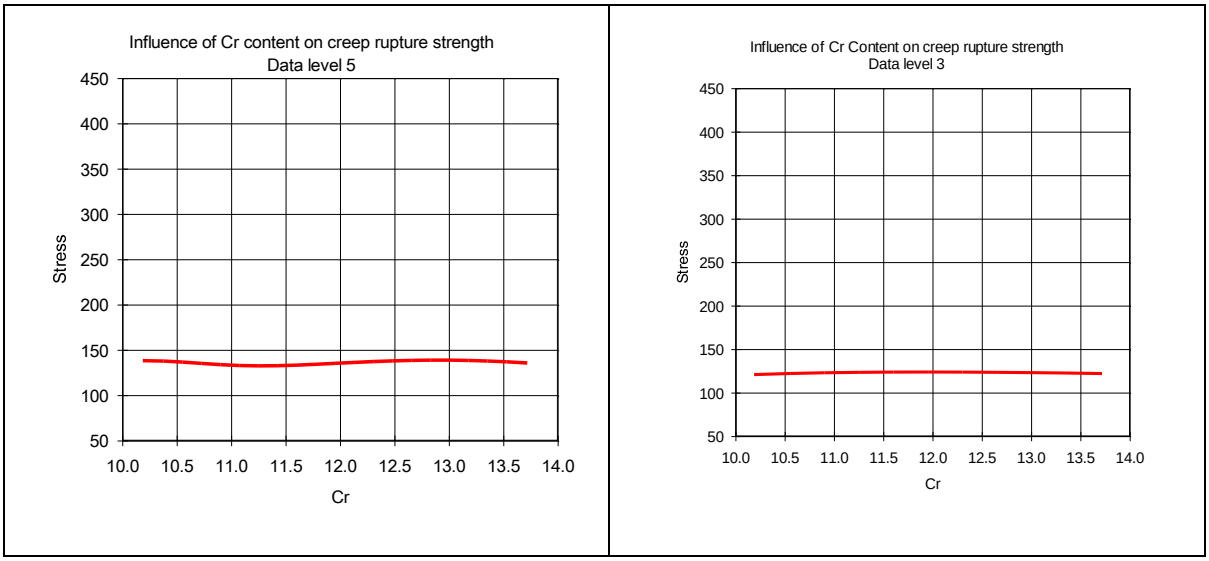

Figure 113: Influence of Cr concentration on the creep rupture strength as interpreted by the neural network – optimized data level 5 (left) and 3 (right)

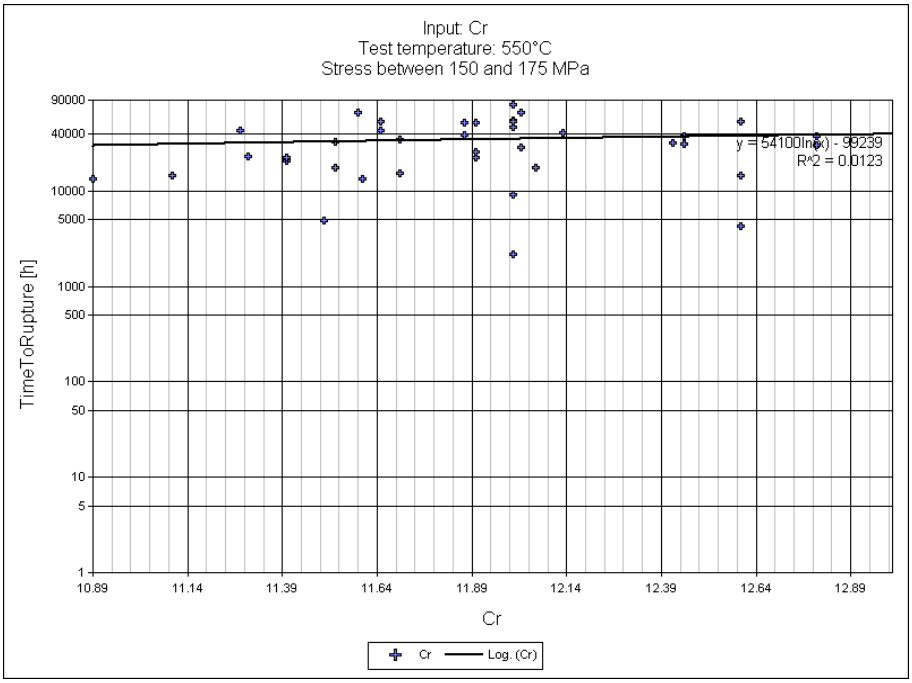

Figure 114: Influence of Cr content on creep rupture strength, experimental data, applied stress level of 150-175 MPa

5.8.5 Influence of V content

Vanadium is known to be carbide-building element, and it forms thermally stable Vanadium-nitrides, which increase the creep strength.

Neural network shows that both level 5 and level 3 confirm this effect, Figure 115, whereas the level 5 gives a similar shape as more drastically shown on Figure 86; this shows the effect of outliners on both regression and neural network analysis.

Level 3, not containing the singular point (cast) does not show this effect, i.e. has a stable growing curve. It is to note that the range of available chemical composition of individual casts is much broader - from 0.15 to 0.5, compared with the standard requirements of 0.25 to 0.35, in which in both cases a small influence is registered. The direct data analysis of the experimental data - Figure 116, shows slightly increasing tendency, mostly due to outliners in the area of 0.45%. The small positive influence described in the literature is in this case reflected by the network.

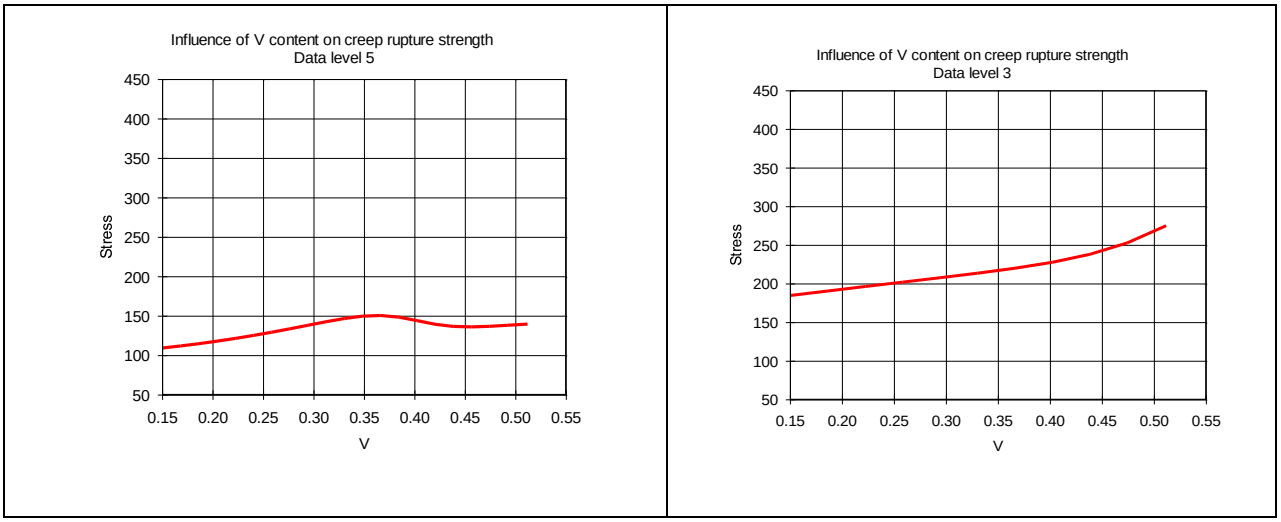

Figure 115: Influence of V concentration on the creep rupture strength as interpreted by the neural network – optimized data level 5 (left) and 3 (right) (NOTE: different data points used for illustration purposes)

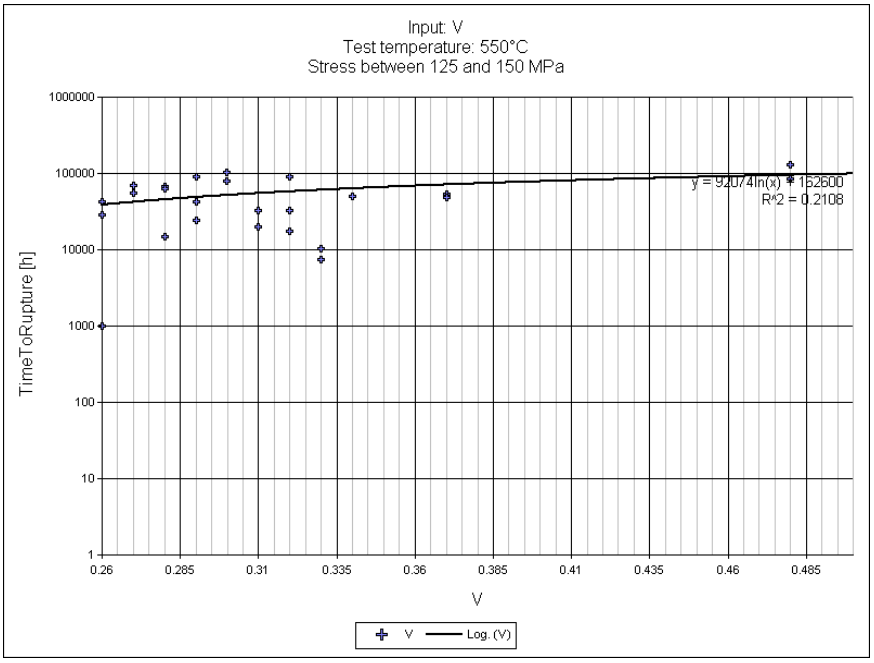

Figure 116: Influence of V content on creep rupture strength, experimental data, applied stress level of 125-150 MPa

5.8.6 Influence of Ni and Mn

As shown already on Figure 85, using common regression analysis gives an optimum at about the same levels as the standard values given in Table 2, i.e. Ni from 0.3 to 0.8% and Mn less than 1%. The neural network on level 5 Figure 117 shows similar tendency; however the network on level 3 looses this effect, and shows stable positive effect; this is mainly due to the fact that level 3 dataset does not include the extreme points present in the level 5 dataset. On the other hand, the direct evaluation of experimental data shows neutral behavior in the interesting area of 125-150 MPa area - Figure 118.

Mn, on the other hand, according to level 5 network, has an optimum at about 0.4-0.5%, whereas the level 3 network shows small decrease of creep rupture strength up to the level 0.4-0.5%, later it does not show any effect. It is to note that, in comparison with other parameters, Mn content in the datasets is lower than the maximum prescribed of 1.04%. Therefore, an analysis of the effect in the whole range was not possible.

The cast 40AN, Figure 72, is a typical example of the effect of higher tempering temperature and high Ni content results in low creep rupture strength. Figure 69 shows the cast 220 la, having high Ni content and tempering temperature of 780-790°C, which again results in creep rupture properties in the lower scatter band.

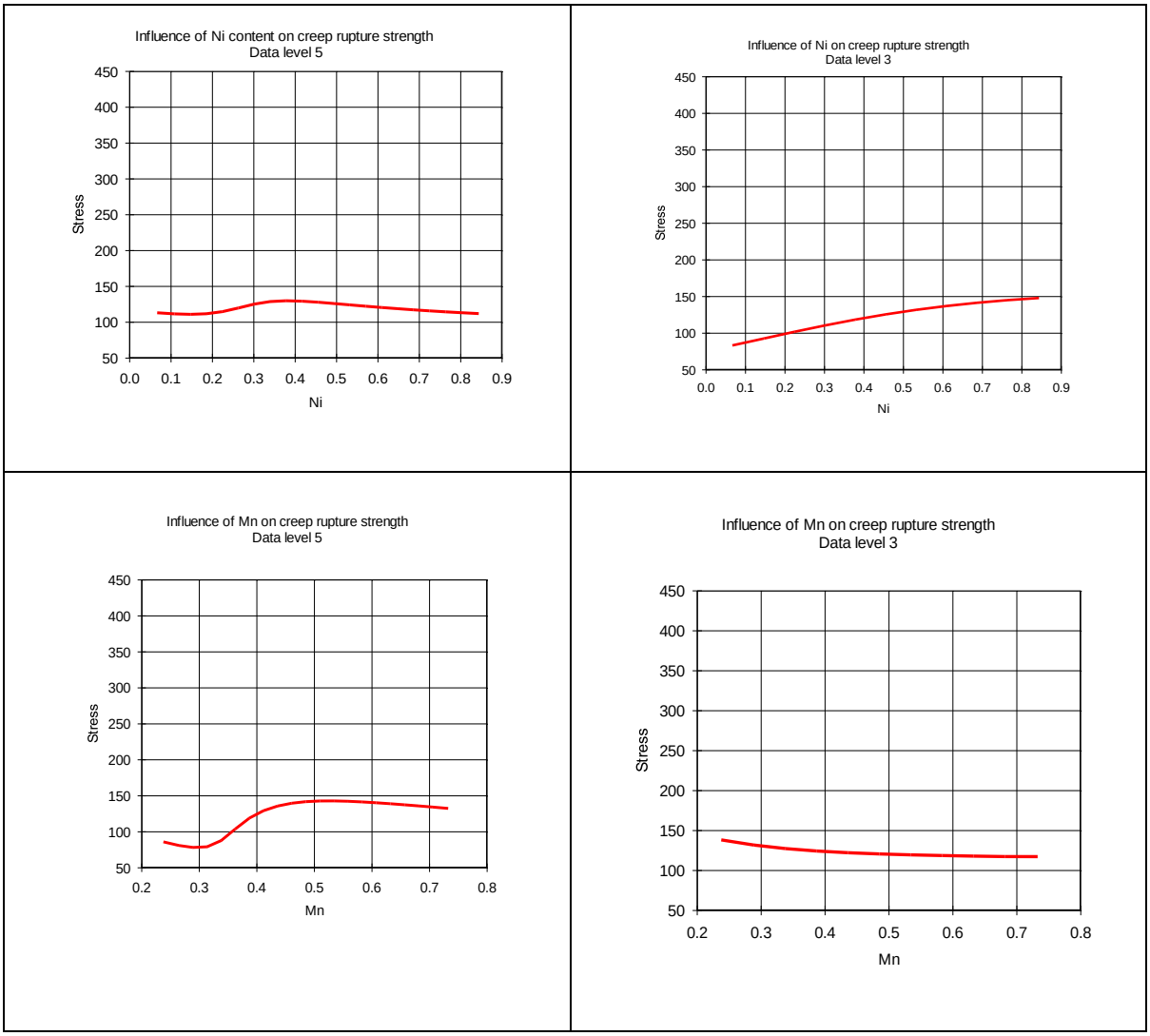

Figure 117: Influence of Ni and Mn concentration on the creep rupture strength as interpreted by the neural network – optimized data level 5 (left) and 3 (right)

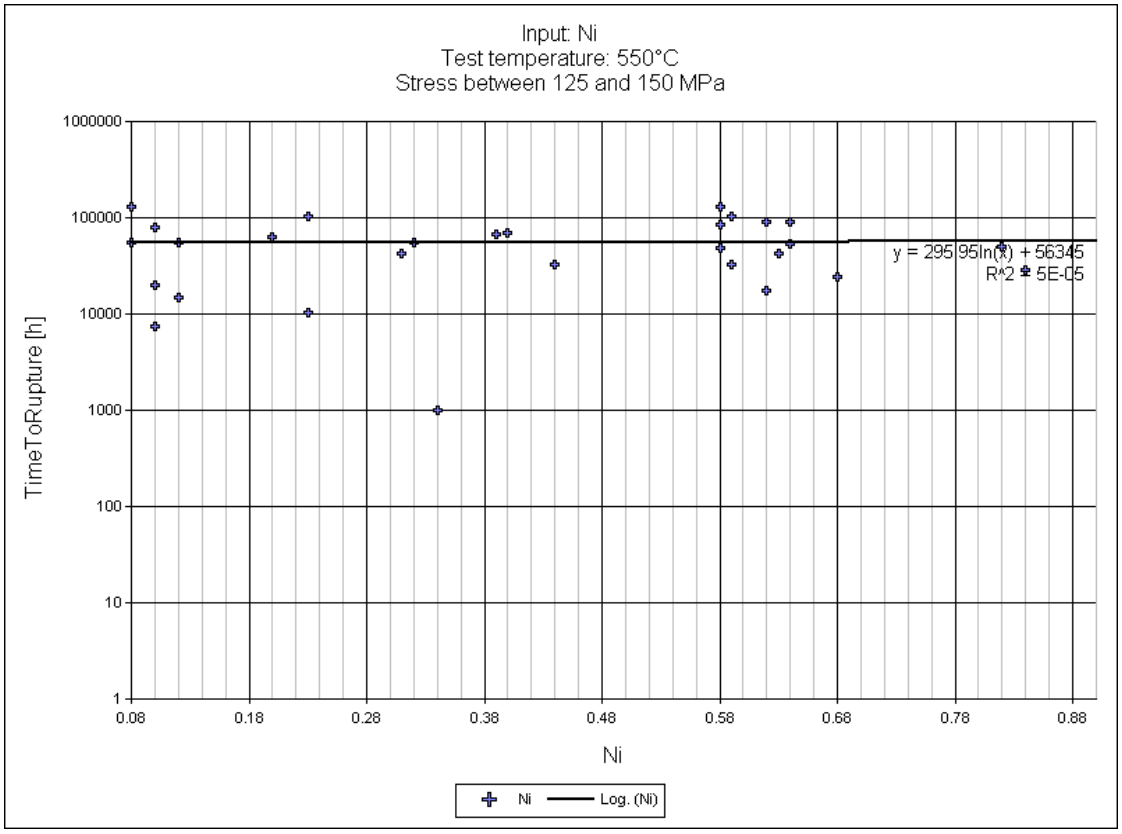

Figure 118: Influence of Ni content on creep rupture strength, experimental data, applied stress level of 125-150 MPa

5.8.7 Influence of W

According to [Mayer 06], W can influence the formation of laves-phase, as well as positively stabilize the $M_{23}C_6$ particles. For the X20CrMoV(W)11-1 the temperatures of 600°C and more laves-phase does not play a role. This can be seen also in the neural network interpretation, in the area where W concentration is defined (0.4-0.6%), it shows relatively stable, decreasing tendency. Level 5 - Figure 119, has an inflection point, due to the evaluation of casts with and without W; the area between 0 and 0.4% is not densely populated. Level 3 network, on the other hand, gives a stable curve; from both curves it might be deduced that the network would predict slightly better behavior of casts without W as with those with W present in their chemical composition. Experimental data - Figure 120, shows the same weak negative influence as the networks.

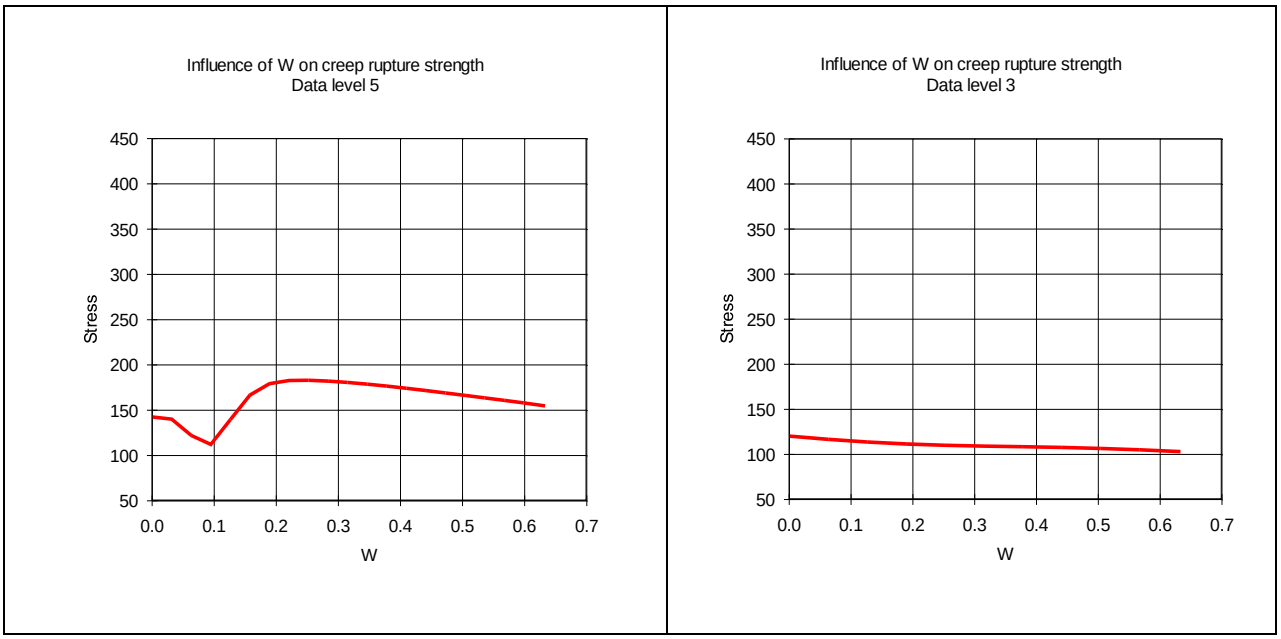

Figure 119: Influence of V concentration on the creep rupture strength as interpreted by the neural network – optimized data level 5 (left) and 3 (right) (NOTE: different data points used for illustration purposes)

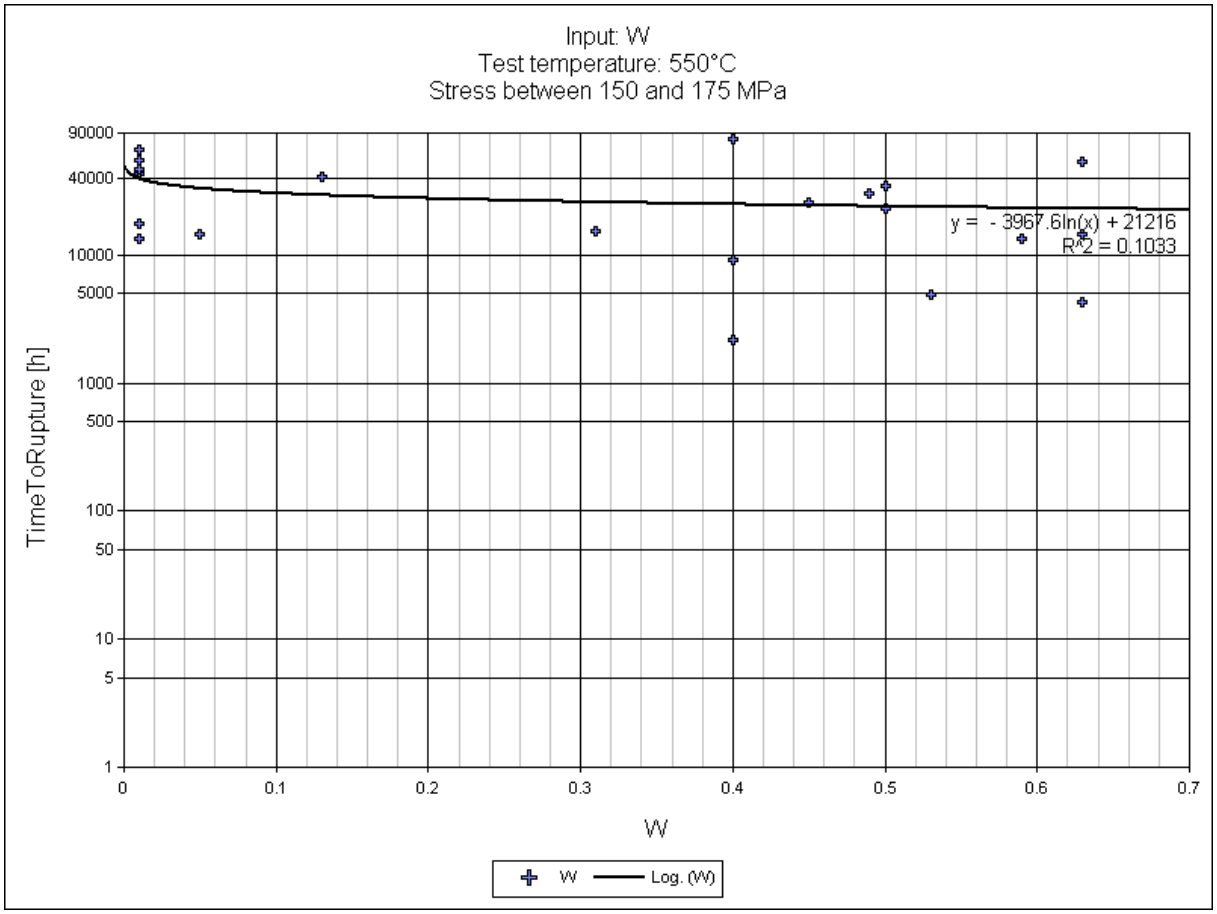

Figure 120: Influence of W content on creep rupture strength, experimental data, applied stress level of 150-175 MPa

5.8.8 Influence of austenitization and tempering temperature

Austenitization temperature was showing in the first assessment Figure 25 high influence on the creep rupture strength. This was found to be the consequence of outliners, ranging from 950°C to 1150°C; whereas the range defined by the standard requirements lies in the 1020-1080°C. This has been the motivation to remove those outliners from the training set as described in the chapter 5.4. This has given a more homogeneous dataset, as demonstrated on Figure 91. The dependency shown on Figure 33, is closely correlated to the strength classes, as defined in Table 8. These groups were established in 60s of the 20th century, and are closely related to the mechanical properties and underlying heat treatment.

According to the neural network interpretation, level 5 - Figure 121, shows mild influence, with an optimum at about 1040-1050°C, whereas the level 3 data again predicts a significant positive influence, explained trough removal of points in the optimized data level in the lower area of the data scatter. However, the duration of austenitization and quenching medium were not evaluated; it is to note that the standard specification prescribes quenching medium air, whereas most of the casts analyzed were quenched in oil. Furthermore, since for a series of casts/data points the product form could not give information about the thickness of original product, therefore the duration of quenching in dependence of the thickness of the product could not be evaluated; although it is to expect that this information might in fact contain a lot of information valuable for the network training.

The interpretation of the influence of the tempering temperature, the same situation is repeated - Figure 122. Level 5 predicts almost no influence, or a decreasing one, whereas the level 3 shows strong, stable increasing influence. Of course, this is based on single point evaluation, at best demonstrated on the Figure 123, which shows also the effect of existence of one “strong” cast at 600°C, it (wrongly) gives the network a tendency to predict that i.e. the same analyzed cast, when tempered at 600°C, would result in creep rupture life of over 275 MPa at 550°C, for 100.000 hours. This effect of the tempering temperature is also to be seen from the direct data evaluation - Figure 124 as well as on isothermal evaluated interdepencies Figure 91. As already mentioned, the effect of tempering duration and medium were not evaluated due to the data incompleteness; however, this might give an

answer to the better modeling of the heat treatment influence on the creep rupture strength.

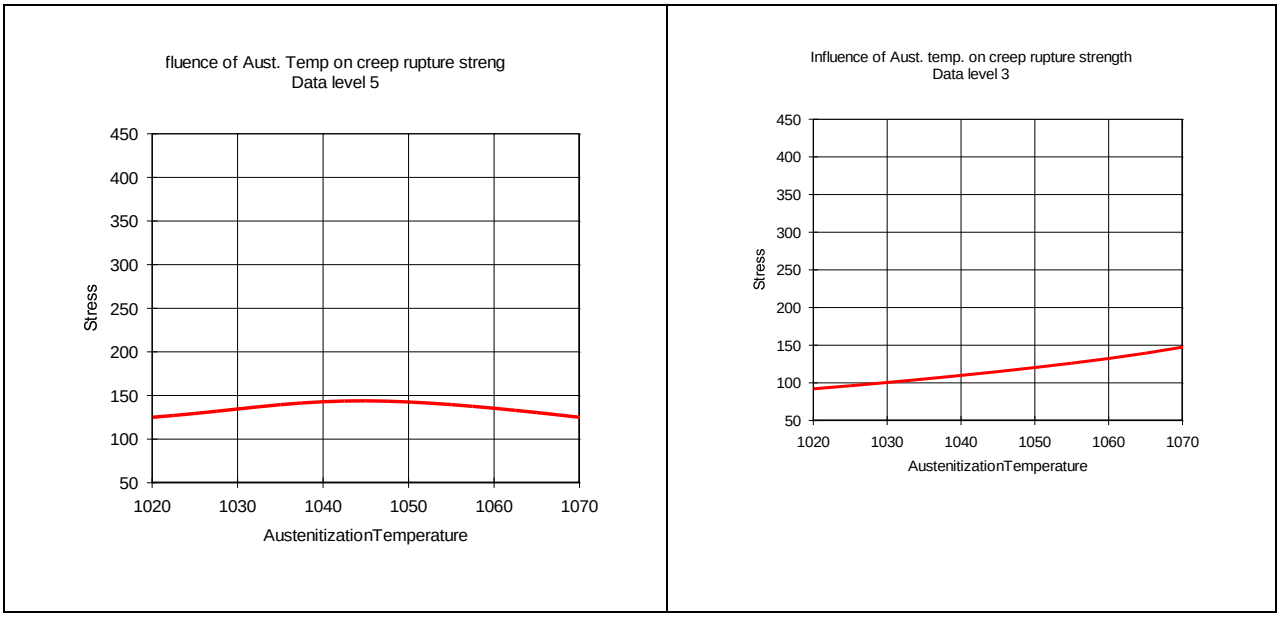

Figure 121: Influence of austenitization temperature on the creep rupture strength as interpreted by the neural network – optimized data level 5 (left) and 3 (right) (NOTE: different data points used for illustration purposes)

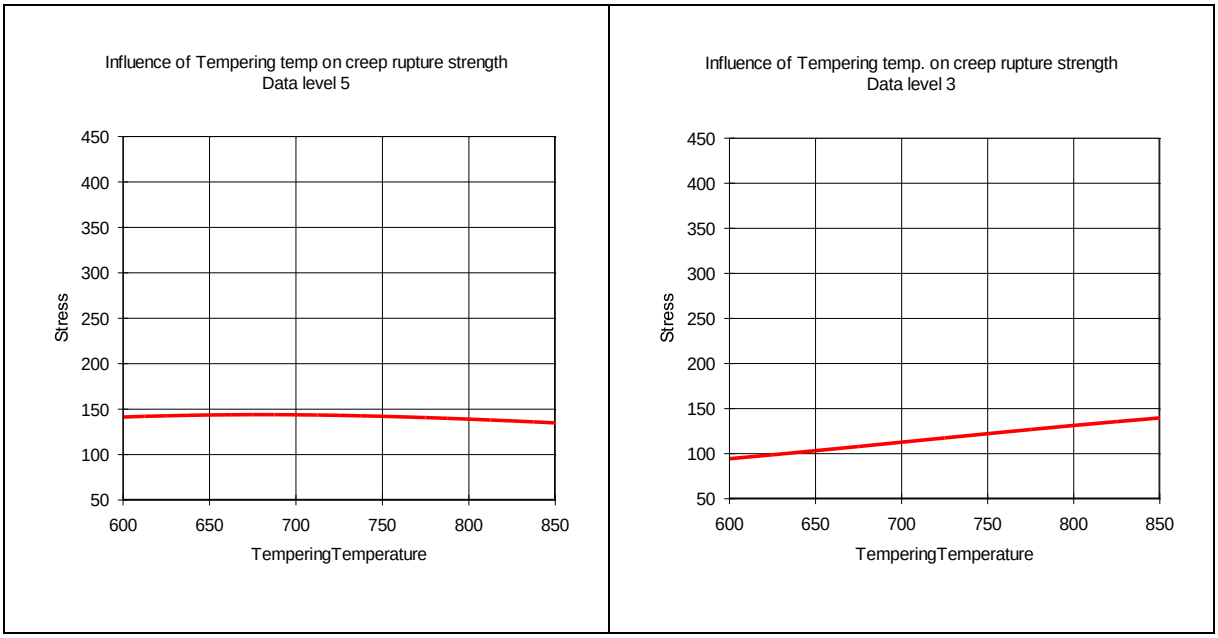

Figure 122: Influence of tempering temperature on the creep rupture strength as interpreted by the neural network – optimized data level 5 (left) and 3 (right) (NOTE: different data points used for illustration purposes)

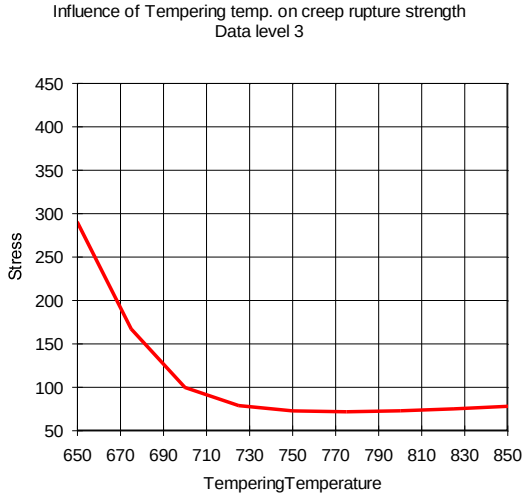

Figure 123: Influence of tempering temperature on the creep rupture strength as interpreted by the neural network – data level 3, data point 6, 100.000 hours, 550°C

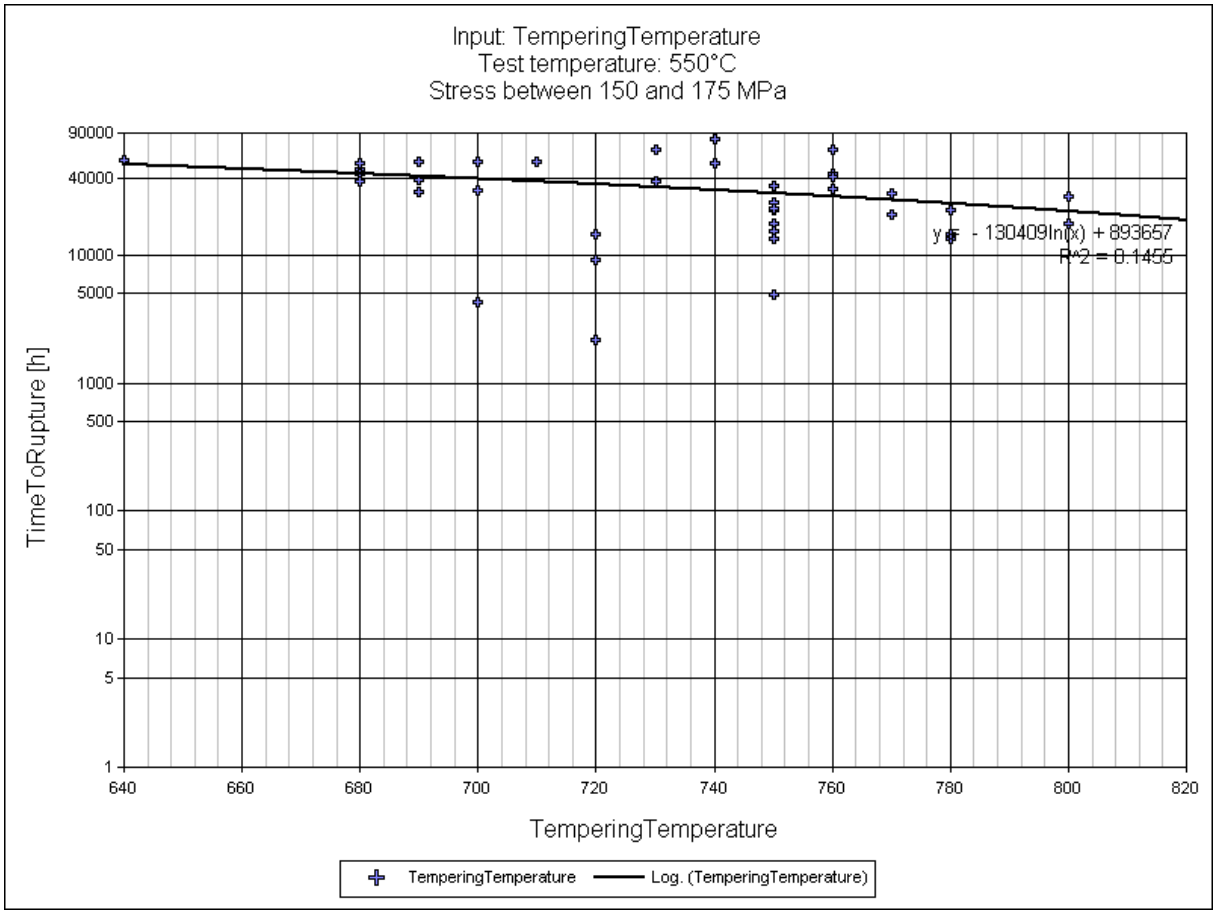

Figure 124: Influence of tempering temperature on creep rupture strength, experimental data, applied stress level of 150-175 MPa

5.8.9 Influence of mechanical properties at room temperature

Figure 125 shows the effects of mechanical properties at room temperature. Both networks show stable creep rupture strength with the increase of $R_{p0,2}$ at room temperature, which is in line with the data analysis shown on Figure 87.

The same situation is repeated for R_m at room temperature. This trend is in line with the isothermal analysis shown on Figure 88.

Direct evaluation of data in the range of 150-175 MPa at 550°C Figure 126 shows similar pattern behavior as given by the network on level 3.

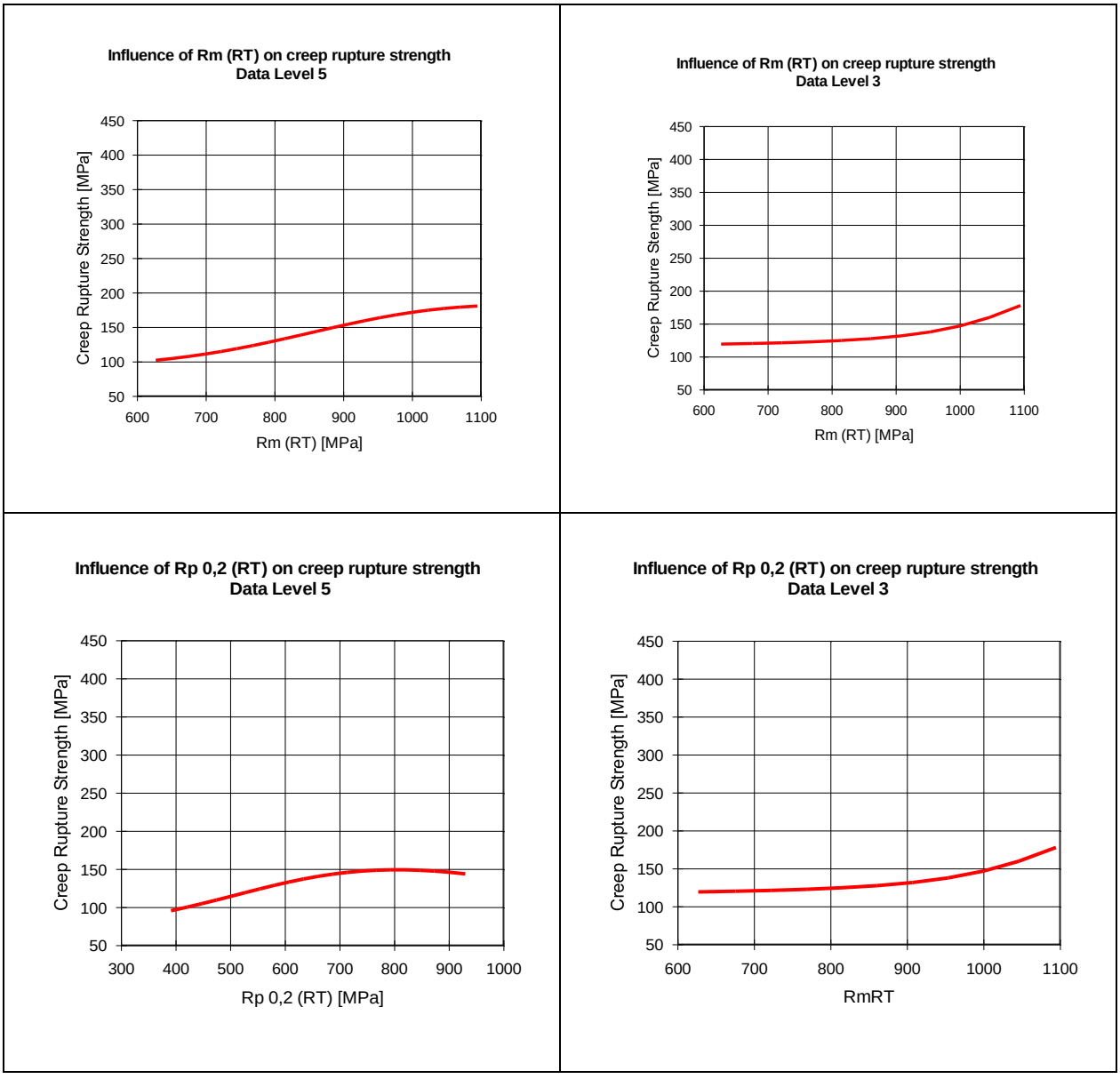

Figure 125: Influence of ultimate tensile strength R_m and $R_{p0,2}$, room temperature, on the creep rupture strength as interpreted by the neural network – optimized data level 5 (left) and 3 (right)

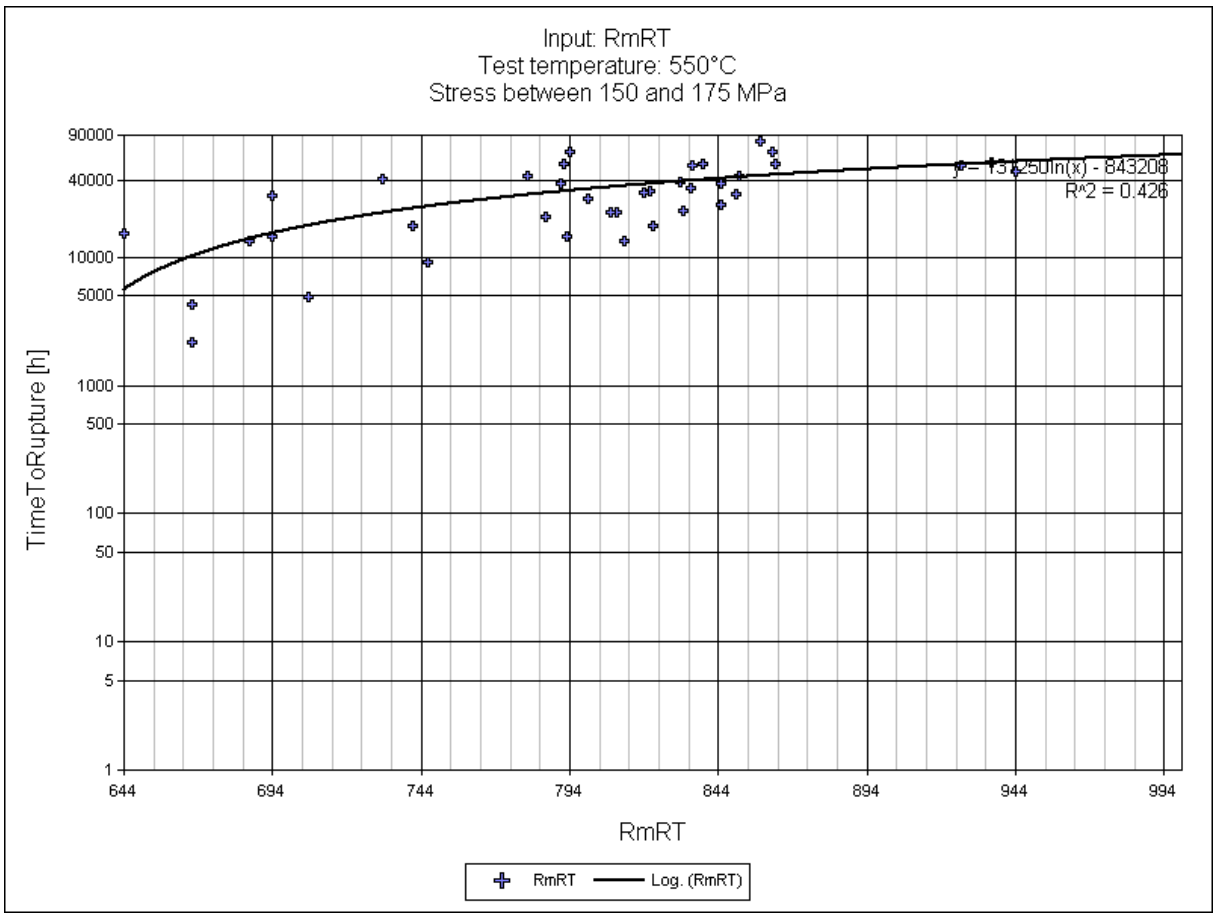

Figure 126: Influence of R_m at room temperature on creep rupture strength, experimental data, applied stress level of 150-175 MPa

5.9 Verification of optimized neural network

The verification has been done with the same datasets as given in the chapter 4.8. Figure 127 shows the cast 220 K/21 that in the previous network training - Figure 67, was predicted to have much lower characteristics than the measured ones, and is correctly predicted at level 5. Figure 128 shows the same cast prediction, and here we see almost completely accurate reproduction of the behavior of the cast by the network.

Figure 129 and Figure 130 show the prediction for the cast 220 K/20, shown in previous training under Figure 68. In the previous network training, the network was repeating the data very accurately, causing the intercept of the predicted line with the average creep rupture strength line. After the data optimization, the level 5 curve, Figure 129, keeps the trend of the short-time tests, indicating less than av-

erage curve in the long-term range, which might be interpreted as a conservatism of the network, still not giving the intercept in the previous training. The level 3 data, Figure 130, shows excellent prediction and at the same time, the trend of the average creep rupture strength line is correctly repeated, indicating the ability of the network to predict properly long-time range values.

Cast 220 la, shown on Figure 69, was having too optimistic predictions in the long-time range according to the network from the first training. Figure 131 shows network level 5 stable, conservative predictions. However, the experimental data contains two data points with the stress levels of 120 and 130 MPa that have been broken in a short period of about 100 hours; this kind of behavior was not (and cannot be) interpreted by the network correctly. Nevertheless, the network predicts less than average cast. Figure 132, level 3 neural network, shows that the network is more closely predicting the cast behavior, giving very close results at the time of rupture, following the upper break point. This figure also demonstrates again the network's ability to adjust to the different creep behavior over time.

On Figure 70, the prediction of the neural network for the cast 220Rb103a, featuring intercept of the average creep rupture line, is again calculated with the neural network of level 5 - Figure 133. The network predicts an average behavior, keeping the trend line at the level of average creep rupture strength, i.e. the intercept is no longer present.

Finally, both networks were tested on ability to predict the weak behavior of the cast 40AN, not included in the training population. The level 5 training, although indicating from the single input analyses that it is able to predict such behavior, did not recognize it and was still predicting an average cast - Figure 134. However, network on level 3 did predict weak, below lower scatter bound line behavior of the cast - Figure 135. At the same time, in order to test the network flexibility and ability to generate stable prediction, a 100.000 hours point was extrapolated (from the point of view of the data for the cast; from point of view of the network range, it is rather interpolation), and indeed that point stays stable below the lower bound line.

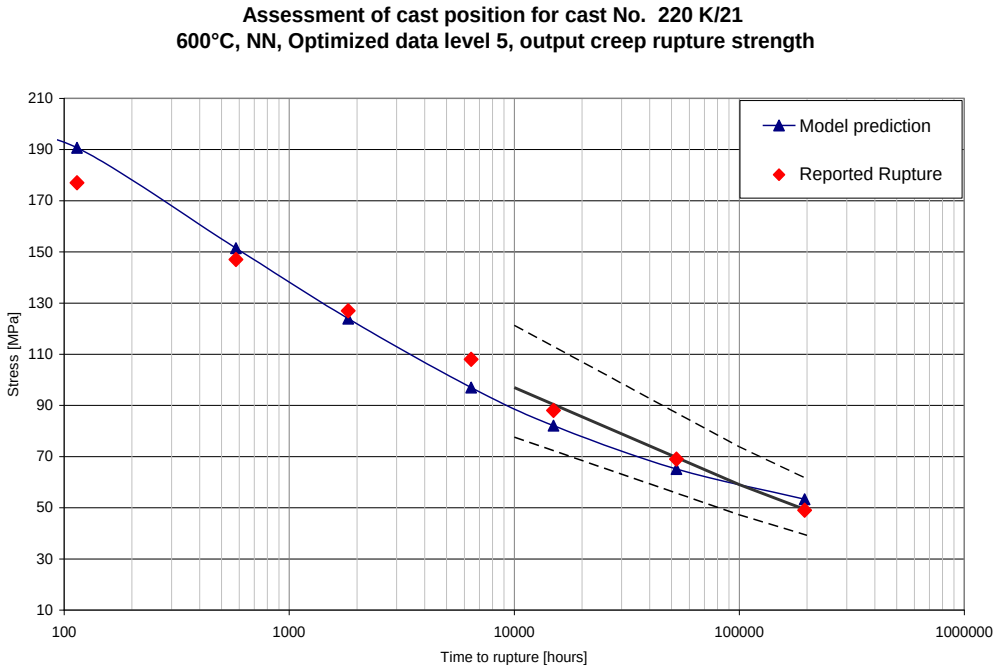

Figure 127: Comparison of model prediction (▲), experimental data (◆) and average creep rupture strength values and corresponding scatter band of the material X20CrMoV11-1 (thick and dashed lines), cast analysis 220 K/21 – 600°C, data level 5

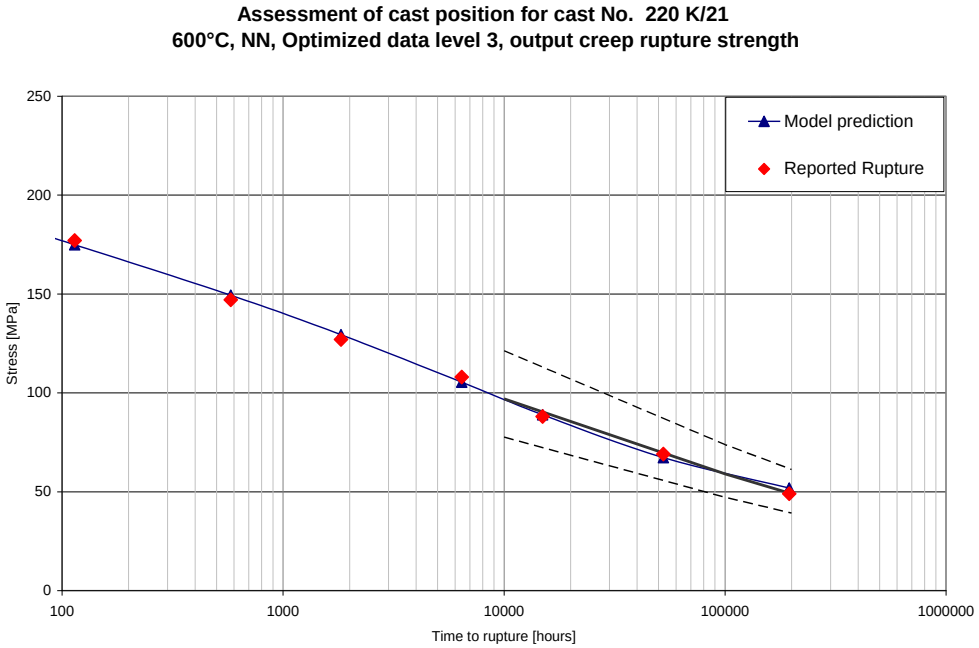

Figure 128: Comparison of model prediction (▲), experimental data (◆) and average creep rupture strength values and corresponding scatter band of the material X20CrMoV11-1 (thick and dashed lines), cast analysis 220 K/20 – 600°C, data level 3

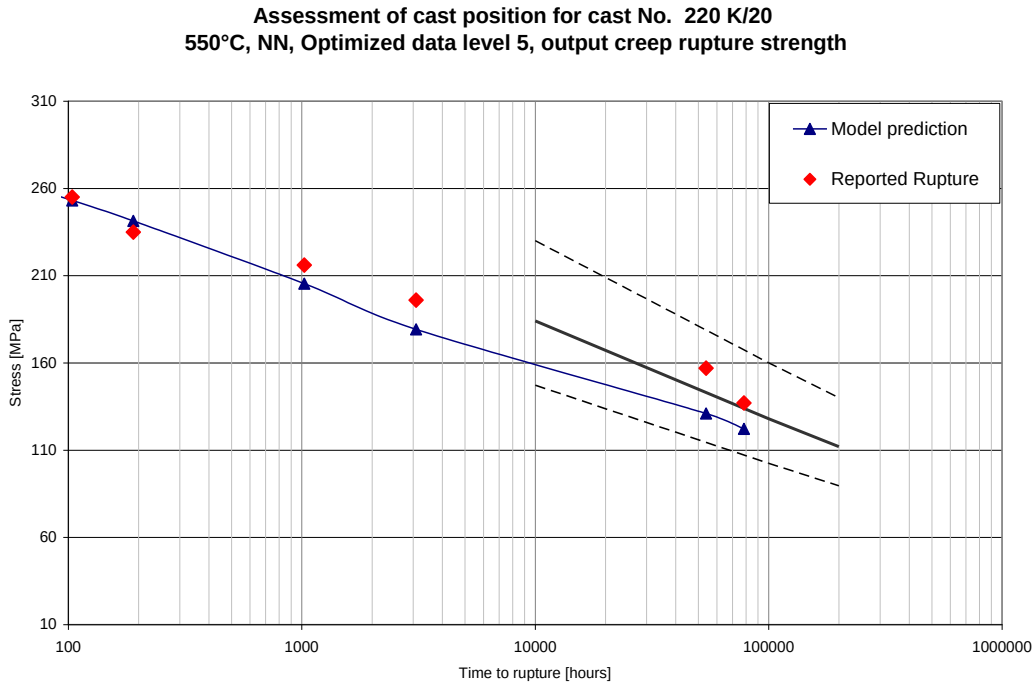

Figure 129: Comparison of model prediction (▲), experimental data (◆) and average creep rupture strength values and corresponding scatter band of the material X20CrMoV11-1 (thick and dashed lines), cast analysis 220 K/20 – 550°C, data level 5

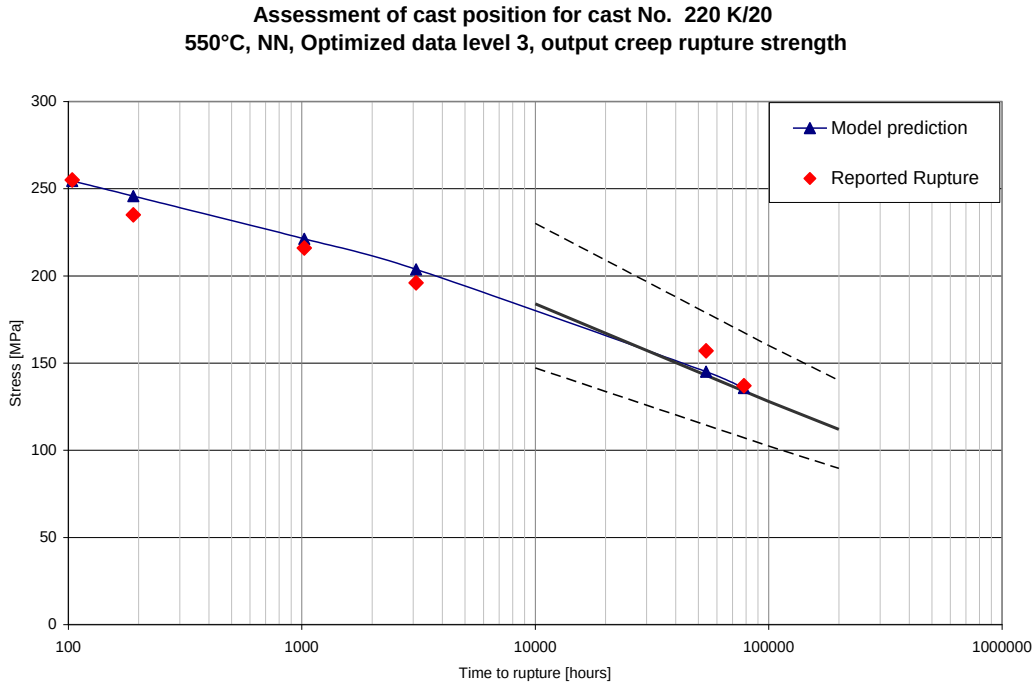

Figure 130: Comparison of model prediction (▲), experimental data (◆) and average creep rupture strength values and corresponding scatter band of the material X20CrMoV11-1 (thick and dashed lines), cast analysis 220 K/20 – 550°C, data level 3

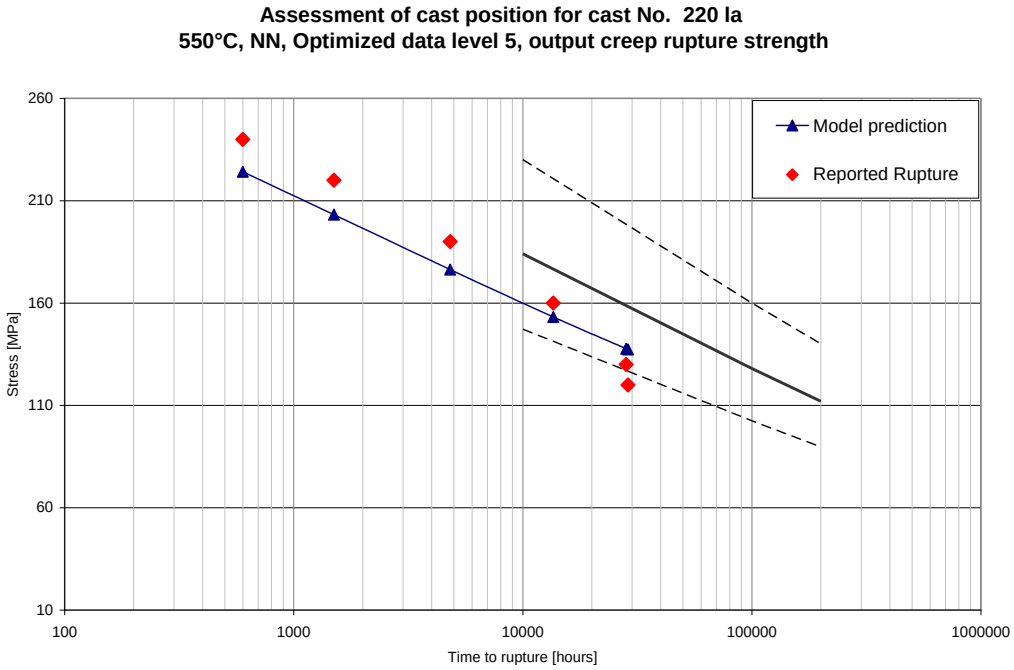

Figure 131: Comparison of model prediction (▲), experimental data (◆) and average creep rupture strength values and corresponding scatter band of the material X20CrMoV11-1 (thick and dashed lines), cast analysis 220 la – 550°C, data level 5, product form pipe

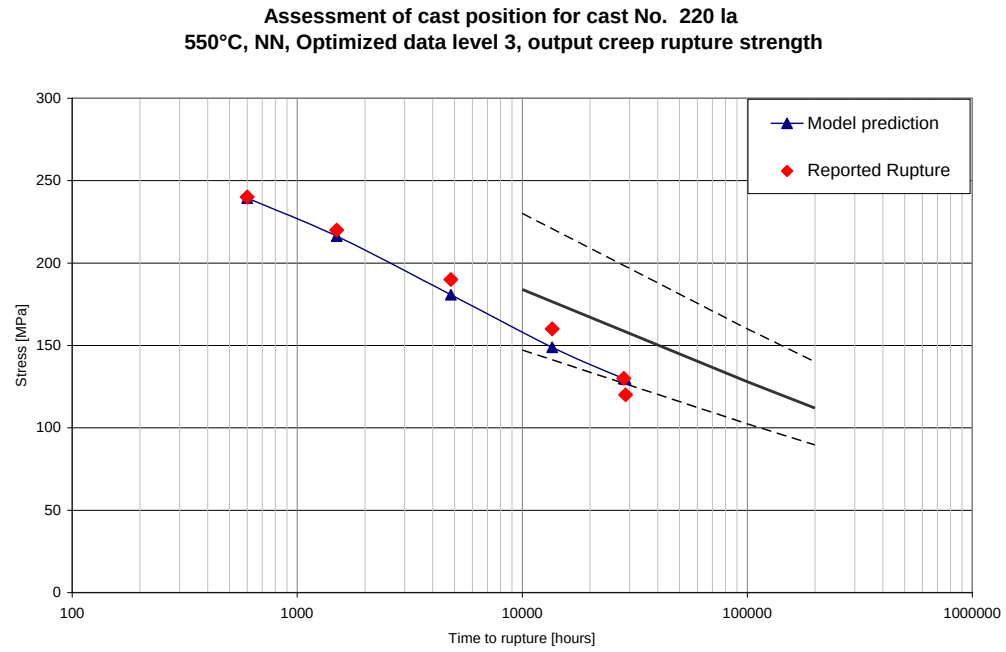

Figure 132: Comparison of model prediction (▲), experimental data (◆) and average creep rupture strength values and corresponding scatter band of the material X20CrMoV11-1 (thick and dashed lines), cast analysis 220 la – 550°C, data level 3, product form pipe

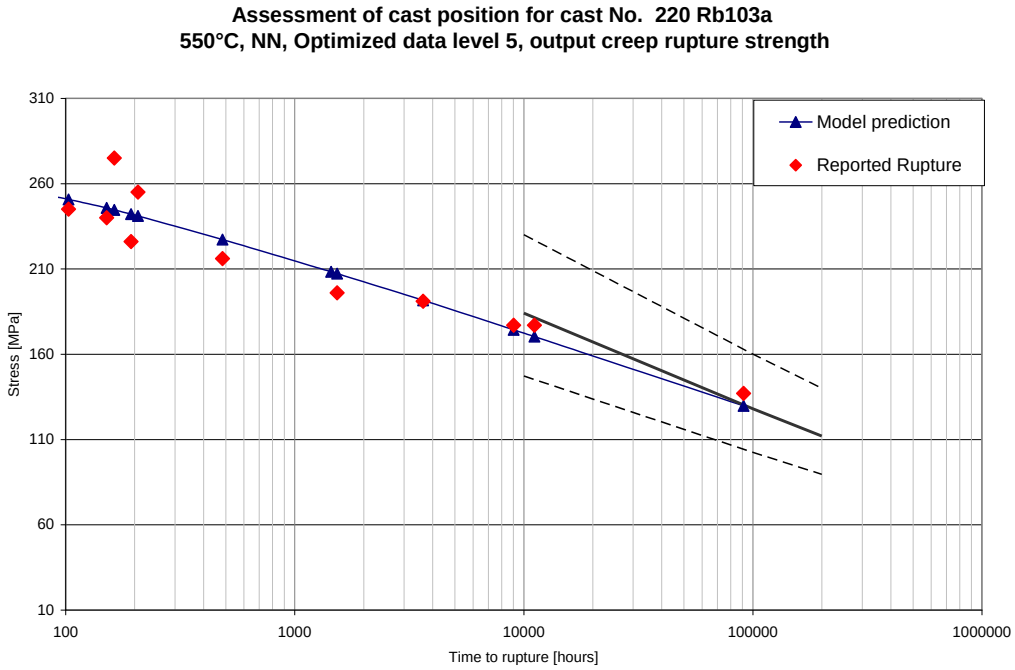

Figure 133: Comparison of model prediction (▲), experimental data (◆) and average creep rupture strength values and corresponding scatter band of the material X20CrMoV11-1 (thick and dashed lines), cast analysis 220 Rb103a – 550°C, data level 5, product form pipe

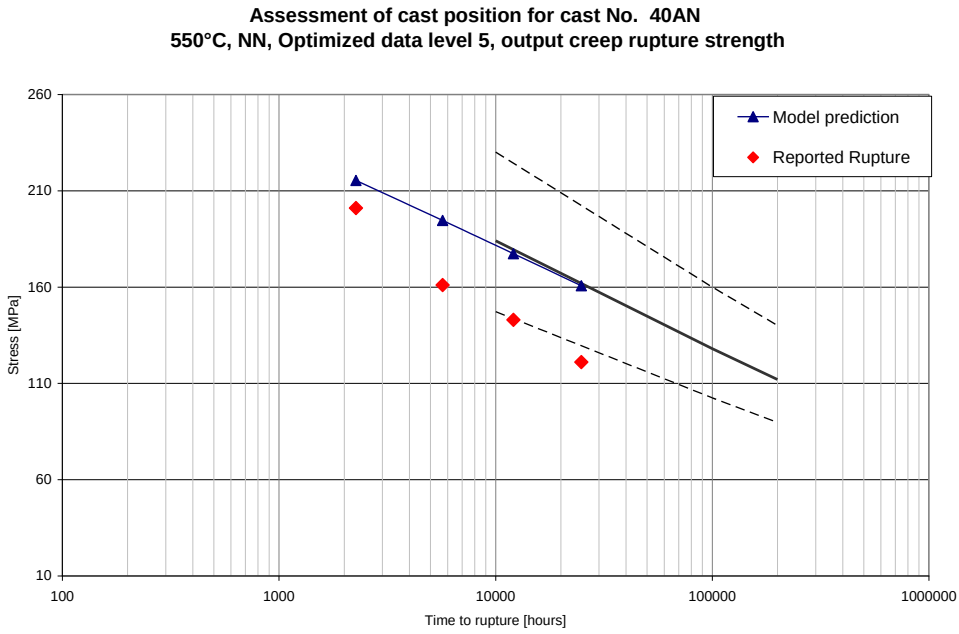

Figure 134: Comparison of model prediction (▲), experimental data (◆) and average creep rupture strength values and corresponding scatter band of the material X20CrMoV11-1 (thick and dashed lines), cast analysis 40AN – 550°C, data level 5, product form pipe

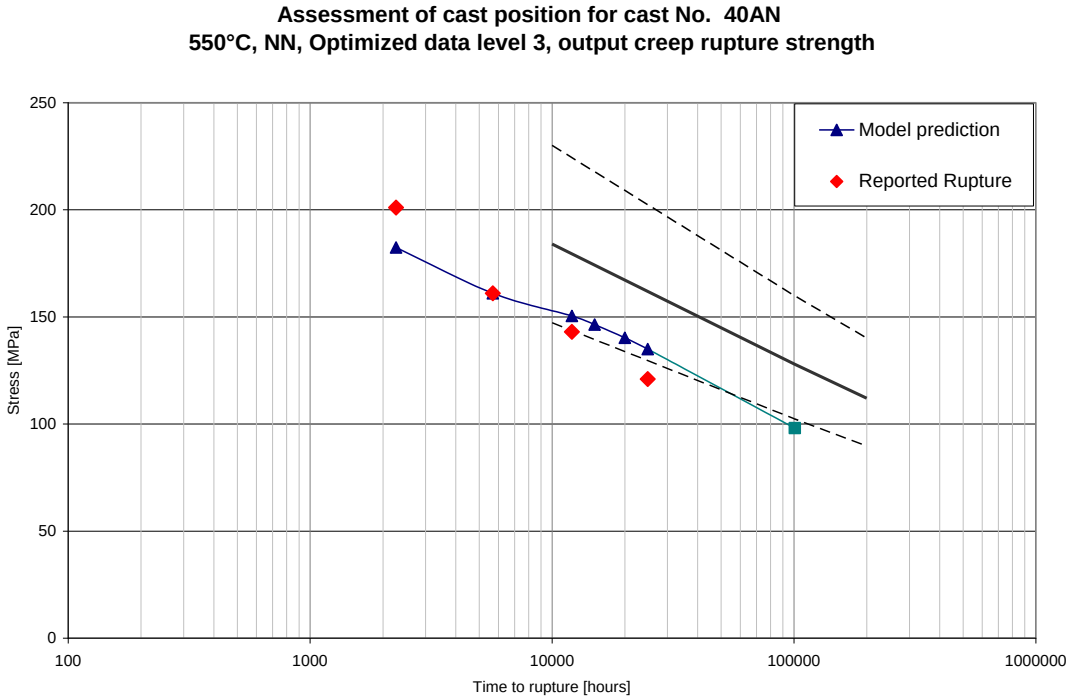

Figure 135: Comparison of model prediction (▲), experimental data (◆) and average creep rupture strength values and corresponding scatter band of the material X20CrMoV11-1 (thick and dashed lines), cast analysis 40AN – 550°C, data level 3, product form pipe

5.10 Application on a power plant component

One of the practical applications of the network is to assess the real position of the particular component in the scatter bound, and then, using i.e. TRD 508: 1978 code, determine its exhaustion due to creep.

TRD 508: 1978 defines the calculation line to be at 0.8 average time to rupture, see Figure 136. Time to rupture is determined according to the lower bound curve, and then the number of hours component was used at the given stress and temperature level is divided by the time to rupture according to the lower bound curve. This is then repeated for each temperature and stress level the component has been working in, and then the results are summed up in order to determine the overall component exhaustion due to creep [TRD 508: 1978], Annex 1, Section 2.3.

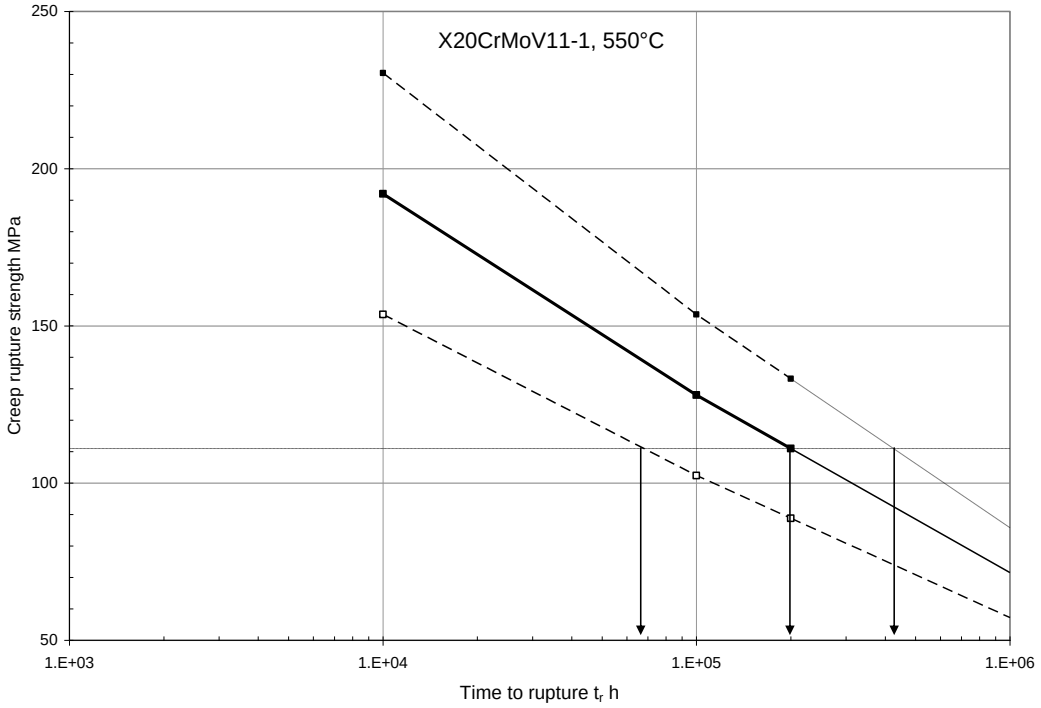

Figure 136: Schematic representation of creep exhaustion calculation according to TRD 508: 1978

Selected component is a T-piece, with the inner diameter of 230 mm, wall thickness of 48.4 mm, the stress equivalency factor is 0.74. Operating temperature is 545°C, and operating pressure 205 bar. Temperature allowance for uncertainties in temperature measurements is set to 5K, giving the reference temperature for the exhaustion calculation of exactly 550°C. According to the delivery certificate, the component's chemical composition is: C 0,17%, Cr 10,3%, Mo 1,1%, V 0,26%. Room-temperature mechanical properties are: R_{mt}= 840 MPa und $R_{p0.2}$=670 MPa.

For the calculation of the exhaustion, overall data for one year of operation (including the outage time) of about 8800 hours has been evaluated, and the corresponding pT matrix has been established – see Figure 137.

According to the standard material values for creep rupture strength and TRD 508 procedure, an exhaustion of 0.58% was calculated. Neural network, on the other hand, gives an assessment of the component's material to be slightly higher than the average, Figure 138. This, in turn, even when calculating with the safety factor of 0.8 (20% lower scatter bound according to TRD 508: 1978), gives yearly exhaustion of 0.48%. This is a reduction of about 20% creep exhaustion in one year.

Creep pressure-temperature-matrix

Operating hours input [h] for each pressure-temperature class

p-T-Classes	T = 510 ÷ 520	T = 520 ÷ 530	T = 530 ÷ 540	T = 540 ÷ 550	T = 550 ÷ 560	T = 560 ÷ 57
p = 0 ÷ 50	0:00:00	0:00:00	0:00:00	0:00:00	0:00:00	0:00:00
p = 50 ÷ 100	55:34:26	188:45:31	384:53:48	192:14:03	0:45:19	0:00:00
p = 100 ÷ 150	19:06:37	35:29:47	503:20:45	279:32:10	0:01:35	0:00:00
p = 150 ÷ 170	0:19:56	3:44:12	256:28:11	158:27:54	0:00:00	0:00:00
p = 170 ÷ 180	0:00:00	0:40:32	91:18:19	45:29:10	0:00:00	0:00:00
p = 180 ÷ 190	0:25:02	0:42:35	107:47:33	64:34:06	0:00:00	0:00:00
p = 190 ÷ 200	0:38:44	0:58:44	453:02:24	253:52:52	0:00:00	0:00:00
p = 200 ÷ 205	0:18:43	1:15:32	1382:09:58	740:16:11	0:00:00	0:00:00
p = 205 ÷ 210	1:03:07	1:21:14	460:48:39	255:20:50	0:00:00	0:00:00
p = 210 ÷ 215	0:00:00	0:00:18	6:06:25	0:37:52	0:00:00	0:00:00
p = 215 ÷ 220	0:00:00	0:00:00	0:40:18	0:05:34	0:00:00	0:00:00
p = 220 ÷ 225	0:00:00	0:00:00	0:00:03	0:00:00	0:00:00	0:00:00
p = 225 ÷ 230	0:00:00	0:00:00	0:00:00	0:00:00	0:00:00	0:00:00
p = 230 ÷ 235	0:00:00	0:00:00	0:00:00	0:00:00	0:00:00	0:00:00
p = 235 ÷ 240	0:00:00	0:00:00	0:00:00	0:00:00	0:00:00	0:00:00
p = 240 ÷ 245	0:00:00	0:00:00	0:00:00	0:00:00	0:00:00	0:00:00
p = 245 ÷ 250	0:00:00	0:00:00	0:00:00	0:00:00	0:00:00	0:00:00
p = 250 ÷ 255	0:00:00	0:00:00	0:00:00	0:00:00	0:00:00	0:00:00
p = 255 ÷ 260	0:00:00	0:00:00	0:00:00	0:00:00	0:00:00	0:00:00

OK

Cancel

Extrapolate

Graph

Total Time:

8759:16:22

p-T-Class edit only

[h, h:mm, h:mm:ss], p: [bar] T: [°C]

Figure 137: Component example – pT Matrix, for one year of component exploitation

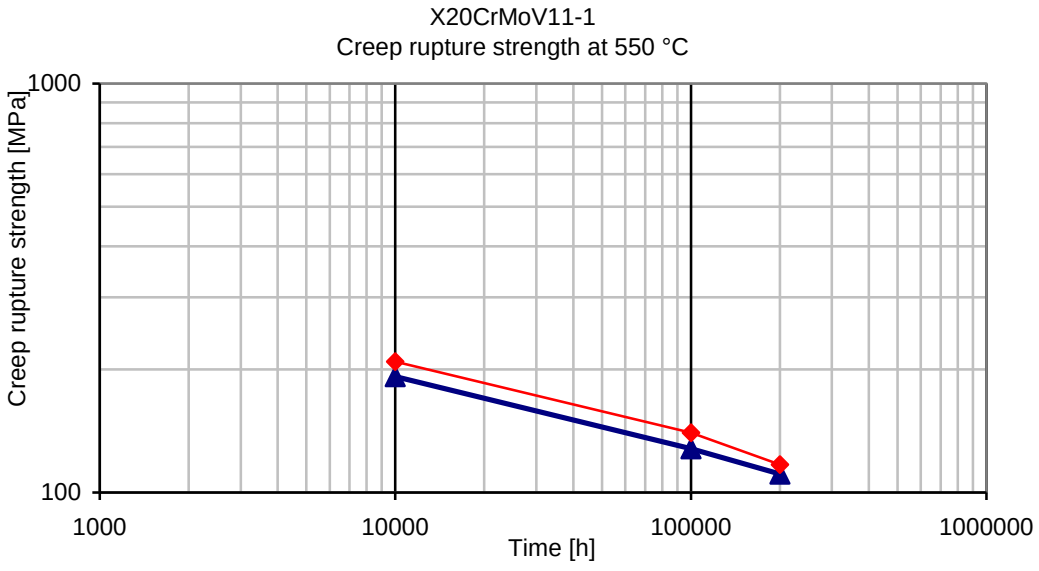

Figure 138: Component example – comparison of standard values (▲) and neural network prediction (◆)

6 Error and confidence levels

The scatter of the experimental data for the network training in any direction is considerable, Figure 48. If only considering applied stress and time to rupture, it is clear that the overall population does not fit in ±20% confidence bounds, Figure 139. If, however, only compliant data to the current standard specification is analyzed – i.e. 314 data points and 37 chemical composition specifications, then, the population becomes more homogeneous, Figure 140. This suggests as it is known from literature, that the specification of the material was fixed only after a great number of tests were conducted and experience with both heat treatment and chemical composition have been gained. Figure 140 also shows that even the compliant population does not fit the ±20% confidence bounds of standard specification, whereas the applied time-temperature parameter Orr-Sherby Dorn (see 3.2.1 Time-Temperature Parameters) suggests a slightly lower values for average creep rupture strength then defined in the standard specification.

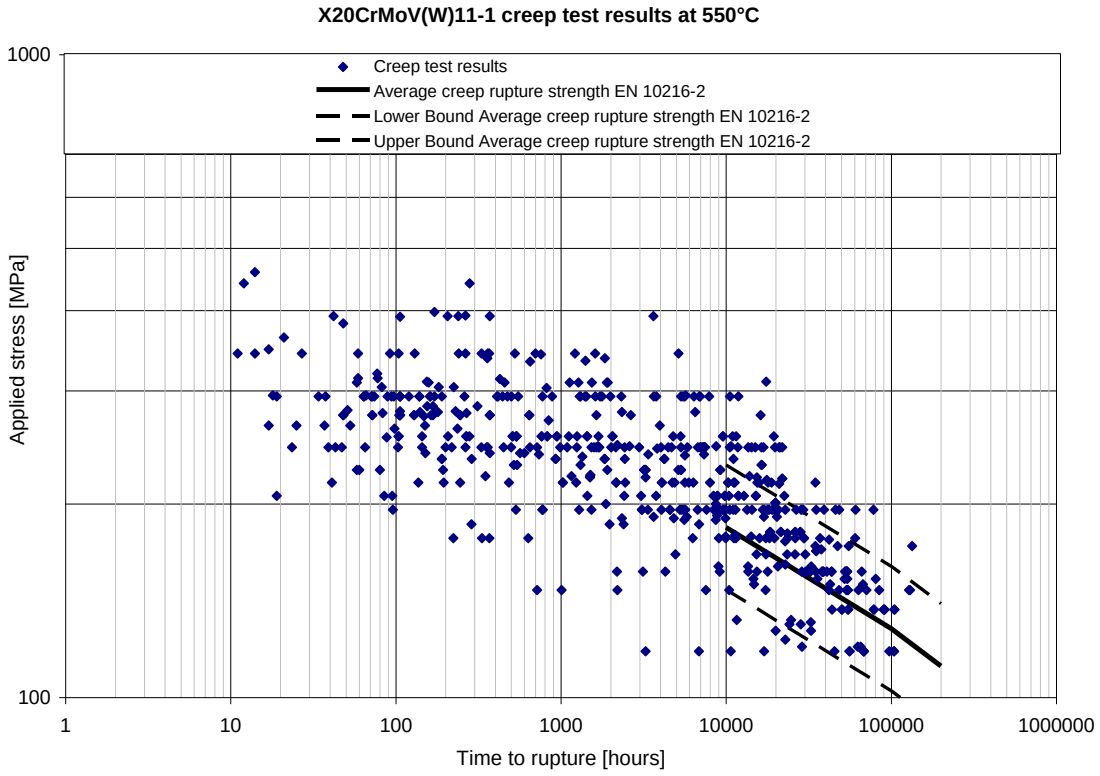

Figure 139: Data scatter test data compared with standard requirements

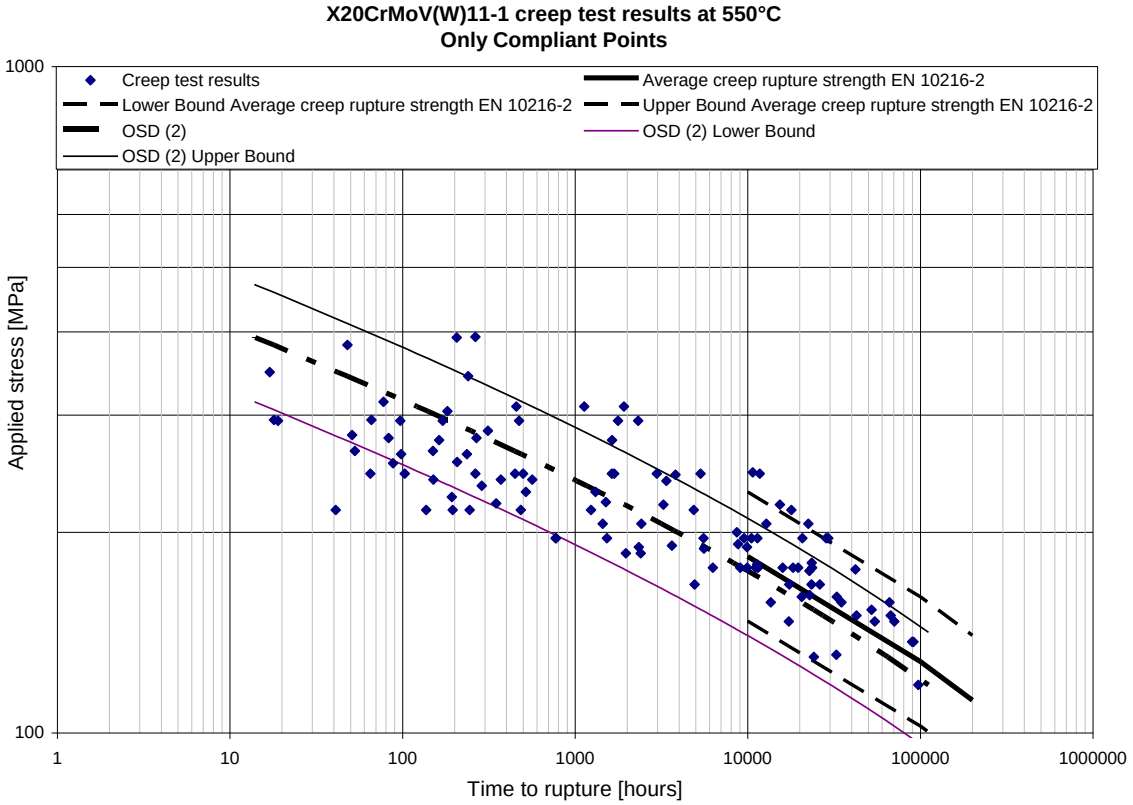

Figure 140: Orr-Sherby Dorn analysis of compliant-only data points

6.1 Residuals

Neural network itself is characterized by residuals, i.e. it tends to minimize the square distance between predicted and measured output values. DataEngine training models are based on residual minimization, both on mean and max scale. Furthermore, the learning criteria itself are optimized so no over fitted network can be constructed, unless using the same dataset for the training and testing. Therefore, the resulting residuals are not tending to 0, but rather staying in the range of ca. ±10 MPa, and extreme values going up to 50 MPa error – see Figure 141. Overall, the optimally trained networks were showing a residual value of ca. 10 MPa, whereas the lower data levels tend to give lower residuals, mainly due to the less possible outcomes, i.e. less data for training while having more features to assess. The learning algorithm applied (SuperSAB and Resilient Propagation, see 3.4.5), are working both on minimization of residuals, however, at each 1000 steps during the training was performed against the test dataset, and the network giving the best test results (minimum residuals and max. testing error) was kept as basis for the next training epoch.

Based on mean residual error of ca. 10 MPa, it means that each predicted point has an inherited error of ± 8-10 MPa, depending on the level of the network. Distribution of residuals is shown on Figure 141. For comparison, Orr-Sherby Dorn regression was applied on the same dataset, and the resulting residuals are shown on Figure 142. Also, Orr-Sherby Dorn would be characterized by a mean residual error of ca. 49 MPa. Here the network shows its comparative advantage to describe the behavior of the real dataset much more closely than a common regression. Of course, it is to note that the purpose of the network is to predict the behavior of the single data point as accurately as possible, whereas the Orr-Sherby Dorn is predicting the behavior of the whole population. It would be interesting to test the residuals for the “average neural network curve” against the data points, in order to make a complete comparison of goodness of fit for both methods. The only problem for such an exercise is the definition of the average representative of the overall population, as the mean values of all the inputs do not reflect interdependencies between the different input variables; i.e. mechanical properties at room temperature are rather a function of the other input variables, such as chemical composition elements and heat treatment, then independent variables. Also, there are (weak) interrelations between chemical composition elements; this is also a fact that speaks against selecting average values for the average representative of the population.

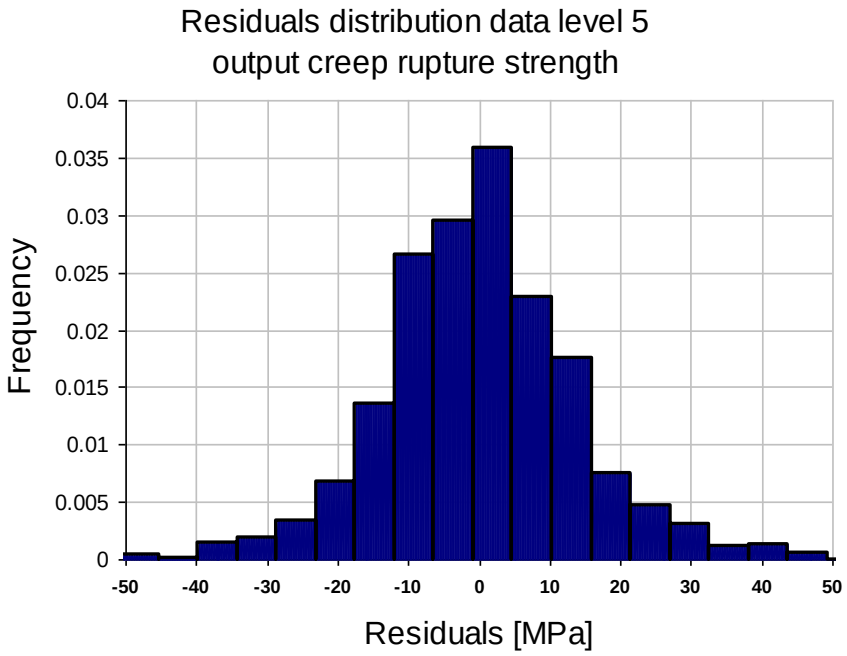

Figure 141: Distribution of residuals for the optimized network level 5

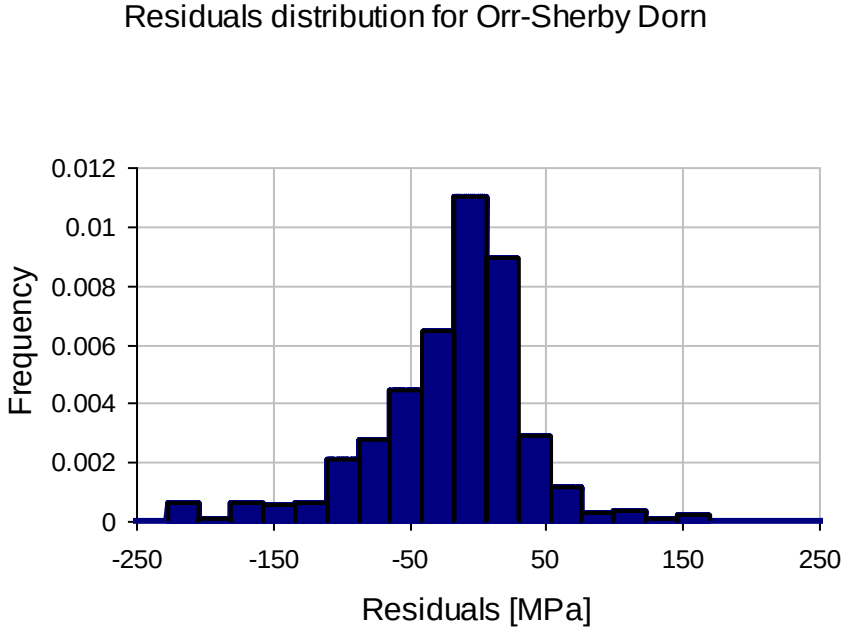

Figure 142: Distribution of residuals for the Orr-Sherby Dorn regression applied on level 5 data

6.2 Neural network as regression

If we consider the neural network as regression form, resulting in an analytical (although in form of “black box”) description of dependencies between input varia-

bles and output variable(s), that also has a deterministic character (i.e. multiple calculation of same dataset yields always the same result), then it is possible to apply the regression analysis and confidence level calculations as for any other regression, based on residuals.

The confidence bound calculation can be, due to the fact that here we do predict the behavior of the cast in the scatter bound, performed on overall population behavior, or on the level of single cast prediction. Overall population error is reflecting the scatter of the data itself, i.e. is giving new 95% confidence bound lines. They are applicable on each of the predicted points, and therefore applicable also on the cast behavior prediction. On the other hand, individual casts have different scatter, and when comparing predicted vs. experimental values, one can construct individual scatter bands for the given single cast. Both are demonstrated on the Figure 143 and Figure 144.

Figure 143 shows a very large scatter in the data of the cast itself. Therefore, the prediction confidence lines are going (due to the smaller number of points as in the overall population) a little bit over the overall population scatter bands.

Figure 144 shows a cast with very narrow scatter in the data; here is the difference between individual cast and overall population behavior clearly visible, i.e. although the number of points is much less than for the overall population and due to homogeneity of the data, the resulting individual scatter band for the cast is much narrower that the scatter band of the overall population.

As demonstrated on the Figure 144, for a homogeneous cast behavior it is for sure an advantage to apply the individual scatter band lines to the prediction rather than those of the overall population. However, this is only possible when comparing the cast results with the network prediction, therefore, requiring existing performed tests. If this is not the case, the application of overall confidence bound of the overall population is the only choice.

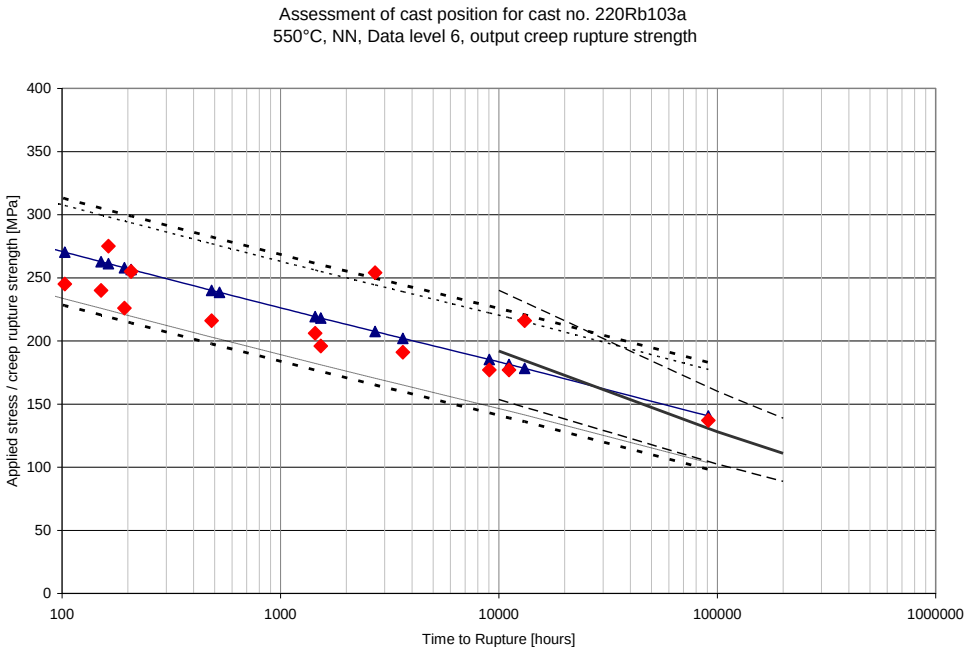

Figure 143: Comparison of model prediction (▲), experimental data (◆) and average creep rupture strength values and corresponding scatter band of the material X20CrMoV11-1 (thick and dashed lines), cast analysis 220Rb103a – 550°C, data level 6; the thick and thin dotted lines represent the overall population and individual cast confidence bounds

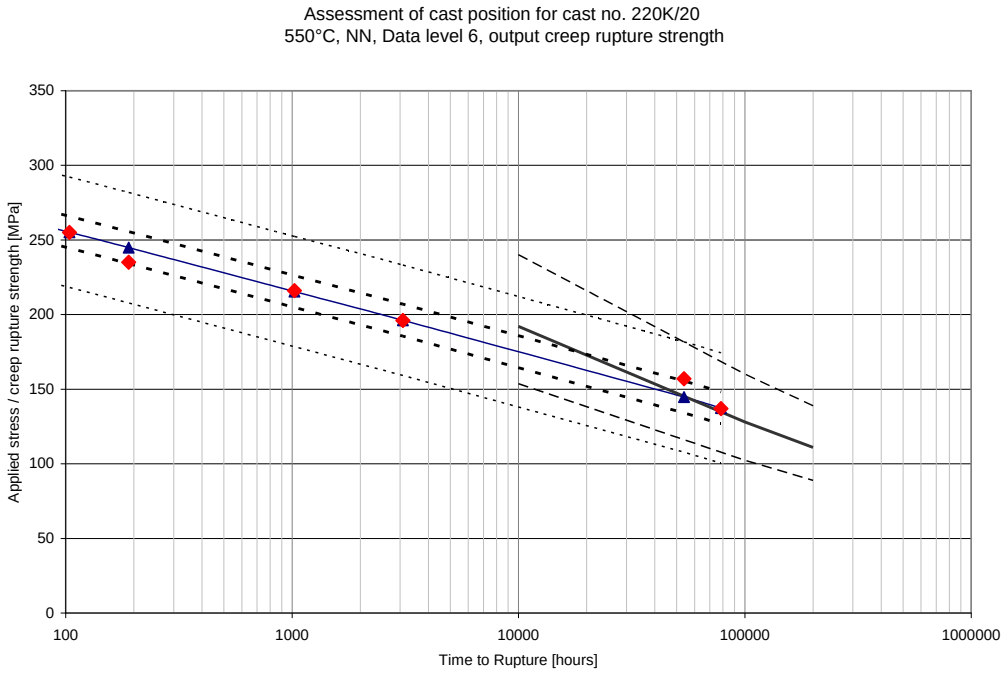

Figure 144: Comparison of model prediction (▲), experimental data (◆) and average creep rupture strength values and corresponding scatter band of the material X20CrMoV11-1 (thick and dashed lines), cast analysis 220K/20 – 550°C, data lev-

el 6; the thick and thin dotted lines represent the overall population and individual cast confidence bounds

6.3 Sensitivity of the network

Furthermore, the sensitivity of the network has been tested - Figure 145. The inputs have been varied in the given range, i.e. population of similar data points around the working point have been constructed, and then the neural network has been used to calculate the outcomes for 10.000, 100.000 and 200.000 hours. The results show comparable results as the mean residual error of ca. ±10 MPa, and pretty much consistent, i.e. giving an even scatter around the working line.

Other possible ways of error handling are use of non-linear regression procedures, as described in similar applications of neural networks on modeling of physical phenomena by Ho 01 and Shao 97.

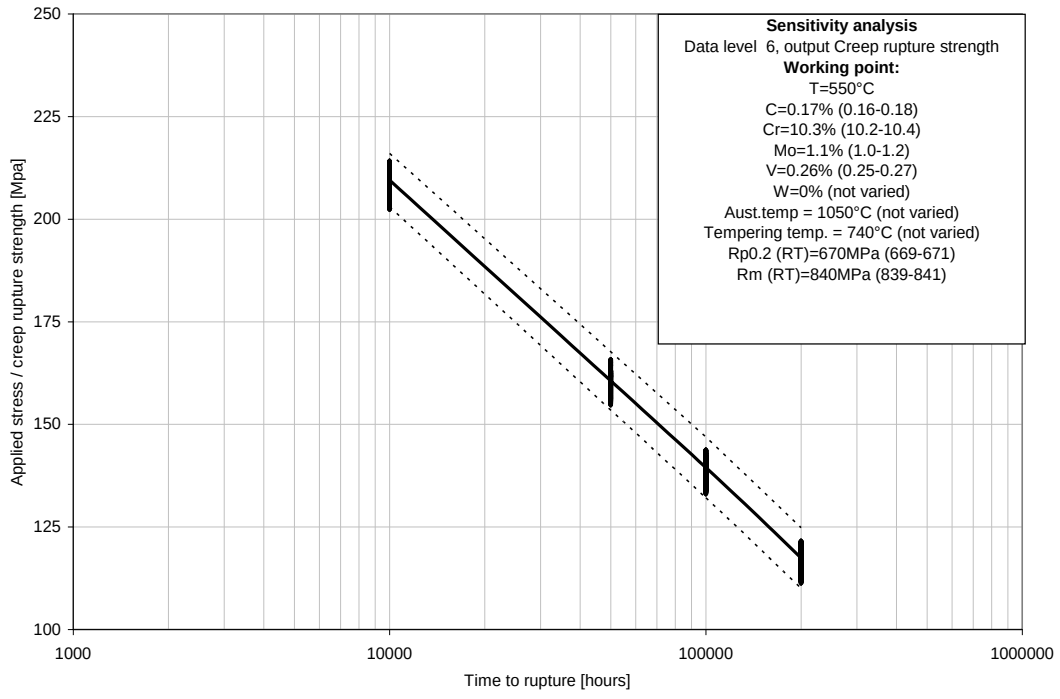

Figure 145: Sensitivity analysis, working point T=550°C, C=0.17% (0.16-0.18), Cr=10.3% (10.2-10.4), Mo=1.1% (1.0-1.2), V=0.26% (0.25-0.27), $R_{p0.2}$ (RT)=670MPa (669-671), R_m (RT)=840MPa (839-841), level 6, output creep rupture strength

7 Summary

This work has demonstrated the application of neural networks on prediction of creep rupture properties of a specific cast based on data contained in material certificates of a power plant component. More specifically, the goal was to predict the position of the given cast in the scatter band associated with the specific material. To this goal, model material X20CrMoV11-1 was selected and commercial software DataEngine used for training and verification of the network.

As the database for the assessment process, the data from the German “Arbeitsgemeinschaft warmfester Stähle“ for the model material was used. The database contained very heterogeneous data points, due to the historic development of the material specification for the X20CrMoV11-1. Also, the database contained more than one single product, heat treatment or chemical analysis specification, and in almost all cases covering wider range than defined in contemporary standards. If applying the current standard specifications, as defined in 4.2, out of 177 initial casts available for the analysis, only 37 would remain for analysis. If we consider that also the data quality, i.e. number of features available for the classification has been different for different casts and data points, this reduction to compliant-only specification would make the task at hand impossible.

Therefore, a combination of data mining and discovery, expert judgment and comparison of the results with the experience and knowledge available about the material in more than 6 decades of exploitation, were utilized to assess the quality of the networks trained. The judgment path taken is partially described in this work, and it demonstrates the complexity of the problem at hand. For each step taken, a complex analysis path was utilized, and various methods of data evaluation have been used.

During the process, it is clearly demonstrated that the pure data selection and training of the network does not produce desired results. Pure neural network software utilization, without consideration of the underlying physical and metallurgical knowledge might easily mislead the user into “discovering” new, non-existing dependencies, and in the end, lead to unfounded conclusions. Both awareness of the metallurgical properties of the given steel, as well as understanding of the ef-

fects of the underlying data structure and distribution of single inputs is required for successful application of the neural network technology.

On the other hand, it has been shown that neural networks, considered as both analytical and empirical method at the same time, given the proper data selection and careful training and results evaluation, can give much better prediction results as the classical analytical methods considering just three dimensions (stress, time, temperature) can give. Neural networks have the ability to describe the complex behavior such as creep phenomena in time and the ability to flexion in the long-time creep range. Furthermore, as shown in some examples, the neural network predictions in the extrapolated areas tend to be stable, although this has yet to be investigated further, on more numerous examples, and in the allowable range.

The problem of interdependency of the input variables such as chemical composition, heat treatment and mechanical properties can be overcome using the neural network model; the empirical model seems to detect and interpret the weak dependencies correctly, moreover, the known, either based on production and exploitation experience or on analytical/expert test data evaluation, dependencies are successfully being repeated by the network.

The big challenge is assessment of the inherited network errors and uncertainties of the network predictions. As demonstrated, the network prediction error over the standard data set is significantly lower, when considering single creep test results; on the other hand, the network scatter is characterized by the scatter of the data, therefore making the prediction characterizing the network to have comparable prediction power as the classical analytical methods. Furthermore, the scatter of the input variables and their inhomogeneous distribution over the range of (allowable) values have significant influence on the uncertainties of the network prediction, as already demonstrated by the i.e. [Badeshia 01].

It is a fact that the mechanical and creep properties of a cast are the result of its chemical composition and heat treatment, that, in turn, determine its microstructure and thus define its properties. It might be of great use to utilize this knowledge (i.e. microstructure) for the better prediction of the mechanical and creep properties of steel. However, since the underlying data set did not contain microstructural data, and most of the tests were conducted in the 60’s until 80’s of last century,

this path could not be taken, although the analysis performed hints that this might be the path that would yield much more reliable predictions of the creep properties.

The path for such, enhanced, analysis might require inclusion of additional measurable quantities that were not used in this work, such as hold time for both austenitization and tempering, scaled down on the thickness of the cast/product tested, as well as other non-quantifiable parameters, such as austenitization and tempering medium (i.e. oil, air). Further, from micro structural properties, the ASTM grain size, number of MX, $M_{23}C_6$, and other participates might be used, as well as the assessment of the structure. These inputs could be then used for assessment of the mechanical properties first at room temperature, in order to ensure much broader dataset available for the assessment, and then established interdependencies might be applied / repeated towards the creep characterization of a material specification.

To this goal, a selection of material with both narrow specification concerning the chemical composition and heat treatment and a broad database of test points representing different possible chemical compositions and heat-treatment variations should be selected. P91 and P92 specifications might be, from point of view of availability of the data and contemporary utilization, right candidates for such an evaluation, as the preliminary analysis of their data availability and consistency of the data is promising (Figure 44).

8 References

AGW 69 — Ergebnisse deutscher Zeitstandversuche langer Dauer. Verlag Stahleisen, Düsseldorf 1969

AiF 92 — AIF-Projekt 234 D; Gefügeänderung und Zeitstandschädigung bei Langzeitbeanspruchung TU Chemnitz/MPA Stuttgart, 1991 bis 1992

ASME BPVC: 2004 — ASME Boiler and Pressure Vessel Code:2004

ASTM E112: 1996 — ASTM E112:1996, Standard Test Methods for Determining Average Grain Size

AVIF 198 — D. Balos, K. Maile und W. Müller: Abschlussbericht des Forschungsprojekts Bewertung der Streubänder im Langzeitverhalten von warmfesten Stählen mit Hilfe der Anwendung von Data Mining-Methoden (AVIF 198), 2007

Badeshia 01 — H. K. D. H. Badeshia: Design of ferritic creep-resistant steels. ISIJ International, Vol- 41 (2001), no. 6, pp. 626 -640

Badeshia 05 — H. K. D. H. Bhadeshia: Microstructural Stability Of Strong 9-12 Wt% Cr Steels, Proceedings of Super-High Strength Steels, 2-4 November 2005, Rome, Italy, Associazione Italiana di Metallurgica, pp. 1-10.

Bendick 92 — W. Bendick und I. Zylla: Eigenschaften des Werkstoffs X20CrMoV 121 nach Betriebsbeanspruchung und Zeitstandschädigung. VGB Konferenz „Restlebensdauer 1992“, VGB Essen

Bendick 93 — W. Bendick, I. Zylla, H. Müsch, O. Wachter: Eigenschaften des Werkstoffs X20CrMoV121 nach Betriebsbeanspruchung und Zeitstandschädigung; in VGB Kraftwerkstechnik 73, 1993, Heft 3

CEN CWA 15261-3:2005 — CEN CWA 15261-3:2005: Measurement uncertainties in mechanical tests on metallic materials - Part 3: The evaluation of uncertainties in creep testing

Cole 00 — D. Cole, C. Martin-Moran, A.G. Sheard, H. K. D. H. Bhadeshia and D. J. C. MacKay: Modelling Creep Rupture Strength of Ferritic Steel Welds, Science and Technology of Welding and Joining, Vol. 5, 2000, 81-90

Danielsen 06 — H. K. Danielsen and J. Hald: Behaviour of Z phase in 9-12% Cr Steels. Energy Materials. Vol.1, No. 1, p. 49 – 57, 2006.

DataEngine 02 — DataEngine – Software und Handbücher der MIT – Management Intelligenter Technologien GmbH, Aachen 2002 (4. Auflage)

DIN 17175 — DIN 17175 Nahtlose Rohre aus warmfesten Stählen Technische Lieferbedingungen

Dobers 73 — H. Dobers und B. Melzer: Einfluss der Kaltverformung auf die Zeitstandfestigkeit warmfester Rohrstähle. Neue Hütte 18 (1973), Seite 304 – 307.

Dok 02 — A. Doktorowski: Datenbasierte Modellierung der Gefügebildung bei der γ–α–Umwandlung von Stählen. Freiberger Forschungshefte B 319, TU Bergakademie Freiberg 2002

ECCC 05 — ECCC Recommendations, 2005, 'Creep data validation and assessment procedures', Holdsworth, S.R. et al. eds., publ. ETD, (a) Vol.1 - Overview, (b) Vol.2 - Terms and terminology, (c) Vol.3 - Data acceptability criteria, Data generation, (d) Vol.4 - Data exchange and collation, (e) Vol.5 – Data assessment (uniaxial data), (f) Vol.6 - Residual life assessment and microstructure, (g) Vol.7 – Assessment of creep crack initiation in testpieces and components, (h) Vol.8 – Assessment of multi-axial creep test data, (i) High temperature component assessment.

EN 10088: 2005 — CEN EN 10088:2005 - Stainless steels - Part 1: List of stainless steels

EN 10213-2:1995 — CEN EN 10213-2:1995 - Technical Delivery Conditions for Steel Castings for Pressure Purposes - Part 2: Steel Grades for Use at room temperature and at elevated temperatures

EN 10216-2:2002 — CEN EN 10216-2:2002 - Seamless Steel tubes for pressure purposes – technical delivery conditions; Part 2: Non-alloy and alloy steel tubes with specified elevated temperature properties

EN 10222-2: 2000 — CEN EN 10222-2:2000 - Steel forgings for pressure purposes; Part 2: Ferritic and martensitic steels with specified elevated temperature properties

EN 10269: 1999 — CEN EN 10269:1999 - Steels and nickel alloys for fasteners with specified elevated and/or low temperature properties

EN 10291: 2000 CEN EN 10291:2000 - Metallic materials -Uniaxial creep testing in tension – Methods of test

EN 10302: 2002 CEN EN 10302:2002 – Creep resisting steels, nickel and cobalt alloys

EN 10314: 2002 CEN EN 10314:2002 - Method for derivation of minimum values of proof strength of steel at elevated temperature

EN 12952-3:2001 CEN EN 12952-3:2001 - Water-tube boilers and auxiliary installations – Part 3: Design and calculation of pressure parts

EN 12952-2:2001 CEN EN 12952-2:2001 - Water-tube boilers and auxiliary installations – Part 2: Materials for pressure parts of boilers and accessories

Fabritius 85 H. Fabritius und H. Weber: Zur Betriebssicherheit von Anlagen nach langer Betriebsbeanspruchung im Zeitstandbereich. Sonderheft VGB Konferenz „Werkstoffe und Schweißtechnik im Kraftwerk 1985“. VGB Essen„

Ho 01 S. L. Ho, M. Xie, L. C. Tang, K. Xu, and T. N. Goh: Neural Network Modeling With Confidence Bounds: A Case Study on the Solder Paste Deposition Process. IEEE Transactions On Electronics Packaging Manufacturing, Vol. 24, No. 4, October 2001

Howard 88 Howard E. Boyes: Atlas of Creep and Stress-Rupture Curves, ASM International, 1988 (second printing 1997)

ISO2605-1: 1976 ISO2605-1:1976 (Withdrawn) Steel products for pressure purposes – Derivation and verification of elevated temperature properties – Part I: Yield or proof stress of carbon and low alloy steel products

ISO2605-2: 1976 ISO2605-2:1976 (Withdrawn) Steel products for pressure purposes – Derivation and verification of elevated temperature properties – Part II: Proof stress of austenitic steel products

ISO2605-3: 1985 ISO2605-3:1985 Steel products for pressure purposes – Derivation and verification of elevated temperature properties – Part III: An alternative procedure for deriving the elevated temperature yield or proof stress properties when data are limited

IS0 15608: 2000 CR IS0 15608, Welding - Guidelines for a metallic material grouping system (ISO/TR 15608:2000).

ISO 9327-2: 1999 ISO 9327-2: Steel forgings and rolled or forged bars for pressure purposes – technical delivery conditions – Part 2: Non-alloy and alloy (Mo, Cr and CrMo) steels with specified elevated temperature properties

ISO 9329-2: 1997 ISO 9329-2: Seamless steel tubes for pressure purposes – technical delivery conditions – Part 2: Unalloyed and alloyed steels with specified elevated temperature properties

Jesper 85 H. Jesper, H. R. Kautz: Eigenschaften, Verarbeitung und Bewährung des Stahles X20CrMo(W)V 12 1 im Kraftwerk. VGB Konferenz „Werkstoffe und Schweißtechnik im Kraftwerk 1985“. VGB Essen.

Jovanovic 99 Jovanovic, M. Magueur: Technical Report: Task 3.1: Applicability of Advanced Statistical Methods and Task 3.2: Trial Application of advanced analysis methods for uncertainties in remaining life assessment (combined report), 1999, Code of Practice for the Determination of Uncertainties in Mechanical Tests on Metallic Materials (UNCERT) Contract SMT4-CT97-2165

Kalwa 85 G. Kalwa, State of the Development and Application Techniques of the Steel X20CrMoV12-1, Nuclear Engineering and Design, 84 (1985), 87-95

Kalwa 91 G. Kalwa, E. Schnabel: Umwandlungsverhalten und Wärmebehandlung der martensitischen Stähle mit 9-12%Cr; in Mannesmann-Mitteilung 1089/1991

Kelly 07 James Kelly: Heat resistant alloys, Rolled Alloys Technology

Maile 04 K. Maile, M. Rauch, P. Seliger und A. Reuter: Charakterisierung der Schädigungsentwicklung zur Lebensdauerbewertung von Rohrleitungskomponenten aus den neuen 9 %-Chromstählen Abschlussbericht zum AVIF-Forschungsvorhaben Nr. A152, 2004. MPA Universität Stuttgart und Siempelkamp Prüf- und Gutachter-Gesellschaft mbH Dresden

Maile 04a K. Maile; J. Hald, Editor: K. Yagi; G. Merckling; T.-U. Kern; H. Irie; H. Warlimont: 2.3.9 12Cr-1Mo-V steel (J. Hald, K. Maile); 2.3 High Cr steels, pp. 170-180, Landolt-Börnstein, Advanced Materials and Technologies, VIII/2B, 2004

Maile 99 K. Maile: Fortgeschrittene Verfahren zur Beschreibung des Verformungs- und Schädigungsverhaltens von Hochtemperaturbauteilen im Kraftwerksbau, Shaker Verlag, ISSBN, 1999

Marx 86 — P. Marx, K. Kautz, Rajinder Singh Dev, Lehrhefte für die Ausbildung zum Kraftwerker, Heft 5 Werkstoffkunde, Dritte Ausgabe 1986

Masuyama 04 — F. Masuyama; Editor: K. Yagi; G. Merckling; T.-U. Kern; H. Irie; H. Warlimont: 2.4.12 23Cr-18Ni-3Cu-1.5W-Nb-N steel (F. Masuyama); 2.4 Austenitic stainless steels, pp. 275-278, Landolt-Börnstein, Advanced Materials and Technologies, VIII/2B, 2004

Mayer 06 — Statusreport: Werkstoffentwicklungen zur Effizienzsteigerung von fossilen Kraftwerken. Fachausschussbericht 6.023. Stahlinstitut VdEH im Stahlzentrum Düsseldorf, 2006

Melzer 91 — Melzer, B.: Eine neue Methodik zur Ermittlung der realen Lebensdauer-Verknüpfung von werkstoffkundlicher Vor-Ort Untersuchung und Lebensdauerberechnung. VDl-Berichte Nr. 852, 1991, Pages 777 to 785

Melzer 92 — B. Melzer, P. Seliger und W. Illmann: Verbesserte Lebensdauerabschätzung kriechbeanspruchter Röhrbögen mittels bauteilspezifischer Kennwerte. VGB Konferenz „Restlebensdauer 1992“, VGB Essen

Melzer 03 — B. Melzer, P. Seliger: 1991 bis 2000 - das Jahrzehnt der warmfesten 9-bis 12 %-Chromstahle in Europa, VGB PowerTech 3/2003, Pages 83 to 96

MINAMI 87 — Yusuke MINAMI and Hideto KIMURA: Effect of $M_{23}C_6$ and MC Carbides on the Creep Rupture Strength of 18%Cr-10%Ni-Ti-Nb Steel, Transactions of the Iron and Steel Institute of Japan Vol.27 (1987), No.4 pp.299-301

Morinaga 94 — M. Morinaga, R. Hashizume and Y. Murata: Materials for advanced power engineering; part I, Kluwer Academic Publshers, Dordrecht (1994), 314

Petri 82 — R. Petri, E. Schnabel und P. Schwaab: Zum Legierungseinfluss auf die Umwandlungsausscheidungsvorgänge bei der Abkühlung warmfester Röhrenstähle nach dem Austenitisieren. Teil II - 12%ige Chromstähle. Archiv Eisenhüttenwesen 52 (1982), S. 27 – 32

Petri 83 — Ruth Petri and Paul Schwaab: Atlas of precipitates in Steels, Verlag Stahleisen mbH, Duesseldorf, 1983

Polcik 98 — O. Polcik: Modellierung des Verformungsverhaltens der warmfesten9-12% Cr-Stähle im Temperaturbereich von 550 – 650°C. PhD-Thesis, Erlangen, Shaker Verlag 1998.

RDC — A. Jovanovic, D. Balos : “ALIAS-RDC – Reduce Design Conservatism HSS” - Task 5, 6, 7 and 8 Final report, RDC/T5/MPA/10-1

Schenk 85 — Schenk, U.: Richtreihe für die Ausgangsgefüge der sowjetischen Rohrstähle 12 Ch 1 MF und 15 Ch 1 M 1 F Werkstoff-Mitteilung für den Kraftwerksanlagenbau 42. Zweite Auflage Kraftwerks- und Anlagenbau AG, Abt. Werkstofftechnik, Dresden 1985

Schieferstein 60 — U. Schieferstein: Einige Bemerkungen zum Zeitstandverhalten von CrMoV-Stählen mit 12% Cr. . Internationale Aussprache über das Langzeitverhalten warmfester Stähle am 24./25. 06.1960 in Düsseldorf

Schinn 60 — R. Schinn: Streuung der Zeitstandfestigkeit des Stahls X20CrMoV12 1, eine Gemeinschaftsauswertung deutscher Versuche. Internationale Aussprache über das Langzeitverhalten warmfester Stähle am 24./25. 06.1960 in Düsseldorf.

Schnabel 87 — E. Schnabel, P. Schwaab und H. Weber: Metallkundliche Untersuchungen an warmfesten Stählen, Stahl und Eisen 107, 1987, Seite 691 - 696

Schubert 92 — J. Schubert, W. Jakobeit, K. Schneider: Einfluss des Reinheitsgrades, der Kaltverformung und des Schweißens auf das Zeitstandverhalten von X20CrMoV121-Rohrstahl bei 550°C; in Materialwissenschaft und Werkstofftechnik , 1992, Heft 23, S.18-28

Shao 97 — R. Shao, E. B. Martin, J. Zhang and A. J. Morris: Confidence bounds for neural network representations, Computers & Chemical Engineering, Volume 21, Supplement 1 , 20 May 1997, Pages S1173-S1178; 6th International Symposium on Process Systems Engineering and 30th European Symposium on Computer Aided Process Engineering

Stackeljan 96 — J. Strakeljan, D. Behr: Verfahren zur Merkmalsauswahl, Symposium, Anwendungen von Fuzzy Technologien und Neuronalen Netzen; 11. - 12. Dezember 1996, Berlin, Pages 87 to 94

TRD 301:1979 — TRD 301: 1979, Cylindrical shells under internal pressure

TRD 508: 1978 — TRD 508: 1978 Zusätzliche Prüfungen an Bauteilen, berechnet mit zeitabhängigen Festigkeitskennwerten

VGB 05 Richtreihe zur Bewertung der Gefügeausbildung und –schädigung zeitstandbeanspruchter Werkstoffe von Hochdruckrohrleitungen und Kesselbauteilen. VGB-TW 507 2. Ausgabe 2005; VGB PowerTech Service GmbH, Essen

Wilhelmsson 80 H. Wilhelmsson und H. Törnblom.. Creep properties, creep rupture strength, cold working, stress relieving, annealing, ferritic steel, austenitic steel HT17, HT9 (X20CrMoV12- 1), 8R40, bending, steam generator tubes. Stiftung für Wärmebehandlung - SV project 96 (1980), Studsvik Energiteknik AB, 611 82 Norköping

Zheng-Fei Hu Zheng-Fei and Yang Zhen-Guo: Identification of the Precipitates by TEM and EDS in X20CrMoV12.1 After Long-Term Service at Elevated Temperature, Journal of Materials Engineering and Performance (2003) 12:106-111